Role of adhesin proteins in *Chlamydia* infection

Inaugural dissertation

for the attainment of the title of doctor
in the Faculty of Mathematics and Natural Sciences
at the Heinrich Heine University Düsseldorf

presented by

Alison Favaroni
from Perugia (Italy)

Düsseldorf, February 2017

from the Institute for Functional Microbial Genomics
at the Heinrich Heine University Düsseldorf

Contents

Abbreviations

° C	Celsius degree
%	Percentage
2D	Second dimension
aa	Amino acid
AB	Aberrant body
Aβ	Amyloid β
AFM	Atomic Force Microscopy
AP	Alkaline phosphate
AT	Autotransporter
ATP	Adenosine triphosphate
BN	Blue Native
bp	Base pair
BSA	Bovine serum albumin
C.	*Chlamydia*
Co-	Co-refolded
cOMC	*Chlamydia* outer membrane complex
DNA	Deoxyribonucleic acid
dNTPs	Deoxy nucleotides
E.	*Escherichia coli*
e.g.	*"exempli gratia",* for example
EB	Elementary body
EGFR	Epidermal growth factor receptor
ER	Endoplasmic reticulum
et al	*"et alia",* and others
Fig.	Figure
FITC	NHS-Fluorescin
FKS	Fetal bovines serum
FT	Flow through
g	Grams
GAGs	Glycosaminoglycans
GST	Glutathione-S-Transferase
h	Hours
HBSS	Hanks buffered salt solution
His	Histidine-tag

hMW	High Molecular Weight
hpi	Hours post infection
HS	Heparan sulfate
IM	Inner membrane
Inc	Inclusion membrane protein
INF	Interferon
Kd	Dissociation constant
kDa	Kilo Dalton
L	Liter
LGV	Lymphogranuloma venereum
LPS	Lipopolysaccharide
M	Molarity
mA	Milliampere
mg	Milligram
min (´)	Minutes
Mix-	Mixed
ml	Milliliter
mM	Millmolar
MOI	Multiplicity of infection
Momp	Major outer membrane protein
MPa	Mega Pascal
MW	Molecular weigth
nM	Nanomolar
nm	Nanometer
nt	Nucleotide
OD	Optical density
OM	Outer membrane
OMC	Outer membrane complex
OmcA	Outer membrane protein A
OmcB	Outer membrane protein B
ON	Overnight
PAGE	Polyacrylamide gel electrophoresis
PBS	Phosphate buffered saline
PCR	Polymerase chain reaction
PD	Passenger domain
Pel	Pellet
PFA	Paraformaldehyde

PG	Peptidoglycan
pH	*pondus hydrogenii*
PID	Pelvic inflammatory disease
pmol	Picomolar
Pmp	Polymorphic membrane protein
r	Recombinant
RB	Reticulate body
Ref.	Reference
RNA	Ribonucleic acid
Rpm	Revolutions per minute
RT	Room temperature
SDS	Sodium dodecyl sulphate
sec (´´)	Seconds
SEC	Size exclusion chromatography
SN	Supernatant
SS	Signal sequence
T3SS	Type 3 secretion system
T5SS (TVSS)	Type 5 secretion system
Tarp	Translocated actin-recruiting phosphoprotein
TEM	Transmission electron microscopy
U	Unit
μg	Microgram
μl	Microliter
μm	Micrometer
UV	Ultraviolet
V_0	Void volume
VSV	VSV-G epitope tag
WB	Western blot
x g	Acceleration due to gravity

Summary

Members of the genus *Chlamydia* are Gram negative bacteria, which can cause infections in several organisms. *C. trachomatis* and *C. pneumoniae* are responsible for widespread infections in humans, causing urogenital and respiratory tract infections, respectively. *Chlamydiae* exist in two morphological forms, the infectious elementary body (EB) and the metabolically active reticulate body (RB) and are obligate intracellular pathogens; therefore the adhesion is the first and essential step for the establishment of the infection; however the molecular details are ill-defined. In an attempt to identify new adhesin proteins for *C. pneumoniae*, a yeast display screening was performed and three hypothetical proteins were identified as adhesin candidates (Yaa1, Yaa2 and Yaa3). Yaa1 has been recently characterized as an adhesin and invasin and re-named LIPP, while Yaa2 and Yaa3 are still uncharacterized proteins. Polymorphic membrane proteins (Pmps) form a family of *Chlamydia* adhesins, with 9 members in *C. trachomatis* and 21 in *C. pneumoniae* and are relevant candidates for the development of a vaccine. Pmps are characterized by multiple GGA(I, L, V) and FxxN motifs along the functional passenger domain (PD). The PDs of many Pmps are processed during the infection. PD fragments of all 9 *C. trachomatis* and of representative *C. pneumoniae* Pmps harboring a high density of motifs (motif-rich) are characterized as adhesins and are relevant for the infection. Furthermore, a recombinant fragment of *C. pneumoniae* Pmp21, harboring only two motifs (motif-poor) is able to oligomerize, forming protofibrillar structures.

In the first part of this work, motif-rich and motif-poor protein fragments of the 9 *C. trachomatis* Pmps were produced and shown to interact with other Pmp proteins, independently of the density of motifs. Motif-poor (Ac, Fc and Gc) and motif-rich (D, H and I) Pmp proteins interacted strongly with each other, forming different species of homomeric and heteromeric high molecular weight (hMW) complexes with different characteristics when analyzed by Blue Native-PAGE, followed by second dimension SDS-PAGE and Size Exclusion Chromatography. Electron microscopy revealed that homomeric complexes formed small protofibrils, while heteromeric protofibrils were significantly longer.

Homomeric and heteromeric Pmp oligomers had different adhesion strength to human cells. Interestingly, the adhesion-incompetent Ac Pmp was present in the adhesive fraction when in a heteromeric complex with adhesion-competent Pmps. Moreover, adhesion-competent but not adhesion-incompetent oligomers, pre-incubated with human cells, could

block a subsequent *C. trachomatis* infection, showing their relevance for the infection. Conversely, adhesion-incompetent oligomers loaded onto the EB surface inhibited the infection, possibly by masking naturally exposed functional Pmp structures on the *Chlamydia* cell surface; while adhesion-competent oligomers loaded onto the EB surface did not impair the infectivity, possibly by binding and substituting the function of naturally exposed Pmp structures on the *Chlamydia* cell surface.

Taken together, these data show the ability of *C. trachomatis* Pmps to generate homomeric and heteromeric complexes relevant for the infection. *C. trachomatis* may use Pmp complexes *in vivo* as adhesin structures, in order to reach the human receptor and, at the same time, using the numerous possible combinations of Pmp heteromeric complexes as a decoy mechanism, in order to escape the immune response.

In the second part of this work the hypothetical *C. pneumoniae* protein Yaa3, identified in the yeast display screening, was analyzed. Yaa3 harbors a DUF720 domain, found only in other two proteins in *C. pneumoniae* and in the three homologous proteins in other *Chlamydia* species. The Yaa3 homologue in *C. trachomatis* harbors a type 3 secretion signal, suggesting that Yaa3 may be type 3 secreted as well. A protocol for heterologous expression, purification and refolding of Yaa3 was established. Recombinant Yaa3 could bind human cells and pre-incubation of human cells with rYaa3 inhibited a *C. pneumoniae* infection. A polyclonal anti-Yaa3 antibody detected expression of Yaa3 associated with the bacteria at 24 h post infection.

These data indicate that Yaa3 might be type 3 secreted within the inclusion and loaded onto the EB cell surface, thus could be used in the next round of infection as an adhesin, relevant for the infection.

Analyzing *C. trachomatis* Pmp oligomers and characterizing a novel *C. pneumoniae* adhesin candidate, further steps were taken in understanding the complex mechanisms, which *Chlamydia* adopts in order to establish the infection.

1. Introduction

The *Chlamydiae* phylum is composed of Gram-negative bacteria which are obligate intracellular parasites of eukaryotic cells and are responsible for a variety of infections in humans and animals. Despite the different tropism, all *Chlamydiae* species share a unique developmental cycle, which comprehends two morphological forms: the infectious, extracellular elementary body (EB) and the intracellular, metabolically active reticulate body (RB).

1.1 Taxonomy

The first reference to a chlamydial infection (trachoma) occurred in Chinese documents of 27th century BC and in Egyptian papyrus of 15th century BC. In Europe, an epidemic spread was observed after the troops of Napoleon came back from Egypt at the beginning of the 19th century. At the end of the 19th century, immigrants coming from Europe were screened for signs of trachoma in the immigration center of Ellis Island in New York, before being allowed to enter the country. With the development of scientific methods, in 1910 bacteria were isolated from conjunctival scrapings and the observation of intracellular vacuoles led to the current name of "*Chlamydia*", derived from "*Chlamys/khlamus*", which in Greek means mantle. In the following years, agents responsible for sexually transmitted diseases and for psittacosis were isolated. Due to the obligate intracellular life cycle and the inability of growing in artificial media, *Chlamydiae* were classified as viruses (Hu, Harding-Esch et al. 2010). The first suggestion that *Chlamydia* might be bacteria came in 1942, but was only confirmed in 1966 (Moulder 1966).

Chlamydial taxonomy has always been object of discussion, leading to several changes in the last decades. The first classification attempt was made in the 1980 in the *Approved List of Bacterial Names* where the family of *Chlamydiaceae* included one genus (*Chlamydia*) with two species: *C. trachomatis* and *C. psittaci*. In the following years, *C. pneumoniae* and *C. pecorum* were identified (Grayston, Kuo et al. 1986, Grayston 1989, Fukushi and Hirai 1992). Between 1997 and 1999, all species, including *Chlamydia*-like species, were unified by comparative analyzes of ribosomal RNA (rRNA) 16S and 23S. According to this classification, the order *Chlamydiales* was divided in 4 families (*Chlamydiaceae, Parachlamydiaceae, Waddliaceae* and *Simkaniaceae*). In the *Chlamydiaceae* family two genera were identified with a total of nine species: *Chlamydia* (*C. trachomatis, C. suis* and

C. muridarum) and *Chlamydophila* (*C. pneumoniae, C. psittaci, C. pecorum, C. caviae, C. abortus* and *C. felis*) (Everett and Andersen 1997, Everett, Bush et al. 1999) Given discordant opinions in the field, in 2009 Stephens and collaborators analyzed a greater number of conserved genes and proposed the unification of *Chlamydia* and *Chlamydophila* in one genus "*Chlamydia*" (Stephens, Myers et al. 2009), confirmed in 2014 with a comparison between *C. psittaci* and *C. trachomatis* (Qin, Xie et al. 2014), and officially adopted in 2010 (Greub 2010, Bavoil, Kaltenboeck et al. 2013). In the meantime, new species have been identified and included in the genus: *C. ibidis, C. gallinaceae* and *C. avium* (Vorimore, Hsia et al. 2013, Sachse, Laroucau et al. 2014). Recently, all species currently belonging to the family *Chlamydiaceae* were compared with an extended analysis of POCP (percentage of conserved proteins), confirming the current taxonomy and provides a reliable method to classify new species (Pillonel, Bertelli et al. 2015, Pannekoek, Qi-Long et al. 2016) (Fig 1).
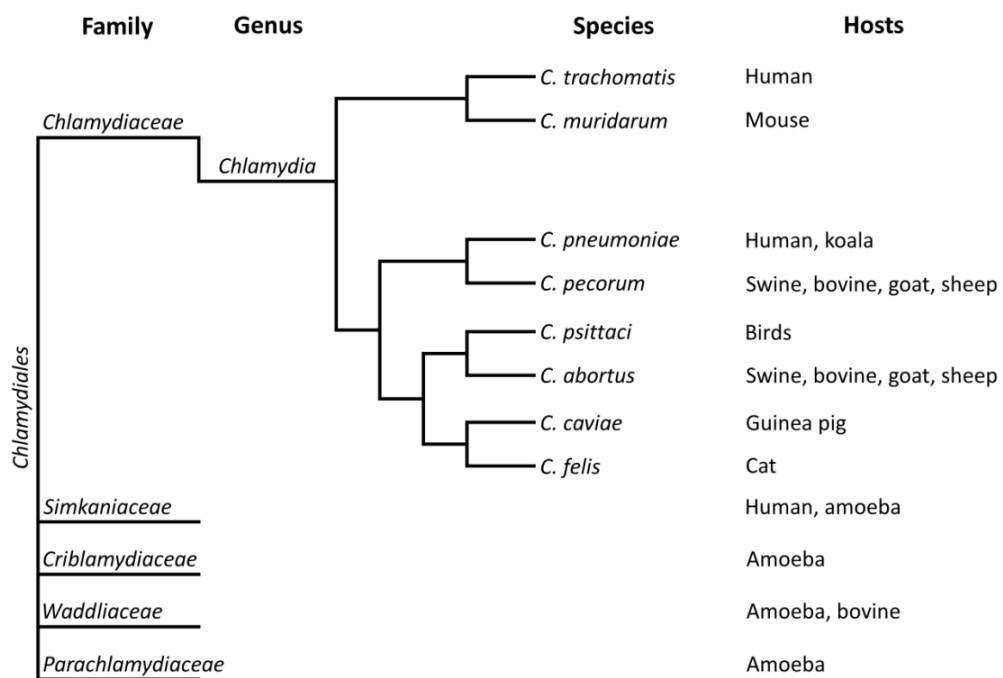
Figure 1. Taxonomy of the order *Chlamydiales*. Overview of families included in the order *Chlamydiales* and species belonging to the genus *Chlamydia*. Host organisms are indicated on the right. Length of line is not representative of phylogenetic distances (modified after Pillonel et al. 2015 and Pannekoek et al. 2016).

1.2 Genome and genetics

For many years, the whole genome sequencing of the different species has been the most important tool to investigate chlamydial biology, given the lack of genetic techniques for

manipulation of the genome of *Chlamydia*. The first sequenced genome was an isolate of *C. trachomatis* serovar D in 1998 (Stephens, Kalman et al. 1998) and genomes from ten chlamydial species are now sequenced (Mojica, Huot Creasy et al. 2011, Voigt, Schofl et al. 2012, Donati, Huot-Creasy et al. 2014, Holzer, Laroucau et al. 2016).

The chlamydial genome is one of the smallest prokaryotic genomes, composed by one circular chromosome of only approximately 1 Mbp and is highly conserved in genes responsible for functions shared among the species, like metabolism (Clarke 2011). Despite the high rate of conserved genes, genetic diversity among the different species is found in part in the *ompA* gene, which encodes the Major outer membrane protein (MOMP), in the family of polymorphic membrane proteins (*pmps*) and in a region called "plasticity zone". Genes found in this highly variable region are involved in species-specific niche adaptation, pathogenicity and host immune response avoidance (Taylor, Nelson et al. 2010). Genetic diversity among the species is also due to the fact that genomes from different species have a different size and harbor a different number of genes, for example, *C. pneumoniae* (genome of ~1.21 Mbp) harbor approximately 250 additional genes, which are not found in *C. trachomatis* (genome of ~1.04 Mbp) (Grimwood and Stephens 1999, Crane, Carlson et al. 2006).

Extensive natural DNA recombination has been observed mostly among *C. trachomatis* different serotypes; different inclusions can indeed fuse during co-infection *in vitro* and *in vivo* (Jeffrey, Suchland et al. 2010). Only in 2011 the first success in genetically manipulation of *C. trachomatis* has been reported (Wang, Kahane et al. 2011). Since then, the molecular toolbox have been expanded and, up to date, several mutant strain libraries of *C. trachomatis* and *C. muridarum* have been produced by random mutagenesis and by plasmid-based transformation (Sixt and Valdivia 2016).

1.3 *Chlamydiae* cause widespread infections

Of all *Chlamydiae* species, only three are known to date to cause diseases in humans: *C. trachomatis*, *C. pneumoniae* and *C. psittaci*. The other species belonging to the *Chlamydia* genus are responsible for a wide range of pathogenesis in the animal kingdom (Fig.1).

1.3.1 Chlamydial infections in animals and transmission to humans

C. muridarum, *C. caviae* and *C. felis* are mainly responsible for infection in domestic animals. *C. muridarum* is the corresponding murine pathogen of *C. trachomatis*, while

C. felis and *C. caviae* are responsible for conjunctivitis in cats and guinea pigs. *C. pecorum* and *C. abortus* can infect the urogenital and intestine tract of ovine and bovine, leading to spontaneous abortion and infertility (Rohde, Straube et al. 2010). Besides the suffering of the animals, these infections cause significant economic damages (Rodolakis and Laroucau 2015). *C. psittaci* is the responsible agents for avian chlamydiosis in more than 450 species of birds, infecting the respiratory tract (Hulin, Oger et al. 2015). Recently, it was shown that *C. gallinaceae*, and not *C. psittaci* as previously thought, is the endemic chlamydial species in chickens (Guo, Li et al. 2016). *C. psittaci* can be transferred from infected birds to humans via inhalation of infected aerosol. Humans infected with *C. psittaci* can develop flu-like symptoms and severe infections like pneumoniae and myocarditis, which can be fatal and create outbreaks in people who work in direct contact with infected animals (Miyairi, Laxton et al. 2011, Laroucau, Aaziz et al. 2015). Recently, transmission of *C. abortus* from animals to humans was reported, causing atypical pneumoniae (Ortega, Caro et al. 2015). Furthermore, besides being a human pathogen, *C. pneumoniae* has been found in many animal hosts, such as koalas, reptiles and horses (Bodetti, Jacobson et al. 2002). Even though cases of *C. pneumoniae* transmission between animals and humans have not been reported, Myers and co-workers suggested that the *C. pneumoniae* strains adapted to human might be evolved from zoonotic infections (Myers, Mathews et al. 2009).

1.3.2 *C. pneumoniae*

C. pneumoniae infection occurs via inhalation of infected aerosol and in immune competent humans is often asymptomatic. It was estimated that 75 % of adult people have been infected with the pathogen. *C. pneumoniae* can infect the upper respiratory tract, causing mild symptoms like pharyngitis and sinusitis and the lower respiratory tract, causing bronchitis and pneumoniae, which can be very severe in immune compromised patients (Jama-Kmiecik, Frej-Madrzak et al. 2015). Moreover, *C. pneumoniae* is one of the major agents of community-acquired pneumonia (6-20 % of cases) (Blasi, Tarsia et al. 2009). *C. pneumoniae* infections can produce chronic inflammation and have been associated with a variety of chronic diseases such as asthma, atherosclerosis, sarcoidosis and Alzheimer diseases (Shima, Coopmeiners et al. 2016). In support of this observation is the ability of *C. pneumoniae* to infect several cell types (e.g. lung epithelial cells, vascular endothelial cells, monocytes), but whether *C. pneumoniae* is the primary agent or a co-factor for chronic diseases is still object of investigation (Belland, Ouellette et al. 2004).

Moreover, *C. pneumoniae* infection is also found in association with lung cancer (Hua-Feng, Yue-Ming et al. 2015).

1.3.3 *C. trachomatis*

C. trachomatis is the leading agent of sexually transmitted diseases (STDs) and infectious blindness worldwide. Each year, *C. trachomatis* is responsible for 131 million new urogenital infections and up to date 8 million people are irreversibly visually impaired by trachoma (Resnikoff, Pascolini et al. 2004, WHO 2016). *C. trachomatis* is subdivided in 19 serovars. Serovars A, B, Ba and C infect ocular epithelia and repeated infections followed by inflammations produce scars, leading to blindness, in particular in third world countries (Hu, Harding-Esch et al. 2010). Serovars D, Da, E, F, G, Ga, H, I, Ia, J and K infect the urogenital tract of both males and females. Infection in men is asymptomatic in 50 % of the cases and, when the infection manifests, causes epididymitis and proctitis. The majority of women infected (75 %) shows no symptoms and therefore the infections remain untreated. *C. trachomatis* can migrate from the vaginal tract to the upper genital tract and create a status of chronic inflammation, leading to the development of salpingitis, endometritis and pelvic inflammatory disease (PID), which can have the outcome of ectopic pregnancies and infertility. Furthermore, urogenital *C. trachomatis* infections represent a risk factor for acquisition of HIV and development of cervical carcinoma (Witkin and Linhares 2002, Malhotra, Sood et al. 2013). Serovars L1, L2, L2a and L3 infect the urogenital tract as well, but can spread to the lymphatic system, causing a severe systematic infection called lymphogranuloma venereum (LGV). If LGV is not properly treated, it can produce chronic lacerations of internal tissues (Stoner and Cohen 2015).

Chlamydial infections can be treated with antibiotics such as tetracycline and its derivates, but there are reports of failure of treatment (Di Francesco, Favaroni et al. 2013). Despite the presence of therapeutic procedures, the high rate of asymptomatic infected women will develop chronic inflammation; therefore a vaccine is urgently needed to prevent the irreversible outcomes.

1.4 The infectious cycle of *Chlamydia*

All chlamydial species are characterized by a unique developmental cycle, which comprehends two morphological forms: the elementary body (EB) and the reticulate body (RB) (Fig. 2). Even though the stages of the life cycle are the same, different species need different amount of time to complete all stages, for example the *C. trachomatis* cycle is

48 h, while *C. pneumoniae* needs 72 h. The EB (0,3 μm) is the infectious, spore-like form. The electron dense EB phenotype is due to a highly condensed nucleoid due to histone-like proteins. The presence of cross-linked proteins of the outer membrane complex (cOMC) allows the EB to survive in the extracellular environment, resisting to the osmotic and physical stress. Once the EBs are internalized within the inclusion, they differentiate to the RBs by reducing the EBs cross-linked complexes. The RBs can then replicate during the mid-cycle. The RB is larger than the EB (1 μm) and represents the intracellular, non-infectious, but metabolically active form. Electron microscopy analysis showed that RBs have a granular cytoplasm with diffuse, fimbrial DNA (Abdelrahman and Belland 2005). Besides replication, RBs are responsible for nutrient acquisition and transport, ATP generation and production of machineries for mRNA production and translation, protein folding and transport (Saka, Thompson et al. 2011).

EBs have long been considered metabolically inactive; however, recent studies showed that they have indeed metabolic activities, depending on D-glucose-6-phosphate (Omsland, Sixt et al. 2014). Under environmental stress, lack of nutrients, host immune response or antibiotic treatment, RBs can transit to a so-called aberrant body (AB). ABs are living, enlarged and non-dividing forms, representing a stage of persistence. This stage is reversible; once the stress is gone, ABs can turn back into active RBs and complete the infectious cycle (Elwell, Mirrashidi et al. 2016).
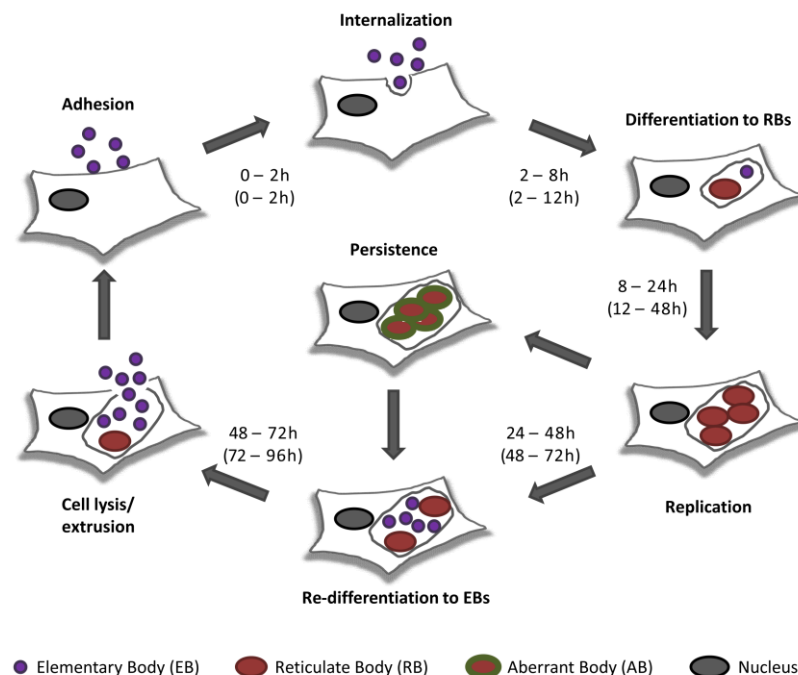
Figure 2. Schematic representation of the life cycle of *Chlamydiae*. Time points of the different phases of the life cycle are indicated for *C. trachomatis* (Hammerschlag 2002). Time points of the *C. pneumoniae* infections are indicated in brackets (Wolf, Fischer et al. 2000).

1.4.1 The chlamydial outer membrane complex (cOMC)

Being Gram-negative bacteria, *Chlamydiae* have an inner membrane (IM) and an outer membrane (OM), separated by the periplasmic space.

The chlamydial OM contains Lipopolysaccharide (LPS), an endotoxin commonly found in Gram-negative bacteria. Chlamydial LPS is actually a Lipooligosaccharide (LOS), consisting of a longer and less toxic lipid A bound to a trisaccharide core (Rund, Lindner et al. 1999, Nguyen, Cunningham et al. 2011).

A peculiar characteristic of the chlamydial cell envelope is the absence of a classical peptidoglycan (PG) structure. Even though all enzymes for PG synthesis are functional and *Chlamydia* is sensitive to penicillin treatment, the classical Gram-negative murein could not be detected. This phenomenon is known as the "*Chlamydia* anomaly" (Barbour, Amano et al. 1982, Hatch 1996, McCoy and Maurelli 2006, Klockner, Otten et al. 2014, Jacquier, Viollier et al. 2015). Recently, microscopy analysis showed that PG could form rings during the mid-late cycle, suggesting a role during chlamydial division (see paragraph 1.4.6) (Liechti, Kuru et al. 2014). In absence of a classical PG structure, the actual stability and structure of chlamydial EBs is due to inter- and intramolecular disulphide cross-linking of the cysteine-rich proteins, forming the chlamydial outer membrane complex (cOMC) (Hackstadt, Todd et al. 1985, Hatch 1996).

The cOMC is a sarkosyl-insoluble network of cross-linked proteins, which has been described for the first time in *C. psittaci* 6BC in 1995 and it involves some of the chlamydial adhesins known so far (Everett and Hatch 1995).

MOMP (outer membrane complex protein A, encoded by the gene *ompA*), a protein of 40 kDa, is the major component of the cOMC and it represents the 60 % of the outer membrane proteins (OMPs) (Feher, Randall et al. 2013). The *ompA* gene is a "mid-cycle gene", MOMP is therefore present in similar amount in EBs and RBs and is characterized as a porin (Confer and Ayalew 2013). The protein is a trimer with the monomers bound by disulphide bridges forming a predicted 16-stranded β-barrel structure (Sun, Pal et al. 2007, Feher, Randall et al. 2013). MOMP is anchored in the OM by five hydrophobic conserved constant segments (CS1-CS5), which are connected by four variable segments (VS1-VS4) exposed on the surface (Kim and DeMars 2001). The VSs are highly variable sequences, which define MOMP differences among *C. trachomatis* strains and serovars and represent antibody epitopes; while CSs are recognized by T cells (Kim and DeMars 2001). In addition to the porin function, *C. trachomatis* MOMP is characterized as an adhesin (see paragraph 1.4.2).

OmcA (outer membrane protein A) is the small cysteine-rich lipoprotein of the cOMC (12 kDa) with a C-terminal hydrophobic region anchored in the OM and a N-terminal hydrophilic region which faces the periplasmic space (Hatch 1996).

Cysteine-rich OmcB (outer membrane protein B) is the second most abundant protein in the cOMC. C-terminal region of OmcB is highly conserved among chlamydial species, while the variable N-terminal region is species-specific and mediates binding to heparan sulfate (HS)-like glycosaminoglycans (GAGs) on the host cell, suggesting a role in tissue tropism (Moelleken and Hegemann 2008, Fechtner, Stallmann et al. 2013). Even though for long time OmcB was considered a periplasmic protein, in 1995 its binding to human HeLa cells was demonstrated (Ting, Hsia et al. 1995) (see paragraph 1.4.2).

Besides these major proteins, many other proteins were found to be part of the cOMC such as OprB, PorB, ring proteins of type 3 secretion system (T3SS), members of the Pmp family (e.g. *C. trachomatis* PmpB, PmpC, PmpE, PmpF, PmpG and PmpH). A total of 17 proteins were identified in the cOMC of *C. trachomatis* L2, but the isolation and analysis of this complex is challenging, therefore further studies are required. Interestingly, *C. pneumoniae* Pmp21 is part of the cOMC, while its homologue in *C. trachomatis* (PmpD) is associated with the outer membrane, but is not linked to the cOMC, probably due to the lack of cysteine residues in its β-barrel. (Mygind, Christiansen et al. 2000, Tanzer and Hatch 2001, Birkelund, Morgan-Fisher et al. 2009, Swanson, Taylor et al. 2009, Liu, Afrane et al. 2010, Molleken, Schmidt et al. 2010, Becker and Hegemann 2014). Many of the low-abundance proteins identified in the cOMC are adhesins, but not all chlamydial adhesins are part of the cOMC.

1.4.2 Adhesion

Chlamydia is an obligate intracellular pathogen, therefore the adhesion of the EBs to the host cells and their subsequent internalization are the essential steps for the establishment of the infection. The adhesion of the EB to the target cells is a multifactorial process and is still not fully understood. Different *Chlamydia* species exhibit different cell tropism and, already in 1976, it was suggested that different species may use different mechanisms of infection (Kuo and Grayston 1976). A two-steps interaction process has been proposed, in which reversible electrostatic interactions establish the first contact between the EB and the host cell, followed by irreversible specific interactions between chlamydial adhesins and host cell receptors (Campbell and Kuo 2006). The first reversible interaction is represented for many, but not all, chlamydial species by a low-affinity interaction of OmcB with

heparan sulfate (HS)-like glycosaminoglycans (GAGs) (Dautry-Varsat, Subtil et al. 2005). GAGs are long, linear polysaccharides, components of the extracellular matrix of mammalian cells and are involved in several functions, such as cell adhesion, cell differentiation and can be recognized by pathogenic adhesins. The high variety of GAG chains is due to enzymatic activities and is strictly regulated (Mikami and Kitagawa 2016). It was shown already in 1973 and again in 1992 that pre-treatment of human cells or EBs with heparin (a HS-like GAG) inhibited *C. trachomatis* attachment and infectivity (Kuo, Wang et al. 1973, Zhang and Stephens 1992). Interestingly, HS-GAGs reduce infectivity of different biovars of *C. trachomatis* at different levels; LGV biovars infectivity is highly blocked by low concentrations of HS-GAGs; while trachoma and urogenital biovars infectivity is not completely blocked even at high HS-GAGs concentrations. Furthermore, *C. trachomatis* serovar E infectivity is not affected by exogenous heparin. This can be explained by the different tropism of the biovars; LGV infects the basolateral domains of the mucosal epithelia, and is therefore highly dependent on GAGs, while serovar E infects the apical site of the cells (Davis and Wyrick 1997, Campbell and Kuo 2006, Moelleken and Hegemann 2008). Surprisingly, when *C. trachomatis* serovar B and L2 were incubated with heparin, the binding was saturated, suggesting the presence of GAG receptors also on the EB surface itself (Chen, Zhang et al. 1996). Not only *C. trachomatis* is able to bind HS-GAGs, but pre-treatment with heparin could also reduce *C. pneumoniae* and *C. muridarum* infections (Wuppermann, Hegemann et al. 2001, Yan, Silvennoinen-Kassinen et al. 2006, Elwell, Mirrashidi et al. 2016).

In 2001, *C. trachomatis* L2 OmcB, a surface protein and part of the cOMC, was identified as the first adhesin responsible for binding to the HS-GAGs. Also in *C. pneumoniae*, *C. caviae*, *C. psittaci* and *C. trachomatis* trachoma and LGV biovars OmcB adhesion to host cells is dependent on HS-GAGs, while OmcB of *C. trachomatis* serovar E adheres to the human cell in a HS-GAG independent manner (Stephens, Koshiyama et al. 2001, Campbell and Kuo 2006, Moelleken and Hegemann 2008, Fechtner, Stallmann et al. 2013). The OmcB motif responsible for interaction with HS-GAGs has been identified in the variable N-terminal region and consists of hydrophobic (X) and basic (B) amino acids: XBBXBX. OmcB binding to the human cells establishes the first reversible adhesion step and defines the different cell tropism of *Chlamydia* species (Moelleken and Hegemann 2008, Fechtner, Stallmann et al. 2013).

C. trachomatis LPS seems to have an active role in the attachment of the EBs to human cells and is presumably associated with the CFTR (cystic fibrosis transmembrane

conductance regulator), an apical anion channel in the plasma membrane of epithelial cells (Ajonuma, Fok et al. 2010, Hegemann and Moelleken 2012). Interestingly, despite the fact that in Gram-negative bacteria LPS is highly immunogenic, the antibodies produced against LPS are not able to neutralize a *C. trachomatis* and a *C. psittaci* infection, but they could inhibit a *C. pneumoniae* infection (Peterson, de la Maza et al. 1998, Fadel and Eley 2008). These data are confirmed by *in vivo* data; sera from *C. pneumoniae* infected patients diagnosed with acute myocardial infarction were indeed found positive for anti-LPS antibodies (Saikku 2000).

MOMP, the most prominent component of the cOMC (see paragraph 1.4.1), is characterized as an adhesin, able to bind HS-GAGs. Furthermore, post-translational glycosylation of MOMP suggests binding to the mannose-6-phosphate-receptor / insulin-like growth factor receptor 2 (M6PR/IGFR2) (Raulston 1995, Mehlitz and Rudel 2013). Of all species, *C. muridarum* was the only one whose infection could be inhibited by anti-MOMP neutralizing antibodies, while antibodies produced against *C. trachomatis* MOMP are not able to neutralize the infection (Su, Raymond et al. 1996). Moreover, immune sera could recognize *C. trachomatis* and *C. psittaci* MOMP, which is therefore considered immunogenic in these species, but not *C. pneumoniae* MOMP, which is not able to adhere to human cells (Campbell, Kuo et al. 1990, Campbell and Kuo 2006, Molleken, Schmidt et al. 2010).

Other proteins are found to be involved in the attachment of EBs to human cells. *C. pneumoniae* Pmp21 is characterized as adhesin and invasin, interacting with the epidermal growth factor receptor (EGFR) on epithelial cells. *C. pneumoniae* Pmp6 and Pmp20 could also adhere to the human cells, but they could not bind the EGFR (explained more in detail in paragraph 1.6.3) (Molleken, Schmidt et al. 2010, Molleken, Becker et al. 2013). The nine *C. trachomatis* Pmps are also identified as adhesins and are relevant for the infection, but their human receptor is still unknown (Becker and Hegemann 2014) (explained more in detail in paragraph 1.6.3).

C. pneumoniae heat shock protein 60 (Hsp60), also known as GroEL1, mediates adhesion to human cells, but also its receptor is still unknown (Wuppermann, Molleken et al. 2008). Recently two new adhesins have been characterized. CPn0473 (LIPP) has been identified as a novel *C. pneumoniae*-specific adhesin, which binds directly to the lipids of the human membrane (Fechtner, Galle et al. 2016). Ctad1 has been identified as a new *C. trachomatis* adhesin, binding to the β1-integrin receptor and an yet unknown α-receptor (Stallmann and Hegemann 2016).

In addition to the already mentioned adhesins, *C. trachomatis* EBs adhesion is mediated by several receptors and molecules on the human cells, but it is still not known which chlamydial structures are involved. The fibroblast growth factor receptor (FGFR) is thought to be secreted by the infected cell and create a bridge between an unknown structure on the EB surface and the neighboring uninfected cell. Platelet-derived growth factor receptor (PDGFR) and ephrin receptor A2 (EPHA2) are also involved in the EBs adhesion and in the signaling cascades (Kim, Jiang et al. 2011, Subbarayal, Karunakaran et al. 2015, Elwell, Mirrashidi et al. 2016). Six membrane receptors (PDGFR, β2-integrin, CXCR7, VEGF, VCAM1 and GTP-binding protein) have been suggested to play a role in the adhesion of *C. pneumoniae* EBs, but none has been proved to be essential, while the presence of apolipoprotein E4 enhances *C. pneumoniae* adhesion (Gerard, Fomicheva et al. 2008, Wang, Johnston et al. 2010). The protein disulfide isomerase (PDI) is used by several *Chlamydia* species and mediates attachment of EBs to the human cells, but not via direct interaction, suggesting the presence of a non-identified host protein behaving as a bridge. The reducing enzymatic activity of PDI seems to be important not for EBs adhesion, but for chlamydial uptake (Abromaitis and Stephens 2009) (Fig. 3).
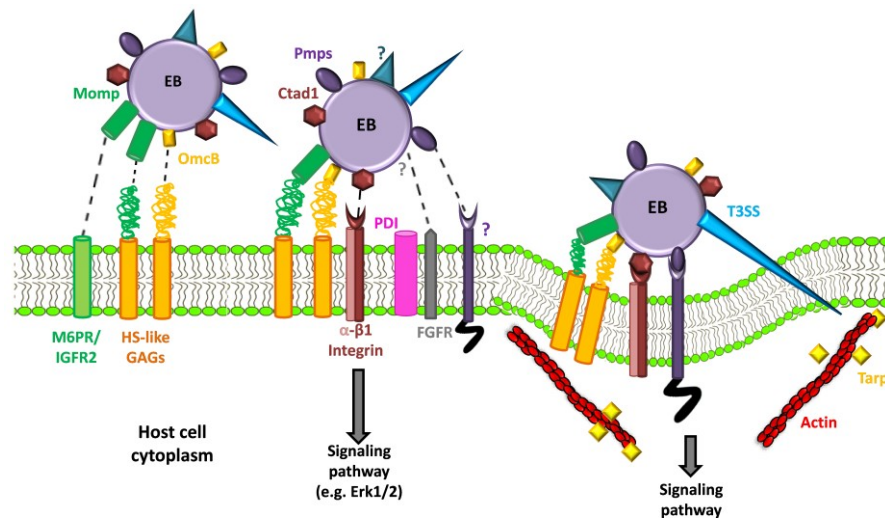
Figure 3. *C. trachomatis* adhesion. Schematic representation of *C. trachomatis* adhesion to human cells. MOMP: Major outer membrane complex, OmcB: Outer membrane protein B, Pmps: Polymorphic membrane proteins, Ctad1: *C. trachomatis* adhesin 1, T3SS: Type 3 secretion system, HS-like GAGs: Heparan sulfate-like glycosaminoglycans, M6PR: Mannose 6 phosphate receptor, IGFR2: Insulin-like growth factor receptor 2, FGFR: Fibroblast growth factor receptor, PDI: Protein disulfide isomerase and Tarp: Translocated actin-recruiting phosphoprotein.

1.4.3 Internalization of EBs

Adhesion of EBs to human cells induces actin remodeling, contributing to the internalization of chlamydial particles (Carabeo, Grieshaber et al. 2002). Several factors

are involved in this process, such as signaling cascades from the activated receptors and bacterial proteins injected into the host cell cytoplasm. Phosphorylation events occur early in the cycle, within the first 5 minutes; they are described as stable for several hours in *C. trachomatis*, while they are more transient and less strong in *C. pneumoniae*. In the *C. pneumoniae* infection, two main signaling pathways are activated: PI 3-kinase and MEK-ERK pathway (Coombes and Mahony 2002, Dautry-Varsat, Subtil et al. 2005). In particular, *C. pneumoniae* infection of epithelial cells *in vitro* showed activation of the ERK1/2 pathway, due to MEK-dependent phosphorylation, and, in a second moment, Akt activation by PI 3-kinase phosphorylation. Inhibition of these pathways blocked the bacteria internalization, but not the adhesion to the human cells (Coombes and Mahony 2002). Furthermore, Pmp21 biding to EGFR leads to the receptor activation, recruitment of Grb2 and c-Cbl adaptors and activation of the ERK1/2 cascade (Molleken, Becker et al. 2013). ERK1/2 signaling cascade is also activated by *C. trachomatis* Ctad1 binding to β1-integrin (Stallmann and Hegemann 2016).

Different signaling molecules are involved in the process of internalization of chlamydial particles, such as GTPases of the RHO-family, which play a role in actin polymerization. Different GTPases are recruited in a species-specific manner (Bastidas, Elwell et al. 2013); Moreover, Rac1 is responsible for *C. trachomatis* invasion of the human cells (Carabeo, Grieshaber et al. 2004), while Cdc42 and Arf6 are required for *C. caviae* entry (Subtil, Wyplosz et al. 2004).

In addition to the signaling cascades, bacterial effector proteins are injected in the host cell cytoplasm by the type 3 secretion system (T3SS) (explained in more detail in paragraph 1.5.1). One of the first effector proteins secreted in the host cell by *C. trachomatis* is Tarp (Translocated actin-recruiting phosphoprotein), which is phosphorylated in the first 5 minutes of the infection and is observed at the inner leaflet of the host membrane (Clifton, Fields et al. 2004, Clifton, Dooley et al. 2005). Tarp can directly nucleate and bundle actin via its F- and G-actin binding domains; furthermore its N-terminal phosphorylation domain is likely involved in signaling cascades, by recruiting effector proteins, such as Sos1, Vav2, Shc1 and Rac1 (Jiwani, Alvarado et al. 2013, Elwell, Mirrashidi et al. 2016). Even though Tarp homologues in other chlamydial species lack the tyrosine-rich domain, the *C. pneumoniae* homologue Cpn0572 can also bind directly to F-actin and remodel its cytoskeleton (Zrieg 2009, unpublished data).

All these factors together lead to membrane remodeling, which in the *C. pneumoniae* infection is mediated by lipid-rafts harboring sphingomyelin, but independent from clathrin

(Korhonen, Puolakkainen et al. 2012, Fechtner, Galle et al. 2016). On the other hand, *C. trachomatis* uptake is mediated by clathrin-dependent microdomains of the host membrane, independent of lipid-rafts (Gabel, Elwell et al. 2004).

1.4.4 Formation and remodeling of the inclusion

The uptake leads the EBs in a membrane-bound compartment called "inclusion" (Fields and Hackstadt 2002). During the chlamydial cycle, the inclusions migrate along microtubules to the Peri-Golgi region, by recruiting the host motor protein Dynein (Grieshaber, Grieshaber et al. 2006, Damiani, Gambarte Tudela et al. 2014), exchanging nutrients and effector proteins with the host cells and avoiding fusion with the lysosomes (Hackstadt 2000). These processes are achieved by constant remodeling of the inclusion membrane profile, using host and bacterial proteins. Rab GTPases are essential players in controlling the intracellular vesicular trafficking. Rab1, Rab4 and Rab11, involved in endosome recycling and transportation from the endoplasmic reticulum (ER) to the Golgi, are recruited by all *Chlamydia* species. Many of the known recruited Rabs are species-specific, for example Rab6 is only recruited by *C. trachomatis* inclusions (Rejman Lipinski, Heymann et al. 2009, Damiani, Gambarte Tudela et al. 2014). Another class of recruited host factors is phosphoinositide (PI) lipid kinases, which regulate cellular signaling and vesicular tracking (Vicinanza, D'Angelo et al. 2008); for example phosphatidylinositol-4-phosphate (PI4P) is recruited at the inclusion by lipid kinase OCRL1, activated by Rabs. This recruitment may mask the inclusion, mimicking as a Golgi component (Moorhead, Jung et al. 2010). SNARE proteins, involved in controlling vesicle fusions, are recruited by *Chlamydia* in order to manipulate inclusion trafficking and nutrient acquisition (Brunger, Cipriano et al. 2015). One last recruited protein family known so far are members of the sorting nexin family (SNX), used to control the Golgi endosomal pathway (Aeberhard, Banhart et al. 2015, Elwell, Mirrashidi et al. 2016).

In addition to the recruitment of the aforementioned host proteins, *Chlamydia* species express a unique family of effector proteins, named inclusion membrane proteins (Incs). Incs are expressed in the early stage of the infection and during the mid-cycle, contributing in the establishment of the inclusion and facilitating substance exchange with the host cell. Inc proteins share little identity and are identified in 5 *Chlamydia* species (55 in *C. trachomatis,* 92 in *C. pneumoniae,* 68 in *C. felis,* 79 in *C. caviae* and 54 in *C. muridarum*). Interestingly, according to bioinformatic analysis, in all 5 species only 23 Incs are conserved, showing a high degree of divergence among different species (Lutter,

Martens et al. 2012). Incs harbor a characteristic hydrophobic domain, which inserts in the inclusion membrane, exposing the C- and N-terminus to the host cytosol, forming homo- and hetero-typic oligomers (Gauliard, Ouellette et al. 2015). *Chlamydia* uses Incs to recruit host proteins to the inclusion in order to modulate several functions, such as avoiding fusion with lysosome, acquiring nutrients, masking the inclusion and redirecting apoptosis signals (Moore and Ouellette 2014).

1.4.5 Differentiation of EBs into RBs

After EBs have been internalized and the inclusion has been established, EBs undergo a primary differentiation process into the metabolically active RBs (12 hpi in *C. pneumoniae* and 2-8 hpi in *C. trachomatis*) (Wolf, Fischer et al. 2000, Abdelrahman and Belland 2005). Even though the signals initiating the process are still unknown, two are the key events responsible for the differentiation of EBs into RBs. The first event is the release of the condensed chromatin of the EBs from the histone-like proteins Hc1 and Hc2, by an unknown trigger signal (Grieshaber, Fischer et al. 2004). Decondensed DNA can now be transcribed and early-genes are therefore expressed. The most relevant early-genes known are the conserved and *Chlamydia*-specific *euo* (*early upstream ORF*), *incs*, genes encoding proteins responsible for replication of the RBs (e.g. ribosomes) and genes encoding proteins relevant for metabolism (e.g. ATP) (Shaw, Dooley et al. 2000). The second event is the reduction of the disulfide bridges of the cOMC, resulting in a more permeable membrane, not resistant to environmental and osmotic stress, but able to guarantee passage of necessary substances (Abdelrahman and Belland 2005).

1.4.6 RBs replication

Metabolically active RBs within the inclusion are able to replicate by binary fission, accumulating up to 1000 new chlamydial particles (Hammerschlag 2002). The increase in RBs results in an enlargement of the inclusions, supported by modification of the inclusion membrane (as described in 1.4.4). This stage of infection (8-24 hpi in *C. trachomatis* and 12-48 hpi in *C. pneumoniae*) represents the most active transcription phase, expressing the so-called mid-cycle genes. Mid-cycle genes encode mainly outer membrane components, proteins involved in metabolism, T3SS effectors and Pmp proteins (Nicholson, Olinger et al. 2003).

As already mentioned, treatment with penicillin can inhibit chlamydial growth, even though *Chlamydia* species lack the classic layer of peptidoglycan (PG), phenomenon

known as the "*Chlamydia* anomaly" (see paragraph 1.4.1) (Moulder 1993, McCoy, Sandlin et al. 2003). Genome sequencing of *C. trachomatis* revealed that *Chlamydia* has indeed the necessary genes for its biosynthesis; in particular the protein MurA (responsible for the first step of PG synthesis) is expressed right before RB division. Furthermore, PG could be visualized as ring structures during the mid-late cycle, strongly suggesting an involvement of PG during the division of the RBs (Stephens, Kalman et al. 1998, McCoy, Sandlin et al. 2003, Henrichfreise, Schiefer et al. 2009, Liechti, Kuru et al. 2016).

1.4.7 Re-differentiation of RBs into EBs and EBs release

After RBs replication within the inclusion, signals, which are not yet understood, initiate the asynchronous re-differentiation of RBs into EBs. It is speculated that the key trigger event is the lack of sufficient T3SS structures, which leads to detachment of RBs from the inclusion membrane, but further investigations are required (Bavoil, Hsia et al. 2000, Wilson, Timms et al. 2006). This stage is characterized by the expression of so-called late-cycle genes, such as genes encoding for proteins involved in condensing chromatin, proteins of the cOMC (e.g. OmcB and OmcA), building the EB-characteristic structure, resistant to environmental and osmotic extracellular stress (Nicholson, Olinger et al. 2003, Abdelrahman and Belland 2005).

When RBs are completely re-differentiated, EBs are ready to leave the host cell and start a new round of infection. *C. pneumoniae* EBs are released between 72 and 96 hpi, while *C. trachomatis* EBs are released between 48 and 72 hpi. Chlamydial EBs can be released in two different processes. The first process is common among intracellular bacteria and involves lysis and death of the host cells. The second process is the extrusion of the intact inclusion. This process, uncommon among other bacteria, is slower than host cell lysis and involves the actin cytoskeleton (Hybiske and Stephens 2007).

1.4.8 Persistence

Chronic *Chlamydia* infections can lead to serious health problems, such as PID in *C. trachomatis* infected women and atherosclerosis and arthritis in *C. pneumoniae* infected patients (Beatty, Morrison et al. 1994, Hammerschlag 2002). Chronic infections can be due to repeated infections with the same or different *Chlamydia* serovars or even species, or can be a consequence of a persistent state of infection. Persistent forms of *Chlamydia* (aberrant bodies, ABs) were described for the first time in *C. psittaci* in 1980 (Moulder, Levy et al. 1980) and appear as aberrant, enlarged RBs, which are viable and can replicate

their DNA, but are not able to divide. Persistence can be induced *in vitro* by several factors, such as treatment with antibiotics like penicillin, absence of nutrients, iron and amino acids (Hogan, Mathews et al. 2004, Abdelrahman and Belland 2005). Interestingly, *C. trachomatis*, but not *C. pneumoniae* penicillin-induced persistence can be reversed when the treatment is withdrawn (Wolf, Fischer et al. 2000). IFN-γ, induced by the host immune response to the infection, can also induce a stage of persistence by blocking the production of tryptophan, essential for chlamydial development (Muramatsu, Brothwell et al. 2016). The characteristics of gene expression during a persistence stage is still not clear, as different models present different transcriptome profiles, possibly dependent on the triggering signal. In general, the persistence phase of the chlamydial cycle is dangerous for the host, because it allows survival of the bacteria during adverse conditions and, afterwards, reactivation of ABs in infectious EBs (Wyrick 2010).

1.5 The protein secretion systems in Gram-negative bacteria

Gram-negative bacteria are equipped with several systems in order to deliver virulence factors across the outer membrane (OM) and into the host cell: the six secretion systems (type 1-6), the mycobacterial type 7, the chaperone-usher and the Curli secretion systems. Type 2, type 4, type 5 and chaperone-usher secretion systems act in a two-step mechanism; unfolded or folded proteins are first inserted into the periplasm via a N-terminal Sec signal sequence or Tat-transport and, afterwards, the proteins are exported through the OM in a separate process. Type 5 secretion systems are also named autotransporters, because they can transport themselves through the OM. Type 1, type 3 and type 6 secretion systems are able to deliver effector proteins directly through the bacterial inner membrane (IM) and OM in one step (Costa, Felisberto-Rodrigues et al. 2015).

Type 3 and type 5 secretion systems play important roles in the different stages of the *Chlamydia* developmental cycle.

1.5.1 Type 3 secretion system

Type 3 secretion system (T3SS) is a complex structure, formed by more than 20 different subunits, which is able to transport effector proteins from the bacterial cytosol directly into the host cell cytoplasm, passing through bacterial inner and outer membrane and the host cell membrane and therefore it is also called "injectisome", formed by a basal structure and a needle (Gerlach and Hensel 2007). The basal structure resembles the flagellar basal body and supports the whole apparatus, anchoring it to the bacterial membrane through an IM

and an OM ring, connected by a neck region in the periplasm. The needle is anchored to the basal structure and is formed by several copies of the same protein (protomer), assembled in a symmetric spiral, forming a channel through which effector proteins can be transported. When the needle reaches the host cell membrane, a set of proteins, called needle tip complex, assemblies the support for the translocon complex, formed by integral membrane proteins, creating a pore in the host cell membrane (Chatterjee, Chaudhury et al. 2013). In order to achieve the right functioning of the system, T3SS chaperones within the bacterial cytosol are required to regulate and assist structural proteins and to establish a hierarchy for secretion of T3SS effectors (Cornelis 2006, Lara-Tejero, Kato et al. 2011). Chlamydial T3SS is still poorly understood, compared to the T3SS from other Gram-negative bacteria, but the system is highly conserved. Interestingly, chlamydial genes encoding T3SS structural proteins are located in three loci, while genes encoding effector proteins are not strictly present in the plasticity zone, but are also found along the chromosome (Mueller, Plano et al. 2014). T3SS structures have been observed on the surface of *C. trachomatis* EBs, where the type 3 apparatus is present in a density of around 20 structures per cell in a polarized manner and is activated upon contact with the host cell membrane (Fields, Mead et al. 2003, Nans, Saibil et al. 2014). In the early phases of the infectious cycle, EBs inject pre-loaded effector proteins in a hierarchal manner; *C. trachomatis* Tarp is the first secreted protein known, responsible for recruiting actin and remodeling the host cytoskeleton, facilitating internalization of the EBs (Clifton, Dooley et al. 2005). Chlamydial T3SS is active through the mid-cycle and its activity is registered till the mid-late phase, when T3SS apparatuses on RBs are predicted to detach from the inclusion membrane and trigger the re-differentiation of RBs to EBs (Bavoil, Hsia et al. 2000).

Not all structural proteins of chlamydial T3SS are known so far; CopB and CopD have been identified as two membrane proteins of the translocon complex, with a high similarity to *Yersinia* translocon complex YopB/YopD. The protein forming the needle (CdsF) has been identified, together with its chaperones (CdsE and CdsG) via bioinformatic approaches. The needle in anchored to the bacterial surface by the basal structure via the OM ring protein CdsC, predicted as a hexamer, according to OM rings from other bacteria. The periplasmic protein CdsJ in bound to the IM ring, probably through direct interaction with the IM ring component CdsD. The structure of the IM ring components is very complex; the putative C-ring of chlamydial T3SS is formed by CdsQ, on the inner side of the IM, which is able to interact with CdsD and several other cytosolic proteins, such as

CdsV, CdsL, CdsS and CdsT. The IM ring creates the platform to support the substrate-chaperone complexes (Peters, Wilson et al. 2007, Betts, Twiggs et al. 2008, Spaeth, Chen et al. 2009, Betts-Hampikian and Fields 2010). At least 7 chlamydial T3SS chaperones have been identified (Slc1, Scc1, Scc2, Scc3, Scc4, Ct274 and Mcsc) and are responsible for regulating effector secretion by keeping effectors in an unfolded status, likely required for transport through the needle and avoiding effectors degradation and unspecific interactions with other proteins. Unfortunately, the molecular mechanisms of secretion are still not understood (Chen, Bastidas et al. 2014, Mueller, Plano et al. 2014).

T3SS effector proteins are characterized by a non-predictable N-terminal secretion sequence, which allows heterologous T3 secretion in other Gram-negative bacteria, like *Yersinia* (da Cunha, Milho et al. 2014). Beyond the aforementioned Tarp and Incs (see paragraphs 1.4.3 and 1.4.4), effector proteins secreted by chlamydial T3SS are responsible for cytoskeleton modifications, for remodeling inclusion membrane identity, interfering in the host cell signaling pathways, immune response and apoptosis (Beeckman and Vanrompay 2010).

1.5.2 Type 5 secretion system

The type 5 secretion system (T5SS) is a two-step mechanism through which bacteria can secrete virulence factors in the extracellular space. Members of this family are characterized by the presence of a N-terminal Sec sequence, which allows Sec-dependent protein transportation through the IM and a central functional passenger domain (PD), secreted in the extracellular space through a C-terminal β-barrel, responsible for creating a pore in the OM (Gawarzewski, Smits et al. 2013). Five types of T5SS are known so far and comprehend one, or more subunits. Type Vb is characterized by two subunits, expressed simultaneously, but not covalently linked. The functional passenger domain (first subunit) is transported through the OM by the second subunit, the 16-stranded β-barrel, linked to a periplasmic sequence, responsible for protein-protein interaction (POTRA). Type Vc (trimeric autotransporter) is formed by three identical subunits, which form the passenger domain, connected via three α-helices to the 12-stranded β-barrel OM pore. Type Vd is the latest discovered T5SS and is characterized by a passenger domain, connected covalently to a C-terminal β-barrel, with similar characteristics to the type Vb. Type Ve is an autotransporter with the opposite order of the subunits. In this subgroup, the β-barrel is located at the N-terminus site of the functional PD (Bernstein 2015). Finally, type Va or autotransporter (AT), the simplest secretion system known so far, is classically described

as a single polypeptide with a N-terminal Sec signal sequence, a central PD and a C-terminal β-barrel. Sec sequence leads the protein in the periplasm and then is cleaved off. Findings for *E. coli* EspP AT suggest that in the periplasm specific chaperones might bind to the PD, preventing its misfolding (Ruiz-Perez, Henderson et al. 2010). The β-barrel is inserted then in the OM and exposes the PD in the extracellular space (Leo, Grin et al. 2012) (Fig. 4). Up to date, the exact mechanism of export of PD through the OM is not clear; however, different models have been proposed. According to the "Hairpin model", the linker sequence, which connects the PD to the β-barrel, forms a hairpin-like structure inside the β-barrel, pushing the unfolded PD outside the cell, through the pore. Another model was proposed, the "Omp85 model", in which the AT folds partially in the periplasm with the help of chaperones such as BAM, responsible for transporting the AT to the OM. Once BAM dissociates, the AT can complete its folding (Dautin and Bernstein 2007, Gawarzewski, Smits et al. 2013).
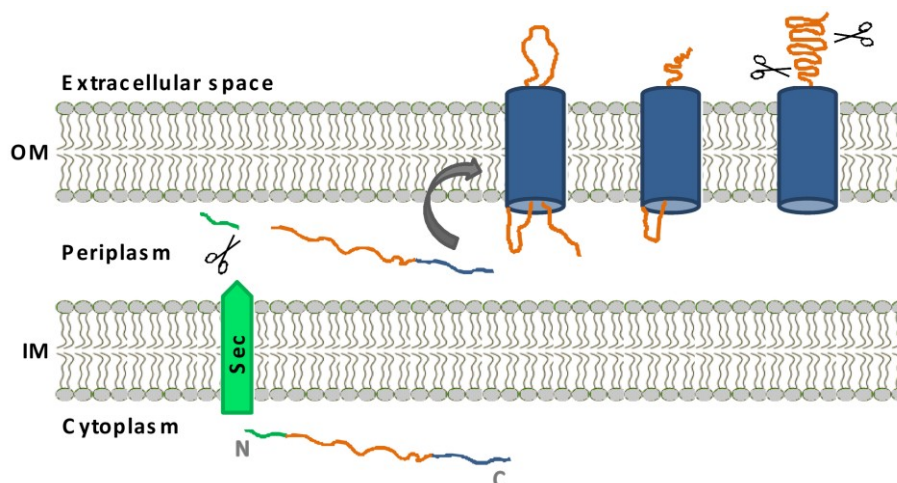
Figure 4. Schematic representation of secretion of a T5SS autotransporter (Va). N-terminal Sec sequence (green) leads the protein in the periplasm, through the inner membrane (IM), where it is cleaved off. Once in the periplasm, the C-terminal β-barrel (blue) forms a pore in the outer membrane (OM), through which the presumably unfolded passenger domain (PD) (orange) is translocated into the extracellular space. In the extracellular space, the PD folds in its final functional conformation and can be cleaved in functional fragments (Henderson, Navarro-Garcia et al. 2004).

Crystal structure of members of AT family revealed their structural characteristics. The structure of the C-terminal domain is formed by multiple antiparallel strands, forming the β-barrel, which creates a hydrophilic pore. Furthermore, one or more α-helical sequences at the C-terminus of the PD can insert themselves in the β-barrel and help maintaining the pore architecture. This structure is highly conserved among AT members; for example, structural studies revealed that *Neisseria meningitis* NalP and *E. coli* EspP share only 15 %

sequence similarity, but both are characterized by a 12-stranded β-barrel, with a similar pore diameter (Barnard, Dautin et al. 2007, Dautin and Bernstein 2007). On the other hand, structures of AT passenger domains revealed a β-helix structure, formed by several β-strands, separated by turns or loops. Different ATs differ from each other in specific characteristics, such as length, number of loops and β-strands, but they share the typical β-helix structure. For example, *Bordetella pertussis* Pertactin and *E. coli* Hbp PDs, which do not share high sequence identity, are folded in 16 β-strands helix and 24 β-strands helix respectively (Emsley, Charles et al. 1996, Otto, Sijbrandi et al. 2005). Interestingly, the passenger domain exposed on the extracellular space can be cleaved in functional fragments by autocatalytic processes or by specific proteases. In particular cases, such as *E. coli* AIDA, cleaved PD fragments can be found associated with the OM (Charbonneau, Berthiaume et al. 2006, Dautin and Bernstein 2007).

Genome sequencing and bioinformatic analysis suggested that all members of chlamydial Pmp family share a predicted type Va autotransporter structure, with a N-terminal Sec sequence, a C-terminal β-barrel and a central functional passenger domain, containing multiple repeats of motifs GGA(I, L,V) and FxxN (explained more in detail in paragraph 1.6.1) (Henderson and Lam 2001).

1.6 Polymorphic membrane proteins (Pmps)

1.6.1 Pmp characteristics

The first Pmp was identified in 1996 as a 90 kDa major immunogenic protein in *C. abortus* (Longbottom, Russell et al. 1996). In the following years, comparative analysis of *C. trachomatis* and *C. pneumoniae* genomes confirmed the presence of *Chlamydia*-specific genes, homologous to the one identified in *C. abortus* (Kalman, Mitchell et al. 1999). Afterwards, genome sequencing revealed that all *Chlamydia* species harbor members of the Pmp family. Interestingly, members of the Pmp family are very heterogeneous; 9 members have been identified in *C. trachomatis* (PmpA-I) and 21 in *C. pneumoniae* (Pmp1-21) and they represent approximately 5 % of the whole chlamydial coding capacity, suggesting a crucial role during infection (Rockey, Lenart et al. 2000, Molleken, Schmidt et al. 2010). According to genomic comparisons, Pmps have been divided in six phylogenetic subgroups: subgroup A (PmpA and Pmp19), B (PmpB/C and Pmp20), D (PmpD and Pmp21), E (PmpE/F and Pmp15-18), G (PmpG/I and Pmp1-13) and H (PmpH and Pmp14). In particular, subgroup G, which contains two Pmps in *C. trachomatis* (G and

I), is extensively expanded in *C. pneumoniae* with 13 members, highlighting a consistent degree of heterogeneity (Grimwood and Stephens 1999, Rockey, Lenart et al. 2000).

Gene arrangement shows that *pmps* are located in different chromosome areas. *C. trachomatis pmps* are present in two clusters (*pmpA-B-C* and *pmpE-F-G-H-I*), while *C. pneumoniae pmps* are arranged in three clusters. Interestingly, in all genomic arrangements, *pmpD* (*pmp21* in *C. pneumoniae*) is found as a stand-alone gene. Moreover, *pmps* present a very high mutation rate, suggesting that these genes are under evolutionary pressure (Grimwood and Stephens 1999, Crane, Carlson et al. 2006).

All *pmps* from *C. trachomatis* and *C. pneumoniae* are transcribed, but, while all *C. trachomatis pmps* are translated, *C. pneumoniae pmp3/4/5/12/17* harbor a frameshift mutation or an early stop codon, which prevents their translation (Grimwood, Olinger et al. 2001, Tan, Hsia et al. 2010).

High level of heterogeneity is also indicated by Pmps amino acids identities. Pmps within the same subgroup among the same species or between different species share significant sequence identity (e.g. PmpC-PmpB: 43 % and Pmp21-PmpD: 33 %), suggesting similar functions. In contrast, Pmps from different subtypes share lower sequence identities (e.g. PmpE-PmpD: 18 %) (Becker 2013, Vasilevsky, Stojanov et al. 2016). When Pmps from four *Chlamydia* species (*C. pneumoniae*, *C. trachomatis*, *C. psittaci* and *C. abortus*) were investigated by bioinformatics, it was shown that PmpA, PmpB, PmpD and PmpH were the most conserved Pmps among the four species (Van Lent, Creasy et al. 2016).

The high level of heterogeneity among *pmps* genes and the corresponding proteins suggests a correlation of the different *Chlamydia* species and serovars with different tissue tropism, niche adaptation and different diseases (Gomes, Nunes et al. 2006, Vasilevsky, Stojanov et al. 2016). These data together suggest a crucial role of Pmp proteins in *Chlamydia* infection and biology.

All members of the Pmp family are predicted to be T5SS autotransporters (explained in more detail in paragraph 1.5.2). Pmps are indeed characterized by the presence of a N-terminal Sec secretion sequence, a C-terminal domain, rich in tryptophan, which presents β-barrel characteristics, and a central functional passenger domain (PD), which is EB-cell surface exposed and can be cleaved into processed forms (Grimwood and Stephens 1999, Henderson and Lam 2001, Pedersen, Christiansen et al. 2001, Vandahl, Pedersen et al. 2002, Wehrl, Brinkmann et al. 2004, Kiselev, Skinner et al. 2009, Molleken, Schmidt et al. 2010, Tan, Hsia et al. 2010, Saka, Thompson et al. 2011) (Fig. 5). All Pmps are rich in cysteines, mostly located in the PD. In some cases, such as Pmp21, cysteines are found

also in the β-barrel, possibly used to create disulfide bridges in the cOMC (Grimwood and Stephens 1999, Molleken, Schmidt et al. 2010).

A specific characteristic among all Pmps is the presence of two repeated tetrapeptide motifs GGA(I, L, V) and FxxN in the PD (Fig. 5). Regarding the FxxN motif, the first "x" can be any amino acid, except proline; while the second "x" can be any amino acid, except methionine, tryptophan and cysteine (Grimwood and Stephens 1999). The high density of the two motifs is a striking feature of this family; for example, the motif GGA(I) is found only once and only in ten other chlamydial proteins. In general, FxxN and GGA(I, L, V) motifs are found an average of 13,6 and 6,5 times in *C. trachomatis* Pmps and 11,3 and 5 times in *C. pneumoniae* Pmps, respectively; while FxxN and GGA(I, L, V) motifs are found an average of 0,73 and 0,06 times in the whole *C. trachomatis* proteome and 0,84 and 0,01 in the whole *C. pneumoniae* proteome, respectively (Grimwood and Stephens 1999, Rockey, Lenart et al. 2000, Molleken, Schmidt et al. 2010).

Several copies of the FxxN and GGA(I, L, V) motifs are found only in few non-Chlamydia proteins, such as the surface OmpA protein from *Rickettia* (7 FxxN and 7 GGA in *R. conorii*), the virulence factor FHA from *Bordetella pertussis* (1 FxxN and 9 GGA), YfaL from *E. coli* (13 FxxN and 6 GGA), Zonadhesin from *mus musculus* (5 FxxN and 1 GGA) and Mucin 5B from *Homo sapiens* (12 FxxN and 4 GGA). OmpA from *Rickettia* is characterized as an adhesin and invasin, interacting with the α2β1 integrin receptor (Hillman, Baktash et al. 2013). FHA or filamentous hemagglutinin of *Bordetella pertussis* is a virulence factor involved in adherence to the respiratory epithelium and is a candidate for the development of a vaccine (Scheller and Cotter 2015). *E. coli* YfaL is an autotransporter which can mediate cell-cell aggregation and biofilm formation (Wells, Totsika et al. 2010). Murine Zonadhesin is responsible for specific adhesion of sperm cells to the egg cell and its folding is conserved in pigs and primates (Herlyn and Zischler 2008). Finally, human Mucin 5B, like all mucins, is rich in serine and threonine residues and its structure is stabilized by disulfide bridges. Mucins play the important role of clearing the respiratory tract from external particles and pathogens (Thornton, Rousseau et al. 2008). In general, non-chlamydial proteins containing FxxN and GGA(I, L, V) motifs are involved in cell-cell adhesion, but the correlation of this function with the presence of the motifs is not proven.

On the other hand, the presence of the motifs in chlamydial Pmps has been shown to play an important role during adhesion. Naturally cleaved forms of *C. pneumoniae* Pmp21 (N-Pmp21 and M-Pmp21), harboring a high density of motifs, 7 FxxN and 8 GGA(I, L, V)

and 9 FxxN and 7 GGA(I, L, V), respectively (Fig. 5), could bind to human cells in yeast display and in protein-coated beads adhesion assays (Molleken, Schmidt et al. 2010). In order to investigate the role of the motifs, different recombinant fragments of Pmp21 PD were produced, two fragments with a high density of motifs: B-Pmp21, harboring 6 FxxN and 7 GGA(I, L, V) and C-Pmp21, harboring 7 FxxN and 7 GGA(I, L, V) and two recombinant fragments with only two motifs: A-Pmp21, harboring 1 FxxN and 1 GGA(V) and D-Pmp21, harboring 2 FxxN motifs (Molleken, Schmidt et al. 2010). When these fragments were tested for adhesion, all of them could bind human cells in a similar manner in yeast display and in protein-coated beads adhesion assays; only the full-length Pmp21 PD showed a significantly higher adhesion degree in yeast display adhesion assay (Molleken, Schmidt et al. 2010). Interestingly, when one or both motifs were deleted or mutated in A-Pmp21 and in D-Pmp21, these fragments could no longer adhere to human cells; furthermore, a recombinant Pmp21 fragment, harboring 0 motifs, was also not able to bind human cells. These data together show that a minimum of 2 FxxN or 1 FxxN and 1 GGA(I, L, V) motifs are required for adhesion of Pmp21 to human cells (Molleken, Schmidt et al. 2010). Interestingly, despite a similar adhesion capacity, all Pmp21 fragments showed a variable ability to block a *C. pneumoniae* infection, independently from the number of motifs. Only the full-length PD could inhibit the infection of almost 90 % (Molleken, Schmidt et al. 2010). Furthermore, a recent work demonstrated that a minimum of 2 motifs is required for D-Pmp21 oligomerization. Only the wild type D-Pmp21 could generate fibril-like adhesive-competent structures, while the oligomerization rate was significantly lower in D-Pmp21 mutated in its motifs (Luczak, Smits et al. 2016). Moreover, the central PD part of *C. pneumoniae* Pmp2, Pmp6 and Pmp20, with a high density of motifs (7, 24 and 21, respectively) could adhere to human cells (Molleken, Schmidt et al. 2010, Becker and Hegemann 2014).

The central part of the PD of all 9 *C. trachomatis* serovar E Pmps, harboring a high density of motifs, in a range between 10 motifs (PmpC) and 34 motifs (PmpD), showed adhesion to human cells in a similar degree in yeast display adhesion assay, but a variable adhesion capacity in protein-coated beads adhesion assay, where PmpD had the strongest binding, comparable to its *C. pneumoniae* homologue Pmp21, and PmpH (14 motifs) had the lowest adhesion degree (Becker and Hegemann 2014). Moreover, all analyzed Pmps could block a *C. trachomatis* infection in a comparable degree (Becker and Hegemann 2014). Proteasome analysis of *C. trachomatis* L2 identified *in vivo* cleavage sites for 7 of the 9 Pmps (Saka, Thompson et al. 2011). *C. trachomatis* serovar E and L2 Pmps share a very

high sequence identity (between 94 % and 100 %), therefore it can be speculated that also the cleavage sites might be conserved, even though this has not been proven yet. All *C. trachomatis* E adhesive-competent Pmps tested in 2014, rich in the number of motifs, are comparable to the central PD processed forms identified by Mass-spectrometry analysis for *C. trachomatis* L2 Pmps in 2011 (except for PmpA and PmpC, whose cleavage sites were not identified) (Saka, Thompson et al. 2011, Becker and Hegemann 2014). Furthermore, cleavage of *C. trachomatis* L2 PmpB, PmpD, PmpF and PmpG could also produce smaller fragments at the C-terminal of the PD, with a low amount of motifs. Their function has not been identified yet (Saka, Thompson et al. 2011).

Pmp 3D models, generated by Phyre2 (**P**rotein **H**omology/Analog**Y** **R**ecognition **E**ngine V **2**.0) server, predicted a triangular β-helical structure of the core region of the PD rich in the repeated motifs, and the motifs were predicted to be localized at its corners, speculated as platform for interactions (Becker 2013).
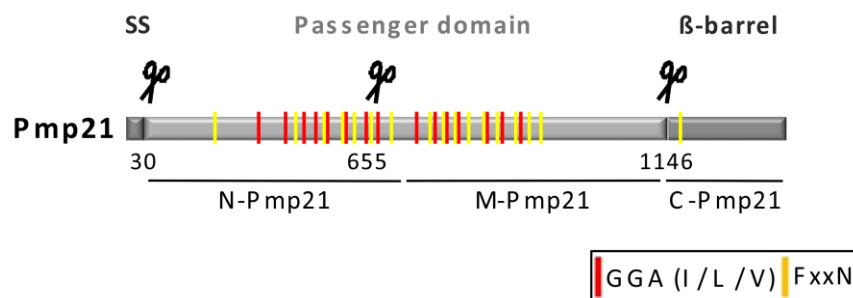
Figure 5. Schematic illustration of a representative Pmp. *C. pneumoniae* Pmp21 autotransporter predicted structure formed by a N-terminal signal sequence (SS), a central passenger domain and a C-terminal β-barrel. Multiple repeats of motifs GGA(I, L, V) and FxxN are shown with red and yellow lines respectively. Scissors represent cleavage sites and the processed fragments formed during infection are indicated with black lines (Wehrl, Brinkmann et al. 2004, Molleken, Schmidt et al. 2010).

1.6.2 Pmp expression during the infection cycle

Only 15 of the 21 transcribed *C. pneumoniae* Pmps are actually expressed in the EBs. On the other hand, all 9 *C. trachomatis* Pmps are transcribed and expressed (Grimwood, Olinger et al. 2001, Montigiani, Falugi et al. 2002, Tan, Hsia et al. 2010).

Different *C. trachomatis* Pmps exhibit heterogeneous expression levels between each other and among different strains; PmpA, for example, shows the least expression level, compared to the other Pmps, but it peaks at 12 hpi and proteomics analysis performed at 18 hpi, showed that PmpA is detected only in RBs (Nunes, Gomes et al. 2007, Saka, Thompson et al. 2011). *PmpD* transcription was upregulated between 12 and 24 hpi, in the stage of differentiation from RBs into EBs and during RB cell division (Kiselev, Stamm et

al. 2007, Saka, Thompson et al. 2011). In general, most of the *C. trachomatis pmps* are transcribed during the mid-cycle, after 24 hpi (PmpB, D, E, G, H), while PmpA and PmpH transcripts were detected also at the early stage of the infection (2 hpi) (Van Lent, Creasy et al. 2016). Interestingly, stress induced by penicillin treatment can influence *pmp* transcription to different degrees (Carrasco, Tan et al. 2011). One example is PmpB, whose transcript is no longer detected at 18 hpi in penicillin-treated samples, while PmpA and PmpD transcription is not affected in comparison to the non-treated cultures, indicating their critical role during chlamydial infection (Van Lent, Creasy et al. 2016, Vasilevsky, Stojanov et al. 2016).

Using a biochemical approach, Saka and co-workers showed that PmpG, E, B, H, C and F proteins are the most abundant Pmps present in EBs at 18 hpi; while PmpI and PmpD are mostly expressed in RBs at the same time point (Saka, Thompson et al. 2011). These data confirmed what Nunes and co-workers observed; *pmpA* and *pmpI* were the least transcribed *pmp* genes, while *pmpF*, *G* and *E* were the most transcribed in three *C. trachomatis* strains (E, D and L2) (Nunes, Gomes et al. 2007). Interestingly, PmpE and PmpF, whose genes are part of the same genomic cluster, show a different level of expression, the more polymorphic PmpF is indeed more expressed. This is possibly due to a premature termination of the *pmpEF* mRNA transcription and suggesting a key role for PmpF in evading the immune response (Nunes, Gomes et al. 2007).

The differential expression of *C. trachomatis* Pmps was further analyzed and it was shown that in the same *in vitro* infection, the same inclusions could express some, but not other Pmps at the same time (Tan, Hsia et al. 2010). In this experimental set-up, 99 % of the inclusions expressed PmpA, D and I and only 1 % of the inclusions were negative for these Pmps, even though they were the least transcribed, as described by Nunes and co-workers. 98-99 % of the inclusions expressed also PmpF and PmpH; while PmpG had the most variable expression frequency (1-10 % of the inclusions were completely negative), in agreement with Nunes data (Nunes, Gomes et al. 2007, Tan, Hsia et al. 2010). Differential expression was also observed *in vitro* for *C. pneumoniae* Pmp10, Pmp20 and Pmp6; while Pmp21 was expressed in all *C. pneumoniae* inclusions (Pedersen, Christiansen et al. 2001, Becker 2013).

Furthermore, all nine *C. trachomatis* Pmps and *C. pneumoniae* Pmp6, 8, 10, 11, 20 and 21 are not only expressed, but they are exposed on the *Chlamydia* surface, detected with specific antibodies in non-permeabilized fixed cells (Vandahl, Pedersen et al. 2002, Molleken, Schmidt et al. 2010, Tan, Hsia et al. 2010, Becker 2013). Interestingly,

processed PD fragments of *C. trachomatis* PmpD and Pmp21 (PmpD homologous in *C. pneumoniae*) could be detected also on the *Chlamydia* surface, even without the membrane-anchoring β-barrel, possibly associated to the full length Pmp PD (Wehrl, Brinkmann et al. 2004, Swanson, Taylor et al. 2009, Molleken, Schmidt et al. 2010) (further explained in paragraph 1.6.4). Specific antibodies produced against *C. trachomatis* PmpD and *C. pneumoniae* Pmp21, Pmp2 and Pmp10 could neutralize a subsequent infection in a species-specific manner, confirming that Pmps are important for the infection (Wehrl, Brinkmann et al. 2004, Finco, Bonci et al. 2005, Crane, Carlson et al. 2006, Molleken, Schmidt et al. 2010). In addition, the anti-PmpD antibody could neutralize infection of 15 different *C. trachomatis* serovars, showing that PmpD is a pan-neutralizing antigen. Interestingly, the presence of antibodies against MOMP and LPS, abundant on the EBs surface, block the binding of pan-neutralizing antibodies against PmpD, possibly acting as a decoy mechanism (Crane, Carlson et al. 2006).

The Pmps surface expression and their ability to generate neutralizing antibodies suggest an important role in adhesion and a role as humoral response targets. Sera from *C. trachomatis*-infected patients were tested for their specific humoral reactivity against all recombinant *C. trachomatis* Pmps. All Pmps were indeed recognized, but in a variable way. PmpD was recognized by most sera, followed by PmpB, C and I; while PmpA was the least recognized Pmp, even though is the most expressed in inclusions *in vitro* (Tan, Hsia et al. 2009, Tan, Hsia et al. 2010). The immunoreactivity of sera seems to depend on many factors; PmpA was mostly recognized by sera of women presenting PID and with no pregnancy success (Taylor, Darville et al. 2011). Sera from women with PID recognized most frequently PmpB and PmpI (Tan, Hsia et al. 2009, Taylor, Darville et al. 2011). A gender bias was also detected, sera from female patients reacted mostly with PmpB, while sera from male patients reacted primarily with PmpD (Tan, Hsia et al. 2009). Furthermore, serological studies showed that some *C. trachomatis* Pmps are recognized only by sera from patients infected with specific *C. trachomatis* serovars (Gomes, Nunes et al. 2006, Nunes, Gomes et al. 2007); for example, PmpD was recognized by sera of serovar E-infected patients, but not by sera of serovar G-infected patients (Nunes, Gomes et al. 2007). Difference in Pmps recognition was also observed in sera from *C. pneumoniae* infected patients (Becker 2013).

These data together suggest that Pmps transcription and expression on the *Chlamydia* surface are highly variable, eliciting a variable humoral immune response, possibly following an antigenic variation mechanism, preventing the immune system from

recognition of the infection (Vasilevsky, Stojanov et al. 2016).

1.6.3 Pmps functions

Passenger domains (PDs) of *C. pneumoniae* Pmp21 and *C. trachomatis* PmpD are naturally processed during the infection and the obtained fragments stay associated with the infectious EBs, where they can be target of neutralizing antibodies, suggesting that Pmp proteins might play a role in the first step of *Chlamydia* infection (Wehrl, Brinkmann et al. 2004, Crane, Carlson et al. 2006, Swanson, Taylor et al. 2009, Molleken, Schmidt et al. 2010).

C. trachomatis L2 PmpD could be detected in Blue Native-PAGE and second dimension analysis as full length PD (p155) and as two cleaved fragments (p73 and p82) from the *Chlamydia* surface. In addition, two other PmpD processed forms were identified at later time points, not associated with the outer membrane, hypothesized as players in interfering with inflammation cascades (Swanson, Taylor et al. 2009).

The role of PmpD in chlamydial adhesion was further analyzed by Kari and co-workers with a *C. trachomatis pmpD* null mutant, created with targeted reverse genetic techniques (Kari, Southern et al. 2014). This study showed that PmpD is actually not essential for chlamydial growth, but might play a role in the RB contact with the inclusion membrane (see paragraph 1.4.7). The absence of PmpD did not impair *C. trachomatis* adhesion to murine cells *in vitro* or in murine infection *in vivo*, but PmpD deficient *C. trachomatis* EBs showed reduced adhesion to human cells *in vitro* and a reduced ocular infection in a non-primate model *in vivo*, suggesting species-specificity. Interestingly, the ocular *in vivo* infection was reduced only in the initial phase of the infection, but did not show differences with WT after 2 weeks. It was concluded that PmpD plays an important role in adhesion and in the early phase of the infection (Kari, Southern et al. 2014).

In 2014, the function of the PD fragments of all 9 *C. trachomatis* Pmps with a high density of motifs were analyzed (see paragraph 1.6.1) (Becker 2013, Becker and Hegemann 2014). All *C. trachomatis* Pmp fragments presented on the yeast cell surface or as recombinant proteins coated on fluorescence beads exhibit adhesion to human epithelial and endothelial cells, but with different adhesion profiles. Furthermore, all Pmps could inhibit a subsequent infection in a species-specific manner (see paragraph 1.6.1) (Becker and Hegemann 2014). Similar experiments were performed with recombinant Pmp21 fragments, all of which showed adhesion to human epithelial cells. Furthermore, pre-incubation of the naturally cleaved Pmp21 fragments with human cells and pre-incubation

of EBs with specific anti-Pmp21 antibodies blocked and neutralized the infection in a species-specific manner (described in more detail in paragraph 1.6.1) (Molleken, Schmidt et al. 2010, Becker and Hegemann 2014). Recombinant PD fragments of *C. pneumoniae* Pmp6 and Pmp20 (serotypes G and B, respectively) with a high density of motifs could also mediate adhesion to human cells and block a subsequent infection (Molleken, Schmidt et al. 2010). Interestingly, pre-incubation of human cells with a mixture of two *C. pneumoniae* or two *C. trachomatis* Pmps from different serotypes (Pmp21-6 and PmpD-G) showed no significant difference than pre-incubation with the two Pmps alone, suggesting overlapping functions of different Pmps, possibly by acting on the same receptor pathway (Becker and Hegemann 2014).

Recombinant Pmp21 fragments lacking the motifs FxxN and GGA(I, L, V) showed significantly reduced adhesion to human cells, compared to recombinant and natural fragments with copies of the motifs. In addition, mutation of the motifs in adhesive-competent fragments resulted in loss of adhesiveness (described in more detail in paragraph 1.6.1) (Molleken, Schmidt et al. 2010). Moreover, the presence of repeated motifs in a recombinant Pmp21 fragment increased its oligomerization phenotype and its adhesive functions (Luczak, Smits et al. 2016). Thus, the presence of at least 2 FxxN or 1 FxxN and 1 GGA(I, L, V) motifs is required for *C. pneumoniae* Pmp21 adhesion to human cells (see paragraph 1.6.1) (Molleken, Schmidt et al. 2010).

EGFR (Epidermal Growth Factor Receptor) was identified as the host receptor responsible for interaction with *C. pneumoniae* Pmp21. Fluorescent beads coated with recombinant Pmp21 could be internalized within the human cells; the Pmp21-EGFR interaction activates the receptor, leading to internalization of *Chlamydia* particles. Since Pmp21 and Pmp6 show overlapping functions, it is hypothesized that also other *C. pneumoniae* Pmps might use the same entry route (Molleken, Becker et al. 2013). Interestingly, *C. trachomatis* PmpD is not able to bind EGFR, even though it shares 33 % sequence identity with Pmp21, possibly indicating tropism-specificity (Becker 2013). Up to date, a host receptor for *C. trachomatis* Pmps has not been identified.

1.6.4 Pmps processing and oligomerization

Specific antibodies directed against *C. trachomatis* L2 PmpD could recognize not only the full length PD (155 kDa), but also two additional bands in EB lysates, suggesting the presence of naturally processed forms of PmpD on the EBs (Crane, Carlson et al. 2006). Further analysis with specific anti-peptide antibodies directed against different domains of

C. trachomatis L2 PmpD revealed that, besides the full length (p155), a N-terminal and a C-terminal PD fragment (p73 and p82 respectively) were present in EB fractions and in infected cells after 24 hpi, time at which *pmpD* is upregulated (Kiselev, Stamm et al. 2007, Swanson, Taylor et al. 2009). Cleavage sites were identified right after the signal sequence (amino acid 53), for p73, and at amino acid 762, between p73 and p82 (Fig. 6A) (Swanson, Taylor et al. 2009). Immunofluorescence analysis revealed that both N- and C-terminal parts of PmpD are localized on the EB surface at 28 hpi with the classical ring-like structure. Interestingly, Blue Native-PAGE analysis of immunoprecipitated samples from the surface of purified *C. trachomatis* L2 EBs using anti-PmpD antibodies revealed the presence of three complexes (~850, ~530 and ~100 kDa). Using PmpD antibodies in second dimension analysis, PmpD full length PD (p155) and the two cleaved PmpD fragments p73 and p82 could be detected as part of the high molecular weight complexes of ~850 and ~530 kDa, even though p73 does not harbor the membrane bound β-barrel (Swanson, Taylor et al. 2009). Later in the cycle (30-36 hpi), analysis of infected cells showed the presence of another PmpD fragment, non-associated with the bacteria cell envelope (p111), which can be cleaved in two additional fragments (p73 and p30) (Fig. 6A). Since the p30 fragment contains a NLS sequence, it is speculated that the late processed PmpD fragments might play a different role during the infection, such as interfering with the inflammatory processes (Swanson, Taylor et al. 2009).

In the same year, PmpD cleavage was also shown not only for *C. trachomatis* L2, but also for other two serovars (A and D) (Kiselev, Skinner et al. 2009).

Proteomic analysis of *C. trachomatis* L2 infected cells revealed that the majority of PmpD (40 %) was present in RBs at 18 hpi, while only 1 % of total PmpD was found in the EBs (Saka, Thompson et al. 2011). Taken together, these data suggest that PmpD might have multiple functions during the infection, other than the ability to mediate adhesion of the EBs to human cells (Becker and Hegemann 2014).

In the aforementioned proteomic analysis, several semitryptic peptides were identified by mass spectrometry analysis for 7 *C. trachomatis* L2 Pmps (except PmpA and PmpC), indicating an extensive proteolytic cleavage activity and generation of numerous Pmp processed forms (see paragraph 1.6.1), whose functions are still unclear (Saka, Thompson et al. 2011).

Cleaved forms of *C. pneumoniae* Pmp6, 20 and 21 have also been identified (Vandahl, Pedersen et al. 2002). Similarly to PmpD, Pmp21 is processed at two sites, right after the signal sequence and right before the C-terminal domain, generating three fragments (N-,

M- and C-Pmp21) (Fig 5-6B). Interestingly, N-Pmp21 and M-Pmp21, not containing the membrane translocator domain, could be detected associated to the OM and are accessible to antibodies (Wehrl, Brinkmann et al. 2004, Molleken, Schmidt et al. 2010). Recombinant N-Pmp21 not only mediates adhesion, like M-Pmp21, but plays a role in activation of monocytes and mediates cytokines production (Wehrl, Brinkmann et al. 2004, Molleken, Schmidt et al. 2010).

PmpD is cleaved not only in *C. trachomatis* and *C. pneumoniae*, but also its homologue is cleaved in *C. abortus* (Pmp18D). Pmp18D processed forms were also detected associated with the *Chlamydia* OM after 24 hpi (Wheelhouse, Sait et al. 2012).

It is still not known whether Pmps harbor an autoproteolytic activity or if the cleavage is due to chlamydial or human proteases.
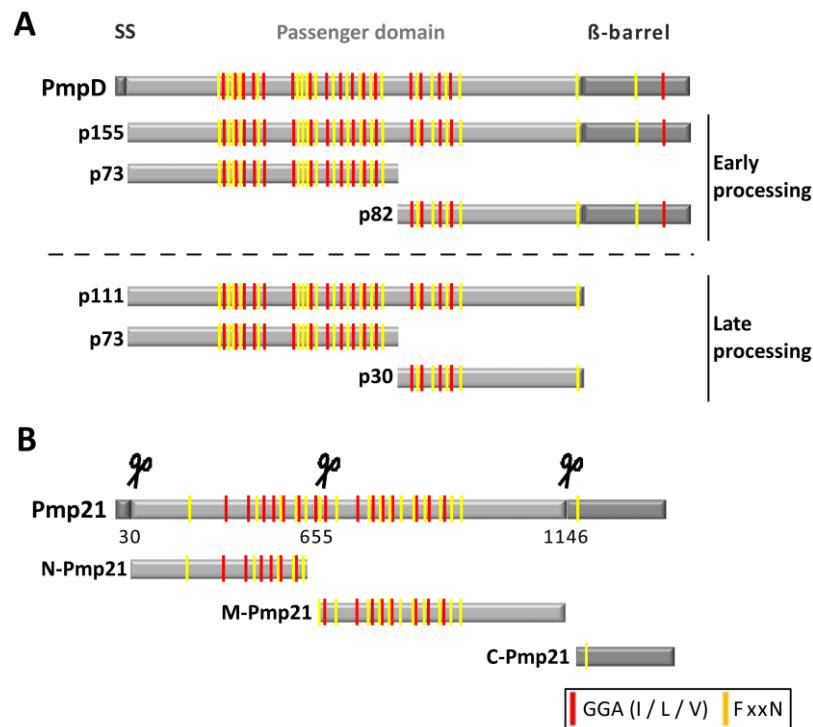
Figure 6. Schematic illustration of Pmp processing. A. *C. trachomatis* PmpD is cleaved in the early stage of the infection and the full length (p155) and two generated processed fragments (p73 and p82) are found associated to the EB-cell surface. A second cleavage is detected later in the infection (30-36 hpi), generating three soluble fragments (p111, p73 and p30) (according to Swanson, Taylor et al. 2009). **B.** *C. pneumoniae* Pmp21 is cleaved at three sites, generating N-, M- and C-Pmp21 processed forms. Soluble N- and M-Pmp21 fragments, found in the OM, are target for antibodies, and might act as adhesins (according to Wehrl, Brinkmann et al. 2004 and Molleken, Schmidt et al. 2010). SS: signal sequence. FxxN and GGA(I, L, V) are shown in yellow and red, respectively.

The fact that processed PD fragments of Pmp21 and PmpD could be detected being associated with the chlamydial OM raised the hypothesis that Pmps could form oligomeric structures on the chlamydial surface (Wehrl, Brinkmann et al. 2004, Swanson, Taylor et al.

2009, Molleken, Schmidt et al. 2010).

Phyre2 3D models of Pmps predicted a triangular β-helical structure of the PD core region, with the motifs localized at its corners. These structures were speculated to be responsible for interactions (Hegemann and Moelleken 2012) (see paragraph 1.6.1).

The first data concerning Pmp oligomerization came from *C. pneumoniae* Pmp21. Naturally processed M-Pmp21 has the ability to interact with itself and with other representative *C. pneumoniae* Pmps *in vitro* (Becker 2013). Recently, a recombinant C-terminal fragment of Pmp21, containing only two motifs, was investigated for functional oligomerization and it showed the ability to form homomeric oligomers, which in electron microscopy pictures exhibits rod-shape protofibrils structures. Interestingly, the homomeric oligomers had an increased ability to adhere to human cells and to block a subsequent infection, when compared with the monomeric form. Furthermore, the presence of the motifs is essential for oligomerization (Luczak, Smits et al. 2016).

1.6.5 Pmps as vaccine candidates

Protective host response against *Chlamydia* is a controversial topic, for long investigated. Immune response to a *Chlamydia* infection is polarized in the direction of Th1 cell activation, recruiting CD4$^+$ and CD8$^+$ T cells at the site of infection (Schautteet, De Clercq et al. 2011, Ziklo, Huston et al. 2016). Incubation of human cells with recombinant *C. pneumoniae* Pmp20 and Pmp21 led to the production of IL-6, IL-8, MCP-1 cytokines and activation of the NF-KB inflammatory pathway (Niessner, Kaun et al. 2003, Wehrl, Brinkmann et al. 2004). Studies on *C. trachomatis* infection in murine models showed that protective immunity is mostly accomplished by CD4$^+$ T cells expressing IFN-γ and TNF-α (Morrison, Feilzer et al. 1995, Perry, Feilzer et al. 1997). Following *C. trachomatis* reinfection, specific immune cells secreting cytokines and chemokines are recruited, inducing increased inflammation and creating tissue damage and scarring, which is the beginning of PID (Darville and Hiltke 2010). Thus, in response to a chlamydial infection, T cells can have a dual role, protecting the host and clearing the infection, but also lead to extensive inflammation and create damage (Ziklo, Huston et al. 2016).

Even though effective therapies against *Chlamydia* are available, the majority of infections are asymptomatic and therefore non-treated, or *Chlamydia* persistence status can resist the treatments, leading to severe sequelae like blindness, infertility and PID. Therefore, the development of an effective vaccine is considered a priority (de la Maza and de la Maza 1995, Chavez, Vicetti Miguel et al. 2011). The first attempts for vaccination against

trachoma were performed in the 1960s with live attenuated *Chlamydia* particles on humans and primates, but they were unsuccessful (Schautteet, De Clercq et al. 2011). More recently, mice were vaccinated with live attenuated or inactivated *Chlamydia*, but they did not elicit full protection (Peterson, You et al. 1999, Olivares-Zavaleta, Whitmire et al. 2010, Yu, Karunakaran et al. 2011). The vaccination with attenuated or inactivated particles has the advantage of providing native antigens and does not require adjuvants, but, on the other hand, reactivation of the bacterial virulence can take place (Schautteet, De Clercq et al. 2011). Different strategies were therefore developed, such as immunization with EB-purified antigenic subunits, recombinant proteins and antigen-encoding plasmid DNA. Vaccination with plasmid DNA carrying the genes of interest can generate a balanced Th1/Th2 response and provide endogenously produced native antigens. Negative aspects of DNA vaccination concern the possibility that plasmid DNA is integrated in the host genome and that auto-antibodies against DNA can be produced (Schautteet, De Clercq et al. 2011). The most studied vaccination strategies against *Chlamydia* are recombinant protein and antigen vaccination. Up to date, vaccinations with MOMP are the most investigated, being MOMP a dominant antigen of the chlamydial outer membrane complex. MOMP is a promising candidate for vaccine development, as indicated by recent studies, but is not sufficient to elicit complete protection (Kari, Whitmire et al. 2009, Tifrea, Pal et al. 2014).

As explained in paragraphs 1.6.3 and 1.6.4, specific antibodies directed against different Pmps were detected in sera from infected patients (Tan, Hsia et al. 2010) and anti-PmpD antibody could pan-neutralize *C. trachomatis* infections (Crane, Carlson et al. 2006). Furthermore, Pmps are interesting because they harbor T cell epitopes (Coler, Bhatia et al. 2009). These data make Pmps valuable candidates for the development of a subunit vaccine. PmpE, F, G and H peptides were identified with an immunoproteomic approach from MHC II dendritic cells of *C. muridarum* and *C. trachomatis* infected mice, respectively and exhibit partial protection in mice against *C. muridarum* and *C. trachomatis* infection, respectively (Karunakaran, Rey-Ladino et al. 2008, Yu, Jiang et al. 2009, Yu, Karunakaran et al. 2012, Karunakaran, Yu et al. 2015). Interestingly, in both murine models, immunization with a combination of the four peptides (PmpEFGH) showed a greater protection than each of the four peptides alone. Furthermore, the PmpEFGH in combination with MOMP and Th1 adjuvants was the most effective protective (Yu, Karunakaran et al. 2012, Yu, Karunakaran et al. 2014, Karunakaran, Yu et al. 2015).

In general, Pmps are considered good candidates for vaccine development because they are surface localized and stimulate neutralizing antibody production by being presented to CD4^{+} T cells. Moreover, a multisubunit vaccine might provide synergic effects and elicit a stronger immune response, also considering that Pmps are heterologously transcribed and expressed (Vasilevsky, Stojanov et al. 2016).

1.7 Identification of new *C. pneumoniae* adhesins

The adhesion of EBs to host cells is the essential step for the establishment of the infection. Several chlamydial proteins and human molecules have been identified as involved in the adhesion process, but the whole process and all the players involved are still not fully characterized (see paragraph 1.4.2). Tools to genetically modify *C. trachomatis* are available since a few years, but *C. pneumoniae* still lacks the possibility of being genetically manipulated (Wang, Kahane et al. 2011, Sixt and Valdivia 2016). Several heterologous systems have been therefore developed to identify new chlamydial adhesins. Candidate proteins can be heterologously expressed on the bacterial surface; for example the heterologous protein can be fused to the autotransporter proteins AIDA-I of *E. coli*, which will transport the protein of interest on the cell surface. *E. coli* expressing the candidate proteins on the cell surface can then be used to perform adhesion assays (Casali, Konieczny et al. 2002). Heterologous expression of proteins is also possible in yeast cells using the so-called yeast display system, in which the protein of interest is fused to the Aga2 protein. Aga2 is linked by disulfide bonds to the cell surface exposed Aga1. Once the protein of interest fused to Aga2 is expressed on the surface of yeast cells, adhesion assays can be performed (Moelleken and Hegemann 2008, Nobbs, Vickerman et al. 2010, Chen 2016).

In 2009, several *C. pneumoniae* hypothetical proteins were selected and screened for their adhesive capacity using a yeast display system. Seven proteins were selected for the screening according to three criteria. The first parameter was their potential localization on the EB cell surface (Montigiani, Falugi et al. 2002). The second parameter was the late expression during the *C. pneumoniae* cycle, according to a transcription microarray assay performed by G. Murra in the laboratory (Murra 2009). Candidate proteins identified by the first two parameters were then compared to the proteins present in the COMP database, which predicts membrane localization (Fechtner 2009). Of the seven proteins identified using these three parameters, four were yeast cell surface presented. Adhesion assays of the yeast cells expressing these proteins with human epithelial cells were then performed

and the binding was analyzed by counting the number of bound yeast cells microscopically. Three of the four candidates showed adhesion ability to human cells, when compared to the Aga2-Invasin positive control and therefore named "Yet Another Adhesin" (Yaa1, Yaa2 and Yaa3) (Fechtner 2009). Of the three proteins analyzed, Cpn1006 (Yaa3), was the protein which could mediate the best binding of yeast cells to human cells.

Cpn0473 (Yaa1), identified in the yeast display, has been recently characterized as an adhesin and invasin specific for *C. pneumoniae* and was re-named LIPP (**L**ipid dependent **I**nternalization **P**romoting **P**rotein). LIPP could be detected on the chlamydial cell surface and rLIPP could bind human cells and initiate internalization of the *Chlamydia* particles, in a lipid-raft dependent manner. Interestingly, when human cells were pre-incubated with rLIPP, the subsequent *C. pneumoniae* infection was boosted, indicating a peculiar *modus operandi*, not observed so far for chlamydial adhesins (Fechtner, Galle et al. 2016). Cpn0498 (Yaa2) and Cpn1006 (Yaa3) showed their potential as adhesin candidate for *C. pneumoniae*, but their functions are still unknown.

1.8 Functional amyloids

Amyloidosis is a term which defines a group of diseases caused by proteinaceous amyloid deposits. Macroscopic observations of white granules present in organs of deceased patients took place already in the 17th century and they have been named as "amyloid" by the German doctor Rudolph Virchow in 1854, who observed an abnormality similar to cellulose in the *corporea amylacea* of the nervous system (Sipe and Cohen 2000).

Even though amyloids represent a heterogeneous group of proteins, they all share some striking characteristics. Amyloids analyzed by Transmission Electron Microscopy (TEM), Atomic Force Microscopy (AFM), and from X-ray fiber diffraction appear as fibrils of around 10 nm diameter and variable length. These fibrils can be stained with specific dyes, such as Thioflavin and Congo red (Chiti and Dobson 2006). Amyloidogenic proteins have a high degree of sequence diversity, but they are characterized by a similar quaternary structure. X-ray fiber diffraction analysis showed that the amyloid fibrils are formed by antiparallel β-sheet structures, arranged perpendicularly to the filament axis (Makin and Serpell 2005). The analysis of the amyloid structure is becoming more and more detailed with the identification of several new models, such as globular proteins with a triangular projection along the axis, forming β-helical amyloid structures. The β-sheet organization of the fibers provides robustness and stability. Differences in the amyloid fibrils can be

attributed to several factors, such as the length of the β-strand regions, number of β-sheets, the parallel or antiparallel orientation to the axis and presence of disulfides bonds (Makin and Serpell 2005, Chiti and Dobson 2006).

The mechanisms which lead to amyloid formation are not fully understood. Observation made for the amyloid Aβ peptide, causing Alzheimer's disease, showed that the aggregation process is preceded by the formation of low molecular weight oligomers called protofibrils. Protofibrils have spherical structure and have the same characteristics as the mature fibrils, such as β-structure, and are associated with toxicity (Walsh, Hartley et al. 1999, Olzscha, Schermann et al. 2011). The model of formation of the mature amyloid fibrils is called "nucleated growth". According to this model, once the protofibrils create the nucleus, other protofibrils quickly associate in the typical β-helical structure to build the mature fibril (Pedersen, Christensen et al. 2004). The monomeric protein can pass through different stages; from completely unfolded to its native conformation, potentially generating functional fibers and functional oligomers as well as native aggregates, which can lead to protofibril formation and thus, accumulation of mature amyloid fibrils. These processes are highly regulated and several of the intermediate stages can have functional properties (Chiti and Dobson 2006). Interestingly, the amyloid fibrils formed by the same protein can exhibit different morphogenesis. Aβ peptide monomers incubated under the same conditions can generate polymorphic fibrils in length and shape within the same sample, as observed by TEM, cryo-EM and 3D reconstruction. This polymorphism could be the result of different inter-residue interactions for the same polypeptide, which has itself a fixed 3D structure (Meinhardt, Sachse et al. 2009).

Accumulation of amyloid fibrils within the cells or in the extracellular space might lead to severe disease, such as Alzheimer, Huntington and Parkinson diseases. In disease-related amyloid accumulation, the assembly of fibrils might be the result of protein misfolding and accumulation of toxic intermediates (Chiti and Dobson 2006).

Even though amyloids are usually associated with diseases, not all fibrils are toxic, but living organisms have developed a regulated expression of amyloids, responsible for essential functions. These fibrils are called "functional amyloids" (Fowler, Koulov et al. 2007, Romero and Kolter 2014). Amyloid proteins have been found in many living organisms, such as bacteria, yeast and humans. In humans, functional amyloids might help the organism in several functions. The amyloid protein Pmel17 is involved in skin pigmentation, by creating the core of melanin (Berson, Theos et al. 2003). Another

example of human functional amyloid is β-endorphin, which might be required for storage of adrenocorticotropic hormones in secretory granules (Maji, Perrin et al. 2009).

In bacteria, amyloid fibrils are mostly associated with adhesion and biofilm formation functions. One of the best known examples for functional amyloids is *E. coli* protein Curli (Romero and Kolter 2014). Curli fibrils are formed by assembly of the protein CsgA, secreted by its own secretion machinery, forming long and complex β-structured fibers of 6-12 nm diameter, able to bind Thioflavin and Congo red (Fig. 7A). Several proteins are involved in CsgA polymerization, keeping the process tightly regulated; environmental conditions, such as lack of nutrients and temperature can indeed influence the expression of the Curli secretion machinery (Barnhart and Chapman 2006). Curli fibers are the main component of the *E. coli* extracellular matrix and play an important role in the initial phase of biofilm formation (Zogaj, Bokranz et al. 2003, Hufnagel, Depas et al. 2015). *E. coli* strains not producing Curli present indeed a different, immature biofilm, compared to the WT strains (Kikuchi, Mizunoe et al. 2005, Hufnagel, Depas et al. 2015). Moreover, Curli mediates *E. coli* adhesion to human cells *in vitro* and induces IL-1β and inflammation pathways, by binding to the TLR2 and NLRP3 receptors on human cells (Hufnagel, Depas et al. 2015, Rapsinski, Wynosky-Dolfi et al. 2015). It is proposed that internalization of *E. coli* cells into host cells is mediated by binding of Curli with fibronectin, followed by interaction with integrin receptor (Gophna, Oelschlaeger et al. 2002, Oh, Hubauer-Brenner et al. 2016).

Curli is not the only relevant example for functional amyloids. The yeast *Candida albicans* presents on its cell surface an adhesin with amyloid characteristics, called Als5p (Alsteens, Dupres et al. 2009). Interestingly, Als5p is not found as very long filaments as Curli, but is presented on the surface of *Candida* in patches. When the patches were pulled by mechanical force using an atomic force microscope, the Als5p amyloid nanodomains were exposed and could cluster and propagate. The nanodomains are positive for amyloid staining and are not generated in strains in which the amyloid sequences within Als5p are mutated (Garcia, Lee et al. 2011, Chan, Joseph et al. 2015).

Recently, analysis of a subdomain of *C. pneumoniae* Pmp21 showed that this protein domain has the ability to form homomeric oligomers with elongated shape, rich in β-sheets and positive for Thioflavin staining, resembling amyloid protofibrils. Despite the fact that Pmp21 has amyloid characteristics, the filaments formed are significantly shorter than the filaments observed for *E. coli* Curli (Fig. 7B). Interestingly, the Pmp21 amyloid-like

protofibrils promote adhesion to human cells and exhibit relevance for the chlamydial infection (Luczak, Smits et al. 2016).
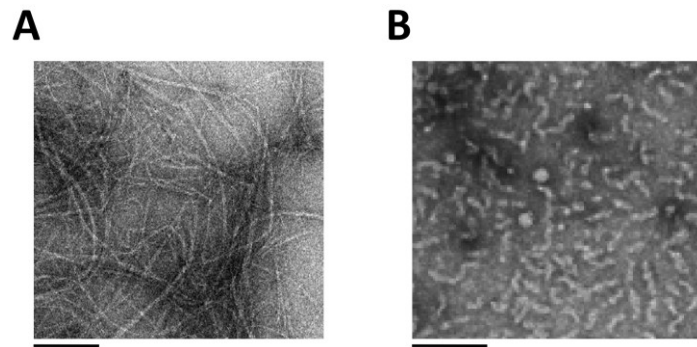
Figure 7. EM pictures of amyloid fibers. A. *E. coli* Curli fiber formed by CsgA monomer after 22 hours incubation, scale bar: 200 nm (Taylor, Hawthorne et al. 2016). **B.** Fiber-like structures formed by C-terminal domain of *C. pneumoniae* Pmp21, scale bar: 100 nm (Luczak, Smits et al. 2016).

1.9 Objectives of this work

Adhesion of the *Chlamydia* EB is the first and essential step for the establishment of the infection; however, this process is still not fully understood. The aim of this work was to characterize *C. trachomatis* adhesins and a new *C. pneumoniae* adhesin candidate.

The first part of this work focused on investigating the oligomerization ability and the functional properties of the *C. trachomatis* Polymorphic membrane proteins (Pmps), which play an important role during adhesion. First of all, Pmps ability to form homomeric oligomers should be analyzed and, considering that *C. trachomatis* has 9 Pmps and all of them are exposed on the cell surface, the ability of different Pmps to interact with each other and generate heteromeric oligomers should be investigated. The adhesion-mediating passenger domain (PD) of all Pmps is characterized by the presence of two repeated motifs FxxN and GGA(I, L, V). In order to study the role of the motifs, the oligomerization ability should be investigated for *C. trachomatis* Pmp domains harboring a high density of motifs and for Pmp domains with a low number of motifs and, if possible, their structures should be analyzed. Moreover, the homomeric and heteromeric Pmp oligomers should be characterized for their adhesion ability and their relevance for the infection.

The second part of this work focused on characterizing a recently identified new *C. pneumoniae* adhesin candidate (Yaa3). Yaa3 is a hypothetical protein; therefore its localization and expression during the chlamydial infection cycle should be investigated. Furthermore, the Yaa3 adhesion capacity and relevance for the *C. pneumoniae* infection should be characterized.

2.   Materials

2.1 Materials, machines and devices

Materials	Source
Amicon Ultra-15 centrifugal filter units 3 kDa cut-off	Merck Millipore
NativePAGE™ Novex™ 3-12% Bis-Tris protein gels, 10-well	Thermo
Cell scraper (23 cm), sterile	Nunc
Cell culture polystyrol flasks, 25 cm^2, sterile	Nunc
Cell culture polystyrol flasks, 75 cm^2, sterile	Nunc
Cell culture plates (24-wells and 96-wells), sterile	Nunc
Cryo tubes (1,8 ml)	Nunc
Dialysis clips	Pierce
Dialysis tubes, 12-15 kDa cut-off	Serva
Electroporation cuvettes	Bio-Rad
Cuvettes, disposable	Sarstedt
Falcon tubes (15 ml and 50 ml), sterile	Sarstedt
Formvar carbon-coated copper grids (S162)	Plano
Glass beads (ø 0,5 mm)	Braun
Glass centrifugation tubes	Korex
Glass coverslips for cell culture (ø 12 mm)	Thermo
Glass flasks (50 ml, 500 ml, 1000 ml, 5000 ml)	Schott
HiTrap™ 5 ml Chelating HP	GE Healthcare
Micro tubes with screw cap, 2 ml, sterile	Sarstedt
Microscope slides	Diagonal
Mini-centrifugation columns (500 µl)	Thermo
MST capillaries NT.115 series, standard treated	Nano Temper
Needles	Braun
PCR reaction tubes (0,5 ml)	Sarstedt
Petri dishes	Sarstedt
Pierce spin columns snap cap	Thermo
Pipette tips (20 µl, 200 µl, 1000 µl)	Sarstedt
Protein purification columns	Thermo
PVDF membrane for Western Blots	Millipore
Reaction Tubes (1,5 ml and 2 ml), sterile	Sarstedt
Round Bottom Centrifugation Tubes, 12 ml, sterile	Greiner
Superose6, 10/300 GL columns	GE Healthcare
Ultracentrifugation tubes	Beckman Coulter
Whatman blotting paper	VWR

Machines and devices	Source
Äkta protein purification system	GE Healthcare
BioPhotometer	Eppendorf
C2 confocal microscope	Nikon
Centrifuge Avanti J-25; rotors JLA10.500, JA25-50	Beckman Coulter
Centrifuge Megafuge 1.0R	Heraeus
Centrifuge Biofuge Pico	Heraeus
Centrifuge Biofuge Primo R	Heraeus
Centrifuge Rotanta 460R	Hettich
Centrifuge J2-21; rotors JA-10, JA-20	Beckman Coulter
Digital balance TE3102S	Sartorius
Electron microscope E902	Zeiss

Electronic analytical balance H110	Sartorius
Electrophoresis power supply EPS	Bioscience
Electroporation system Gene Pulser	Bio-Rad
Gel documentation system	Bio-Rad
Homogenizer Precellys 24	Bertin Technologies
Incubator HEPA class 100	Thermo
Incubator Memmert BE Modell 600	Heraeus
Incubator Multitron	Infors
Inverted microscope Axiovert 25C	Zeiss
Isopropanol freezing box	Roth
Magnetic stirrer	IKA
Microwave	Bosch
Monolith NT.115	Nano Temper
Nano-Drop 2000C	Peqlab
PCR Thermocycler C1000	Bio-Rad
PCR Thermocycler PTC-200	Mj Research
pH-Meter pH 720	inoLab
Plasma cleaner femto	Electronic diener
Pulse generator 100 GE, sealing machine	Polystar
Safety bench Hera safe	Heraeus
SDS-electrophoresis apparatus SE-260	Hoefer
Shakers Orbitron	Infors
Shakers Unitron	Infors
Speed-Vac vacuum concentrator SC110	Savant
Syringe series 702 Microliter	Hamilton
Thermoblock	Labnet
Ultrasonic Homogenizer Sonopuls HD 2200	Bandelin
Ultrasonic bath RK 102 H	Bandelin
Vortex Genie 2	Scientific Industries
Western blot apparatus Pierce G2 Fast Blotter	Thermo
XCell SureLock™ Mini-Cell Electrophoresis System	Thermo

2.2 Chemicals and reagents

Chemicals and reagents	Source
4-(2-hydroxyethyl)-1-piperazineethanesulfonic acid (HEPES)	Sigma
4′,6-diamidin-2-phenylindol (DAPI)	Sigma
5-bromo-4-chloro-3-indolyl-phosphat (BCIP)	Sigma
Acetic acid	Roth
Acrylamide (Rodiphorese 35)	Roth
Adenine	Sigma
Agar	BD
Agarose	Biozym
Alanine	AppliChem
AminoLink coupling resin	Thermo
Ammonium chloride (NH_4Cl)	Merck
Ammonium persulfate (APS)	Roth
Ammonium sulfate ((NH_4)$_2SO_4$)	AppliChem
Amphotericin B	Life technologies
Ampicillin	Sigma
Arginine	AppliChem
Asparagine	AppliChem
Aspartic acid	Roth
β-Mercaptoethanol	Roth
Bis Tris	Acrows Organics

Materials

Biofreeze	Biochrom
Bovine serum albumin (BSA)	Serva
Bradford reagent	Bio-Rad
Bromophenol blue	Serva
Calcium Chloride (CaCl$_2$)	Riedel-de Haën
Calf thymus carrier-DNA (ss-DNA)	Sigma
Casein peptone	BD
Cell dissociation solution	Sigma
Chloramphenicol	Serva
Complete protease inhibitor cocktail	Roche
Complete His-Tag Purification Resin	Roche
Coomassie brilliant blue G250	Serva
Cycloheximide	Sigma
Cysteine	AppliChem
D(+)-Galactose	AppliChem
D(+)-Glucose	Roth
D(+)-Raffinose	Sigma
Deoxynucleoside-5'-Triphosphate (dNTPs)	Fermentas
Dimethylformamide (DMF)	Roth
Dimethyl sulfoxide (DMSO)	Sigma
Dithiothreitol (DTT)	Sigma
DMEM cell culture medium	Gibco
DTSSP (3,3'-dithiobis(sulfosuccinimidyl propionate))	Thermo
Ethanol 96 %	J. T. Baker
Ethidium bromide solution, 10 mg/ml	Roth
Ethylenediaminetetraacetic acid (EDTA)	AppliChem
EZ-Link Sulfo-NHS-Biotin	Thermo
Fetal bovine serum (FKS)	Sigma
Ficoll	Sigma
Gentamycin	Life technologies
Gastrografin	Bayer
Glutamine	AppliChem
Glutamic acid	Sigma
Glutathion agarose	Thermo
Glycerin	Roth
Glycine	Fluka
Guanidine-HCl	Serva
Hanks buffered salt solution (HBSS)	Gibco
Heparin	Sigma
Hydrogen chloride (HCl)	Roth
Histidine	Roth
Imidazole	Sigma
Immersion Oil 518F	Zeiss
Immersion Oil Type A	Nikon
Isoleucine	Roth
Isopropanol	Roth
Isopropyl β-D-1-thiogalactopyranoside (IPTG)	Roth
Kanamycin	Roth
Leucine	AppliChem
Lithium acetate (LiAc)	Roth
Lysine	Sigma
Magnesium chloride (MgCl$_2$)	Roth
Methanol	Riedel-de Haën
Methionine	AppliChem
Milk powder	Roth

Materials

NHS-activated sepharose	GE healthcare
NHS-Fluorescin	Thermo
Ni-NTa agarose	Qiagen
Nickel(II) sulfate (NiSO$_4$)	Sigma
Nitro Blue Tetrazolium (NBT)	Serva
Non-essential amino acids (MEM)	Gibco
NP-40	Sigma
Paraformaldehyde (PFA)	Sigma
Phenol-chloroform	Roth
Phenylalanine	Acros
Phenyl methane sulfonyl fluoride (PMSF serine protease inhibitor)	Sigma
Plasmocin	InvivoGen
Polyethylene glycol (PEG)	Sigma
Ponceau S	Sigma
Potassium Acetate (KAc)	Sigma
Potassium chloride (KCl)	Roth
Potassium dihydrogen phosphate (KH$_2$PO$_4$)	Th. Geyer
Potassium hydroxide (KOH)	Roth
Protein G agarose	Thermo
Proline	Roth
Reduced L-glutathione (GSH)	Sigma
Serine	Roth
Sodium acetate (NaCH$_3$COO)	Sigma
Sodium bicarbonate (NaHCO$_3$)	Fluka
Sodium chloride (NaCl)	Fisher
Sodium cyanoborohydride (NaCNBH$_3$)	Thermo
Sodium deoxycholate	Sigma
Sodium dihydrogen phosphate (NaH$_2$PO$_4$)	Roth
Sodium dodecyl sulfate (SDS)	Roth
Sodium fluoride (NaF)	Sigma
Sodium hydroxide (NaOH)	Roth
Sodium lauroyl sarcosinate (Sarkosyl)	Sigma
Sodium orthovanadate (Na$_2$VO$_4$)	Sigma
Sodium phosphate dibasic (Na$_2$HPO$_4$)	AppliChem
Streptavidin agarose	Thermo
Sucrose	Roth
Tetramethylethylenediamine (TEMED)	Roth
Threonine	AppliChem
Tricine	AppliChem
Triethanolamine	Merk
Tris hydroxymethyl aminomethane (Tris)	VWR
Triton X-100	Sigma
Tryptone	BD
Tryptophan	Roth
TurboFect	Thermo
Tween 20	AppliChem
Tyrosine	AppliChem
Uracil	Sigma
Urea	Sigma
Uranyl acetate	Provided by the CAi (HHU Düsseldorf)
Valine	AppliChem
Vitamin solution (MEM)	Biochrom
Vectashield	Vector laboratories
Xylen-Cyanol FF	Sigma

Yeast extract	BD
Yeast nitrogen base (YNB)	BD

2.3 Solutions and buffers

Solutions and buffers	Composition
1 X PBS	137 mM NaCl 2,7 mM KCl 10 mM Na_2HPO_4 1,8 mM KH_2PO_4 pH 7,4 (HCl/NaOH)
4 X SDS protein blue marker buffer	272 mM Tris-HCl 8-32 % SDS 0,08 % Bromophenol blue 40% Glycerin pH 6,8 (HCl/NaOH)
4 X SDS running gel buffer	1,5 M Tris-HCl 0,4% SDS pH 8,8 (HCl/NaOH)
4 X SDS stacking gel buffer	0,5 M Tris-HCl 0,4% SDS pH 6,8 (HCl/NaOH)
BCIP solution	0,5 g BCIP in 10 ml DMF
Blocking solution (Western blot)	3 % Milk powder 0,05 % Tween 20 in PBS
Buffer A1 (Denaturing lysis buffer)	6 M Guanidine HCl 20 mM Tris-HCl 0,5 M NaCl 0-20 mM Imidazole 1 mM β-Mercaptoethanol (βME) pH 8 (HCl/NaOH)
Buffer A2 (Protein purification buffer)	6 M Urea 20 mM Tris-HCl 0,5 M NaCl 1 mM β-Mercaptoethanol (βME) 50-500 mM Imidazole pH 8 (HCl/NaOH)
Buffer B (Denaturing lysis buffer)	8 M Urea 0,1 M NaH_2PO_4 10 mM Tris/HCl pH 8,0
Buffer C (Protein purification buffer)	8 M Urea 0,1 M NaH_2PO_4 10 mM Tris/HCl pH 6,3
Buffer P1 (Plasmid preparation)	50 mM Tris/HCl pH 8,0 10 mM EDTA pH 8,0 100 μg/ml RNAse A
Buffer P2 (Plasmid preparation)	200 mM NaOH 1 % SDS
Buffer P3 (Plasmid preparation)	2,55 M KAc pH 5,5

Coomassie brilliant blue solution	0,008 % Coomassie G-250 35 mM HCl in water
Coupling buffer	0,2 M $NaHCO_3$ 0,5 M NaCl pH 8.3
Detection buffer (Western blot)	0,1 M Tris/HCl pH 9,5 0,1 M NaCl 50 mM MgCl2
DNA blue marker buffer	0,1 % Bromophenol blue 0,1 % Xylen-Cyanol FF 15 % Ficoll 10 mM Tris/HCl 10 mM EDTA
Hepes buffer (Native lysis buffer)	0.1 M HEPES pH 7.4
Hepes/KOH (MST buffer)	238.3 g HEPES KOH pellets to adjust pH to 9 In 1 L water
Lithium acetate buffer	1M Lithium acetate, pH 8,4-8,9
Native PAGE™ Anode Buffer	1 X Native PAGE™ Running buffer
Native PAGE™ Cathode Buffer Additive (20X)	1g Coomassie G-250 in 250 mL water
Native PAGE™ Light Blue buffer	10 ml Running buffer (20X) 1 ml Cathode Buffer Additive (20X) 189 ml water
Native PAGE™ Running buffer (20X)	50 mM Bis Tris 50 mM Tricine pH 6.8
Native PAGE™ Sample buffer (4X)	50 mM Bis Tris 6 N HCl 50 mM NaCl 10 % Glycerol 0.001 % Ponceau S pH 7,2
NBT solution	0,5 g NBT in 10 ml of 70 % DMF
PEG	50 % PEG in H_2O
Phospholysis buffer	1 % NP-40 1 % Triton X100 20 mM Tris/HCl pH 7,5 140 mM NaCl 2 mM EDTA 1 mM Na_2VO_4
Ripa buffer (Native lysis buffer)	50 mM Tris-HCl, pH 7,4 1 % NP-40 0,5 % Sodium deoxycholate 0,1 % SDS 150mM NaCl 2 mM EDTA 50 mM NaF
SDS-PAGE running buffer	0,05 M Tris/HCl pH 8,3 0,2 M Glycine 0,1 % SDS
SPG buffer	75 g Sucrose 0,52 g KH_2PO_4

	1,53 g Na_2HPO_4 0,72 g Glutamic acid diluted in in 1 L of H_2O pH 7,5
Stripping buffer (Nickel columns)	500 mM NaCl 20mM NaH_2PO_4 50 mM EDTA pH 7,4
Transfer buffer (Western blot)	25 mM Tris 150 mM Glycine 10 % Methanol 0,05 % SDS
TSE buffer (Periplasmic fraction extraction)	25 mM Tris 0,25 M Sucrose 2,5 mM EDTA

2.4 Enzymes

2.4.1 Restriction enzymes

Restriction enzymes were used to cut vectors for homologous recombination (see paragraph 3.2.3) and for digestion of plasmids to verify the presence of the insert. The enzymes were used according to the Thermo-Fisher instructions, with the appropriate buffers. Enzymes used: *AvaI, AvaII, HindIII, NdeI, XhoI*.

2.4.2 Other enzymes

Other enzymes	Source
All-in HiFi polymerase	HighQu
Lysozyme	Sigma
Proteinase K	Roche
RNAse A	Qiagen
Taq-polymerase	Self-made (Irina Volfson)
Trypsin	Invitrogen

2.5 Antibodies

2.5.1 Primary antibodies

Antibody	Reactivity	Origin	Dilution	Source
Anti-147	CPn0147	Rabbit	IF 1:50	Dissertation Herbst 2011
Anti-Actin	Human Actin	Mouse	WB 1:2000	Sigma
Anti-DnaK	C. tr. DnaK heat shock Protein	Mouse	IF 1:50	(Birkelund, Lundemose et al. 1990)
Anti-GST	GST-Tag	Rabbit	WB 1:1000 IF 1:50	Santa Cruz
Anti-His	5 Histidine Tag	Mouse	WB 1:2500	Roche
Anti-LPS	Chlamydial LPS	Mouse	IF 1:20	US Biological
Anti-Momp	C. tr. Momp	Mouse	WB 1:500	Santa Cruz

			IF 1:100	
Anti-OmcB	C. pn. OmcB	Rabbit	WB 1:2500	(Moelleken and Hegemann 2008)
Anti-Pmp6	C. pn. Pmp6	Rabbit	WB 1:200 IF 1:20	(Becker 2013)
Anti-Pmp20	C. pn. Pmp20	Rabbit	WB 1:200 IF 1:20	(Becker 2013)
Anti-M-Pmp21	C. pn. Pmp21	Rabbit	WB 1:200 IF 1:20	(Molleken, Schmidt et al. 2010)
Anti-VSV	VSV-Tag	Mouse	WB 1:1000	Santa Cruz
Anti-Yaa3	Cpn1006 (Yaa3)	Rabbit	WB 1:100 IF 1:50	Favaroni (This work)

2.5.2 Secondary antibodies

Antibody	Origin	Dilution	Source
Alexa Fluor 488-Mouse	Goat	IF 1:200	Invitrogen
Alexa Fluor 488-Rabbit	Goat	IF 1:200	Invitrogen
Alexa Fluor 594-Mouse	Goat	IF 1:200	Invitrogen
Alexa Fluor 594-Rabbit	Goat	IF 1:200	Invitrogen
AP-Anti-Mouse	Goat	WB 1:7500	Promega
AP-Anti-Mouse	Goat	WB 1:7500	Promega
AP-Anti-Streptavidin	Rabbit	WB 1:1000	Sigma

2.6 Kits

Kits	Source
PeriPreps™ Periplasting Kit	Epicenter Biotechnologies
Plasmid Midi Kit	Qiagen
QIAquick Gel Extraction Kit	Qiagen

2.7 DNA and protein size standards

Ladder	Standards size	Source
O' Gene Ruler™ DNA Ladder Mix	10.000, 8.000, 6.000, 5.000, 4.000, 3.500, 3.000, 2.500, 2.000, 1.500, 1.200, 1.000, 900, 800, 700, 600, 500, 400, 300, 200, 100 [bp]	Fermentas
Page Ruler™ Prestained Protein Ladder	170, 130, 100, 70, 55, 40, 35, 25, 15, 10 [kDa]	Fermentas
Page Ruler™ Plus Prestained Protein Ladder	250, 130, 100, 70, 55, 35, 25, 15, 10 [kDa]	Fermentas
NativeMark unstained protein standard	1236, 1048, 720, 480, 242, 146, 66, 25 [kDa]	Thermo
Standard proteins preparation for Size Exclusion Chromatography (SEC)	Blue Dextran: 2000 kDa Thyroglobulin: 669 kDa Ferritin: 440 kDa BSA: 67 kDa Ribonuclease A: 13,7 kDa	GE Healthcare

2.8 Oligonucleotides

The oligonucleotides used were synthesized by Biomers and diluted in H_2O to the concentration of 50 μmol/μl. The numbers of the list refer to the internal oligonucleotides collection.

2.8.1 Oligonucleotides for cloning

The oligonucleotides designed for cloning via homologous recombination in yeast (see paragraph 3.2.3) have a region of around 40 nt of homology to the vector and a region of around 20 nt of homology to the gene.

Number	Name	Sequence (5´-> 3)
C-1475	1006 pKM32 hin (pFA3)	AACTATGAGAGGATCTCACCATCACCATCAC CATACGGATATGTCTATAACCACCTTAGGG
C-1476	1006 pKM32 her (pFA3)	TGAGGTCATTACTGGATCTATCAACAGGAGT CCAAGCTCATCCTAGGGGTTTATTCAGTTG
C-2395	Cpn1006pET24n fwd (pFA1)	TAGAAATAATTTTGTTTAACTTTAAGAAGGA GATACATATGTCTATAACCACCTTAGG
C-2396	Cpn1006pET24n rev (pFA1)	CTTTGTTAGCAGCCGGATCTCAGTGGTGGTG GTGGTGGTGTCCTAGGGGTTTATTCAGTT
C-2415	pSL4linkCpn1006 fw (pFA2)	TGCTGGTCTGCTGCTCCTCGCTGCCCAGCCGG CGATGGCCATGTCTATAACCACCTTAGG
C-2416	pSL4linkCpn1006 rev (pFA2)	CCGGATCTCAATGGTGATGGTGATGATGGTG GTGATGGTGTCCTAGGGGTTTATTCAGTT
C-2569	Cpn1006pET24a40 FWD (pFA4)	AGAAATAATTTTGTTTAACTTTAAGAAGGAG ATATACATATGCTTCTTTTACAAGCAATT
C-2570	Cpn1006pET24a40aa REV (pFA4)	CTTTGTTAGCAGCCGGATCTCAGTGGTGGTG GTGGTGGTGTCCTAGGGGTTTATTCAGTT
C-2695	1006RVFT28	GAGGCAGATCGTCAGTCAGTCAATGGTGATG GTGATGGTGTCCTAGGGGTTTATTCAGTT
C-2788	GALYaa3FDW	TGGCGACCATCCTCCAAAATCGGATCTGATC GAAGGTCGTATGTCTATAACCACCTTAGG
C-2789	GALYaa3REV	TGTGGGGGGAGGGCGTGAATGTAAGCGTGAC ATAACTAATTCAATGGTGATGGTGATGGT
C-2790	METYaaFDW	CTAATTACATGACTCGAGGTCGACGGTATCG ATAAGCTTGATGTCTATAACCACCTTAGG
C-2791	METYaaREV	GTCAGATACATAGATACAATTCTATTACCCCC ATCCATACTCAATGGTGATGGTGATGGT
C-2798	FwdPmpAC-term (pFA7-8)	AATAATTTTGTTTAACTTTAAGAAGGAGATAT ACATATGTCCCTAGATCGACACAATTCT
C-2799	REVPmpAC1-term (pFA7)	TTTGTTAGCAGCCGGATCTCAGTGGTGGTGGT GGTGGTGGGTGAGCAAGATTTCCATTTG
C-2800	REVPmpAC2-term (pFA8)	CTTTGTTAGCAGCCGGATCTCAGTGGTGGTG GTGGTGGTGGCCTAAGTTATGAGAGGCTG
C-2801	FwdPmpAN-term (pPH1)	ATAATTTTGTTTAACTTTAAGAAGGAGATATA CATATGGAAATGGAATTAGCTATTTCTG
C-2802	REVPmpAN-term	TTTGTTAGCAGCCGGATCTCAGTGGTGGTGGT

	(pPH1)	GGTGGTGGCCTTCGAAAGTAATTTGTTG
C-2803	FwdPmpEC-term (pFA9)	AAATAATTTTGTTTAACTTTAAGAAGGAGAT ATACATATGGAGGGGGGCGCTATCTATAT
C-2804	REVPmpEC-term (pFA9)	TGTTAGCAGCCGGATCTCAGTGGTGGTGGTG GTGGTGACTATTTTTTAAGCTTTCTGTTG
C-2805	FwdPmpEN-term (pPH2)	AATAATTTTGTTTAACTTTAAGAAGGAGATAT ACATATGAGAGAGGTTCCTTCTAGAATC
C-2806	REVPmpEN-term (pPH2)	TTTGTTAGCAGCCGGATCTCAGTGGTGGTGGT GGTGGTGATAGATAGCGCCACCTTTTCC
C-2807	FwdPmpFC-term (pFA10)	AAATAATTTTGTTTAACTTTAAGAAGGAGAT ATACATATGCCGTTTACCCAAAATCCGAC
C-2808	REVPmpFC-term (pFA10)	CTTTGTTAGCAGCCGGATCTCAGTGGTGGTG GTGGTGGTGGTTTCTTCCTGAATGCACCA
C-2809	FwdPmpFN-term (pPH3)	AATAATTTTGTTTAACTTTAAGAAGGAGATAT ACATATGAATGAAACAGATACGCTACAG
C-2810	REVPmpFN-term (pPH3)	CTTTGTTAGCAGCCGGATCTCAGTGGTGGTG GTGGTGGTGAGCTTGCGTGTCCGGTATAT
C-2811	FwdPmpGC-term (pFA11)	AAATAATTTTGTTTAACTTTAAGAAGGAGAT ATACATATGGATGGTGGAGCGATTTATTT
C-2812	REVPmpGC-term (pFA11)	TTTGTTAGCAGCCGGATCTCAGTGGTGGTGGT GGTGGTGTGCTGAATGCGCAGATCGTAT
C-2813	FwdPmpGN-term (pPH4)	ATAATTTTGTTTAACTTTAAGAAGGAGATATA CATATGGAAATCATGATTCCTCAAGGAA
C-2814	REVPmpGN-term (pPH4)	TTTGTTAGCAGCCGGATCTCAGTGGTGGTGGT GGTGGTGCATAGCAGAGAAACTGGTGAC
C-2921	VSVFWD (pFA14)	GGATCCGAATTCGAGCTCCGTCGACAAGCTT GCGGCCGCATACACCGATATCGAGATGAACA GGCTGGGAAAG
C-2922	VSVREV (pFA14)	ACTCAGCTTCCTTTCGGGCTTTGTTAGCAGCC GGATCTCACTTTCCCAGCCTGTTCATCTCGAT ATCGGTGTA
C-2923	15FWD (pFA15)	AAATAATTTTGTTTAACTTTAAGAAGGAGAT ATACATATGTCCCTAGATCGACACAATTC
C-2924	15REV (pFA15)	GATCTCACTTTCCCAGCCTGTTCATCTCGATA TCGGTGTAGGTGAGCAAGATTTCCATTT
C-2925	C2FWD (pFA12-13)	ATAATTTTGTTTAACTTTAAGAAGGAGATATA CATATGGTTACTGCATCTTCTGATAATC
C-2926	C2REV (pFA12)	CTTTGTTAGCAGCCGGATCTCAGTGGTGGTG GTGGTGGTGAGATGGGGGTTCCACCGCTTC
C-2927	C3REV (pFA13)	TTTGTTAGCAGCCGGATCTCAGTGGTGGTGGT GGTGGTGCAAGCCTTGTTTGACTGTGAC
C-2928	16FWD (Gc in pFA14)	AAATAATTTTGTTTAACTTTAAGAAGGAGAT ATACATATGGATGGTGGAGCGATTTATTT
C-2929	16REV (Gc in pFA14)	GATCTCACTTTCCCAGCCTGTTCATCTCGATA TCGGTGTATGCTGAATGCGCAGATCGTA
C-3156	AcHisVSVREV (pFA16)	CGGATCTCACTTTCCCAGCCTGTTCATCTCGA TATCGGTGTA GTGGTGGTGGTGGTGGTG

2.8.2 Oligonucleotides for sequencing

Number	Name	Sequence (5´-> 3)
C-673	Seq pKM33 vorne (pFT8)	TACTTGAAATCCAGCAAGTAT
C-795	seq pKM32 tim her(hin)	TTTCGTCTTCACCTCGAGAAA
C-796	seq pKM32 tim her	GGTCATTACTGGATCTATCAA
C-803	GST Protease GenX His seq her	CAAGCTGTGACCGTCTCCG
C-1292	pFT25 seq-rev	CAATAAAAAACGCCCGGCGG
C-2095	Seq_ pET24a_Fwd	GATAACAATTCCCCTCTAG
C-2096	Seq_ pET24a_Rev	CTTTCGGGCTTTGTTAG
C-2097	Seq-_ pET28b_Rev (pSL4)	CCAACTCAGCTTCCTTTC
C-2098	Seq-_ pET28b_Fwd (pSL4)	GGATAACAATTCCCCTCTAG
GATC	T7 promoter	TAATACGACTCACTATAGGG

2.9 Plasmids

The numbers of the list refer to the internal plasmid collection.

Number	Name	Construct, reference
1612	pFT8	Expression vector with N-term. GST and C-term. His-tag (Fechtner)
1740	pKM50	Expression vector pKM32 with *inv497* (Invasin) from *Y. pseudotuberculosis* (Moelleken)
1936	pGro7	Expression vector: Chaperones *groES-groEL* (Takara)
1938	pG-Tf2	Expression vector: Chaperones *groES-groEL-tig* (Takara)
1939	pTf16	Expression vector: Chaperone *tig* (Takara)
1941	pKM32	Expression vector with N-term. His-Tag and with integrated *CEN6 ARS URA3* from pAC2 (Moelleken)
1972	pST42	Expression vector pFT25 with *ct017* (Ctad1) and C-term. His-tag (Stallmann)
1998	pEB39	Expression vector pKM32 with *pmpG* fragment G (29-732 aa) (Becker)
2003	pEB44	Expression vector pKM32 with *pmpD* fragment D (269-918 aa) (Becker)
2063	pET24a	Expression vector pET24a with C-term. His-tag with integrated *CEN6 ARS URA3* from pAC2 (Engel)
2132	pFT28	Expression vector pFT8 with *cpn1006* (*yaa3*), N-term. GST and C-term. His-tag (Fechtner)
2135	pFT31	Expression vector pFT25 with *cpn1006* (*yaa3*) and C-term. His-tag (Fechtner)
2138	pFT34	Expression vector pFT25 with *cpn0473* and C-term. His-tag (Fechtner)
2175	pEB66	Expression vector pKM32 with *pmpA* fragment A (154-608 aa) (Becker)
2176	pEB67	Expression vector pKM32 with *pmpB* fragment B (138-811 aa) (Becker)
2177	pEB68	Expression vector pKM32 with *pmpC* fragment C (171-735 aa) (Becker)
2178	pEB69	Expression vector pKM32 with *pmpE* fragment E (88-380 aa) (Becker)
2179	pEB70	Expression vector pKM32 with *pmpF* fragment F (112-510 aa) (Becker)
2180	pEB71	Expression vector pKM32 with *pmpH* fragment H (111-422 aa)

		(Becker)
2181	pEB72	Expression vector pKM32 with *pmpI* fragment I (137-518 aa) (Becker)
2197	pSL4	Expression vector pET22b+ with a N-term. PelB sequence, integrated *CEN6 ARS URA3* from pAC2 and a N-term. His-tag (Luczak)
2270	pFA1	Expression vector pET24a with *cpn1006* (*yaa3*) and C-term. His-tag, generated with the oligonucleotides C-2395 / C-2396 (Favaroni)
2271	pFA2	Expression vector pSL4 with *cpn1006* (*yaa3*) and N-term. His-tag, generated with the oligonucleotides C-2415 / C-2416 (Favaroni)
2380	pFA3	Expression vector pKM32 with *cpn1006* (*yaa3*) and N-term. His-tag, generated with the oligonucleotides C-1475 / C-1476 (Favaroni)
2387	pFA4	Expression vector pET24a with *cpn1006* deletion version (*yaa3Δ*) (41-161 aa) and C-term. His-tag, generated with the oligonucleotides C-2569 / C-2570 (Favaroni)
2505	pFA7	Expression vector pET24a with *pmpA* fragment Ac (408-608 aa), generated with the oligonucleotides C-2798 / C-2799 (Favaroni) (Favaroni)
2506	pFA8	Expression vector pET24a with *pmpA* fragment Ac2 (408-692 aa), generated with the oligonucleotides C-2798 / C-2800 (Favaroni) (Favaroni)
2507	pFA9	Expression vector pET24a with *pmpE* fragment Ec (336-678 aa), generated with the oligonucleotides C-2803 / C-2804 (Favaroni)
2508	pFA10	Expression vector pET24a with *pmpF* fragment Fc (505-748 aa), generated with the oligonucleotides C-2807 / C-2808 (Favaroni)
2509	pFA11	Expression vector pET24a with *pmpG* fragment Gc (401-726 aa), generated with the oligonucleotides C-2811 / C-2812 (Favaroni)
2512	pFA14	Expression vector pET24a with C-term. VSV-tag, instead of His-tag, generated with the oligonucleotides C-2921 / C-2922 (Favaroni)
2513	pFA15	Expression vector pFA14 with *pmpA* fragment Ac and C-term. VSV-tag, generated with the oligonucleotides C-2923 / C-2924 (Favaroni)
2514	pPH1	Expression vector pET24a with *pmpA* fragment An (52-252 aa), generated with the oligonucleotides C-2801 / C-2802 (Hanisch)
2515	pPH2	Expression vector pET24a with *pmpE* fragment En (19-219 aa), generated with the oligonucleotides C-2805 / C-2806 (Hanisch)
2516	pPH3	Expression vector pET24a with *pmpF* fragment Fn (26-226 aa), generated with the oligonucleotides C-2809 / C-2810 (Hanisch)
2517	pPH4	Expression vector pET24a with *pmpG* fragment Gn (29-229 aa), generated with the oligonucleotides C-2813 / C-2814 (Hanisch)
2518	pPH6	Expression vector pKM32 with *pmpA* fragment Ash (154-407 aa) (Hanisch)
2524	pPH13	Expression vector pET24a with *pmpE* fragment Efl (26-678 aa) (Hanisch)
2525	pSL15	Expression vector pET24a with *pmpA* fragment Afl (52-692 aa) (Luczak)
2526	pSL17	Expression vector pET24a with *pmpF* fragment Ffl (26-748 aa) (Luczak)
2542	pFA12	Expression vector pET24a with *pmpC* fragment C2 (800-1300 aa), generated with the oligonucleotides C-2925 / C-2926

2543	pFA16	Expression vector pFA14 with *pmpA* fragment Ac with C-term. His-tag and VSV-tag, generated with the oligonucleotides C-2095 / C-3156 (Favaroni)
		(Favaroni)

2.10 Cells and cell lines

2.10.1 Eukaryotic cells and cell lines

Human cells:

HEp-2 cell line: Epithelial laryngeal carcinoma cell line of human origin, HeLa morphology, 46 chromosomes (ATCC No: CCL-23)

Saccharomyces cerevisiae:

CEN.PK 2-1C: *MATa leu2-3,112 ura3-52 trp1-289 his3-Δ1 MAL2-8C SUC2* (Entian, Schuster et al. 1999)

2.10.2 Prokaryotic cells and cell lines

Escherichia coli:

XL₁Blue: *supE44 hsdR17 recA1 endA1 gyrA96 thi relA1 lac-[F' proAB lacIp ZΔM15 Tn10(Tetr)]* (Stratagene)

BL21:   *F⁻ompT hsdSB(rB⁻mB⁻) gal dcm (DE3)* (Invitrogen)

Rosetta: *F-ompT hsdSB(rB⁻ mB⁻) gal dcm (DE3) pRARE (Cam^R)* (Nonages)

ArcticExpress RIL: *E. coli B F⁻ ompT hsdS(rB⁻ mB⁻) dcm+ Tetr gal λ (DE3) endA Hte [cpn10cpn60 Gentr] [argU ileY leuW Strr]*

Chlamydia pneumoniae:

GID: Giessen isolate of a patient with acute bronchitis (Jantos, Heck et al. 1997)

Chlamydia trachomatis:

Serovar E: DK-20 (Institute of Ophthalmology, London)

2.11 Media

2.11.1 Media for cell culture and *Chlamydia* cultivation

500 ml DMEM GlutaMAX™ (Dulbecco's Modified Eagle Medium)

50 ml FKS (heat-inactivated for 1 h at 56 ° C), final concentration: 10%

5 ml MEM non-essential amino acids (100 X), final concentration: 1 X

5 ml MEM vitamins (100 X), final concentration: 1 X

5 ml Amphotericin B (250 µg/ml), final concentration: 2,5 µg/ml

500 µl Gentamycin 50 mg/ml, final concentration: 50 µg/ml

Cycloheximide, final concentration: 12 µl/ml (*Chlamydia* cultivation)

2.11.2 Media for *S. cerevisiae* cultivation

YPD$^+$ medium:

20 g Glucose

10 g Yeast extract

20 g Casein Peptone

13,5 g Agar (only for plates)

2 ml Adenine stock solution (2 mg/ml)

4 ml Tryptophan stock solution (5 mg/ml)

Dissolved in 1 L H$_2$O and autoclaved

SD-minimal medium:

20 g Glucose

20 g Agar (only for plates)

1,7 g Yeast Nitrogen Base

5 g Ammonium sulfate

2 g Amino acid mix
(For selection, the corresponding amino acid or nucleobase
is not added in the mix)

The components are dissolved at final volume of 1 L with H$_2$O, after adjusting the pH at 6.0 and afterwards the solution is autoclaved.

Amino acid mix +24:

The mix is composed of amino acids, nucleobases and chemicals, in the combination appropriate for selection. The mix is mixed for 15´ with sterile grinding balls.

Amino acid	Amount	Amino acid	Amount
Adenine	0,5 g	Leucine	10,0 g
Alanine	2,0 g	Lysine	2,0 g
Arginine	2,0 g	Methionine	2,0 g
Aspargine	2,0 g	Para- aminobenzoic acid	2,0 g
Aspartic acid	2,0 g	Phenylalanine	2,0 g
Cysteine	2,0 g	Proline	2,0 g
Glutamine	2,0 g	Serine	2,0 g
Glutamic acid	2,0 g	Threonine	2,0 g
Glycine	2,0 g	Tryptophan	2,0 g
Histidine	2,0 g	Tyrosine	2,0 g
Inositol	2,0 g	Uracil	2,0 g
Isoleucine	2,0 g	Valine	2,0 g

2.11.3 Media for *E. coli*

LB medium:

10 g Bacto Tryptone

5 g Yeast extract

5 g NaCl

8 g Glucose (Optional, for protein expression)

13,5 g Agar (only for plates)

The components are dissolved in 1 L H_2O and autoclaved. After cooling at room temperature, antibiotics are added (Ampicillin: 50 µg/ml, Kanamycin: 10 µg/ml for liquid medium and 15 µg/ml for plates and Chloramphenicol: 20 µg/ml).

3. Methods

3.1 Cultivation of different organisms

3.1.1 Cultivation of HEp-2 epithelial human cells

3.1.1.1 Cell culture medium

500 ml minimal essential DMEM (1X) + GlutaMAX (Dulbecco's Modified Eagle Medium, Thermo Fisher Scientific) was supplemented with

- 50 ml FKS (heat-inactivated for 1 h at 56 ° C)
- 5 ml MEM vitamins (100X)
- 5 ml MEM non-essential amino acids (100X)
- 5 ml Amphotericin B (250 mg/ml)
- 500 µl Gentamycin (50 mg/ml)

3.1.1.2 Passaging adherent cells by trypsinization

- Cell culture medium is removed from 75 cm^2 flask with confluent HEp-2 cells
- Cells are washed with 10 ml HBSS (Hank's balanced salt solution)
- Cells are incubated at 37 °C with 5 ml trypsin solution until cells are detached
- Trypsin solution is neutralized with the addition of 5 ml culture medium
- The solution is transferred in a 12 ml centrifuge tube and centrifuged at 500 rpm for 10´ (Rotanta 460R)
- Cell pellet is resuspended in 5 ml cell culture medium and diluted in cell culture medium
- For passage in 75 cm^2 flask, 1 ml of cell suspension in 15 ml cell culture medium
- For passage in 25 cm^2 flask, 0,5 ml of cell suspension in 5 ml cell culture medium
- For passage in 25 cm^2 flask, 0,5 ml of cell suspension in 5 ml cell culture medium
- For passage in 24-well plates, cell suspension was diluted 1:10-1:30 with cell culture medium and place 1 ml in each well.
- Cells were incubated for 2-3 days at 37 °C and 6 % CO_2

3.1.1.3 Freezing human epithelial HEp-2 cells

- Confluent cells are detached by trypsinization (see paragraph 3.1.1.2)
- After centrifugation, cell pellet is resuspended in 1 ml Biofreeze
- Solution is transferred in a cryo-tube and frozen in a isopropanol freezing box at -80 °C

3.1.2 Cultivation of *Saccharomyces cerevisiae*

S. cerevisiae strain *CEN.PK2* is cultivated at 30 °C with shaking in selection medium, lacking the marker amino acid, which is present in plasmid-expressing cells.

3.1.3 Cultivation of *Chlamydia*

Chlamydia is cultivated in monolayers of human epithelial HEp-2 cells in cell culture medium (see paragraph 3.1.1.1) with the addition of 12 µl/ml Cycloheximide (100 mg/ml), responsible for inhibiting human cells replication, in favor of *Chlamydia* growth. *Chlamydia* is stored at -80 °C in SPG (Sucrose phosphate glutamate) buffer.

3.1.3.1 Infection, passaging and harvesting *Chlamydia* from adherent cells

- 1 ml of *Chlamydia* (approx. 10^7 IFU/ml) stored in SPG is thawed and mixed with 4 ml cell culture medium

- The final volume of 5 ml of *Chlamydia* suspension is added to the confluent layer of HEp-2 cells in 25 cm^2 flasks

- Flasks are then centrifuged at 3000 rpm at 30 °C for 60′ (Rotanta 460R) to allow the attachment and uptake of *Chlamydia* in human cells

- Cells are incubated for 1h in the incubator at 37 °C, 6 % CO_2

- The medium is changed with 5 ml per flask of cell culture medium + Cycloheximide

- Infected cells are incubated for 2 days (*C. trachomatis*) or 3 days (*C. pneumoniae*) in the incubator at 37 °C, 6 % CO_2

- After incubation, infected cells were detached from the flasks, using a sterile cell scraper and the suspension is collected in 50 ml centrifugation tubes

- Cells are disrupted by sonication for 45′′ and centrifuged at 3000 rpm for 10′ (Rotanta 460R) to remove cells debris

- Supernatant is transferred in new 50 ml centrifugation tubes and centrifuged again

- The supernatant is diluted 1:2 / 1:4 and used to infect new flasks with confluent HEp-2 cells

- Supernatant is diluted 1:1 in SPG buffer and stored at -80 °C (*Chlamydia* pool)

3.1.3.2 Purification of chlamydial EBs by gastrografin gradient

- Supernatant obtained from infected cells, out of 32 25 cm^2 flasks (see paragraph 3.1.3.1) is transferred to a sterile ultracentrifugation tube and centrifuged at 15,000 rpm, for 30′ at 4 °C

- The chlamydial pellets are resuspended in 1 ml SPG buffer, using an ultrasound bath and frozen at -80 °C

- The *Chlamydia* pellets are thawed and centrifuged at 15,000 rpm, for 30′ at 4 °C (Biofuge Primo R)

- The obtained pellets are resuspended in 1 ml final volume of HBSS

- The *Chlamydia* suspension is added on top of 9 ml of 30 % gastrografin in a sterile glass tube and centrifuged in J2-21 rotor (Beckmann) at 30,000 g for 1 h at 4 °C

- The EBs pellet is washed with 1 ml HBSS, transferred in a centrifugation tube and centrifuged at 15,000 rpm for 30′ at 4 °C (Biofuge Primo R)

- The EBs pellet is finally resuspended in 1 ml SPG and aliquots are frozen at -80 °C

3.1.3.3 Determination of *Chlamydia* infectious rate (inclusion-forming units (IFU)/ml)

- The obtained Chlamydia suspension is diluted in cell culture medium 1:10 to the dilution 10^{-10}

- 100 µl of dilution is added in triplicates to confluent HEp-2 cells grown in 96-well plates

- Infected 96-well plate is centrifuged at 3000 rpm for 15′ at 30 °C (Rotanta 460R) and afterwards incubated for 1 h in the incubator at 37 °C, 6 % CO$_2$

- Medium is substituted with 200 µl/well of cell culture medium + Cycloheximide and incubated at 37 °C, 6 % CO$_2$ for 1 day (*C. trachomatis*) or 2 days (*C. pneumoniae*)

- The infected cells are washed with HBSS and fixed with 96 % methanol for 5′ at RT

- After washing three times with HBSS, the inclusions are stained with FITC-conjugated antibody against LPS (*C. pneumoniae*) or with anti-Momp antibody (*C. trachomatis*)

- The inclusions are counted using a C2 confocal microscope and the number of IFU/ml of the initial suspension is calculated

3.1.3.4 Stationary chlamydial infection of human cells

Stationary infection is performed on 24-well plate during functional experiments, such as infection blocking assay and infection with protein-coated EBs

- *Chlamydia* EBs (MOI 10) are mixed in a final volume of 300 µl cell culture medium and added to each well

- The infected cells are incubated for 2 h in the incubator at 37 °C, 6 % CO_2

- Medium is exchanged with 1 ml/well of cell culture medium + Cycloheximide

- Infected cells are incubated for 1 day (*C. trachomatis*) or 2 days (*C. pneumoniae*)

- After washing three times with HBSS, the inclusions are stained with FITC-conjugated antibody against LPS (*C. pneumoniae*) or with anti-Momp antibody (*C. trachomatis*)

- The inclusions are counted using a C2 confocal microscope

3.1.3.5 Genomic chlamydial DNA extraction from infected cells

- Chlamydial pellets obtained by ultracentrifugation at 15000 rpm, for 30´ at 4 °C (see paragraph 3.1.3.2) is resuspended in 1 ml H_2O and centrifuged again

- Chlamydial pellet is resuspended in 100 µl H_2O using the ultrasound bath RK 102 H for 30'' and centrifuged again

- Chlamydial pellet is resuspended in 100 µl H_2O using the ultrasound bath RK 102 H for 30'' and by gently pipetting

- 10 µl of Proteinase K (40 mg/ml) are added and incubated for 1 h at 55 °C and then 10´ at 100 °C

- 140 µl of H_2O are used to mix the solution and 250 µl of Phenol-Chloroform are added

- The suspension is centrifuged at 13,000 rpm for 10´ at RT (Biofuge Primo R)

- The upper phase (200 µl) is transferred in a new centrifugation tube

- 20 µl of sodium acetate and 200 µl of isopropanol are added and the suspension is frozen for 30´ at -80 °C

- The suspension is thawed on ice and centrifuged at 15,000 rpm for 30´ at 4 °C (Biofuge Primo R), the pellet washed with 500 µl off 70 % ethanol and centrifuged again

- DNA pellet is dried and resuspended in 50 µl H_2O

3.1.3.6 Preparation of protein extract from *Chlamydia*-infected cells for SDS-PAGE analysis

- Infected cells from a 25 cm^2 flasks are incubated with 500 µl of Phospholysis buffer for 20′ at RT
- The suspension is transferred in an Eppendorf tube
- 50 µl DTT and 125 µl protein loading buffer are added
- The mix is boiled for 20′ at 100 °C and used for SDS-PAGE analysis

3.1.4 Cultivation of *Escherichia coli*

E. coli strains XL1-Blue, Rosetta and BL-21 were cultured in LB medium in aerobic conditions at 37 °C with shaking (140 rpm). *E. coli* arctic cells (DE3)RIL were cultured in LB medium in aerobic conditions at 30 °C with shaking (250 rpm) for 3-5 hours, afterwards the temperature was lowered at 10 °C for 30′ at the same shaking conditions. Plasmid transformants in liquid cultures were selected with the addition of Ampicillin (50 µg/ml), Kanamycin (10 µg/ml) or Chloramphenicol (20 µg/ml).

3.1.4.1 Production of electrocompetent *E. coli* cells

- *E. coli* strain from the collection is plated on a LB solid medium + selection marker and incubated at 37 °C overnight
- *E. coli* colonies are gown in 50 ml of LB medium + selection marker overnight at 37 °C
- *E. coli* is inoculated in 1 L of LB medium + selection marker at the initial OD$_{600}$ = 0.05 and let it grow by shaking at 37 °C till it reaches OD$_{600}$ = 0.6-0.8
- The 1 L culture is cooled on ice for 1 h and centrifuged at 5000 rpm for 15 min at 4 °C (Beckmann J2-21, JLA10.500).
- Cell pellets are washed twice with 1 L sterile, ice-cold H$_2$O and centrifuged again
- Cell pellets are resuspended in 20 ml of 10 % glycerol and transferred in a 50 ml centrifugation tube
- The suspension is centrifuged at 5000 rpm for 20 min at 4 °C
- Cell pellet is resuspended in 2 ml of 10 % glycerol
- 50 µl aliquots are transferred in Eppendorf tubes and frozen for 1′ in liquid nitrogen
- Electrocompetent *E. coli* cells are finally frozen at -80 °C
- Transformation efficiency is determined by a test-transformation of *E. coli* cells with 1 µl of 0.01 ng pBIISK+

3.1.4.2 Production of chemical competent *E. coli* cells

• *E. coli* strain from the collection is plated on a LB solid medium + selection marker and incubated at 37 °C overnight

• *E. coli* colonies are gown in 5 ml SOB medium (20 mM $MgSO_4$) + selection marker overnight at 37 °C

• *E. coli* is inoculated in 1 L of SOB medium + selection marker at the initial OD_{600} = 0.05 and let it grow by shaking at 37 °C till it reaches OD_{600} = 0.6-0.8

• The 1 L culture is cooled on ice for 1 h and centrifuged at 5000 rpm for 15 min at 4 °C (Beckmann J2-21, JLA10.500).

• Cell pellets are resuspended with 20 ml of sterile ice-cold FSB buffer and transferred in a 50 ml centrifugation tube

• The suspension is cooled for 10′ on ice and centrifuged at 5000 rpm for 15 min at 4 °C

• Cell pellet is resuspended in 4 ml of sterile ice-cold FSB buffer

• 140 µl of DMSO is added, the suspension is gently mixed and cooled on ice for 15′

• Again 140 µl of DMSO is added, the suspension is gently mixed

• 10 µl aliquots are transferred in Eppendorf tubes and frozen for 1′ in liquid nitrogen

• Electrocompetent *E. coli* cells are finally frozen at -80 °C

• Transformation efficiency is determined by a test-transformation of *E. coli* cells with 1 µl of 0.01 ng pBIISK+

3.2 Biomolecular methods

3.2.1 Polymerase chain reaction (PCR)

Specific synthetic oligonucleotides (primers) are constructed with homology to the edges of the gene fragment of interest and, after DNA denaturation, are able to anneal to the target sequence. The DNA of interest is then amplified by a thermostable DNA polymerase.

3.2.1.1 PCR on chlamydial genomic DNA or from plasmid DNA

For PCR on chlamydial genomic DNA or plasmid DNA, 60 nt primers are constructed with homology to the gene of interest (20 nt) and homology to the vector (40 nt) in which the gene will be inserted. The annealing temperature of the primers is calculated on the 20 nt of homology to the gene with the following formula:

2 x (Adenine + Thymine) + 3 x (Guanine + Cytosine)

The elongation temperature depends on the DNA polymerase used. For PCR products which do not need proof-reading, Taq polymerase is used; while for PCR products which require error check, All-in HiFi polymerase was used. The elongation time depends on the length of the gene to be amplified (Taq: 1 min / kb, All-in: 30 sec / kb).

PCR-Mix:

Taq-Polymerase:

x µl 100 ng DNA
1 µl Oligonucleotide 1 (50 pmol)
1 µl Oligonucleotide 2 (50 pmol)
5 µl dNTP (4 mM)
5 µl Polymerase buffer (10X)
4 µl $MgCl_2$ (25 mM)
0.3 µl Taq polymerase (1 U/µl)
Up to 50 µl with H_2O

All-in HiFi polymerase:

x µl 100-500 ng DNA
1 µl Oligonucleotide 1 (50 pmol)
1 µl Oligonucleotide 2 (50 pmol)
10 µl All-in HiFi buffer
0,5 µl All-in HiFi polymerase (2 U/µl)
Up to 50 µl with H_2O

PCR-Run:

Taq-Polymerase:

- Denaturation:	5´ at 95 °C	
- Denaturation:	1´ at 95 °C	
- Annealing:	1´ at 45-55 °C	x 35 cycles
- Elongation:	1-3´ at 72 °C	
- Final Elongation:	7´ at 72 °C	
- Cooling:	Forever at 16 °C	

All-in HiFi polymerase:

- Denaturation:	1´ at 95 °C	
- Denaturation:	15´´ at 95 °C	
- Annealing:	15´´ at 55-65 °C	x 35 cycles
- Elongation:	1-3´ at 72 °C	
- Final Elongation:	30-90´´ at 72 °C	
- Cooling:	Forever at 16 °C	

3.2.1.2 PCR on yeast cells

To verify that yeast cells carry the plasmid generated by homologous recombination, single yeast colonies were picked with a pipette tip, resuspended in 15 µl H_2O and yeast cells are opened using the microwave at 600W for 15´´. The PCR is then performed with Taq polymerase.

PCR-Mix:

15 µl H_2O containing yeast colony
0,3 µl Oligonucleotide 1 (50 pmol)
0,3 µl Oligonucleotide 2 (50 pmol)
0,24 µl dNTP (25 mM)
3 µl Polymerase buffer (10X)
1,8 µl $MgCl_2$ (25 mM)
0.3 µl Taq polymerase (1 U/µl)
Up to 30 µl with H_2O

PCR-Run:

- Denaturation:	10´ at 95 °C	
- Denaturation:	1´ at 95 °C	
- Annealing:	1´ at 45-55 °C	x 40 cycles
- Elongation:	1´ at 72 °C	
- Final Elongation:	7´ at 72 °C	
- Cooling:	Forever at 16 °C	

3.2.2 Separation of DNA by agarose gel electrophoresis

Agarose gel electrophoresis is used to separate DNA fragments according to their size. Agarose gel is prepared by solving 0.7-1 % agarose in H_2O, with the addition of 1 µg / ml ethidium bromide (DNA intercalating dye). DNA samples are mixed with the DNA blue marker, loaded on the agarose gel and separated at 140 V (electrophoresis). The ethidium bromide makes the DNA fragments visible under UV light. To determine the DNA sizes, 5 µl of DNA protein standard (Gene Ruler DNA Ladder Mix) is run in the gel.

3.2.2.1 DNA elution from agarose gel

Sections of the agarose gel containing the desired DNA fragments separated by electrophoresis are cut out of the gel. The gel sections are dissolved and the DNA is eluted in H_2O using the "QIAquick Gel Extraction Kit", according to the manufacture protocol.

3.2.3 Transformation and homologous recombination in *S. cerevisiae*

Plasmid transformation in yeast is performed following the lithium acetate (LiAc) method (Gietz, Schiestl et al. 1995). The gene of interest is amplified by PCR with specific oligonucleotides (see paragraph 3.2.1). The PCR product and a linearized empty vector are transformed together in yeast. The homology of the primers to the linearized vector allows the integration of the gene of interest in the vector by homologous recombination.

- 5 ml of liquid YPD medium is inoculated with one colony of the *CEN.PK2* yeast strain and incubated with shaking (140 rpm) overnight at 30 °C

- 50 ml of YPD main culture is inoculated with the overnight culture (OD_{600} 0,1) and incubated with shaking at 30 °C for 4-5 h, until the culture contains 2 x 10^7 cells / ml (OD_{600} 1)

- The culture is harvested in a 50 ml centrifugation tube at 3500 rpm for 5′ at 30 °C (Megafuge 1.0 R)

- The medium is discarded, the cell pellet is resuspended in 25 ml of sterile H_2O and centrifuged again

- The water is discarded, the cell pellet is resuspended in 1 ml of 100 mM LiAc and transferred in a microfuge tube

- Cell pellets are obtained by centrifugation at 13000 rpm for 15′′ at RT (Biofuge Pico)

- Cell pellet is resuspended in 500 µl of 100 mM LiAc (2 x 10^9 cells / ml)

- For the transformation, 50 µl cell aliquots are transferred in new reaction tubes and centrifuged again at 13000 rpm for 15˝ at RT and the LiAc is discarded

- Carrier ss-DNA (2 mg/ml) is denatured at 100 °C for 5´ and quickly chilled on ice

- The "transformation mix" is added to the cell pellet in the following order:
  - 240 µl sterile PEG (50% w/v)
  - 36 µl of 1 M LiAc
  - 50 µl of ss-DNA
  - x µl (0.1-10 µg) linearized vector + DNA fragment (1:3 ratio) or plasmid DNA (positive control) or linearized vector only (negative control)
  - to the end volume of 360 µl with sterile H_2O

- The tubes are vigorously vortexed to resuspend the cell pellet completely

- The solution is incubated for 30´ at 30 °C

- The solution is incubated for 30´ at 42 °C

- The tubes are then centrifuged at 8000 rpm for 15˝ at RT (Biofuge Pico)

- Cells are resuspended in 100-200 µl H_2O

- 20 % and 80 % of each suspension is plated on selective plates and incubated for 2-3 days at 30 °C

- Single colonies are then picked and streaked on selective plates and used for further investigations or for plasmid isolation

3.2.4 DNA isolation from *S. cerevisiae*

DNA is isolated from *S. cerevisiae* using glass beads to disrupt the yeast cells and then applying the principle of alkaline lysis (Fink, J.B. et al. 1983).

- A single yeast colony carrying the desired plasmid is cultured into 5 ml selective liquid medium (incubated overnight with shaking at 140 rpm, 30 °C)

- 2 ml of the overnight culture are transferred into 2 ml tubes and centrifuged at 13000 Rpm (Biofuge Pico) for 5˝

- The cell pellet is resuspended in 1 ml H_2O and centrifuged at 13000 Rpm (Biofuge Pico) for 5˝

- The supernatant was discarded and the pellet is completely resuspended in 300 µl P1 buffer with 100 µg/ ml RNase

- 300 µl of P2 buffer and 2/3 of the volume of sterilized glass beads are added to break the cells with strong vibrating with 2 rounds of 20˝ at 6500 rpm (Precellys 24)

- The suspension is centrifuged at 2000 rpm (Heraeus Biofuge Pico) for 2 min and 500 µl of the supernatant is collected in a new 1,5 ml microfuge tube

- 250 µl of P3 buffer is added to the supernatant, mixed and placed on ice for 10 min

- The tube is centrifuged at top speed for 15´ and the supernatant (750 µl) obtained is transferred into a new microfuge tube

- 750 µl of ice-cold isopropanol is added and the suspension is mixed and incubated for 15´on ice

- The DNA is obtained by centrifugation at top speed for 30´ (Heraeus Biofuge Pico)

- The supernatant is removed and the pellet is washed with 500 µl of 70% ethanol and centrifuged at top speed for 10´ (Heraeus Biofuge Pico)

- The pellet containing the DNA is dried down using the speed-vac for 10´ and the dried pellet is resuspended into 20 µl of cold sterilized H_2O

- 2-10 µl of this suspension is used for *E. coli* transformation

3.2.5 Transformation in *E. coli*

3.2.5.1 One-minute transformation

One-minute transformation is a fast method to transform DNA in *E. coli* cells. The transformation efficiency is relatively low, therefore the procedure is recommended for transformation of pure plasmid DNA and it should be avoided for plasmids which contain Kanamycin resistance gene.

- 7-10 µl DMSO competent *E. coli* cells are thawed on ice

- *E. coli* cells are mixed with 1-2 µl plasmid DNA (~100 ng)

- The mix is incubated at 42 °C for 1´ and then on ice for 5´

- 100 µl of LB medium is added and the suspension is plated on agar LB + selection antibiotic and incubated at 37 °C overnight

3.2.5.2 Electroporation

- Sterilized electroporation cuvette is incubated on ice before use

- 10 µl electrocompetent *E. coli* cells are thawed on ice

- 5-10 µl DNA is placed at the bottom of the cuvette

- 10 µl *E. coli* cells are added to the DNA in the cuvette

- 100 µl sterilized H_2O is added in the cuvette

- Electroporation is performed using Bio-Rad Gene Pulser (2.1 KV, 200 Ohm and 25µF)

- Electroporated cells are resuspended in 1 ml of LB medium and incubated at 37 °C for 45´ min with shaking at 140 rpm

- Cells suspension is centrifuged at 13000 for 1´ and about 80% of the supernatant is removed

- The cell pellet is resuspended in the rest of the supernatant (about 200 µl), plated on agar LB + selection antibiotic and incubated at 37 °C overnight

3.2.6 Plasmid DNA isolation from *E. coli*

The method for plasmid DNA isolation from *E. coli* cells is based on alkaline lysis, modified by Qiagen (Sambrook and Maniatis 1989).

3.2.6.1 Plasmid DNA mini-preparation

- A single *E. coli* colony carrying the desired plasmid is cultured into 2 ml selective liquid LB medium (incubated overnight with shaking at 140 rpm, 37 °C)

- The overnight culture is transferred into 1.5 ml tube and centrifuged at 13000 Rpm (Heraeus Biofuge Pico) for 1´

- The cell pellet is resuspended in 100 µl P1 buffer with 100 µg/ ml RNase and vortexed until the pellet is resuspended

- 100 µl of P2 buffer is added to the suspension, mixed gently and placed at room temperature for 5´

- 100 µl of P3 buffer is added to the suspension, mixed gently and placed on ice for 15´

- The suspension is mixed gently and centrifuged at 13000 rpm for 10´

- The supernatant (300 µl) is transferred in a new microfuge tube, mixed vigorously with 1 ml ice-cold 98 % ethanol and placed on ice for 10´

- The suspension is centrifuged at 13000 for 20-30´

- The supernatant is discarded and the pellet is washed with 500 µl of 70 % ethanol

- The tube is centrifuged at 13000 for 10´

- The pellet containing the plasmid DNA is dried down using the speed-vac for 10´

- The dried pellet is resuspended into 100 µl of cold sterilized H_2O

3.2.6.2 Plasmid DNA midi-preparation

For the isolation of larger amount of plasmid DNA, a single *E. coli* colony carrying the desired plasmid is cultured into 50 ml selective liquid LB medium (incubated overnight

with shaking at 140 rpm, 37 °C) and the plasmid DNA is purified using the plasmid midi kit from Qiagen, according to the manufactory protocol.

3.2.7 Digestion of plasmid DNA with restriction enzymes

To linearize plasmid vector and to verify the correct insertion of a gene in the vector, restriction endonucleases are used with the corresponding specific buffers. Plasmid DNA is mixed with the selected enzymes and respective buffers and incubated for 3 hours or overnight at the indicated temperature. The resulting DNA fragments are analyzed by agarose gel electrophoresis.

3.2.8 Measuring DNA concentration

The concentration of the purified plasmid DNA is determined by spectrophotometric measurements at 260 nm by NanoDrop. 1 µl of H_2O is used to equilibrate the system and 1 µl of plasmid DNA is then measured. The absorbance read out is the concentration of DNA (ng/µl). In order to check the DNA purity, the ratio between absorbance of DNA sample at 260 nm and 280 nm is measured. If the value is in the range of 1.8 and 2.0, the plasmid DNA is considered pure.

3.2.9 Sequencing of DNA

The generated plasmids positive by restriction enzyme analysis are sequenced by GATC-Biotech.

3.3 Biochemical methods

3.3.1 Induction of gene expression in *E. coli*

Heterologous protein expression in *E. coli* is under the direct control of an inducible *lac* promoter present in the vector (pKM32) by addition of Isopropyl-β-D-thiogalactopyranosid (IPTG) (XL$_1$Blue *E. coli* strain) or under the control of an inducible T7 promoter present in the pET system based vectors (pET24a, pSL4, pFA15). Induction of T7 promoter is achieved by the expression of T7 RNA polymerase from the genome or a plasmid of DE3 *E. coli* strains (BL21, ArcticExpress and Rosetta *E. coli* strains). The induction of T7 RNA polymerase is under the control of a *lac* promoter, inducible with IPTG.

The success of gene expression is analyzed by SDS-PAGE.

1 ml of *E. coli* culture is adjusted to an OD_{600} of 1, centrifuged at 13000 rpm for 1´ (Biofuge Pico) and the cell pellet is resuspended in 32,5 µl of H_2O. 12,5 µl of protein blue marker and 5 µl of DTT are added to the suspension and boiled for 10´ at 100 °C. 10 µl are loaded on a SDS-PAGE and analyzed by Coomassie staining or immunoblotting.

3.3.1.1 Induction of gene expression in XL1 Blue and (DE3) BL21 and Rosetta *E. coli* strains

- A single *E. coli* colony carrying the desired plasmid is cultured into 2 times 50 ml selective liquid LB medium (incubated overnight with shaking at 140 rpm, 37 °C)
- *E. coli* from the overnight culture is inoculated in ½ L of selective liquid LB medium with an initial OD_{600} of 0.1
- The culture is grown at 37 °C with shaking till the culture reaches an OD_{600} of 0.8-1
- A sample before induction (T_0) is transferred in a new reaction tube and prepared for SDS-PAGE as described in 3.3.1
- Gene expression is induced with 1 mM IPTG and the culture is incubated for 4 hours at 37 °C with shaking
- A sample after induction (T_4) is transferred in a new reaction tube and prepared for SDS-PAGE as described in 3.3.1
- *E. coli* cells are then collected in centrifugation tubes and centrifuged at 5000 rpm, for 10´ at 25 °C (Beckman; JLA 10,500)
- The cell pellet is washed with 40 ml of sterile PBS and collect in a 50 ml centrifugation tube
- The suspension is centrifuged at 4600 rpm for 15´ at 25 °C (Megafuge 1.0R)

The cell pellet is resuspended in 20 ml/L of lysis buffer and incubated overnight before purification or is resuspended in 1 ml of sterile PBS and frozen at – 20 °C

3.3.1.2 Induction of gene expression in ArcticExpress (DE3) RIL *E. coli* strain

- A single *E. coli* colony carrying the desired plasmid is cultured into 50 ml selective liquid LB medium, containing 20 µg/ml Gentamycin (incubated overnight with shaking at 220-250 rpm, 37 °C)
- *E. coli* from the overnight culture is inoculated in 1 L of selective liquid LB medium with an initial OD_{600} of 0.1
- The culture is grown at 30 °C with shaking for 3-5 hours (till the culture reaches an OD_{600} of 0.6-0.8)

- The culture is transferred to 10-13 °C and incubated with shaking for 30′

- A sample before induction (T_0) is transferred in a new reaction tube and prepared for SDS-PAGE as described in 3.3.1

- After temperature equilibration, gene expression is induced with 1 mM IPTG and the culture is incubated for 24 hours at 10-13 °C with shaking

- A sample before induction (T_{24}) is transferred in a new reaction tube and prepared for SDS-PAGE as described in 3.3.1

- *E. coli* cells are then collected in centrifugation tubes and centrifuged at 5000 rpm, for 10′ at 25 °C (Beckman; JLA 10,500)

- The cell pellet is washed with 40 ml of sterile PBS and collect in a 50 ml centrifugation tube

- The suspension is centrifuged at 4600 rpm for 15′ at 25 °C (Megafuge 1.0R)

- The cell pellet is resuspended in 20 ml/l of lysis buffer and incubated overnight before purification or is resuspended in 1 ml of sterile PBS and frozen at − 20 °C

3.3.2 *E. coli* cells lysis to extract heterologous proteins

In order to extract the expressed heterologous protein, *E. coli* cells are lysed under native or denaturing conditions, using lysozyme and Urea or Guanidine-HCl, respectively. Different detergents have been added in the native and denaturing lysis buffers, in order to optimize the amount of soluble heterologous protein Yaa3 (see paragraph 4.2.2.1).

3.3.2.1 *E. coli* cells lysis under native conditions

- *E. coli* cell pellet containing the expressed heterologous protein was resuspended in 20 ml/l of native lysis buffer:

   - PBS +1 mg/ml lysozyme + 1mM PMSF + 1 % Proteases Inhibitor cocktail
   - PBS +1 mg/ml lysozyme + 1mM PMSF + 1 % Proteases Inhibitor cocktail + 1 % triton
   - PBS +1 mg/ml lysozyme + 1mM PMSF + 1 % Proteases Inhibitor cocktail + 1 % triton + 1 % sarkosyl
   - PBS +1 mg/ml lysozyme + 1mM PMSF + 1 % Proteases Inhibitor cocktail + 1 % sarkosyl
   - PBS +1 mg/ml lysozyme + 1mM PMSF + 1 % Proteases Inhibitor cocktail + 0.3 % SDS
   - Ripa buffer, pH 8
   - 50 mM NaH_2PO_4 + 300 mM NaCl + 1 mg/ml lysozyme + 1 % Proteases Inhibitor cocktail
   - 50 mM Tris/HCl + 10 mM EDTA + 10 mM $MgCl_2$ + 1 mg/ml lysozyme

- 20 mM Tris/HCl + 137 mM NaCl + 10 % glycerol + 1 % NP-40

- The suspension is incubated on the wheel at 4 °C, overnight

- In the morning, the suspension is sonicated for 3 times 10′′ on ice

- 32,5 µl of "lysate sample" is transferred in a microfuge tube

- Lysate is then centrifuged at 24000 rpm for 1 h at 4 °C (Beckman; JA 25,50)

- 32,5 µl of "supernatant sample" is transferred in a microfuge tube

- The pellet is resuspended in 20 ml of PBS, 32,5 µl of "pellet sample" is transferred in a microfuge tube

- The supernatant containing soluble *E. coli* proteins and the heterologously produced protein is stored at 4 °C for further analysis

3.3.2.2 *E. coli* cells lysis under denaturing conditions

- *E. coli* cell pellet containing the expressed heterologous protein is resuspended in 20 ml/l of denaturing lysis buffer:

    - Buffer B (containing 8M Urea)
    - Buffer B + 1-3 % triton
    - Buffer B + 1 % triton + 1 % sarkosyl
    - Buffer B + 0.1-0.3 % SDS
    - Buffer B + 300 mM NaCl
    - Buffer A1 (containing 6 M Guanidine HCl)
    - Buffer A1 + 1-3 % triton
    - Buffer A1 + 1 M NaCl
    - Buffer A1 + 10 % ethanol

- The suspension is incubated on the wheel at 4 °C, overnight

- The morning after the suspension is sonicated for 3 times 10′′ on ice

- 32,5 µl of "lysate sample" is transferred in a microfuge tube

- Lysate is then centrifuged at 24000 rpm for 1 h at 4 °C (Beckman; JA 25,50)

- 32,5 µl of "supernatant sample" is transferred in a microfuge tube

- The pellet is resuspended in 20 ml of PBS, 32,5 µl of "pellet sample" is transferred in a microfuge tube

- The supernatant containing soluble *E. coli* proteins and the heterologous produced protein is stored at 4 °C for further analysis

3.3.3 Extraction of *E. coli* outer membrane and periplasmic fractions

3.3.3.1 TSE periplasmic extraction

To separate the periplasmic fraction of *E. coli* cells, a method based on Tris-sucrose-EDTA (TSE) buffer has been adopted (Quan, Hiniker et al. 2013).

- *E. coli* cells containing the expressed protein of interest in the periplasm are harvested by centrifugation at 3760 rpm for 20′ at 4 °C (Beckman)
- The supernatant is carefully removed
- The pellet is gently resuspended in 1 ml of TSE buffer using a wire loop (vortex and vigorous pipetting are not recommended, because they could break the cells and contaminate the periplasmic fraction with cytoplasmic proteins)
- The solution is incubated on ice for 30′
- The solution is centrifuged at 13000 rpm for 30′ at 4 °C
- The supernatant obtained contains the envelope extract (outer membrane and periplasmic fractions) and the pellet the cytoplasmic fraction
- To separate periplasmic and outer membrane fractions, the supernatant is centrifuged at 100′000 g for 1 h at 4 °C. The pellet obtained contains the outer membrane fraction, while the supernatant contains the periplasmic fraction

3.3.3.2 Osmotic shock periplasmic extraction

To separate the periplasmic fraction of *E. coli* cells, a second method based on osmotic shock was used and adapted from the protocol for PeriPreps™ Periplasting Kit (Epicenter Biotechnologies, Madison, WI, USA).

- *E. coli* cells containing the expressed protein of interest in the periplasm are harvested by centrifugation at 3760 rpm for 20′ at 4 °C (Beckman)
- The supernatant is carefully removed
- The pellet is gently resuspended in 0,5 ml of TSE buffer using a wire loop (vortex and vigorous pipetting are not recommended, because they could break the cells and contaminate the periplasmic fraction with cytoplasmic proteins)
- The solution is incubated on ice for 15′
- 0,5 ml of ice-cold H_2O was added
- The solution was incubated on ice for additional 15′

- The solution is centrifuged at 13000 rpm for 30′ at 4 °C

- The supernatant obtained contains the envelope extract (outer membrane and periplasmic fractions) and the pellet the cytoplasmic fraction

- To separate periplasmic and outer membrane fractions, the supernatant is centrifuged at 100′000 g for 1 h at 4 °C. The pellet obtained contains the outer membrane fraction, while the supernatant contains the periplasmic fraction

3.3.4 Purification of heterologously expressed proteins by affinity chromatography

His-tagged or GST-tagged proteins can be purified from *E. coli* cell lysate by affinity chromatography, using columns with Ni-NTa or glutathione agarose, respectively.

3.3.4.1 Purification of GST-fusion proteins under native conditions using manual columns

- The supernatant containing soluble *E. coli* proteins and the heterologous GST-tagged protein of interest is obtained, as described in paragraph 3.3.2.1

- 70 mg of glutathione agarose are diluted in 200 ml / g of H_2O for 1 h, at RT

- The glutathione agarose is washed with PBS and incubated with the supernatant on the wheel at 4 °C for 3 h

- A manual protein purification column, containing a filter, is filled with the supernatant + glutathione agarose and let it flow through

- A sample of 32,5 µl of the "Flow through" is collected for SDS-PAGE analysis

- The agarose and the bound proteins do not flow through the filter

- The column is then washed two times with 10 ml PBS

- A sample of 32,5 µl of the "Washing" is collected for SDS-PAGE analysis

- GST-tagged proteins are eluted from the agarose with 5 times 1 ml of 50 mM Tris + 10 mM reduced Glutathione (5′ incubation time before collection of the elution fractions)

3.3.4.2 Purification of His-fusion proteins under native conditions using manual columns

- The supernatant containing soluble *E. coli* proteins and the heterologous GST-tagged protein of interest is obtained as described in paragraph 3.3.2.1

- 800 µl of Ni-NTa agarose is washed with PBS and incubated with the supernatant on the wheel at 4 °C for 3 h

- A manual protein purification column, containing a filter, is filled with the supernatant + Ni-NTa agarose and let it flow through, at 4 °C

- A sample of 32,5 µl of the "Flow through" is collected for SDS-PAGE analysis

- The agarose and the bound proteins do not flow through the filter

- The column is then washed two times with 10 ml PBS and two times with 10 ml PBS + 40 mM Imidazole, at 4 °C

- A sample of 32,5 µl of the "Washing" is collected for SDS-PAGE analysis

- His-tagged proteins are eluted from the agarose with 5 times 1 ml of 1 M PBS + 500 mM Imidazole (5´ incubation time before collection of the elution fractions) , at 4 °C

3.3.4.3 Purification of His-fusion proteins under denaturing conditions using manual columns

- The supernatant containing soluble *E. coli* proteins and the heterologous His-tagged protein of interest is obtained, as described in paragraph 3.3.2.2

- 800 µl of Ni-NTa agarose is washed with PBS and incubated with the supernatant on the wheel at RT for 2-3 h

- A manual protein purification column, containing a filter, is filled with the supernatant + Ni-NTa agarose and let it flow through

- A sample of 32,5 µl of the "Flow through" is collected for SDS-PAGE analysis

- The agarose and the bound proteins do not flow through the filter

- The column is then washed two times with 10 ml Buffer A1 (or Buffer B) and two times with 10 ml Buffer A2 (or Buffer B) + 50 mM Imidazole (according to the lysis buffer used)

- A sample of 32,5 µl of the "Washing" is collected for SDS-PAGE analysis

- His-tagged proteins are eluted from the agarose with 5 times 1 ml of 1 M Buffer A2 (or Buffer C) + 500 mM Imidazole (5´ incubation time before collection of the elution fractions)

3.3.4.4 Purification of His-fusion proteins under denaturing conditions using His-trap Nickel columns

- The supernatant containing soluble *E. coli* proteins and the heterologous His-tagged protein of interest is obtained, as described in paragraph 3.3.2.2

- HiTrap™ 5 ml Chelating HP (Nickel column) is connected to a peristaltic pump, getting rid of air bubbles

- The column is washed with 3 column volumes of H_2O

- The column is washed with 3 column volumes of Buffer A1

- The supernatant is loaded in the column

- A sample of 32,5 µl of the "Flow through" is collected for SDS-PAGE analysis

- The column is washed with 3 column volumes of Buffer A1 + 20 mM Imidazole

- The column is washed with 3 column volumes of Buffer A2 + 50 mM Imidazole

- A sample of 32,5 µl of the "Washing" is collected for SDS-PAGE analysis

- His-tagged proteins are eluted from the column with 10-15 ml of Buffer A2 + 500 mM Imidazole (collected in 1 ml fractions)

- The column is washed with 3 column volumes of H_2O

- The Nickel sulfate is stripped from the HiTrap column and the column is recharged with new Nickel sulfate, as described in paragraph 3.3.4.4.1

- The column is washed with 3 column volumes of 20 % ethanol and store at 4 °C

3.3.4.4.1 Stripping and recharging Nickel columns

- Connect a HiTrap™ 5 ml Chelating HP to a peristaltic pump, getting rid of air bubbles

- The column is washed with 3 column volumes of H_2O

- The column is washed with 3 column volumes of Stripping buffer

- The column is washed with 3 column volumes of H_2O

- The column is recharged with 10 ml 0,1 M Ni-SO_4

- The column is washed with 3 column volumes of H_2O

- The column is washed with 3 column volumes of 20 % ethanol and store at 4 °C

3.3.4.4.2 Cleaning Nickel columns

- Connect a HiTrap™ 5 ml Chelating HP to a peristaltic pump, getting rid of air bubbles

- The column is washed with 3 column volumes of H_2O

- The column is washed with 3 column volumes of Acetic Acid

- The column is washed with 3 column volumes of H_2O

- The column is washed with 3 column volumes of 0,5M NaOH

- The column is washed with 3 column volumes of H_2O

- The column is washed with 3 column volumes of 1% Triton + 5M Urea

- The column is washed with 3 column volumes of Isopropanol

- The column is washed with 3 column volumes of H_2O

- The column is washed with 3 column volumes of 20 % ethanol
- The Nickel sulfate is stripped from the HiTrap column and the column is recharged with new Nickel sulfate, as described in paragraph 3.3.4.4.1

3.3.5 Refolding of denatured purified proteins

To renature recombinant proteins purified under denaturing conditions, two methods have been used based on buffer exchange: A slow refolding method (dialysis) and a fast refolding method (centrifugation using Amicon columns).

3.3.5.1 Protein refolding by dialysis

- A 5 cm long dialysis tube (12-15 kDa cut-off) is boiled together with the dialysis clips for 10' in H_2O and then cooled on ice-cold sterile H_2O
- The purified recombinant protein is diluted at the desired concentration is the denaturing elution buffer and added in the dialysis tube
- The dialysis tube containing the protein is then closed with the dialysis clips and immersed in 2 L of ice-cold sterile PBS (dialysis buffer)
- Dialysis buffer is exchanged three times every 12 h, for a total of 36 h dialysis
- The refolded proteins are then transferred in a new reaction tube
- The sample is centrifuged at 10000g for 10' at 4 °C to remove precipitated aggregates (Biofuge Primo R) and stored at 4 °C

3.3.5.1.1 Co-refolding

- Two denatured proteins are mixed in the same reaction tube in a 1:1 molar ratio at the total concentration of 1 mg/ml in the elution buffer
- The sample is transferred in a dialysis tube and dialyzed as described in paragraph 3.3.5.1
- The co-refolded proteins are then transferred in a new reaction tube
- The sample is centrifuged at 10.000g for 10' at 4 °C to remove precipitated aggregates (Biofuge Primo R) and stored at 4 °C

3.3.5.1.2 Mixing

- Two already renatured proteins are mixed in the same reaction tube in a 1:1 molar ratio at the total concentration of 1 mg/ml in sterile PBS

- The sample is transferred in a dialysis tube and dialyzed as described in paragraph 3.3.5.1 for 12 h

- The mixed proteins are then transferred in a new reaction tube

- The sample is centrifuged at 10000g for 10' at 4 °C to remove precipitated aggregates (Biofuge Primo R) and stored at 4 °C

3.3.5.2 Protein refolding using Amicon columns

- The purified recombinant protein is adjusted to the desired concentration in the denaturing elution buffer

- The denatured protein is diluted 1:20 in 20 ml of ice-cold sterile PBS or ice-cold sterile PBS + 100-200 mM Arginine (refolding buffer)

- The sample is loaded on a Amicon Ultra-15 Centrifugal Filter Units column and centrifuged at 3500 rpm, 4 °C for 3-6 h (Megafuge 1.0R), until reached the desired final volume

- The sample retained from the Amicon filter, containing the protein, is resuspended by pipetting and transferred in a new reaction tube

- The sample is centrifuged at 10000g for 10' at 4 °C to remove precipitated aggregates (Biofuge Primo R) and stored at 4 °C

3.3.6 Measuring protein concentration with Bradford

The Bradford method for the determination of protein concentration is based on a specific color reaction using Coomassie Brilliant Blue G250. Coomassie dye binds the proteins in the sample and forms complexes with an absorption maximum of $\lambda = 595$ nm, while the not bound dye has an absorption maximum of $\lambda = 465$ nm. The protein concentration of the sample is determined by means of the adsorption values of a standard curve (0 µg - 10 µg, in 2 µg steps) with bovine serum albumin (BSA). The measurement is carried out by adding in a cuvette 790 µl H_2O + 200 µl Bradford reagent and 10 µl protein sample (or 10 µl protein buffer as blank). The mix is incubated 10' at RT and the absorption at 595 nm is determined with the BioPhotometer plus.

The protein concentration is calculated with the formula:

Protein concentration (µg/ml) = absorption sample at 595 nm X dilution factor (100 for 10 µl protein) / Bradford factor (0,057).

3.3.7 EB membrane protein solubilization

In order to analyze EB membrane proteins via mass spectrometry and immunoblotting, HEp-2 cells have been infected with *Chlamydia* EBs in cell culture polystyrol 25 cm^2 flasks. In order to increase the amount of solubilized proteins from the EB membrane, different conditions and detergent were used in addition to the Phospholysis buffer. Cross-linker was used to stabilize the natural protein-protein interactions.

- Infection is carried out till the end of the chlamydial cycle (80 hpi for *C. pneumoniae* and 50 hpi for *C. trachomatis*)
- Osmotic lysis with 1 ml/ flask of deionized H$_2$O for 15', RT
- Resuspend the lysed cells gently by pipetting and transferred in a reaction tube
- Centrifuge at 2000 rpm, 5', RT (Biofuge Pico)
- Transfer the supernatant in a new centrifugation tube and add:

  1.

  - Phospholysis buffer for 15', on the wheel, RT
  - Add detergents for 2h, on the wheel at 4 °C:
    - None
    - + 50 mM DTT
    - + 10 % β-Mercaptoethanol
    - + 10 % β-Mercaptoethanol + 50 mM DTT
    - + 2 mM DTSSP (Stop reaction by incubating with 50 mM Tris, pH 7.5)
    - + 2 % sarkosyl + 2 % SDS + 10 mM DTT + 10 % β-Mercaptoethanol
    - + 2 % sarkosyl+ 2 % SDS + 50 mM DTT

  2.
  - 2 mM DTSSP cross linker (stock: 25 mM in PBS) for 2h, 4 °C on the wheel
    - Stop reaction with 50 mM Tris, pH 7.5, for 15', 4 °C on the wheel
  - Add detergents for 2h, on the wheel at 4 °C:
    - + 2 % sarkosyl+ 2 % SDS + 50 mM DTT
- The solubilized sample is used for co-immunoprecipitation with specific antibodies

3.3.8 Protein separation via SDS-PAGE

In a SDS-PAGE (polyacrylamide gel electrophoresis), denatured proteins are separated according to their monomeric size.

3.3.8.1 SDS-PAGE sample preparation

- X µl protein sample is filled with 32,5 µl H_2O at the desired concentration

- 12,5 µl protein blue marker and 5 µl DTT are added to the sample (final volume 50 µl)

- The mix is boiled on a thermo block for 10-15' at 100 °C

- The sample is cooled on ice and centrifuged for 5'' at 13000 rpm, RT (Biofuge Pico)

3.3.8.1.1 Ethanol precipitation

Samples containing Guanidine-HCl are not able to run into the SDS-PAGE, because the Guanidine-HCl precipitates the SDS. Therefore the Guanidine-HCl is removed from the sample by ethanol precipitation, before SDS-PAGE.

- 25 µl protein sample is mixed with 225 µl ice-cold 96 % ethanol

- The mix is incubated at -20 °C for 10'

- The sample is centrifuged at 13000 rpm for 5', RT (Biofuge Pico)

- Pellet is washed with 250 µl ice-cold 90 % ethanol and centrifuged again

- Ethanol is carefully removed with a pipette tip

- Protein pellet is resuspended in 32,5 µl H_2O + 12,5 µl protein blue marker + 5 µl DTT

- The sample is boiled on a thermo block for 15-20' at 100 °C

- The sample is cooled on ice and centrifuged for 5'' at 13000 rpm, RT (Biofuge Pico)

3.3.8.2 Preparation of SDS polyacrylamide gels

- The running gel mix is prepared with TEMED added right before pouring

- The running gel buffer is poured in between 7 x 9 cm glass and aluminum plates

- The running gel buffer is covered with 1 ml of isopropanol and left till it is polymerized

- The isopropanol is removed carefully, washing with H_2O

- The stacking gel mix is prepared with TEMED added right before pouring

- The stacking gel buffer is added on top of the running gel, without air bubbles

- A comb is inserted in the stacking gel buffer and left till the stacking gel is polymerized

Preparation for 4 SDS-PAGE gels:

Material	Running gel		Stacking gel
	10 %	15 %	
ddH$_2$O	8,4 ml	5 ml	6 ml
4 X running / stacking buffer	5 ml	5 ml	2,5 ml
30 % Acrylamide (30:0.8)	6,7 ml	10 ml	1,5 ml
10 % APS	200 µl	200 µl	200 µl
TEMED	50-100 µl	50-100 µl	50 µl

3.3.8.3 SDS-PAGE electrophoresis

The SDS gel is clamped in the electrophoresis chamber (Hoefer Se 260) after removing the comb and the chamber is filled with 1 X running buffer. 10-25 µl sample is loaded in the pockets. 5-10 µl protein ladder is loaded in one pocket. Electrophoresis takes places at 200 V for 70' (10 % gels) and 80' (15 % gels).

3.3.9 Native protein separation via Blue Native-PAGE

In a Blue Native-PAGE (polyacrylamide gel electrophoresis), the Coomassie brilliant blue G250, present in the buffer confers a negative net charge, while maintaining the proteins in their native conformation. Therefore, native proteins are separated according to their conformation and their size. The Blue Native gel used is NativePAGE Novex Bis Tris Gel system, harboring a 3-12 % Acrylamide gradient, and is used according to the manufacture protocol (Life technologies).

3.3.9.1 Blue Native-PAGE sample preparation

- X µl native protein sample is calculated for the final desired concentration of 1 or 2 µg
- 5 µl Native PAGE Sample buffer (4X)
- Up to 20 µl with H$_2$O

3.3.9.2 Blue Native-PAGE electrophoresis

- The Blue Native gel cassette is removed from the manufactured storing plastic bag
- The tape is removed from the bottom of the cassette
- The comb is removed and the wells are washed with the Cathode buffer
- The cassette is locked into place in the XCell SureLock Mini-Cell
- The inner chamber is filled with Native PAGE Light Blue buffer (Cathode buffer)
- The samples are loaded in the wells

- 5 µl NativeMark unstained protein ladder is loaded in one pocket

- The outer chamber is filled with Native PAGE Anode Buffer

- The XCell SureLock Mini-Cell is closed

Electrophoresis is performed in the cold room at 150 V (8-10 mA) for 60´and then at 250 V (2-4 mA) for 90´.

3.3.10 Protein separation via second dimension SDS-PAGE

- The desired Blue Native band is cut out of the gel (First dimension)

- The first dimension band is placed at the top position in between 7 x 9 cm glass and aluminum plates (cassette)

- The running gel mix is prepared, as indicated in 3.3.8.2 and poured in the cassette

- The running gel buffer is covered with isopropanol and left till it is polymerized

- The isopropanol is removed carefully, washing with H_2O

- The stacking gel mix is prepared, as indicated in 3.3.8.2

- The stacking gel buffer is added on top of the running gel, covering the first dimension band completely, avoiding air bubbles

- A comb is inserted in the stacking gel buffer, to create the pocket for the protein ladder

- Electrophoresis takes places at 200 V for 90', as indicated in 3.3.8.3

3.3.11 Coomassie-staining of SDS-PAGE and Blue Native-PAGE

- SDS and Blue Native gels are transferred in a box containing H_2O

- The gel is heated in a microwave at 600 W for 30' and let it shake at 40 rpm

- The gel is washed with fresh H_2O three times and water is discarded

- The gel is immersed in Coomassie solution (filtered for Blue Native gels)

- The gel is heated in a microwave at 600 W for 10' and let it on the shaker at RT (40 rpm) till the protein bands appear

- Coomassie solution is discarded and the gel is washed with H_2O to remove the staining background

3.3.12 Western blot and immunodetection of SDS-PAGE and Blue Native-PAGE

The proteins in the gel are transferred to a PVDF membrane. The proteins on the membrane can then be visualized using specific antibodies. The primary antibody targets

the protein or the protein tag and the secondary antibody targets the first antibody. The secondary antibody is conjugated with alkaline phosphatase (AP), which, in the presence of BCIP/NBT, catalyzes a color reaction.

3.3.12.1 Protein transfer to a PVDF membrane

- Two Whatman papers (10 x 7) and a PVDF membrane (9 x 7) are cut
- The PVDF membrane is activated with methanol for 5-10', RT
- Whatman papers and PVDF membrane are equilibrated in the 1 X transfer buffer
- The blot is prepared on the metal plate of the Pierce G2 Fast Blotter in the following order: Whatman paper + PVDF membrane + gel + Whatman paper
- The proteins are transferred at 25 V, 1A for 15-30'
- The PVDF membrane is incubated with the blocking solution for 30', RT, shaking

3.3.12.1.1 Protein transfer to a PVDF membrane from a Coomassie-stained gel

- Proteins are transferred to PVDF membrane, as described in paragraph 3.3.12.1
- The proteins are immobilized on the membrane by incubation for 10' in 8 % acetic acid
- The Acetic acid is discarded and the Coomassie staining is removed with methanol
- The membrane is then washed with PBS three times
- The PVDF membrane is incubated with the blocking solution for 30', RT, shaking

3.3.12.2 Protein immunodetection

- The primary antibody is diluted in the blocking solution
- The PVDF membrane is incubated on the wheel with the primary antibody for 2 h, at RT or ON at 4 °C
- The membrane is washed three times every 10' with PBS, shaking at 40 rpm
- The AP-conjugated secondary antibody is diluted in the blocking solution
- The membrane is incubated on the wheel with the secondary antibody for 1 h at RT
- The membrane is washed three times every 10' with PBS, shaking at 40 rpm
- The PVDF membrane is then incubated with 20 ml detection buffer + 33 µl BCIP solution + 33 µl NBT solution
- The membrane is incubated in darkness till the bands appear
- The reaction is stopped by washing with H_2O

3.3.13 Protein separation via Size Exclusion Chromatography (SEC)

Protein separation by SEC is performed with a chromatography column packed with a porous stationary phase, through which the buffer, containing the protein of interest is running. The principle of separation is based on the fact that the proteins in the buffer penetrate the pores of the stationary phase and therefore its elution is delayed according to the velocity of the buffer flow. Smaller proteins, which are retained in the pores longer than larger molecules, are eluted later. Proteins which are larger than the column pores are not able to enter the stationary phase and therefore are not separated and elute in the Void volume (V_0). The retention time, and therefore the separation, does not depend on the proteins molecular mass, but on their size and shape, therefore it is only possible to determine an apparent molecular weight of the eluted proteins, according to the elution of standard globular proteins with known size.

For SEC analysis of Pmp proteins, a Superose 6, 10/300 GL column was connected with an ÄKTA Purifier (GE Healthcare) and washed from the ethanol used for storage. 1 ml of running buffer (PBS) was loaded on the column to wash the loop, followed by loading of refolded Pmp proteins. SEC was performed with a flow rate of 0,3 ml/min in PBS buffer and fractions of 0,5 ml were collected. Protein concentration in the fractions was determined by Bradford assay and protein samples were analyzed by SDS-PAGE. SEC elution profiles were analyzed by PrimeView program (GE healthcare).

Basic parameters	
Sample	700 µl (1 mg/ml) in PBS
Base column volume	23,562 ml
Max pressure	0,5 MPa
Flow	0,3 ml/min

Volume (ml)	Steps
0,00	Gradient 0,0 % B
10,00	Autozero UV
11,00	Injection
12,00	Load
14,00	Fractionation 900 0,5 ml
40,00	Fractionation Stop
40,00	Gradient 100 % B
70,00	End method

3.3.14 Labeling proteins with biotin

- 2,2 mg of EZ-Link Sulfo-NHS-biotin is resuspended in 500 µl of PBS (final concentration: 10 mM)

- X µl of biotin solution is added to the protein in a 20 fold molar excess, according to the calculation:

X µl Biotin = (y mg Protein / z Da of protein molecular weight) x 20 x 100.000

- The protein-biotin solution is incubated on ice for 2 h

- The reaction is quenched with 1 M Tris pH 7,5 at a final concentration of 50 mM

- The solution is dialyzed overnight in PBS at 4 °C

3.3.15 Labeling proteins with FITC

- 1 mg of NHS-fluorescein (FITC) is resuspended in 100 µl of DMSO

- X µl of fluorescin solution is added to the protein in a 20 fold molar excess, according to the calculation:

X µl FITC = (y mg Protein / z Da of protein molecular weight) x 20 x 47.340

- The protein-FITC solution is incubated on ice for 2 h

- The reaction is quenched with 1 M Tris pH 8 (final concentration: 50 mM) for 1h on ice

- The solution is dialyzed overnight in PBS at 4 °C

3.3.16 Protein-Protein interaction assays

3.3.16.1 Far Western-Blot and Far Western Dot-Blot assays

Far Western-Blot is performed to detect direct protein-protein interaction *in vitro*.

   Far Western-Blot:

- 1 µg of prey proteins are separated by SDS-PAGE and blotted on a PVDF membrane (Far Western-Blot)

   Far Western Dot-Blot:

- 1 µg of prey proteins are loaded as a drop on an activated PVDF membrane and let enter via capillary forces at RT.

- The proteins are immobilized on the membrane by incubation for 10' in 8 % acetic acid

- The Acetic acid is discarded and the membrane is washed with PBS three times for 10´

- The denatured prey proteins on the membrane are at first completely denatured with 8 M Guanidine-HCl

- The prey proteins are then slowly renatured, by incubation with several buffers with a decreasing concentration of Guanidine-HCl, in order to restore the native protein conformation

Guanidine-HCl [M]	6	3	1	0,1	0
Glycerin (ml)	5	5	5	5	5
5 M NaCl (ml)	1	1	1	1	1
1 M Tris pH 7,5 (ml)	1	1	1	1	1
0,5 M EDTA (ml)	0,1	0,1	0,1	0,1	0,1
20 % Tween-20 (ml)	0,25	0,25	0,25	0,25	0,25
Milk powder (g)	1	1	1	1	2
1 M DTT (ml)	0,05	0,05	0,05	0,05	0,05
8 M Guanidine-HCl (ml)	37,5	18,6	6,3	0,6	0
H_2O (ml)	3,8	22,8	35	40,8	41,4
Final Volume (ml)	50	50	50	50	50
Minutes / T °C	30/RT	30/RT	30/RT	30/4°C	ON/4°C

- After renaturation, the membrane is incubated with the biotinylated native bait protein (2μg/ml in blocking solution) for 2 h or overnight at 4 °C

- The membrane is washed three times for 10′ with PBS

- The membrane is incubated with the AP-conjugated anti-streptavidin antibody for 1 h

- The membrane is washed three times for 10′ with PBS

- The protein-protein interaction is detected with NBT/BCIP solution

3.3.16.2 Pull-down assay of recombinant proteins via affinity chromatography

Pull-down assays are performed to detect direct protein-protein interaction *in vitro* by immunoaffinity chromatography, using two recombinant proteins fused with different tags.

- VSV-tagged protein X is expressed in *E. coli,* as indicated in paragraph 3.3.1.1

- *E. coli* cells are lysed under native conditions (PBS + 1 mg/ml lysozyme + 1mM PMSF + 1 % Proteases Inhibitor cocktail + 1 % sarkosyl)*,* as indicated in paragraph 3.3.2.1

- The suspension is incubated on the wheel at 4 °C, overnight

- The morning after the suspension is sonicated for 3 times 10′′ on ice

- The lysate is then centrifuged at 24000 rpm for 1 h at 4 °C (Beckman Avanti J-25; JA 25,50)

- The supernatant containing the soluble VSV-tagged protein X is incubated with 1 mg/ml of native His-tagged protein Y for 4 h or overnight on the wheel at 4 °C

- The protein suspension is centrifuged at 12000 rpm for 20′ at 4 °C (Beckman Avanti J-25; JA 25,50)

- The protein suspension is loaded on a HiTrap™ 5 ml Chelating HP Nickel column (with affinity for the His-tag), connected to a peristaltic pump

- A sample of 32,5 µl of the "Flow through" is collected for SDS-PAGE analysis

- The column is washed with 3 column volumes of PBS

- The column is washed with 3 column volumes of PBS + 50 mM Imidazole

- A sample of 32,5 µl of the "Washing" is collected for SDS-PAGE analysis

- His-tagged Protein Y is eluted from the column with 5-6 ml of PBS + 500 mM Imidazole (collected in 1 ml fractions)

- If the VSV-tagged Protein X interacts with the His-tagged Protein Y, both proteins are eluted together in the same elution fractions

- If the VSV-tagged Protein X does not interact with the His-tagged Protein Y, Protein X is found in the flow-through and washing samples, while Protein Y is found in the elution samples.

3.3.16.3 MicroScale Thermophoresis (MST)

Protein-Protein *in vitro* interactions were quantified with MicroScale Thermophoresis, performed in the department of Molecular Mycology, at the Heinrich-Heine-University of Düsseldorf. In MST measurements, a labeled protein at a fixed concentration is mixed with a second protein in 14 different concentrations (serial dilutions 1:1) and loaded on glass capillaries (NT.115 series, standard treated). The proteins in the capillaries are exposed to a temperature gradient, which causes the movement of the molecules (thermophoresis). The movement depends on many parameters, such as molecular size and charge. When the two proteins interact with each other, there will be a change of the labeled protein thermophoresis from the completely non-bound to the completely bound state with the unlabeled protein, depending on its concentration. In each of these forms, the parameters are compared in plots, which are used to fit a curve and elaborate the dissociation constant (Kd). Kd above 600µM indicates no binding between two molecules.

- Protein X is labeled with NHS-Fluorescin and is diluted in HEPES/KOH buffer, pH 9
- 25 nM of labeled protein is mixed with 14 serial dilutions of non-labeled Protein Y (initial concentration 25 µM) at a final volume of 12 µl
- The proteins are incubated for 5´ at RT and then loaded on the capillaries
- MST measurements are performed with Monolith NT.115 (Nano Temper)

3.3.16.4 Co-immunoprecipitation from infected cells

In order to analyze EBs membrane proteins via Mass spectrometry and immunoblotting, chlamydial EB membrane proteins are solubilized as described in paragraph 3.3.7 and co-immunoprecipitated using a specific antibody.

- 150 µl Protein G Agarose is loaded on mini-centrifugation columns and washed with PBS
- 2 µg of purified antibody or serum (1:25 / 1:50) is coupled on the Protein G Agarose
- The suspension is incubated on the wheel for 1-2 h at 4 °C
- The Antibody-Protein G Agarose suspension is incubated with the EB solubilized protein sample on the wheel, overnight at 4 °C
- 100 µl "Input" sample (1/50 of the lysate) is collected for SDS-PAGE analysis
- The day after, the solution is run through the mini-centrifugation column
- 100 µl "Flow through" sample is collected for SDS-PAGE analysis
- The column is washed three times with PBS
- 100 µl "Washing" sample is collected for SDS-PAGE analysis
- The antibody and its bound proteins are eluted from the agarose with three times 80 µl of Glycine pH 2.5, incubating for 5´
- The pH of the elution fractions is neutralized with 15 µl of 1 M Tris, pH 9
- 45 µl of the elution fractions are mixed with 10 µl DTT and 25 µl protein blue marker and analyzed by SDS-PAGE
- The remain elution fraction samples are analyzed by immunoblotting and mass spectrometry analysis

3.3.17 Mass-spectrometry analysis

In order to identify interaction partner of specific proteins, co-immunoprecipitation has been performed as described in paragraph 3.3.16.4 and the sample has been analyzed by Liquid chromatography–mass spectrometry (LC-MS), performed by Dr. Daniel Waldera-

Lupa at the Biological-Medical Research Center (BMFZ) at the Heinrich-Heine-University of Düsseldorf, in the department of Prof. Dr. Kai Stühler.

3.3.18 Transmission Electron Microscopy (TEM)

Recombinant proteins have been analyzed by TEM, in order to visualize their structures. TEM analyses have been performed using the E902 electron microscope (Zeiss) at 80 kv provided from the Centre for Advanced Imaging (CAi) at the Heinrich-Heine-University of Düsseldorf, with the assistance of Mrs. Marion Nissen.

- S162 Formvar carbon-coated copper grids (Plano) are made hydrophilic in a Plasma cleaner (Electronic Diener, Femto), by incubating for 11 seconds at 0,3 mbar
- Recombinant protein is diluted at a concentration of 0,5 μM in PBS
- 10 μl of recombinant protein is loaded on the grids net for 5′ at RT
- The protein solution is removed with the edge of Whatman paper
- The protein on the grid is washed three times with ddH_2O
- The water is removed with the edge of Whatman paper
- The negative staining is achieved by incubating 10 μl of 1 % Uranyl acetate on the grid for 1′ at RT
- The solution is removed with the edge of Whatman paper and dry at RT for 5′
- The grids are stored at RT until TEM is performed

3.3.19 Generation of polyclonal anti-Yaa3 antibody

Polyclonal anti-Yaa3 antibody was generated by Eurogentec (Belgium) with the 87-days standard protocol of immunization of two rabbits with native and denatured recombinant proteins. Recombinant Yaa3 was purified under denaturing conditions (paragraph 3.3.4.3) and refolded in PBS + 200 mM Arginine, using Amicon column (paragraph 3.3.5.2). Four immunizations with 100 μg of recombinant protein are required for each rabbit. Thus, 600 μg of protein is run in a SDS-PAGE and the gel is coomassie-stained. The SDS gel band containing full length Yaa3 is cut and used for the first 3 immunizations. The last immunization is carried out with 100 μg refolded Yaa3.

The serum obtained, containing the polyclonal antibody, is then purified against the specific antigen or depleted against human cells, in order to increase its specificity and purity.

3.3.19.1 Antigen affinity purification of antibodies using NHS-Sepharose

Sera are antigen-purified using NHS-Sepharose. The recombinant protein is coupled to the NHS-Sepharose and then incubated with the antibody. Only the antibodies specific for the protein are able to bind and are subsequently eluted.

- 1,5 ml NHS-Sepharose are loaded on a manual purification column, containing a filter
- The NHS-Sepharose is washed with 20 ml cold 1 mM HCl
- The NHS-Sepharose is washed with 10 ml Coupling buffer
- 1,5 mg of recombinant native protein is mixed with the same volume of Coupling buffer
- The mix is incubated in the column on the wheel ON (or for 4h) at 4°C
- To block the groups which have not react with the NHS, the NHS-Sepharose-protein solution is incubated with 4ml Blocking solution (0,5 M ethanolamine, 0,1 M Tris, pH 8,5) for 4h at 4°C
- The NHS-Sepharose-protein solution is washed three times, alternating 1,5 ml buffer 1 (0,1M Tris, pH 8) and 1,5 ml buffer 2 (0,1 M NaCH$_3$COO, 0,5 M NaCl, pH 4)
- 3 ml of serum containing the polyclonal antibody + 8 ml 0,1 M Tris pH 8 are loaded on the column and incubated with the NHS-Sepharose-protein solution on the wheel ON (or for 4h) at 4°C
- The mix is washed with 10 ml of 10 mM Tris, pH 7.5
- The mix is washed with 10 ml of 500 mM NaCl
- The purified antibody is eluted using acid and basic elution:
- Acid Elution: Antibody is eluted with (2X) 2 ml 100 mM Glycine, pH 2,5, incubating for 5´
- The elution fractions are collected in a 15 ml falcon tube, containing 0,2 ml of 1 M Tris, pH 9, to neutralize the acidic pH
- Basic Elution: Antibody is eluted with (2X) 2 ml 100 mM Triethanolamine, pH 11,5, incubating for 5´
- The elution fractions are collected in a 15 ml falcon tube, containing 0,2 ml of 1 M Tris, pH 8, to neutralize the basic pH
- The concentration of antibody in the elution fractions is measured by Bradford assays
- Aliquots are stored at -20 °C

3.3.19.2 Depletion of sera using fixed cells

In order to decrease the serum background fluorescence on human cells and increasing its specificity for the antigen, the polyclonal serum was depleted against fixed cells.

- Monolayer of confluent human epithelial HEp-2 cells were grown on a 25 cm^2 flask
- Cells were fixed with 1 ml 3 % PFA for 15′ at RT
- Cells were washed three times with HBSS
- Cells were permeabilized with 1 ml methanol for 5, RT
- Cells were washed three times with HBSS
- Serum is diluted 1:25 / 1:50 in HBSS
- 1 ml of diluted serum is added to the fixes cells and incubating with shaking ON at 4 °C
- The serum is rescued and stored at -20 °C

3.3.19.3 Depletion of sera using cell extracts in western blot

In order to increase the serum specificity for the antigen, the polyclonal serum was depleted against *E. coli* and human epithelial HEp-2 cells extracts in western blot.

- Confluent HEp-2 cells from a 25 cm^2 flasks are incubated with 500 µl of Phospholysis buffer for 20′ at RT
- *E. coli* culture of 5 ml is grown overnight, then centrifuged at 5000 rpm for 10′, RT and the pellet resuspended in 500 µl of PBS
- *E. coli* and HEp-2 cell lysates are transferred in new Eppendorf tubes
- 50 µl DTT and 125 µl protein loading buffer are added
- The mixes are boiled for 20′ at 100 °C
- 200 µl of cells lysates are run in SDS-PAGE
- SDS gel is blotted on a PVDF membrane
- The membrane is blocked with for 30` with shaking
- The membrane is incubated with serum diluted 1:5 in 1 % BSA + 0,05 % Tween-20 in PBS, overnight on the wheel at 4 °C
- The serum is rescued and stored at -20 °C

3.4 Cellular biology methods: treatment of cells and bacteria with recombinant proteins

3.4.1 Immunological detection of *Chlamydia* by fluorescence microscopy

3.4.1.1 Fixation and permeabilization of *Chlamydia*-infected and uninfected HEp-2 cells

- Infected and uninfected HEp-2 cells are cultivated on glass coverslips in 24-well plates
- Cell culture medium is removed and cells are washed with 1 ml HBSS
- Cells are fixed with 300 µl 3 % PFA solution, incubated with the cells for 15´ at RT
- The PFA solution is removed and the cells are washed three times with 1 ml HBSS
- Fixed cells can be stored in HBSS at 4 °C for one week
- HBSS is removed and cells are permeabilized with 300 µl methanol or 0,2 % Triton, incubated with the cells for 10´ at RT
- The s is removed and the cells are washed three times with 1 ml HBSS

3.4.1.2 Indirect Immunofluorescence

- Infected and uninfected HEp-2 cells are cultivated on glass coverslips in 24-well plates
- Cells are fixed and permeabilized (as indicated in 3.4.1.1)
- Cells are washed three times with HBSS
- 30 µl of primary antibody diluted in PBS is added to the glass coverslip
- The antibody is incubated with the cells at 30 °C for 30´
- Cells are washed three times with HBSS
- 30 µl of fluorescent-labeled secondary antibody diluted in PBS is added to the glass coverslip
- The antibody is incubated with the cells at 30 °C for 30´
- Cells are washed three times with HBSS
- Cells are dyed with 1 µg/ml DAPI for 10´, RT (to stain DNA)
- Cells are washed three times with HBSS
- 1 µl of Vectashield is placed on a microscopy slide
- The glass coverslips are dried and placed on the Vectashield drop, with the cell side downwards

The coverslips are sealed at the edge with nail polish and can be stored at 4 ° C for several weeks

3.4.2 Adhesion assay with soluble recombinant proteins

Chlamydia proteins adhesive capacity to human epithelial cells is investigated by adding soluble recombinant protein to the human cell monolayer and analyzing the adhesion via immunoblotting.

- A confluent Hep-2 cells monolayer is grown in 24 well-plate ($1X10^6$ cells per well)
- Cells are cooled at 4 °C for 15 min
- Cell culture medium is removed and cells are washed with cold HBSS
- 250µl (25-200 µg/ml) of recombinant protein in cell culture medium are added to the cells and incubated for the desired time points in the incubator at 37 °C or at 4 °C
- Cell culture medium is removed and cells are washed five times with 1 ml HBSS
- The cells are detached from the plate well by incubation with 200 µl of cell dissociation solution for 10 min at 37 °C
- The suspension is transferred in a new tube and pelleted for 5 min at 1000 x g, RT (Biofuge Primo R)
- The supernatant is discarded and the cell pellet is resuspended in 97,5 µl PBS + 37,5 µl protein blue marker + 15 µl of 1 M DTT
- The mix is boiled for 15´at 100 °C
- Evaluation of bound recombinant proteins is performed by immunoblotting

3.4.3 Infection blocking assay with soluble recombinant proteins

In order to investigate the relevance of a *Chlamydia* protein for the infection, soluble recombinant protein is incubated with human cells. If the protein is a functional adhesin, it binds to the human receptors, blocking a subsequent infection with purified EBs.

- A confluent Hep-2 cells monolayer is grown in 24 well-plate ($1X10^6$ cells per well)
- Cell culture medium is removed and cells are washed with HBSS
- 250µl (100-200 µg/ml) of recombinant protein in cell culture medium are added to the cells and incubated for 2 h in the incubator at 37 °C
- Protein solution is removed and cells are gently washed three times with 1 ml HBSS

- 250 µl of purified EBs (MOI 10) in cell culture medium are added to the cells and incubated for 2 h in the incubator at 37 °C (stationary infection)
- EBs solution is removed and medium is substituted with 300 µl cell culture medium + 12 µl/ml Cycloheximide
- Infection is carried out for 24 h (*C. trachomatis*) or 48 h (*C. pneumoniae*) in the incubator at 37 °C
- Cells are fixed and stained with anti-Momp (*C. trachomatis*) or anti-LPS (*C. pneumoniae*) + DAPI
- The number of inclusions is counted using fluorescence microscope

- Heparin control (*C. pneumoniae*): 500 µg/ml of protein is added to the EBs for 30′ on ice. The solution is filled to a final volume of 250 µl and used for stationary infection

3.4.4 Coating *Chlamydia* EBs with soluble recombinant proteins

Chlamydia EBs can be coated with soluble recombinant proteins in order to investigate the proteins impact on the infection.

- 1 µM of recombinant protein is added to purified EBs (MOI 10) at a final volume of 50 µl in HBSS and the solution is incubated on ice for 30′
- To remove unbound proteins, the solutions is centrifuged at 15000 rpm, 4 °C for 20′ (Biofuge Primo R)
- EBs + protein pellet is resuspended in 30 µl cell culture medium
- Coated EBs solution is mixed with 5 µl 1 M DTT + 12,5 µl protein blue marker and analyzed by immunoblotting.

Anti-His or protein-specific antibody: to detect the recombinant protein coated on the EBs. Anti-Momp or anti-LPS: to analyzed the *C. trachomatis* or *C. pneumoniae* EB load.

3.4.5 Infection assay with EBs coated with soluble recombinant proteins

In order to investigate the relevance of a *Chlamydia* protein for the infection, human epithelial cells are infected with purified EBs coated with soluble recombinant protein.

- 1 µM of recombinant protein is used to coat purified EBs (MOI 10), as described in paragraph 3.4.4

- 30 µl of coated EBs are mixed with 270 µl cell culture medium and used to infect a confluent cell layer on glass coverslip

- Stationary infection is carried out for 2 h in the incubator at 37 °C

- Medium is substituted with 300 µl cell culture medium + 12 µl/ml Cycloheximide

- Infection is carried out for 24 h (*C. trachomatis*) or 48 h (*C. pneumoniae*) in the incubator at 37 °C

- Cells are fixed and stained with anti-Momp (*C. trachomatis*) or anti-LPS (*C. pneumoniae*) + DAPI

- The number of inclusions is counted using fluorescence microscope

4. Results

The purpose of this study was to characterize two different aspects of the *Chlamydia* adhesion to the host cell. The first part of this work focused in investigating the characteristics and functions of homomeric and heteromeric complexes formed by different *C. trachomatis* Pmps; while the second part of this work was invested in characterizing Yaa3, a hypothetical *C. pneumoniae* protein, which exhibits adhesive capacity to human epithelial cells.

4.1 *C. trachomatis* Polymorphic membrane proteins (Pmps) form functional oligomers

4.1.1 Motif-rich and motif-poor *C. trachomatis* Pmp proteins

In this work, different domains of selected *C. trachomatis* Pmps, with different characteristics, were investigated for their ability to generate homomeric complexes and for their capacity to interact with each other, forming heteromeric complexes. The functions and relevance of these complexes for the infection was then analyzed. To investigate the role of the motifs in oligomerization and in the complexes functions, six different Pmp domains with a high and a low number of motifs were selected and characterized in more detail.

In order to have a wide representation of the whole Pmp passenger domain (PD), different fragments of all 9 Pmps of *C. trachomatis* serovar E, strain DK-20, were produced, in addition to the adhesive fragments with a high number of motifs characterized so far (Becker and Hegemann 2014) (Fig. 8A). Pmp fragments Ac, B, C, D, En, Fc, Gc, H and I were sent to the laboratory of Prof. Dr. L.M. De la Maza, at the University of California, Irvine, for vaccination studies, in which the immunological response and protection against a *C. muridarum* infection in a murine model was investigated.

The central PD fragments of PmpD (D), PmpH (H) and PmpI (I), carrying a high density of motifs, in total 34, 14 and 15 respectively (motif-rich), and the C-terminal PD fragments of PmpA (Ac), PmpF (Fc) and PmpG (Gc), harboring only two motifs each (motif-poor) were selected. Selected motif-poor Pmp fragments were fused with a C-terminal His tag, while motif-rich Pmp fragments were fused with a N-terminal His tag (Fig. 8B) (see paragraph 3.2.3). All Pmp fragments were expressed in the *E. coli* Rosetta strain, purified under denaturing conditions using HisTrap HP column (GE Healthcare) and refolded via

dialysis at an initial concentration of 1 mg/ml (see paragraphs 3.3.4.4 and 3.3.5). Motif-rich D, H and I were stable in PBS at pH 7.2, while motif-poor Ac, Fc and Gc were stable in PBS at pH 9.0. Subsequent denaturing SDS-PAGE revealed that the different Pmp proteins migrate according to their predicted molecular weight (MW), with some degradation bands seen for Pmps Fc, D, H and I (Fig 8C).

Fragment	FxxN	GGA (I / L / V)
A	14	6 (6 / 0 / 0)
Ac	2	0
Ac2	2	0
Ash	12	6 (6 / 0 / 0)
An	4	2 (2 / 0 / 0)
Afl	14	6 (6 / 0 / 0)
B	6	6 (5 / 1 / 0)
C	6	4 (4 / 0 / 0)
C2	12	4 (4 / 0 / 0)
D	18	16 (11 / 3 / 2)
E	10	8 (8 / 0 / 0)
En	4	4 (4 / 0 / 0)
Ec	1	1 (1 / 0 / 0)
Efl	10	8 (8 / 0 / 0)
F	12	7 (6 / 1 / 0)
Fc	2	0
Fn	5	4 (4 / 0 / 0)
Ffl	13	7 (6 / 1 / 0)
G	11	4 (4 / 0 / 0)
Gc	1	1 (1 / 0 / 0)
Gn	2	2 (2 / 0 / 0)
H	12	2 (2 / 0 / 0)
I	9	6 (6 / 0 / 0)

Fragment	FxxN	GGA (I,L,V)	Tot
Ac	2	0	2
Fc	2	0	2
Gc	1	1 (1,0,0)	2
D	18	16 (11,3,2)	34
H	12	2 (2,0,0)	14
I	9	6 (6,0,0)	15
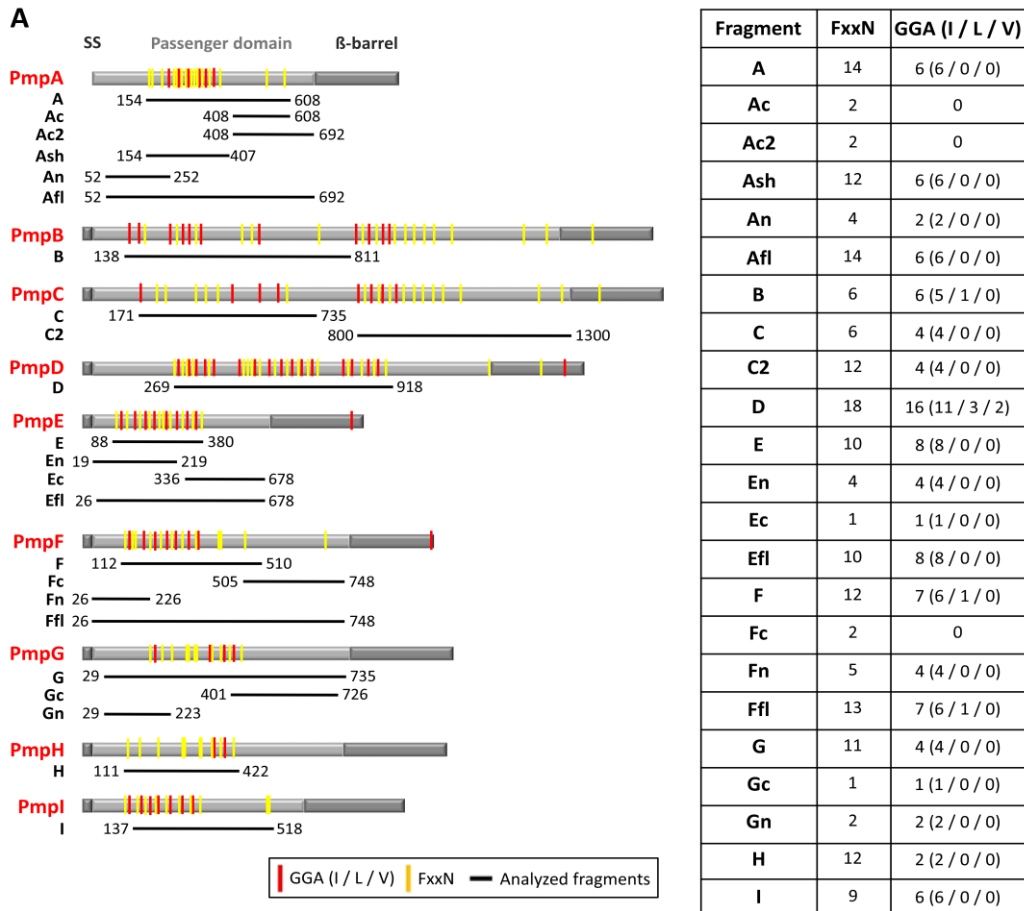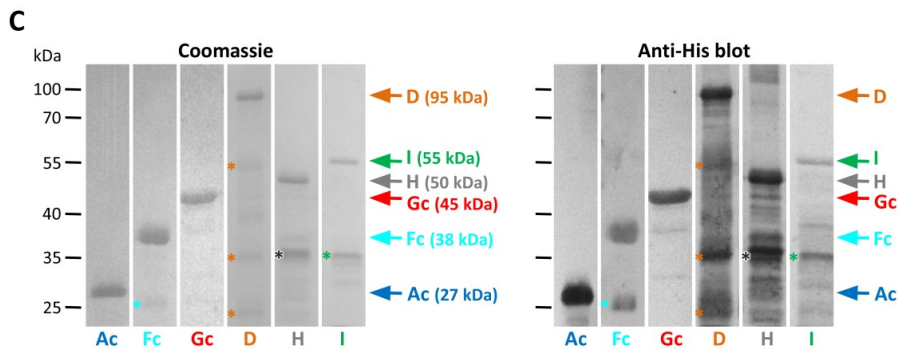
Figure 8. Motif-rich and motif-poor *C. trachomatis* Pmp proteins. A. Schematic representation of all 9 *C. trachomatis* serovar E Pmps. Analyzed recombinantly produced Pmp fragments are marked with a black line and amino acids indicate the position of the fragment within the passenger domain (PD). The table gives the number of FxxN and GGA(I, L, V) motifs present in each protein fragment. The FxxN and GGA(I, L, V) motifs are shown in yellow and red, respectively. SS: signal sequences. Pmp fragments A, B, C, D, E, F, G, H and I were produced as indicated by Becker and Hegemann 2014. Pmp fragments Ac, Ac2, C2, Ec, Fc and Gc were produced by myself, for the purpose of this work. Pmp fragments An, Ash, En, Efl, Fn and Gn were produced by Philipp Hanisch. Pmp fragments Afl and Ffl were produced by Sören Luczak. **B.** Schematic representation of selected Pmps with the analyzed motif-poor (Ac, Fc and Gc) and motif-rich (D, H and I) protein fragments carrying a C-terminal or N-terminal His tag respectively. The numbers indicate the first and the last amino acid of the fragments generated. The theoretical MW is given in kDa. The table gives the number of FxxN and GGA(I, L, V) motifs present in each protein fragment. The FxxN and GGA(I, L, V) motifs are shown in yellow and red, respectively. SS: signal sequences. **C.** SDS-PAGE of 1µg renatured recombinant His-tagged Pmp fragments Ac, Fc, Gc, D, H and I used in this study. Color-coded arrows indicate the fragments with their apparent MW given in brackets and * indicates the main degradation bands. Coomassie staining (left) and anti-His immunoblot (right).

4.1.2 Motif-rich and motif-poor *C. trachomatis* Pmp proteins form high MW homomeric complexes

4.1.2.1 Motif-rich and motif-poor *C. trachomatis* Pmp proteins interact with themselves

Self-interaction of recombinant *C. trachomatis* motif-poor Ac, Fc and Gc and motif-rich D, H and I Pmp proteins were initially tested via Far-Western-dot blot, in which 1 µg of purified recombinant proteins were loaded on a PDVF membrane. The proteins were then renatured on the membrane (prey) and incubated for 2 h with a biotinylated native Pmp protein (bait). If the interaction between prey and bait proteins occurs, the protein bound on the membrane is visualized using an AP-conjugated anti-streptavidin antibody, which has affinity for the biotin tag (Fig. 9A) (see paragraph 3.3.16.1). An anti-His antibody was used to detect the loaded prey proteins (loading control) and rGST as a negative control for interactions. These Far-Western dot blots revealed that Pmps Ac, Fc and D could interact strongly with themselves, compared to the loading control; while Pmps Gc, H and I were

able to self-interact, but in a weaker way, compared to the loading control (Fig. 9B).

Pmps self-interaction was then confirmed and quantified via MicroScale Thermophoresis (MST). In MST, 25 µM of a fluorescin-labeled protein is mixed with the second protein at different concentrations (serial dilutions 1:1, starting from 25 nM) and loaded in 14 capillaries. The capillaries are then exposed to a temperature gradient, causing different molecule movement, depending on many parameters such as molecular size, charge and entropy. The different ratios of the labeled protein and its interaction partner provide a range of partial binding in between the non-bound and the bound forms. At each dilution the parameters are compared and the generated curve is used to elaborate the dissociation constant (Kd). Kd above 400 µM indicates no binding between two molecules (see paragraph 3.3.16.3). MST data revealed that motif-poor Ac, Fc and Gc interacted strongly with themselves, exhibiting Kd values of $1,33 \pm 0,52$ µM, $4,75 \pm 1,02$ µM and $2,52 \pm 0,88$ µM, respectively.
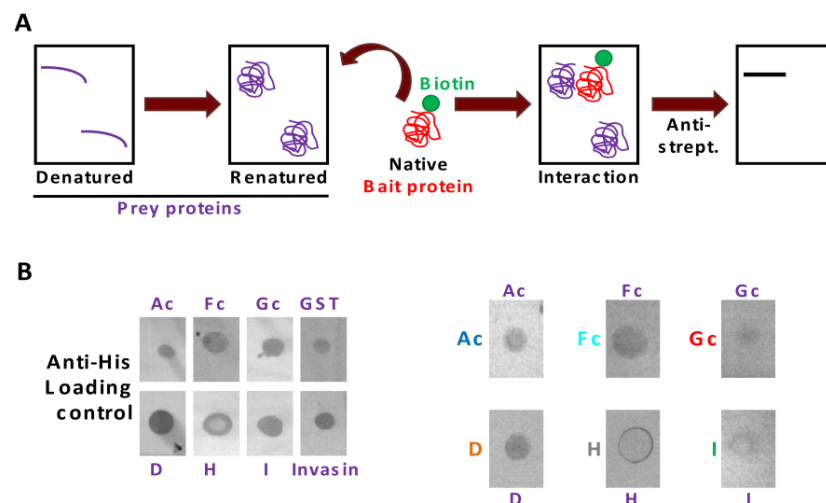
Figure 9. Motif-rich and motif-poor *C. trachomatis* Pmp proteins interact with themselves. **A.** Schematic representation of Far-Western-dot blot assay. 1 µg of denatured prey proteins were loaded on a membrane and renatured on the membrane overnight. 2 µg/ml native biotinylated bait protein was incubated with the membrane for 2 h at room temperature and bound proteins were visualized via an AP-conjugated anti-streptavidin antibody. **B.** Anti-His Far-Western-dot blot loading control of prey proteins (left) and self-interaction of biotinylated motif-poor Ac, Fc and Gc and of motif-rich D, H and I Pmp proteins (right). Prey proteins are indicated in purple, bait proteins are shown on the left side of the membranes.

4.1.2.2 *C. trachomatis* motif-rich and motif-poor Pmp proteins form different species of homomeric oligomers

Next, we investigated the panel of six renatured Pmp proteins (Fig. 8B) by Blue Native-PAGE (BN) for their ability to form oligomeric structures. BN separates proteins and protein complexes according to their size and conformation (see paragraph 3.3.9).

All six Pmp proteins showed one main high molecular weight (hMW) band (Ac: ~1300 kDa, Fc: ~1300 kDa, Gc: ~800 kDa, D: ~1300 kDa, H: ~1000 kDa, I: ~1250 kDa) surrounded by weaker signals, suggesting that each Pmp formed more than one hMW oligomeric species (Fig. 10A). The number of Pmp molecules in each hMW complex was calculated according to the apparent size of the respective monomer (Fig. 8C) and revealed that the six Pmp oligomers adopted different compositions (Ac: 48 monomers, D: 14 monomers, Fc: 34 monomers, Gc: 17 monomers, H: 20 monomers and I: 22 monomers). In addition, Pmp D and Gc proteins showed low MW bands of ~250 kDa and ~50 kDa respectively, indicating the presence of dimers and monomers respectively (Fig. 10A).

The composition of the different Pmp oligomers was further analyzed by Size Exclusion Chromatography (SEC), which separates proteins according to the complex size (see paragraph 3.3.13).

Each Pmp protein presented a specific elution profile. Motif-poor Ac eluted in a broad peak of approximately 400 kDa with two additional shoulders eluting between 18 and 20 ml, suggesting low MW complexes. The presence of Ac in all elution fractions is confirmed by immunoblot analysis. Motif-poor Gc eluted in two peaks with an apparent sizes of ~650 kDa and ~200 kDa respectively and presence of Gc was confirmed by western blot analysis. Motif-rich D eluted in two small hMW peaks of around 1000 and 669 kDa apparent sizes, composed mainly of full-length D, as confirmed by western blots. The majority of PmpD eluted in a peak of ~140 kDa and consisted mostly of 55 kDa PmpD degradation products, as shown by immunoblot analysis of the corresponding elution fractions. Finally, motif-rich I eluted in a major peak, which partially overlapped with the void volume (V_0), of around 2000 kDa apparent size. One smaller peak eluted at around 60 kDa, suggesting the presence of monomers (Fig. 10B). The number of Pmp molecules in each SEC elution peaks was calculated according to the apparent size of the corresponding monomer (Fig. 8C) and showed that the different Pmp hMW oligomers have different composition (Ac: 15 monomers, D: 11 monomers, Gc: 14 monomers and I: 36 monomers). Interestingly, Pmp Ac and I showed a discordant composition of the hMW complexes in BN and SEC analysis; while hMW complexes of Pmp D and Gc had a similar size in BN and SEC analysis (Fig. 10). Taken together, these data indicate that *C. trachomatis* motif-rich and motif-poor Pmps form different species of hMW homomeric complexes, independently from the number of motifs harboring.
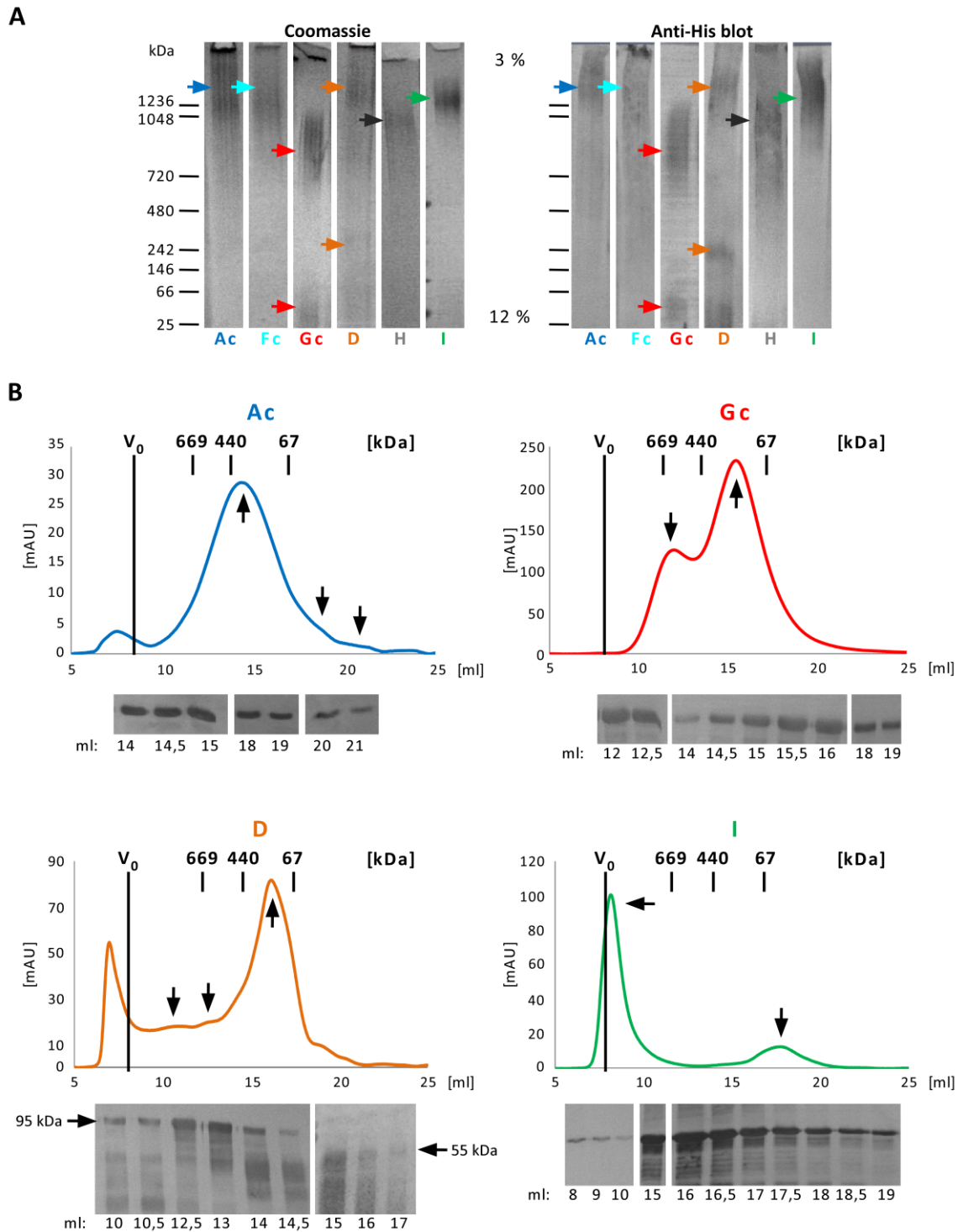
Figure 10. Motif-rich and motif-poor *C. trachomatis* Pmp proteins form high molecular weight (hMW) homomeric complexes. A. Blue Native-PAGE (BN) of 1 μg renatured Pmp proteins Ac, Fc, Gc, D, H and I. Color-coded arrows point to the center of the prominent bands for each Pmp. Coomassie staining of the BN gel (left) and anti-His immunoblot (right). Repetitions: n ≥ 3. **B.** Size exclusion chromatography (SEC) of motif-poor Pmps Ac and Gc and of motif-rich Pmps D and I was performed with a Superose6 column; flow rate 0.3 ml/min. Black line indicates the void volume (V_0) as determined by Blue dextran (~2000 kDa). The elution volume of globular standard proteins is indicated with short black lines, marked with the corresponding MW in kDa. Arrows indicate the relevant peaks within each elution profile. Anti-His immunoblots of relevant SEC fractions are shown at the bottom. Repetition: n = 1.

4.1.3 Motif-rich and motif-poor *C. trachomatis* Pmp proteins interact with each other

In preliminary studies performed in our laboratory, naturally cleaved motif-rich fragments of *C. pneumoniae* Pmp21 (M-Pmp21) interacted with itself and with motif-rich fragments of other *C. pneumoniae* Pmps *in vitro* in Far-Western blots; furthermore, interactions of M-Pmp21 with itself and with motif-rich fragments of Pmp6 and Pmp20 were detected on purified *C. pneumoniae* EBs after immunoprecipitation (Becker 2013). Therefore, the hypothesis was tested that also *C. trachomatis* Pmps would interact with each other.

4.1.3.1 Different fragments of all 9 *C. trachomatis* Pmps interact with most, but not all other fragments of the same or different Pmp

The whole panel of different motif-poor and motif-rich fragments of all 9 *C. trachomatis* Pmps produced (Fig. 8A) were tested for interactions with each other by Far-Western-dot blot. 1 μg prey Pmp proteins were loaded onto a PDVF membrane and renatured. Biotinylated bait Pmps were then incubated for 2 h with the membrane and the prey binding was visualized via AP-conjugated anti-streptavidin antibody (Fig. 9A) (see paragraph 3.3.16.1). As expected, biotinylated GST did not interact with membrane-bound Pmp proteins, but it could interact weakly with itself (Fig. 11A). Far-Western dot blot assays using biotinylated Pmp proteins revealed that all Pmp proteins tested were able to interact with themselves. In addition, the majority of motif-poor and motif-rich Pmp fragments tested interacted with motif-rich A, B, C, D, E, H and I and with motif-poor Fc proteins. In general, all Pmp proteins, motif-poor and motif-rich, showed capacity to interact with other Pmps, but no Pmp could interact with all other fragments (Fig. 11). Specifically, motif-poor Ac, Fc and Gc and motif-rich D, H and I Pmps were able to interact with themselves (Fig. 9B). Motif-poor Ac, Fc and Gc, fragments of different Pmps, presenting similar characteristics (position within the PD and number of motifs), exhibited a comparable pattern, interacting rather than with each other, mostly with motif-rich fragments of the same and of different Pmps (Fig. 11).

These observations suggest Pmp-domain specificity for interaction. Considering the fragments analyzed so far, it was not possible to identify a specific domain, even though motif-rich Pmp proteins seem to be more potent to interact. This observation is in agreement with the model proposed in which the Pmp PD form a triangular β-helix, exposing the motifs at the corners and mediating functional activities and oligomerization (Hegemann and Moelleken 2012).

Figure 11. Different fragments of all 9 *C. trachomatis* Pmps interact with most, but not all other fragments of the same or different Pmp. A. Representative Far-Western-dot blots. Anti-His Far-Western-dot blot shows prey protein loading. Interaction of 2 µg/ml native biotinylated GST was used as negative control. Far-Western-dot blots using biotinylated Ac, Gc, H, D and I are shown as examples. Prey proteins are indicated in purple, bait proteins are shown on the left side of the membranes. **B.** The table shows the interactions of bait Pmp proteins (red) with prey Pmp proteins (purple) in Far-Western-dot blot assays. Green box (+) indicates interaction, red box (-) represents lack of interaction, light green box (+/-) stands for weak interaction and white box for interaction not yet tested.

4.1.3.2 Motif-rich and motif-poor *C. trachomatis* Pmp proteins interact strongly with each other

In order to confirm the physical interaction of selected Pmp proteins, pull-down assays were performed. For this purpose, motif-poor Ac was fused at the C-terminus with a VSV tag (AcV) and expressed in *E. coli.* After cells disruption and centrifugation, the supernatant containing AcV was incubated with His-tagged Pmp proteins and affinity-purified. Bound proteins were analyzed via immunoblotting assays with anti-His and anti-VSV antibodies (Fig. 12A) (see paragraph 3.3.16.2). Control experiments were performed to confirm the specificity of the system. First, AcV protein alone was unable to bind the column, as it was not detected in the elution fractions. Next, AcV was incubated with the unrelated His-tagged CPn0473 adhesin (Fechtner, Galle et al. 2016). After affinity purification, CPn0473, but not Ac, could be detected in the elution fractions, confirming the absence of interaction among the two proteins (Fig. 12B). Finally, in pull-down assays of AcV with His-tagged motif-poor Fc (Fig. 12D) and Gc (Fig. 12C) and with His-tagged motif-rich D (Fig. 12E) and I (Fig. 12F) Pmp proteins, Ac was found in the same elution fractions as the His-tagged Pmps.

In order to confirm and quantify the Pmp interactions with each other, MST measurements were performed as described in paragraph 4.1.2.1. 25 µM of fluorescin-labeled Ac was mixed with different dilutions of a second Pmp and analyzed. MST measurements showed a very strong interaction of motif-rich Ac with motif-rich PmpA full length PD (Kd: 0,723 ± 0,56 µM), while a relatively weaker interaction with motif-poor Pmp Gc (Kd: 10,6 ± 1,1 µM), Pmp Fc (Kd: 5,7 ± 1,73 µM) and Pmp Ec (Kd: 17,5 ± 2,33 µM). In contrast, Ac showed no interaction with GST.

These data together demonstrate that *C. trachomatis* Pmps have the capacity to strongly interact with each other and the ability of interactions is shared among all fragments types (motif-poor and motif-rich). Moreover, all Pmp proteins interacted with most, but not all other Pmp proteins, suggesting domain-specificity.
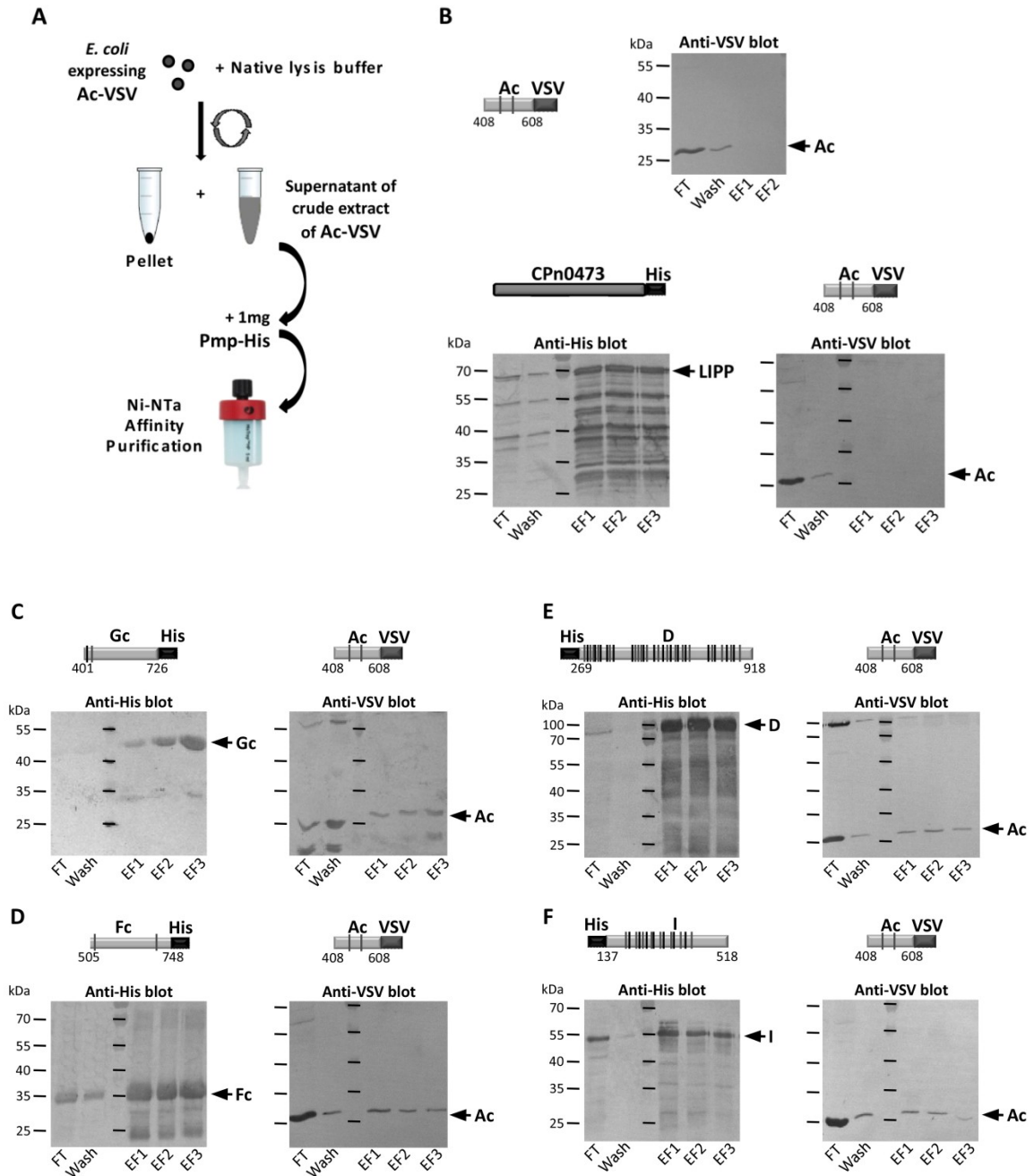
Figure 12. Physical interaction between *C. trachomatis* Pmp fragments. A. Scheme of pull-down assays of motif-poor Pmp Ac fused at its C-terminus with a VSV tag (AcV) with a His-tagged candidate Pmp. Soluble supernatants of *E. coli* cells expressing AcV were incubated with 1 mg/ml recombinant His-tagged Pmp. Ni-NTa affinity purification was performed to elute the His-tagged protein and eventually bound AcV. **B.** Western blot revealed presence of Ac in the Flow-through and in the wash fractions only, but not in the elution fractions in absence of a His-tagged protein and in the presence of His-tagged CPn0473, used as negative control. Interaction between AcV and His-tagged Gc (**C**), AcV and His-tagged Fc (**D**), AcV and His-tagged D (**E**) and AcV and His-tagged I (**F**). Western blots detect the Pmp proteins with anti-His (left) and anti-VSV (right) antibodies. FT: Flow Through, Wash: Washing step, EF: Elution fraction.

4.1.4 Motif-rich and motif-poor *C. trachomatis* Pmp proteins form heteromeric complexes

The ability of Pmps to interact with each other and to form hMW homomeric complexes (see paragraphs 4.1.3 and 4.1.2.2) led to the hypothesis that Pmps could generate hMW heteromeric complexes.

4.1.4.1 Co-refolding of *C. trachomatis* motif-rich and motif-poor Pmp proteins leads to hMW complex formation

In order to investigate whether Pmp interactions may result in heteromeric complex formation, motif-poor Ac, Fc and Gc and motif-rich D, H and I Pmps were co-refolded in an initial 1:1 molar ratio, at a final concentration of 1 mg/ml (Fig. 13) (see paragraph 3.3.5.1.1). The Pmp proteins were co-refolded in different combinations: motif-poor with motif-poor (Ac+Gc, Ac+Fc and Fc+Gc), motif-rich with motif-rich (D+I) and motif-poor with motif-rich (Ac+D, Ac+H and Ac+I).
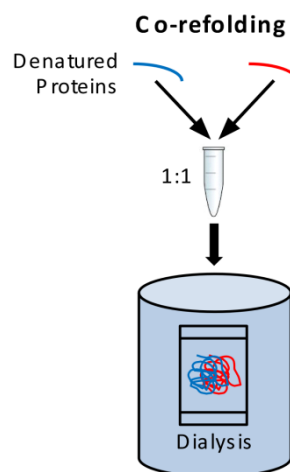
Figure 13. Schematic representation of co-refolding of Pmp proteins. Two different recombinant Pmp proteins were purified under denaturing conditions, mixed in a 1:1 molar ratio at a final concentration of 1 mg/ml and refolded together in the dialysis buffer.

The co-refolded pairs of different Pmps were first analyzed by Blue Native-PAGE (BN) (see paragraph 3.3.9). All co-refolded Pmps migrated as hMW bands of different sizes, surrounded by a weaker signal, suggesting more than one species of complexes, similarly to what was observed for homomeric complexes. Co-refolded motif-poor Fc+Ac migrated as one main band of ~1250 kDa, comparable to both homomeric Fc and Ac complexes (Fig. 14A). Interestingly, a shift was observed for the main bands formed by co-refolded motif-poor Fc+Gc and Ac+Gc complexes. Fc+Gc migrated as a main band of ~1236 kDa, different from both homomeric Fc and Gc bands; and Ac+Gc migrated as a main band of

~1050 kDa, different from both homomeric Ac and Gc bands (Fig. 14A). Co-refolded motif-rich Pmps D+I showed one main band of ~1250 kDa, comparable to homomeric I, but slightly different from homomeric D (Fig. 14B). Similar results were obtained for co-refolded motif-poor Ac with motif rich D, H and I. Ac+D migrated in a main hMW band of ~1050 kDa, slightly different from both homomeric D and Ac bands; Ac+H was detected in a band of ~1300 kDa, comparable to homomeric Ac, but different from homomeric H. Finally, Ac+I migrated in a main band of ~1250 kDa, comparable to homomeric I, but slightly different from homomeric Ac (Fig. 14B).

These results indicated that all co-refolded Pmp pairs form hMW complexes and almost all of them have different sizes compared to the respective homomeric complexes, with the exception of co-refolded Fc+Ac, which formed complexes comparable in size to both Ac and Fc homomeric complexes. In general, in all Pmp preparations, the majority of homomeric and co-refolded Pmps are present as hMW oligomeric forms.
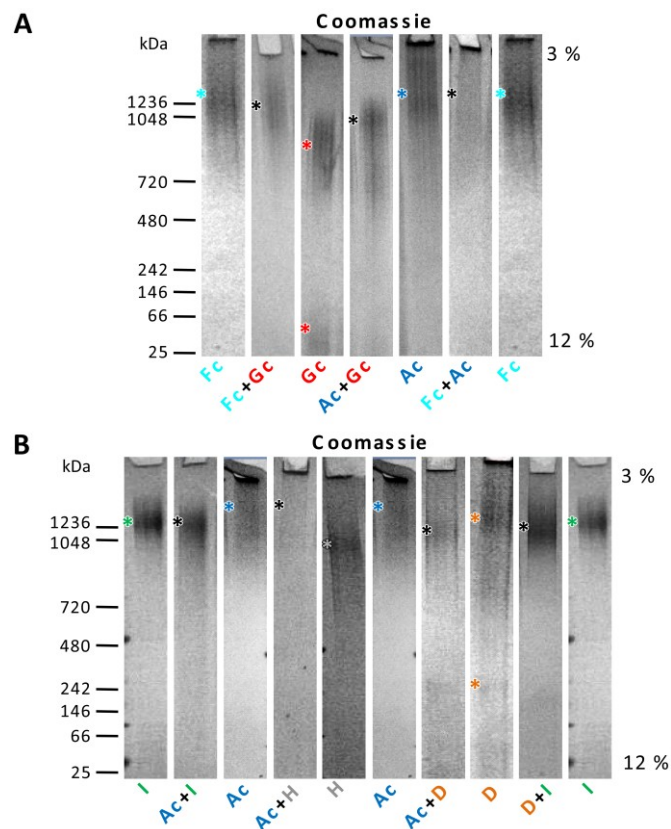
Figure 14. Co-refolded Pmp proteins form hMW complexes. A. Blue Native-PAGE of 1µg refolded complex formed by individual motif-poor Pmps (Fc, Gc and Ac) and co-refolded pairs of motif-poor Pmps (Fc+Gc, Ac+Gc and Fc+Ac). **B.** Blue Native-PAGE of 1µg complex formed by individual motif-rich Pmps (H, I and D), motif-poor Pmp Ac, and co-refolded pairs of motif-rich Pmps D+I and co-refolded pairs of motif-poor and motif-rich Pmps (Ac+D, Ac+H and Ac+I). Main hMW bands formed by homomeric complexes are indicated by color-code *. Main hMW bands formed by co-refolded complexes using two different Pmp proteins are indicated with a black *.

4.1.4.2 Both protein species are present in the hMW co-refolded Pmp complexes

Theoretically, the hMW bands found for the co-refolded pairs of Pmps would consist of the two Pmp proteins. To investigate the distribution of the two Pmp proteins in the hMW co-refolded complexes, sections of Blue Native-PAGE (BN) bands were cut and run in a second dimension SDS-PAGE, which separates the Pmps according to their monomeric size (see paragraph 3.3.10).

Co-refolded motif-rich D+I migrated as a hMW band in first dimension Blue Native-PAGE and both Pmp proteins were separated in a second dimension SDS-PAGE from the same region of the first dimension hMW BN band, but with different intensities, as Pmp I was significantly more prominent than Pmp D, compared to the input sample (Fig. 15).
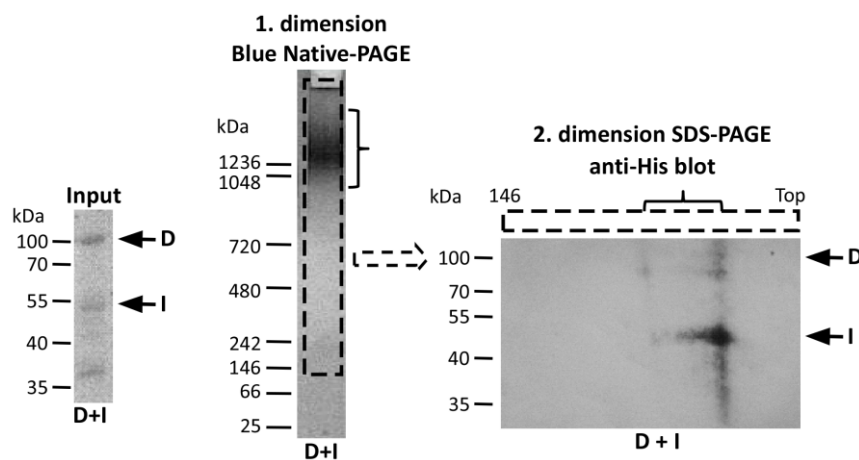
Figure 15. Both protein species are present in the hMW complexes formed by co-refolded motif-rich Pmp proteins. Second dimension SDS-PAGE of co-refolded Pmp complex D+I (set up described in paragraph 3.3.10). 1 µg co-refolded D+I (input, Coomassie-staining) was run in a first dimension Blue Native-PAGE (BN) and the lane containing the hMW complexes (black segmented box) was analyzed by second dimension SDS-PAGE. Black arrows indicate the position of monomeric Pmp proteins. Black bracket indicate the position of the main hMW band in the first dimension BN. The position of the hMW band in first dimension BN does not correspond to the position of the monomeric proteins in second dimension SDS-PAGE because of a compressing effect that the run of the second dimension SDS-PAGE has on the first dimension lane. Repetitions: n ≥ 3.

Both Pmp proteins were separated from the same region of the first dimension hMW BN bands of the co-refolded motif-poor and motif-rich Ac+D and Ac+I complexes (Fig. 16). Ac and D Pmp proteins were detected with similar intensities, together with Pmp D degradation product, while the input presented a slightly higher amount of Ac (Fig. 16A). Both Ac and I Pmps were found in Ac+I hMW and low MW complexes. High MW complexes showed a more prominent presence of Ac Pmp protein, while both Pmps were present in similar amount in the input sample. Both Ac and I Pmps were found in similar amount in Ac+I low MW complexes (Fig. 16B).
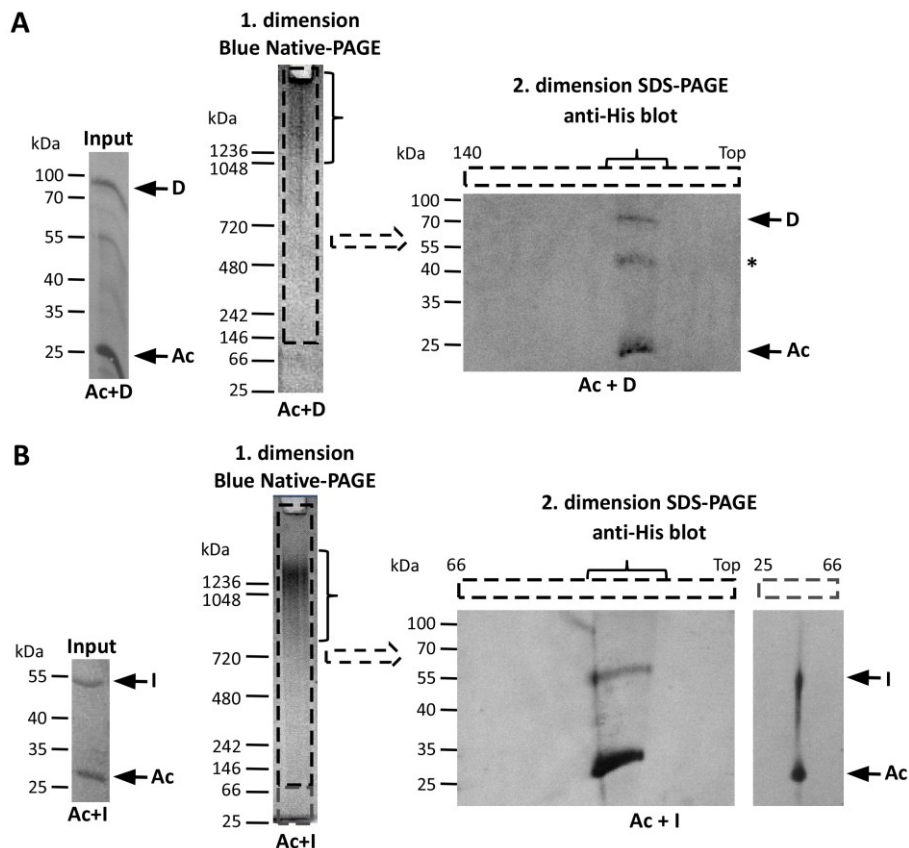
Figure 16. Both protein species are present in the hMW complexes formed by co-refolded motif-poor and motif-rich Pmp proteins. Second dimension SDS-PAGE of co-refolded Pmp complexes Ac+D (**A**) and Ac+I (**B**) (set up described in paragraph 3.3.10). 1 μg co-refolded Ac+D (**A**) and Ac+I (**B**) (input, Coomassie-staining) were run in a first dimension Blue Native-PAGE (BN) and the lanes containing the hMW complexes (black segmented box) or low MW complexes (grey segmented box) were analyzed by second dimension SDS-PAGE. Black arrows indicate the position of monomeric Pmp proteins. * indicates Pmp D degradation band (55 kDa). Black bracket indicate the position of the main hMW band in the first dimension BN. The position of the hMW band in first dimension BN does not correspond to the position of the monomeric proteins in second dimension SDS-PAGE because of a compressing effect that the run of the second dimension SDS-PAGE has on the first dimension lane. Repetitions: n ≥ 3.

Both Pmp proteins were separated from the same region of the first dimension hMW BN bands of co-refolded motif-poor Fc+Ac, Fc+Gc and Ac+Gc (Fig. 17). Interestingly, Fc and Gc Pmp proteins were detected with similar intensities (Fig. 17B); while both Ac+Gc and Fc+Ac hMW complexes showed a more prominent presence of Ac Pmp protein. In both cases, the co-refolded Pmps were present in similar amount in the input sample (Fig. 17A-C). Low MW complexes were also analyzed by second dimension SDS-PAGE. Significant Fc+Ac low MW complexes could not be detected in first dimension BN, and this was confirmed by the absence of both Ac and Fc proteins in second dimension analysis (Fig. 17A). On the other hand, second dimension SDS-PAGE revealed that low MW complexes formed by Fc+Gc and Ac+Gc complexes were formed only by Gc Pmp

fragment (Fig. 17B-C). The presence of Gc in the BN band region of ~25-70 kDa suggest the presence of Gc as monomers, indicating that the hMW complexes Fc+Gc and Ac+Gc are composed mainly of Fc and Ac, respectively, in a ratio with Gc which is different from the initial 1:1 ratio.
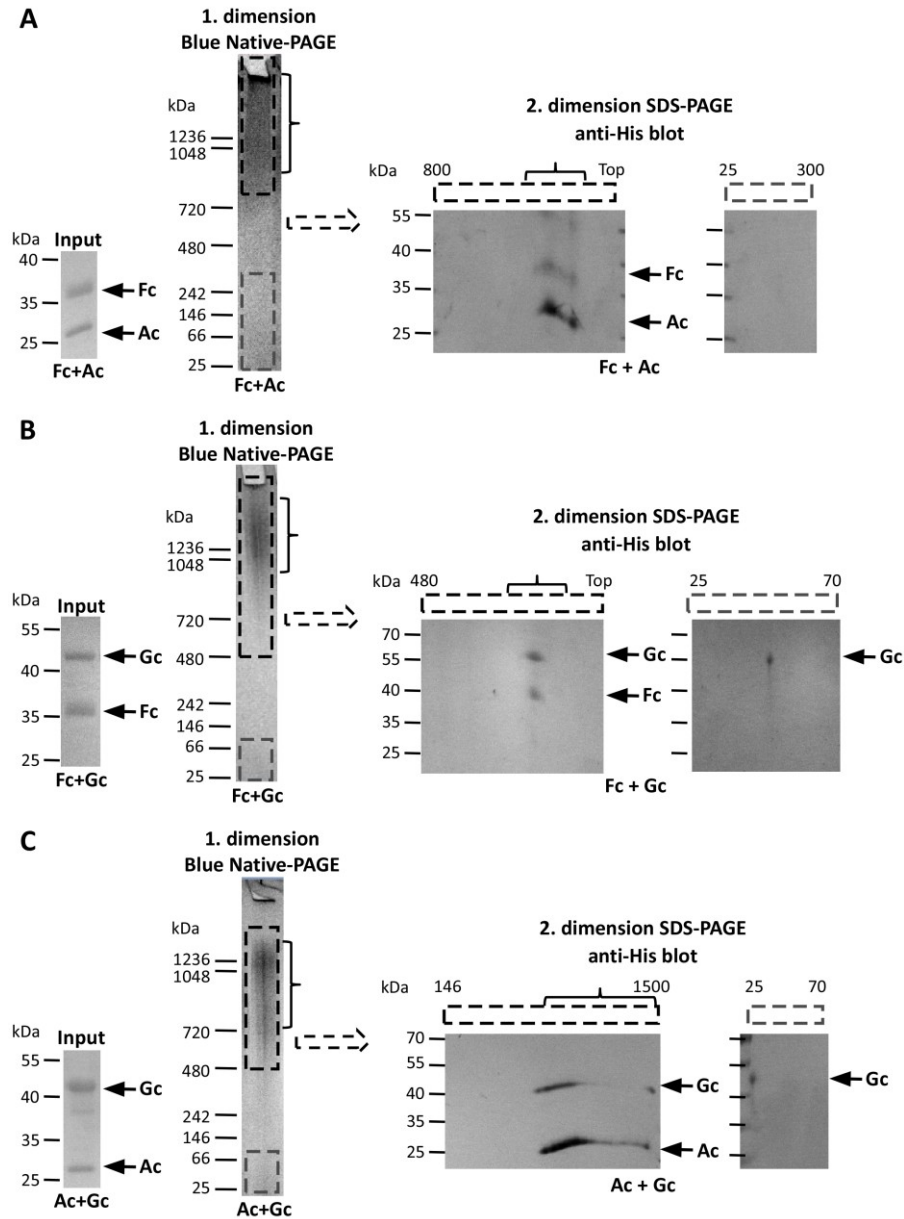
Figure 17. Both protein species are present in the hMW complexes formed by co-refolded motif-poor Pmp proteins. Second dimension SDS-PAGE of co-refolded complexes Fc+Ac (**A**), Fc+Gc (**B**) and Ac+Gc (**C**) (set up described in paragraph 3.3.10). 1 μg co-refolded Fc+Ac (**A**), Fc+Gc (**B**) and Ac+Gc (**C**) (input, Coomassie-staining) were run in a first dimension Blue Native-PAGE (BN) and the lanes containing the hMW complexes (black segmented box) or low MW complexes (grey segmented box) were analyzed by second dimension SDS-PAGE. Black arrows indicate the position of monomeric Pmp proteins. Black bracket indicate the position of the main hMW band in the first dimension BN. The position of the hMW band in first dimension BN does not correspond to the position of the monomeric proteins in second dimension SDS-PAGE because of a compressing effect that the run of the second dimension SDS-PAGE has on the first dimension lane. Repetitions: n ≥ 3.

These data suggest that two co-refolded Pmp proteins can form hMW complexes in which the different proteins are arranged in a ratio different from the initial 1:1 molar ratio. This seems true for mixture of two motif-rich Pmps, for mixtures of two motif-poor Pmps and for mixtures of one motif-poor and one motif-rich Pmp.

4.1.4.3 Co-refolded motif-poor Ac+Gc form complexes with a ratio different from the initial 1:1

When co-refolded in a 1:1 ratio, motif-poor Ac+Gc complexes migrate as a hMW band of ~1050 kDa, different in motility from both homomeric Ac and Gc complexes (Fig. 14A). Second dimension analysis of the hMW band showed that Ac and Gc Pmps were both found in the hMW co-refolded complex, but only Gc was detected in the low MW co-refolded complex (Fig. 17C).

In order to investigate in more detail the distribution of the two Ac and Gc Pmp proteins during co-refolding, motif-poor Ac and Gc Pmp proteins were co-refolded in different initial concentrations, starting from 100 % Gc and 0 % Ac and stepwise reducing until 0 % Gc and 100 % Ac was reached. The same experiment was performed also for Fc+Ac, which does not exhibit any shift in motility in the 1:1 co-refolded hMW complex, compared to the homomeric complexes.

As one might have expected, all complexes formed by co-refolding of Fc+Ac in different percentages migrated in the main hMW band of ~1250 kDa, comparable to the homomeric Fc and Ac complexes alone (Fig. 18B).

Interestingly, the Ac+Gc complex migrated as a hMW band of ~800 kDa, comparable to homomeric Gc complexes, as long as Gc dominated in the mix (99 %, 95 % and 75 %). However, when Ac and Gc were co-refolded in a 50 % : 50 % ratio, the hMW complex shifted and migrated at ~1100 kDa, a motility not observed for both homomeric Ac and Gc complexes alone. As soon as Ac was more prominent in the mixture (75 % and 95 %) the hMW complexes migrated at ~1300 kDa, comparable only with homomeric Ac. Low MW complexes were observed in all co-refolded complex mixtures albeit in decreasing amounts with decreasing amount of Gc in the mixture. This suggests that the low MW complexes are dominated by Gc, as this was already shown for the 1:1 co-refolded Ac+Gc mixture (Fig. 18A).
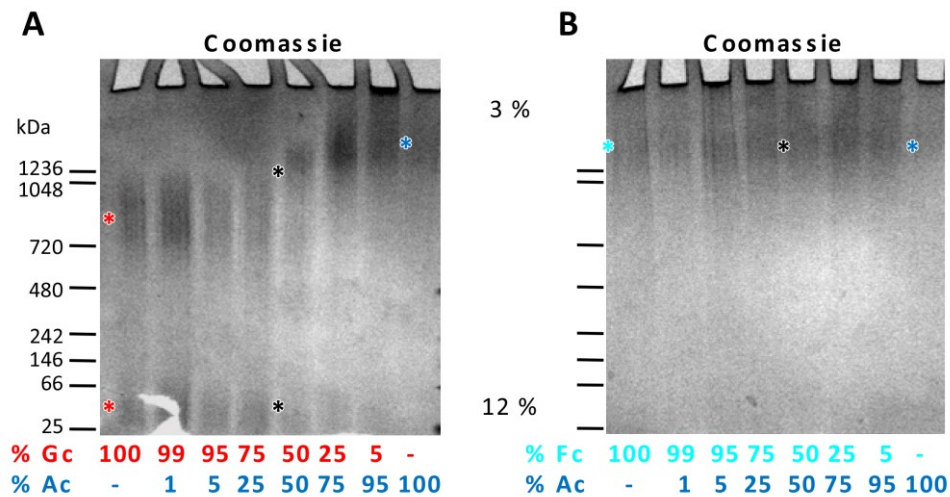
Figure 18. Co-refolded Pmp hMW complexes showed Pmp-dependent motility shifts in Blue Native-PAGE. Blue Native-PAGE of 1 µg motif-poor Pmp complexes Ac+Gc (**A**) and Fc+Ac (**B**) formed by co-refolding of the two Pmp proteins in different percentages, as indicated below the gels. Main hMW bands formed by homomeric Pmp complexes are indicated with color-coded *. Black * indicate hMW complexes formed by 50 % co-refolded Pmp proteins.

To investigate whether the ratio of the two Pmp proteins changes in the hMW complexes formed by co-refolding of Ac and Gc in different percentages (25+75 % and 75+25 %), second dimension SDS-PAGE were performed (Fig. 19B-C). As controls, Ac and Gc were detected in the respective homomeric hMW complexes (Fig. 19A). In the Ac+Gc co-refolded complexes (25 % : 75 %, Fig. 19B and 75 % : 25 %, Fig. 19C), both Ac and Gc Pmp proteins were separated from the same region of the first dimension hMW BN bands. In the hMW complexes of ~700-1500 kDa size, formed by co-refolding of 25 % Ac and 75 % Gc, Ac and Gc are detected in an equal amount, despite Gc is dominant in the input sample (Fig. 19B). In the hMW complexes of ~900-2000 kDa size, formed by co-refolding of 75 % Ac and 25 % Gc, Ac signal is stronger than Gc signal, whereas in the lower MW complexes of ~480-900 kDa size, Ac and Gc were detected in a similar amount, despite Ac is more prominent in the input sample (Fig. 19C).
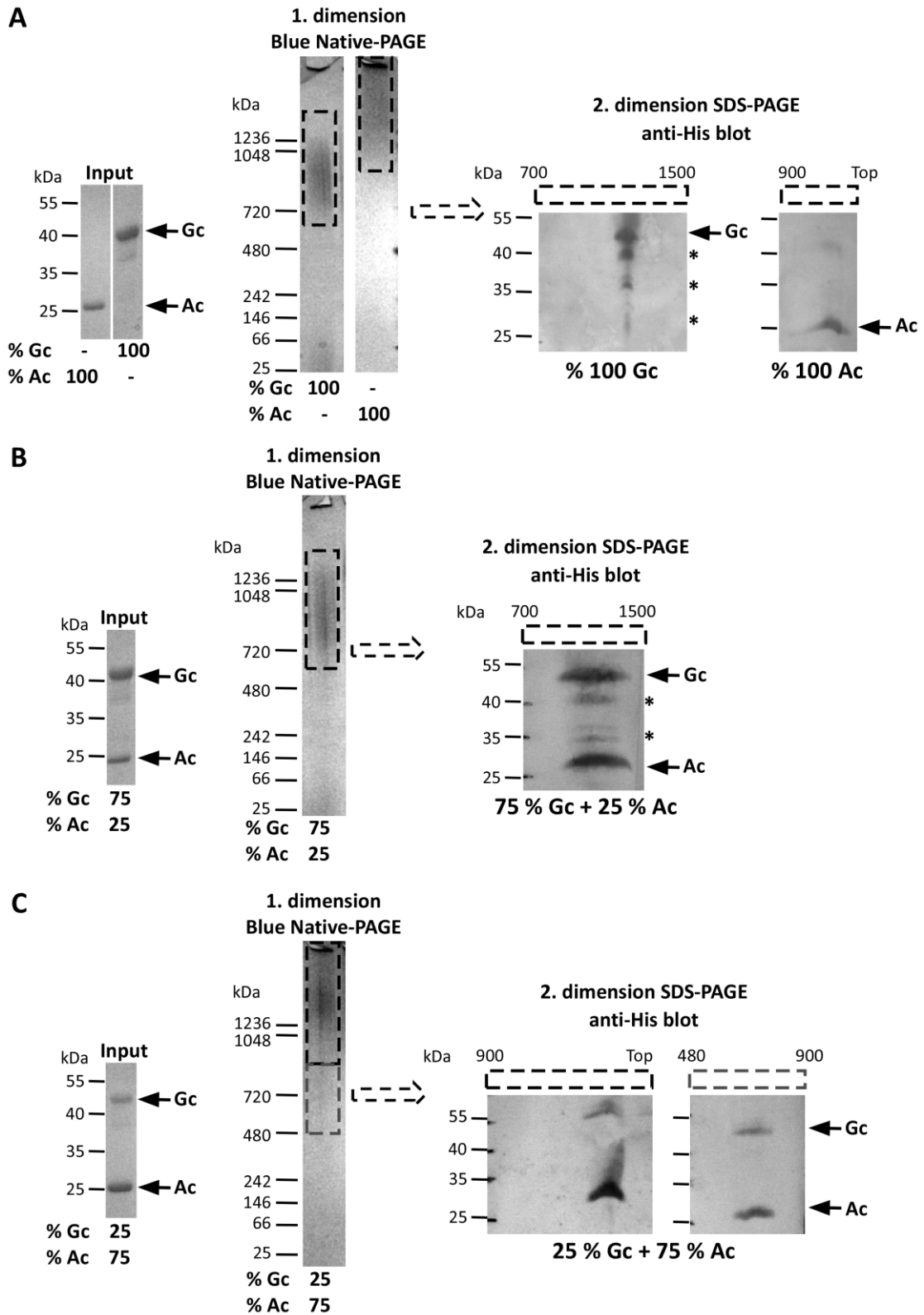
Figure 19. Both protein species are present in the hMW complexes formed by Ac and Gc co-refolded at different concentrations. Second dimension SDS-PAGE of homomeric Ac and Gc complexes (**A**) and of Ac+Gc complexes, formed by co-refolding of Ac and Gc at 25 % + 75 % (**B**) and at 75 % + 25 % (**C**) and separated by Blue Native-PAGE (BN). First dimension BN bands containing the hMW complexes (black and grey boxes) were analyzed by second dimension SDS-PAGE. Arrows indicate the position of monomeric Pmp proteins. * indicate degradation bands.

To confirm the data obtained and further investigate the distribution of the two Pmp proteins in the co-refolded Ac+Gc complex, His-tagged Ac was fused with a VSV tag and co-refolded with a His-tagged Gc in a 1:1 molar ratio. Immunoblotting of the Blue Native-PAGE analysis were performed with an anti-His antibody (which detected both Ac and Gc) and anti-VSV antibody (which detected only Ac). Homomeric Gc Pmp protein was detected only in a main hMW band of ~1000 kDa and in the low MW band of ~30 kDa, while homomeric Ac was detected in a main hMW complex of ~1300 kDa by both anti-His and anti-VSV antibodies, but the signal was very weak, possibly because the majority of the Ac hMW complexes are retained in the gel pockets (Fig. 20).

The co-refolded Ac+Gc complex migrated at the hMW main band of ~1100 kDa and could be detected with both antibodies, suggesting the presence of both Ac and Gc Pmp proteins; while the low MW bands at ~500 and ~30 kDa were detected only with anti-His antibody, but not with anti-VSV antibody, indicating the presence of Pmp Gc only (Fig. 20).
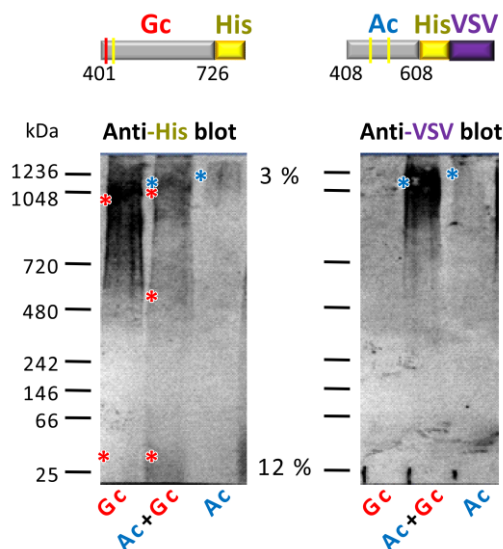
Figure 20. Ac and Gc Pmp proteins distribution in the Ac+Gc complex. Blue Native-PAGE of 1 μg homomeric His-tagged Gc, homomeric His-VSV-tagged Ac, and 1:1 co-refolded Ac+Gc. Immunoblots were performed with an anti-His antibody to detect both Ac and Gc (left) and with an anti-VSV antibody to detect only Ac (right). Color-coded * indicate the presence and position of the two different Pmps in the bands.

In order to determine whether the Ac+Gc complexes formed by co-refolding of Ac and Gc in a 1:1 initial ratio are not saturated and have still the capacity to interact with Ac and Gc homomeric complexes, MST measurements were performed (as described in paragraphs 4.1.2.1 and 3.3.16.3). Fluorescin-labeled homomeric Ac oligomers and fluorescin-labeled homomeric Gc oligomers were mixed with different concentrations of the already co-refolded Ac+Gc mixture (14 serial dilutions 1:1). Only homomeric Ac was still able to bind to the already co-refolded Ac+Gc mixture, however the binding was weaker than to

homomeric Gc or Ac alone (Kd: 45,5 ± 3,2 μM). On the other hand, homomeric Gc oligomers could not bind to the already co-refolded Ac+Gc complex.

Taken together, these data show that during co-refolding, Ac and Gc Pmp proteins are able to interact, forming new complexes (Ac+Gc) with a different size than the two respective homomeric complexes alone. In a 1:1 co-refolding situation, Ac is the most prominent protein in the co-refolded Ac+Gc hMW complex, while Gc is found not only in the hMW complex, but also is present alone as low hMW complex and as monomer. Moreover, homomeric Ac, but not homomeric Gc, can still interact with the already co-refolded Ac+Gc complexes. Thus, it can be hypothesized that Ac is the major component in the complexes formed with Gc.

4.1.4.4 Mixing pre-refolded Pmp proteins results in hMW complexes in Blue Native-PAGE

In order to test whether different Pmp proteins could still interact once they are already in their folded status and if the majority of protein in the mixture still forms hMW complexes, two different motif-poor Pmp proteins were purified from *E. coli* under denaturing conditions and refolded, forming hMW and low MW complexes. Only after refolding, the two Pmps were mixed in a 1:1 molar ratio and incubated overnight in the dialysis buffer (Fig. 21A) (see paragraph 3.3.5.1.2) and the mixed Pmp proteins ("mix") were analyzed by Blue Native-PAGE (see paragraph 3.3.9). For comparison, the corresponding co-refolded complexes ("co-") were loaded side by side with the "mix" probes. Three combinations of motif-poor Pmps were tested (Ac+Gc, Fc+Gc and Fc+Ac). In all combinations, the co-refolded and the mixed complexes migrated at the same main hMW band of ~1000, ~1200 and ~1250 kDa, respectively (Fig 21B). In the mixed Pmp samples it is very likely to found a mixture with a majority of the two homomeric Pmp complexes and a minority of heteromeric Pmp complexes, whose bands are visible as a fused smear, in which the overlapping regions have a size comparable to the co-refolded Pmp complexes.
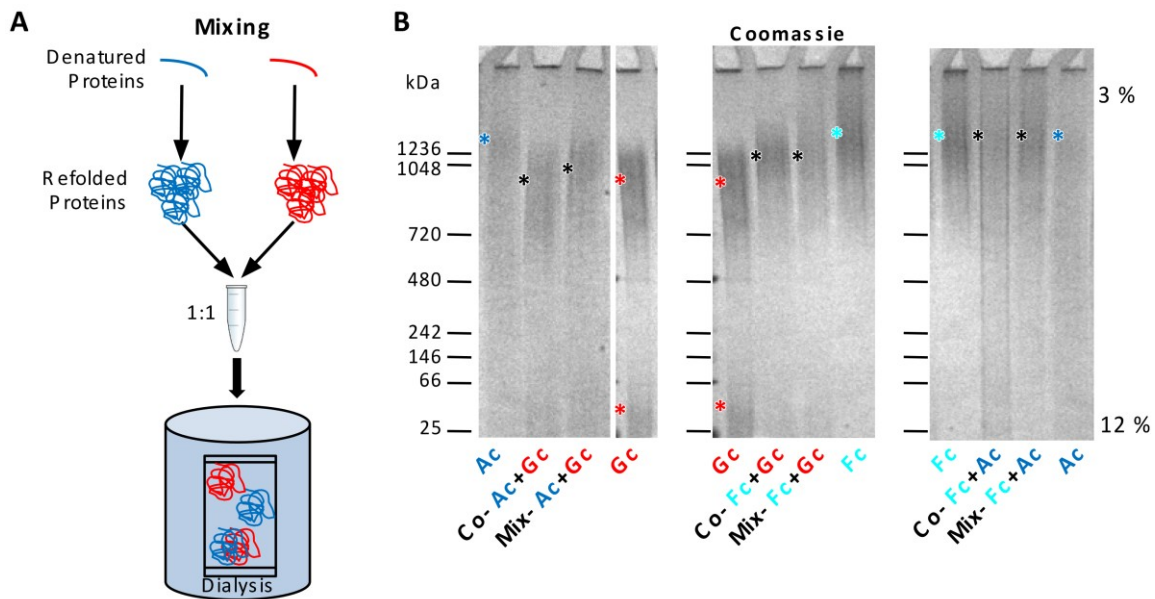
Figure 21. Complexes formed by co-refolding or by mixing of two different Pmp proteins. A.
Schematic representation of mix procedure. Two different recombinant Pmp proteins are purified
under denaturing conditions, refolded individually, mixed in a 1:1 molar ratio at a final
concentration of 1 mg/ml and incubated overnight in the dialysis buffer at 4 °C. **B.** Blue Native-
PAGE of 1 µg complexes formed by co-refolding (Co-) and mixing (Mix-) motif-poor Pmp
proteins Ac+Gc (left), Fc+Gc (center) and Fc+Ac (right) and the respective homomeric complexes.
Color-code * indicate the main homomeric hMW complexes and black * indicate the main co-
refolded and mixed hMW complexes.

4.1.4.5 Co-refolded Pmps form hMW heteromeric complexes with different properties than the respective homomeric complexes

Next we analyzed the hMW complexes formed by different heteromeric, co-refolded Pmps
by Size Exclusion Chromatography (SEC) (see paragraph 3.3.13).

The co-refolded motif-poor Ac+Gc mixture eluted in a main peak of approximately
200 kDa. A hMW shoulder was detected at around 500 kDa. Western blot analysis showed
that both Ac and Gc Pmp proteins were present in similar amount in all elution fractions
(Fig 22A). The co-refolded Ac+I mixture eluted in a hMW peak of ~670 kDa and in a
lower MW peak of ~200 kDa. Both proteins were found in all elution fractions analyzed by
immunoblotting; Ac protein was stronger in the ~670 kDa peak (Fig 22B). The co-refolded
Ac+D mixture eluted in one small hMW peaks of ~400 kDa. Immunoblot analysis revealed
that Ac Pmp protein was strongly dominating compared to Pmp D. In addition, the
majority of the protein eluted in a peak of approximately 140 kDa, also composed mainly
of the Ac Pmp protein with some full length Pmp D and its degradation product of 55 kDa,
as confirmed by immunoblot analysis (Fig 22C). The co-refolded motif-rich D+I mixture
eluted in one hMW shoulder of ~1000 kDa, composed by both D and I Pmps in similar

amount, as indicated by western blots of the relevant fractions. The majority of protein eluted in a ~140 kDa peak and in a shoulder of ~67 kDa, in which both D and I Pmps were detected, albeit at very different amounts (Fig, 22D).

These data confirm that when two Pmps are co-refolded in a 1:1 initial molar ratio, the majority of protein forms different species of hMW complexes, as already observed in Blue Native-PAGE and second dimension SDS-PAGE analysis.
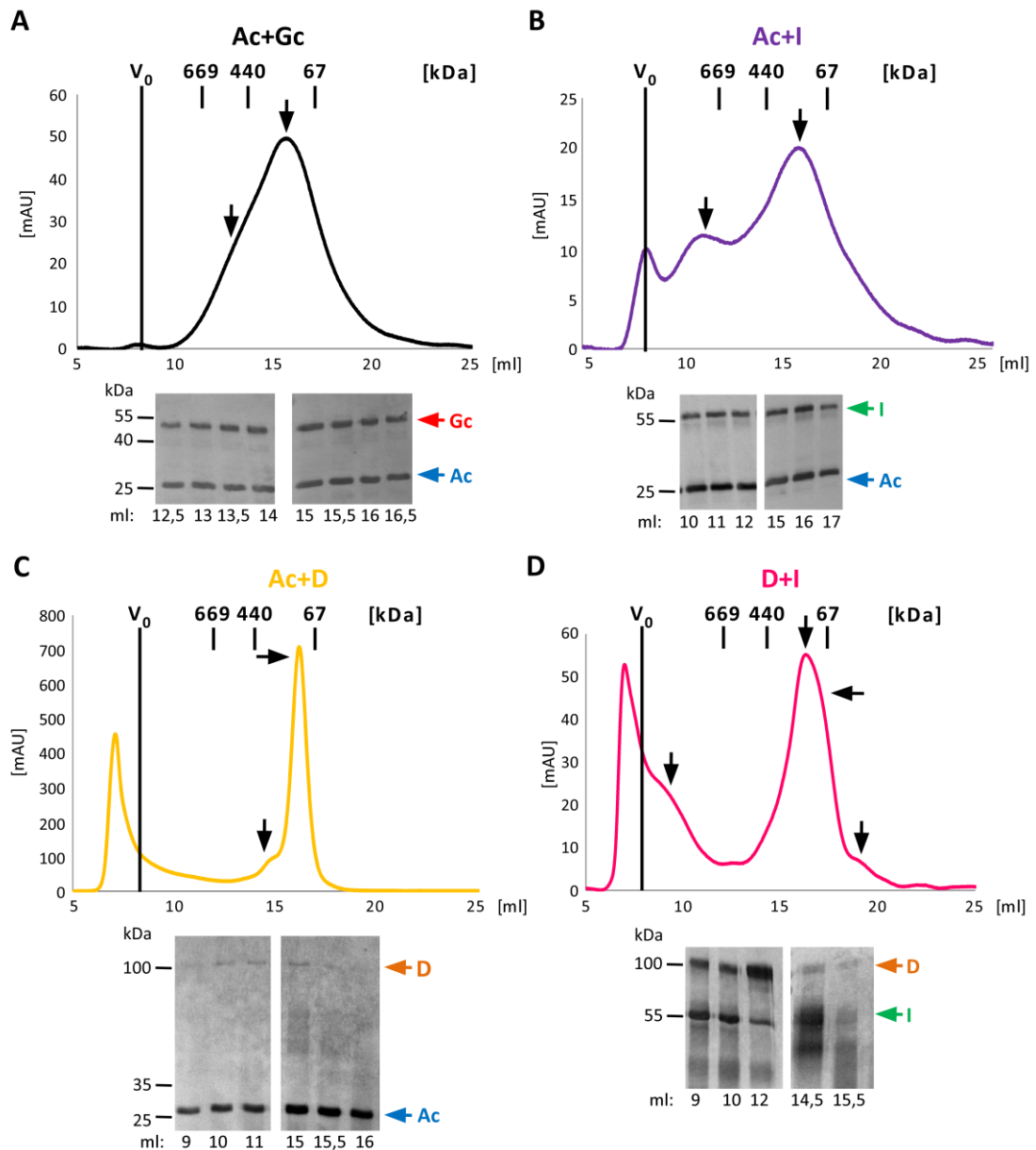
Figure 22. Co-refolded motif-rich and motif-poor *C. trachomatis* Pmps form hMW complexes. Size exclusion chromatography (SEC) of co-refolded Pmps Ac+Gc (**A**), Ac+I (**B**), Ac+D (**C**) and D+I (**D**), each at an initial 1:1 molar ratio, performed with a Superose6 column; flow rate 0.3 ml/min. Black line indicates the void volume (V_0) as determined by Blue dextrane (~2000 kDa). Elution volume of globular standard proteins is indicated with short black lines and their MW is given above the lines. Black arrows indicate the relevant peaks within each elution profile. Anti-His immunoblots of relevant SEC fractions are shown at the bottom. Color coded arrows indicate the different Pmp proteins. Repetition: n = 1.

4.1.4.6 Superimposition of the previously analyzed SEC profiles of the co-refolded Pmp mixtures with the SEC profiles of the respective homomeric Pmp mixtures

The different co-refolded complexes migrated in Blue Native-PAGE differently from the respective homomeric Pmp complexes. In order to determine whether co-refolded complexes are actually heteromeric, elution profiles of the co-refolded Pmp mixtures obtained in the previous experiments (Fig. 22) were superimposed with the elution profiles of the respective homomeric Pmps obtained in the previous experiments (Fig. 10B).

The co-refolded Ac+Gc peak of ~200 kDa overlapped with one peak of homomeric Gc, but it was shifted from homomeric Ac; while the Ac+Gc shoulder of ~500 kDa was shifted from both homomeric and heteromeric Ac and Gc peaks (Fig. 23A). The co-refolded Ac+I mixture eluted in two peaks shifted from both the homomeric Ac and I peaks (Fig. 23B). The co-refolded Ac+D eluted in a ~400 kDa shoulder, overlapping with homomeric Ac, but shifted from homomeric D. The majority of protein eluted in a ~140 kDa peak overlapped completely with homomeric D, but was shifted from homomeric Ac (Fig. 23C). The co-refolded motif-rich D+I eluted in a peak of ~1000 kDa, partially overlapping with both homomeric D and I. D+I peak of ~140 kDa and shoulder of ~67 kDa overlapped with homomeric D, but were shifted from homomeric I peak (Fig. 23D).

In general, all co-refolded Pmp mixtures analyzed (Ac+Gc, Ac+I, Ac+D and D+I) presented a shift in the main peaks, when compared to the main peaks of the respective homomeric Pmps. Furthermore, immunoblot analysis of SEC elution fractions showed that co-refolded hMW complexes are formed by both protein species, mostly organized in a ratio different from the initial 1:1, even when the peaks of the co-refolded complex do not overlap with the peaks of the respective homomeric Pmps (Figs. 22 and 23). Taken together, these data indicate that co-refolding of two different Pmp proteins generate hMW heteromeric oligomers with different properties than the respective homomeric Pmp complexes.
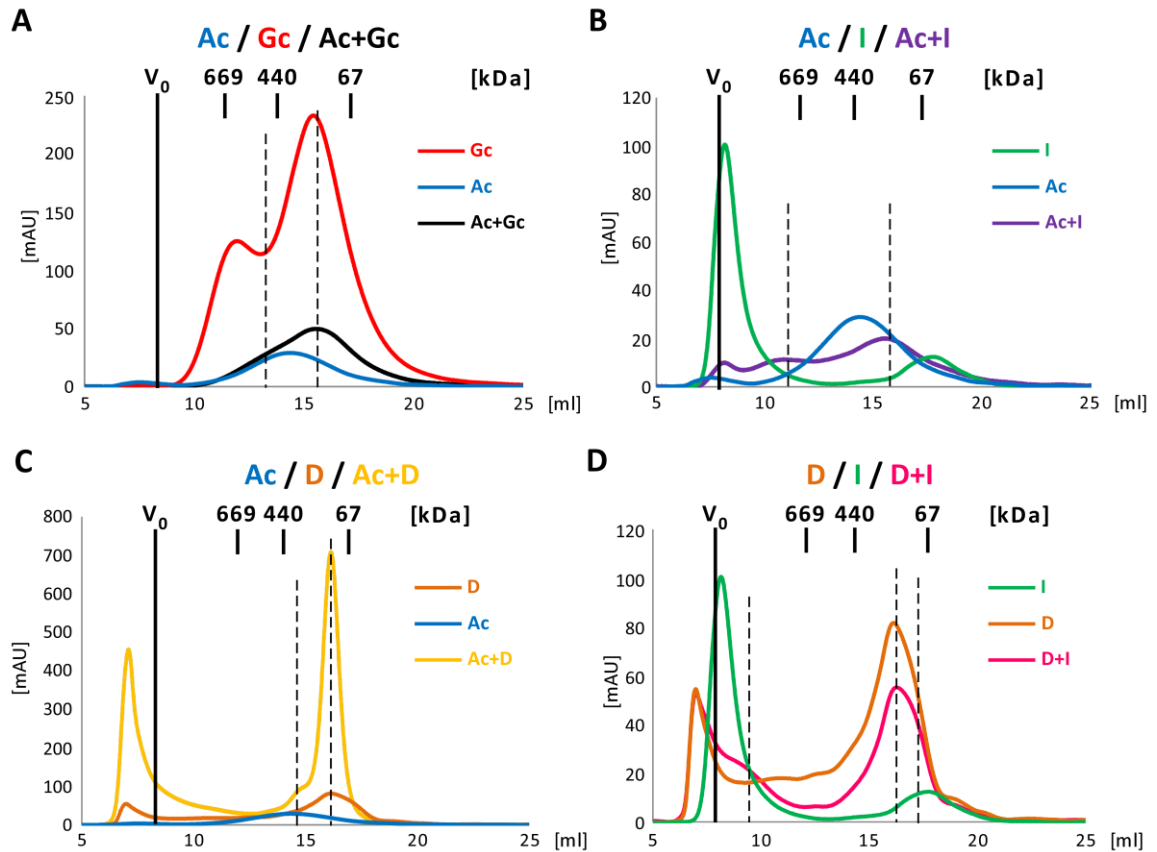
Figure 23. Motif-rich and motif-poor *C. trachomatis* Pmps form hMW heteromeric complexes. Overlap of previously analyzed SEC curves of Pmp complexes formed by 1:1 co-refolded Pmp proteins Ac+Gc (**A**), Ac+I (**B**), Ac+D (**C**), D+I (**D**) (Fig. 22) with the respective homomeric Pmp complexes (Fig. 10B), obtained with a Superose6 column; flow rate 0.3 ml/min. Color codes represent the homo- and heteromeric complexes respectively. Black line indicates the void volume (V_0) as determined by Blue dextrane (~2000 kDa). Elution volume of globular standard proteins is indicated with short black lines and their MW is given above the lines. Black segmented lines indicate peaks specific to the heteromeric Pmp mixtures.

4.1.5 Homomeric and heteromeric Pmp oligomers form protofibril-like structures

A recombinant motif-poor fragment of *C. pneumoniae* Pmp21 formed hMW homomeric oligomers with protofibril-like structures and amyloid characteristics *in vitro* (Luczak, Smits et al. 2016). Therefore, we asked whether the different homomeric and heteromeric *C. trachomatis* Pmp complexes could be visualized by Transmission Electron Microscopy (TEM) (see paragraph 3.3.18).

All homomeric *C. trachomatis* Pmp complexes formed visible structures. Homomeric motif-poor Gc showed small oligomers with round shape, while homomeric motif-poor Ac and motif-rich D and I formed elongated protofibril-like structures, indication of specificity (Fig. 24A).

Likewise, heteromeric motif-poor and motif-rich Ac+D and Ac+I and heteromeric motif-rich D+I Pmp oligomers were visualized by TEM as elongated oligomers (Fig. 24B). Surprisingly, heteromeric motif-poor Ac+Gc Pmp oligomers formed very long and complex protofibril-like structures. In all co-refolded samples, Pmp mixture could be visualized not only as elongated structures, but also as shorter filaments, suggesting the presence of different species of hMW complexes (Fig. 24B).
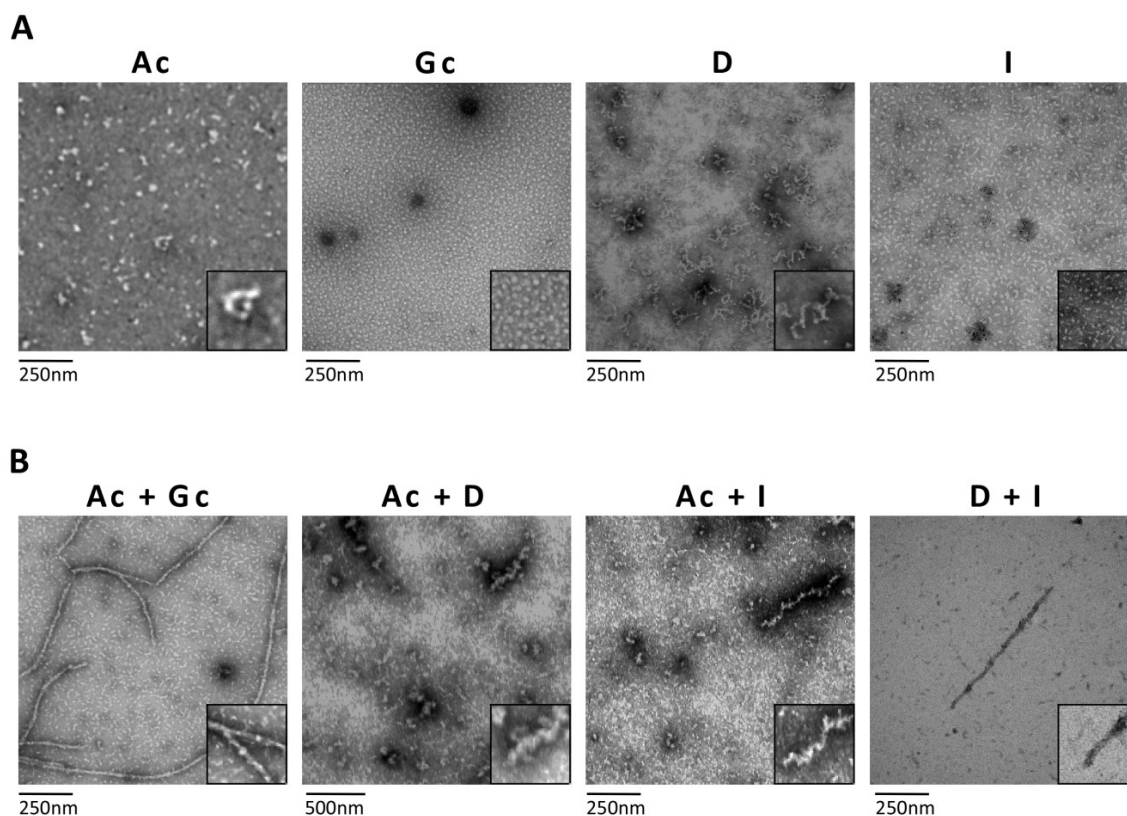
Figure 24. Homomeric and heteromeric complexes form protofibril-like structures. Representative Transmission Electron Microscopy (TEM) pictures of homomeric Ac, Gc, D and I Pmp oligomers (**A**) and heteromeric Ac+Gc, Ac+D, Ac+I and D+I Pmp oligomers, each formed by two co-refolded Pmps in an initial 1:1 molar ratio (**B**). 10 µl of 0,5 µM protein samples were loaded on 200 square mesh copper nets grids and negatively stained with 1% Uranyl acetate. 1:2 enlargements are shown at the bottom right of each picture. The bars indicate the magnification.

The length of the different Pmp oligomers was quantified. Homomeric motif-poor Gc small oligomers presented an average diameter of 12 nm, while homomeric Ac, D and I Pmp elongated structures had an average length of 32, 70 and 29 nm, respectively (Fig. 25A). Heteromeric Ac+D, Ac+I and D+I elongated oligomers had an average length of 207, 120 and 92 nm, respectively; reaching up to 749, 604 and 804 nm, respectively (Fig. 25A). The longest structures visualized were formed by co-refolded Ac+Gc Pmp oligomers, with an average length of 186 nm, reaching up to 2932 nm (Fig. 25A).

Interestingly, when the length of homomeric oligomers was compared with the length of

heteromeric oligomers, it became obvious that all heteromeric protofibril-like structures were significantly longer than the respective homomeric oligomeric structures (Fig. 25A). Despite the differences in length, all Pmp structure presented a similar width, except for heteromeric Ac+D and Ac+I, which showed larger complexes, with an average width of 48 and 52 nm, respectively (Fig. 25B). Homomeric Ac, Gc, D and I presented an average width of 17, 13, 20 and 16 nm, respectively; while heteromeric motif-poor Ac+Gc and motif-rich D+I showed an average width of 18 and 13 nm, respectively (Fig. 25B).
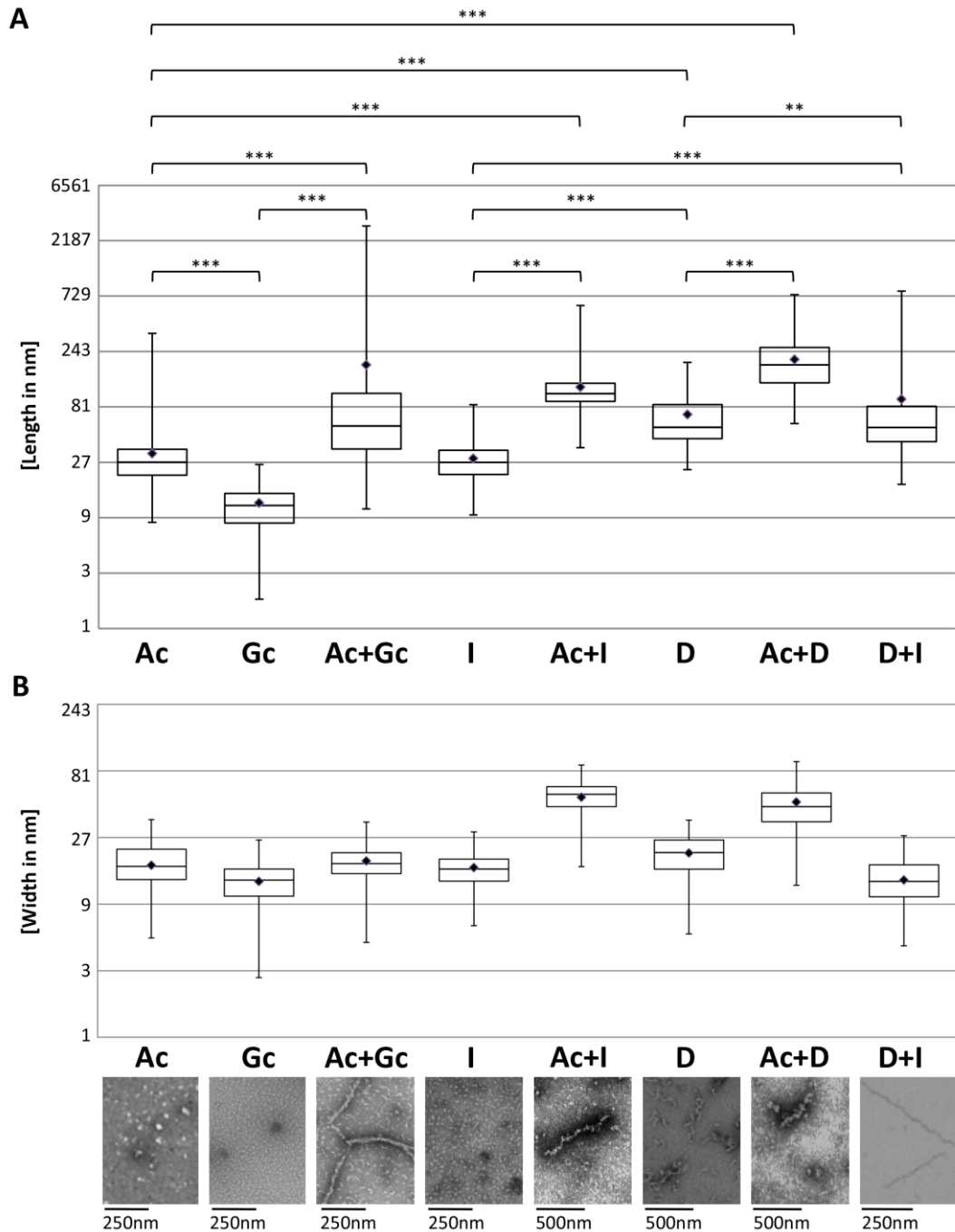
Figure 25. Heteromeric Pmp complexes form longer oligomers than homomeric Pmp complexes. A. Quantification of the length of 100 oligomers from 3 independent pictures, in total 300 oligomers for each homomeric and heteromeric Pmp complex. **B.** Quantification of the width

of 50 oligomers from 2 independent pictures, in total 100 oligomers for each homomeric and heteromeric Pmp complex. **A-B.** Pmp structures were measured with ImageJ and results were displayed in boxplots in a logarithmic scale, base 3. Maximum and minimum values are indicated by the whiskers, 1st and 3rd quantiles indicate 50 % of the total data, separated by the median. P-Value calculations are based on the means shown as black dots. **: $p<0.01$, ***: $p<0.001$. Representative TEM pictures at the bottom. The bars indicate the magnification.

Taken all together, Far-Western blots, MST, Blue native-PAGE, second dimension SDS-PAGE, SEC and TEM analyses support the conclusions that different motif-poor and motif-rich *C. trachomatis* Pmp proteins form hMW oligomeric structures. Different combinations of two different Pmps generate heteromeric hMW complexes, with different characteristics from the respective homomeric oligomers. Most Pmp oligomers form elongated structures, as detected by TEM, indicating that these structures are specific.

4.1.6 Homomeric and heteromeric Pmp oligomers show different binding capacity to human epithelial cells

In order to investigate whether the *C. trachomatis* homomeric and heteromeric Pmp oligomers are functional, the different complexes were tested for their ability to bind human epithelial HEp-2 cells. For this purpose, soluble adhesion assays with recombinant proteins were performed as described in Fig. 26 (see paragraph 3.4.2).
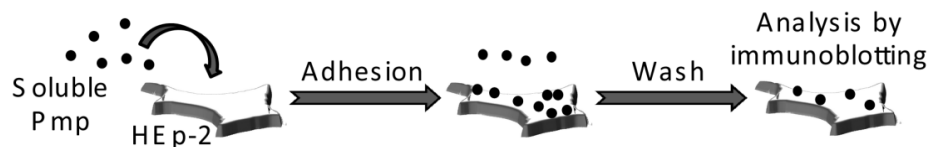
Figure 26. Schematic representation of adhesion assay with soluble recombinant proteins. 100 µg/ml soluble Pmp oligomers were incubated for 1 h at 37 °C with confluent human epithelial HEp-2 cells. Unbound proteins were removed by washing three times with HBSS solution. Cells with bound proteins were solubilized with cell dissociation solution for 10′ at 37 °C and the fractions were analyzed via immunoblotting.

4.1.6.1 *C. trachomatis* homomeric and heteromeric motif-poor Pmp oligomers show different binding capacity

The first adhesion assays focused on motif-poor Pmp proteins. *C. trachomatis* homomeric motif-poor Ac, Fc and Gc, and heteromeric motif-poor Ac+Gc, Fc+Ac and Fc+Gc Pmp mixtures were tested for their ability to bind human epithelial HEp-2 cells. Recombinant GST, used as a negative control, could not bind human cells; while *C. trachomatis* adhesin Ctad1, used as positive control, showed a strong signal in the binding fraction, as has been already published (Stallmann and Hegemann 2016) (Fig. 27). Homomeric motif-poor Fc

mixture could bind strongly to human epithelial cells after 1 hour of incubation (Fig. 27). On the other hand, homomeric motif-poor Ac mixture showed no binding capacity to human cells, while homomeric Gc mixture presented a very weak binding signal; despite both Ac and Gc Pmp proteins harbor two motifs (Fig. 27). In this adhesion assay set-up, heteromeric motif-poor Ac+Gc oligomers showed very weak adhesion to human cells. Only a very weak band for Gc, but not for Ac, was detected in the binding fraction, suggesting that homomeric Gc complexes might be still present in the mixture, together with the heteromeric complexes or that Ac might help Gc in exposing the adhesive domains, mediating a weak binding (Fig. 27). Interestingly, adhesive-competent Fc lost almost all its adhesive capacity when in a heteromeric complex with Ac or Gc. In the Fc+Ac mixture, Ac was not detected in the binding fraction, while a very weak band could be seen for Fc, suggesting the presence of a small portion of homomeric adhesive-competent Fc oligomers in the mixture; while the rest of Fc, as compared to the input control, is probably masked in the heteromeric complexes Fc+Ac by adhesion-incompetent Ac (Fig. 27). In the Fc+Gc mixture, a weak band for both Gc and Fc could be detected. Gc signal in this mixture was stronger than the homomeric Gc signal, while the Fc signal was weaker than the homomeric Fc signal, suggesting that in some of the different heteromeric Fc+Gc complexes formed, Fc is able to bring Gc in the binding fraction; while in the majority of the heteromeric Fc+Gc complexes formed Gc might mask the adhesive-competent Fc Pmp (Fig. 27).

These data show that fragments of different Pmps with similar characteristics (position within the PD and number of motifs) have different binding capacity. Furthermore, they indicate that presence of two motifs is not sufficient for adhesion of *C. trachomatis* recombinant Pmp proteins to human cells in this type of adhesion assay.
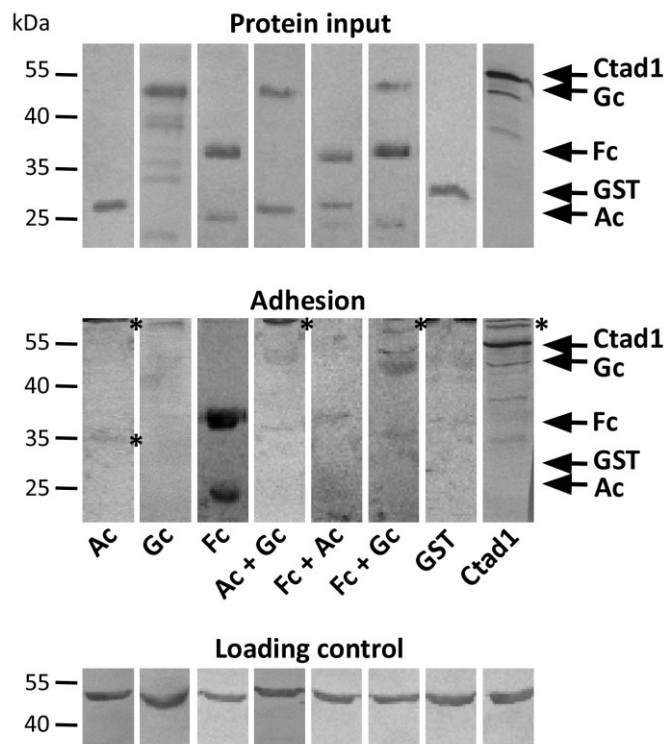
Figure 27. Homomeric and heteromeric motif-poor Pmp oligomers show different binding capacity to human cells. Adhesion capacity of 100 µg/ml renatured homomeric Ac, Fc, Gc Pmp oligomers and of heteromeric Ac+Gc, Fc+Ac and Fc+Gc Pmp oligomers, formed by co-refolding of the two Pmp proteins in a 1:1 initial molar ratio. rGST and rCtad1 were used as negative and positive control respectively. Protein mixture was incubated with human epithelial HEp-2 cells for 1 h at 37 °C. Unbound proteins were washed away and the binding was analyzed by immunoblotting. Anti-His antibody was used to determine the input of soluble recombinant proteins (protein input) and their binding capacity (adhesion). An anti-actin antibody was used to verify the amount of HEp-2 cells (loading control). Unspecific bands are indicated with *. Arrows mark the position of the proteins.

4.1.6.2 Co-refolded and mixed motif-poor Pmp oligomers show different binding capacity

Next, adhesion capacity of oligomers formed by mixing of two Pmps already in their folded status (Fig. 21) was compared with the respective Pmps co-refolded in a 1:1 initial molar ratio. As already shown in figure 27, homomeric motif-poor Fc Pmp oligomers could bind strongly human cells; while homomeric motif-poor Ac showed no binding and homomeric motif-poor Gc presented only a very weak binding capacity (Fig. 28). Mixed heteromeric Ac+Gc Pmp oligomers could not bind human cells in soluble adhesion assays, only a very weak band for Gc was detected, comparable to the binding capacity detected for co-refolded Ac+Gc Pmp oligomers (Fig. 28). Mixed Fc+Ac and Fc+Gc showed also a weak binding capacity, comparable to the respective co-refolded Pmp oligomers. In both mixed oligomers, Fc signal was a little bit stronger than in the co-refolded oligomers,

possibly due to the majority of homomeric complexes present in the mixed samples (Fig. 28). These data suggest that when two different Pmps are mixed already in their renatured status, they organize themselves in hMW complexes, which are different from the hMW oligomers formed by co-refolded Pmps.
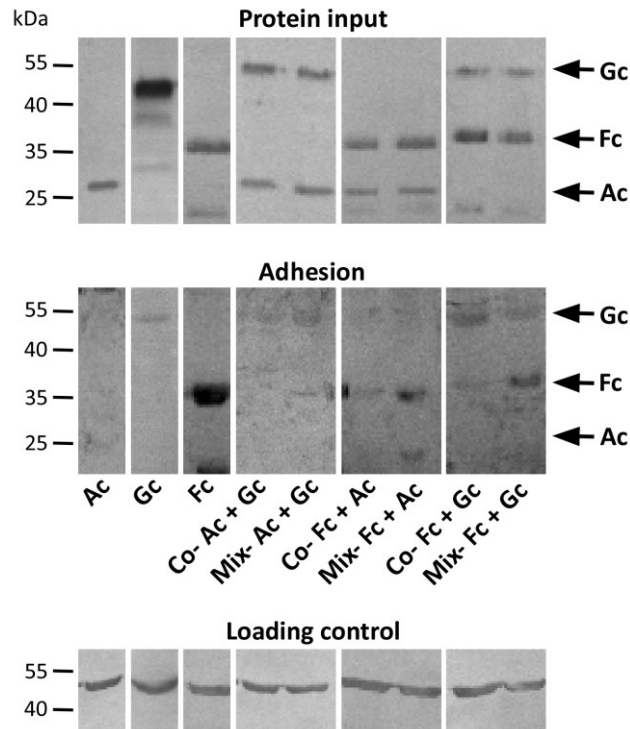
Figure 28. Motif-poor mixed Pmp complexes show different binding capacity than co-refolded Pmp complexes. Adhesion capacity of 100 µg/ml renatured homomeric Ac, Fc, Gc Pmp oligomers and of Ac+Gc, Ac+Fc and Fc+Gc Pmp oligomers, formed by co-refolding of the two Pmps in a 1:1 initial molar ratio (Co-) and by mixing of the two Pmps already in their folded status (Mix-). Protein mixture was incubated with human epithelial HEp-2 cells for 1 h at 37 °C. Unbound proteins were washed away and the binding was analyzed by immunoblotting. Anti-His antibody was used to determine the input of soluble recombinant proteins (protein input) and their binding capacity (adhesion). An anti-actin antibody was used to verify the amount of HEp-2 cells (loading control). Arrows mark the position of the proteins.

4.1.6.3 Adhesive-incompetent Ac is found in the adhesive fractions when in a heteromeric oligomer with adhesive-competent motif-rich Pmps

Soluble adhesion assays were performed for motif-rich homomeric Pmp oligomers and for co-refolded heteromeric D+I, Ac+D, Ac+H and Ac+I Pmp oligomers. Homomeric motif-rich Pmp oligomers H, I and D showed binding capacity in soluble adhesion assays (Fig. 29), confirming the results obtained in yeast adhesion and in protein-coated fluorescent-beads binding assays (Becker and Hegemann 2014). Heteromeric oligomers formed by co-refolding of motif-rich adhesive-competent D and I (D+I) were also able to adhere to human epithelial HEp-2 cells, like the respective homomeric oligomers (Fig. 29).

In contrast, homomeric motif-poor Ac showed no adhesion in this adhesion assay (Fig. 29). Interestingly, when the adhesive-incompetent Ac is in a heteromeric complex with adhesive-competent motif-rich D, H or I (Ac+D, Ac+H and Ac+I), now, also Ac could be detected in the binding fractions (Fig. 29).

These data confirm the adhesion capacity of *C. trachomatis* motif-rich Pmp proteins. Furthermore, the presence of adhesive-incompetent Ac in the binding fractions of heteromeric complexes indicates that Ac can act as building block of adhesive-competent heteromeric oligomers.
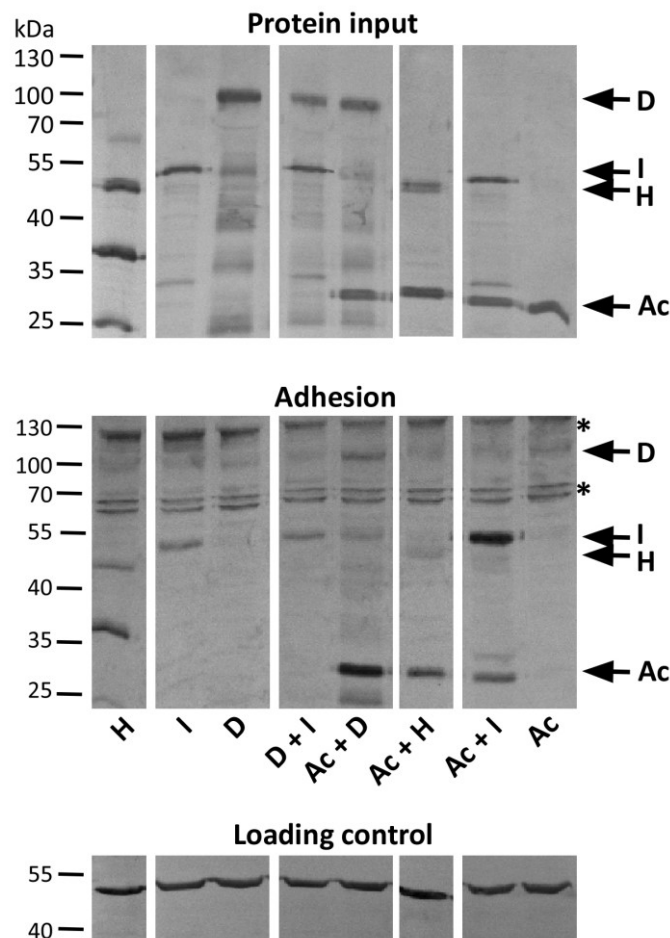
Figure 29. Adhesive-incompetent Ac is found in the adhesive fractions when in a heteromeric oligomer with adhesive-competent D, H and I. Adhesion capacity of 100 µg/ml renatured homomeric motif-rich H, I, D and motif-poor Ac Pmp oligomers, and of heteromeric D+I, Ac+D, Ac+H and Ac+I Pmp oligomers, formed by co-refolding of the two Pmp proteins in a 1:1 initial molar ratio. Protein mixture was incubated with human epithelial HEp-2 cells for 1 h at 37 °C. Unbound proteins were washed away and the binding was analyzed by immunoblotting. Anti-His antibody was used to determine the input of soluble recombinant proteins (protein input) and their binding capacity (adhesion). An anti-actin antibody was used to verify the amount of HEp-2 cells (loading control). Unspecific bands are indicated with *. Arrows mark the position of the proteins.

4.1.6.4 Different fragments of the same Pmp show different adhesion capacity

Considering that different fragments of different *C. trachomatis* Pmp proteins showed different adhesion capacities in soluble adhesion assays (Fig. 27-29); the adhesion capacities of different fragments of the same *C. trachomatis* Pmps were tested, aiming at identifying a domain responsible for Pmp binding to human cells.

Motif-poor, motif-rich and medium motif density fragments of PmpA, PmpE and PmpF were analyzed (Fig. 30A). PmpA motif-rich fragment A (20 motifs) and medium motif density An (6 motifs) showed adhesion to human cells, while motif-poor Ac (2 motifs) was again adhesive-incompetent, with only a very weak signal, compared to the input control (Fig. 30B). PmpE fragment En with medium motif density (8 motifs) was able to adhere to human cells, in contrast to motif-poor Ec (2 motifs), which could only bind very weakly (Fig. 30B). In contrast, PmpF motif-poor Fc (2 motifs) adhered strongly to human cells, almost like motif-rich F (19 motifs), compared to the input control; while the Fn fragment with medium motif density (9 motifs) showed no binding to human cells (Fig. 30B).

From these data is not possible to identify a domain of *C. trachomatis* Pmp PD responsible for adhesion to human cells.
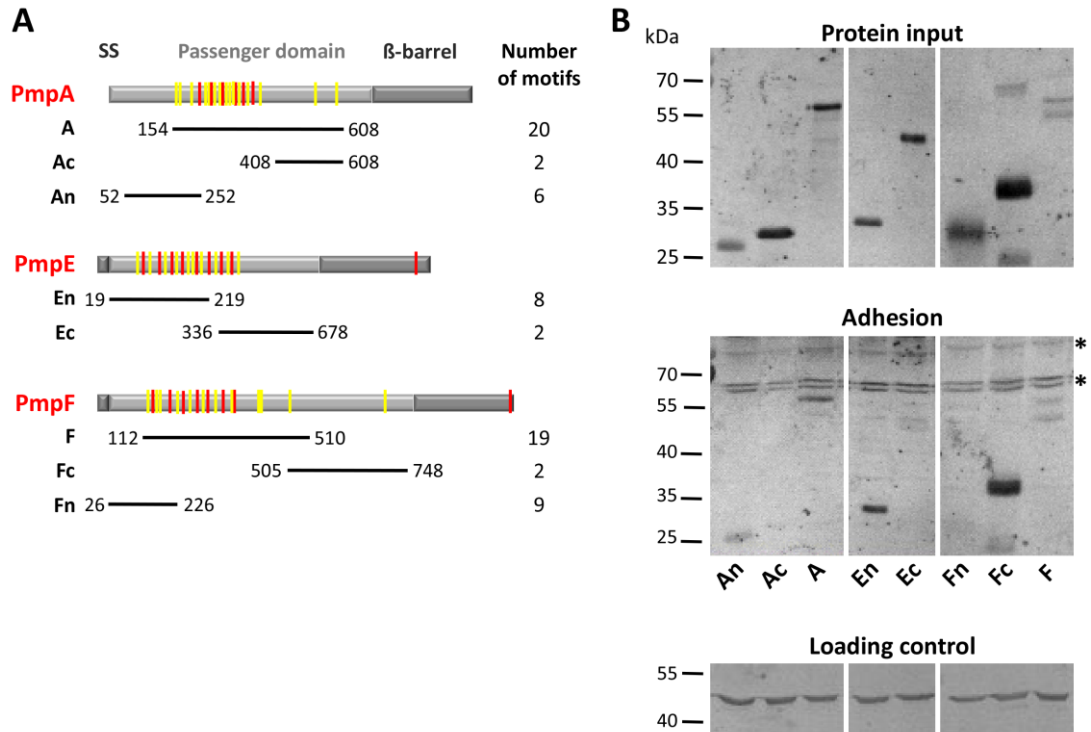
Figure 30. Different fragments of the same *C. trachomatis* Pmp have different adhesion capacity. A. Schematic representation of *C. trachomatis* serovar E PmpA, PmpE and PmpF with the analyzed motif-poor (Ac, Ec and Fc), motif-rich (A and F) and medium motif density (An, En and Fn) protein fragments. The numbers indicate the first and the last amino acid of the fragments generated. The number of motifs in each fragment is indicated on the right. SS: signal sequences

(SS is not predicted for PmpA). **B.** Adhesion capacity of 100 µg/ml of the different PmpA, PmpE and PmpF fragments. Pmps were incubated with human epithelial HEp-2 cells for 1 h at 37 °C. Unbound proteins were washed away and the binding was analyzed by immunoblotting. Anti-His antibody was used to determine the input of soluble recombinant proteins (protein input) and their binding capacity (adhesion). An anti-actin antibody was used to verify the amount of HEp-2 cells (loading control). Unspecific bands are indicated with *.

4.1.7 Homomeric and heteromeric Pmp oligomers show an adhesion-dependent relevance for the *C. trachomatis* infection

Since *C. trachomatis* homomeric and heteromeric Pmp oligomers analyzed in this work showed different adhesion capacities to human epithelial cells, their relevance for a *C. trachomatis* infection was analyzed in two different infection blocking assays.

4.1.7.1 Homomeric and heteromeric Pmp oligomers reduce *C. trachomatis* infection in a different degree

In the first setting, human epithelial HEp-2 cells were pre-incubated with recombinant Pmp proteins and with control proteins. Unbound proteins were washed away and then the cells were infected with *C. trachomatis* EBs. The infection rate was quantified by counting the inclusions formed at 24 hpi (Fig. 31A) (see paragraph 3.4.3).

Upon binding to human receptors, *C. trachomatis* adhesin rCtad1, used as positive control, reduced the infection rate of 60 %; while, pre-incubation of human cells with adhesive-incompetent BSA and rGST, used as negative controls, showed no effect on the infection rate (Fig. 31). Adhesive-incompetent homomeric Ac and Gc and heteromeric Ac+Gc Pmp oligomers pre-incubated with human cells showed no influence on *C. trachomatis* infection, with an infection rate of 99 %, 94 % and 110 % respectively, indistinguishable from the PBS-treated sample and the negative controls BSA and rGST (Fig. 31).

In contrast, adhesive-competent homomeric I and D Pmp oligomers pre-incubated with human cells reduced the infection rate by 53 % and 55 % respectively. Adhesive-competent heteromeric Ac+I and Ac+D Pmp complexes also reduced the *C. trachomatis* infection by 60 % and 53 % respectively, compared to the PBS-treated sample, similarly to the positive control Ctad1. Heteromeric D+I Pmp oligomer, formed by co-refolding of the two adhesive-competent D and I Pmps, showed no additive effect, reducing the infection by 57 %, compared to the PBS-treated sample, similar to the two homomeric Pmp D and I alone (Fig. 31). These data indicate that adhesive-competent Pmp oligomers are able to bind and block human receptors used by *C. trachomatis* EBs to infect the host cells,

proving their role in the *C. trachomatis* infection.
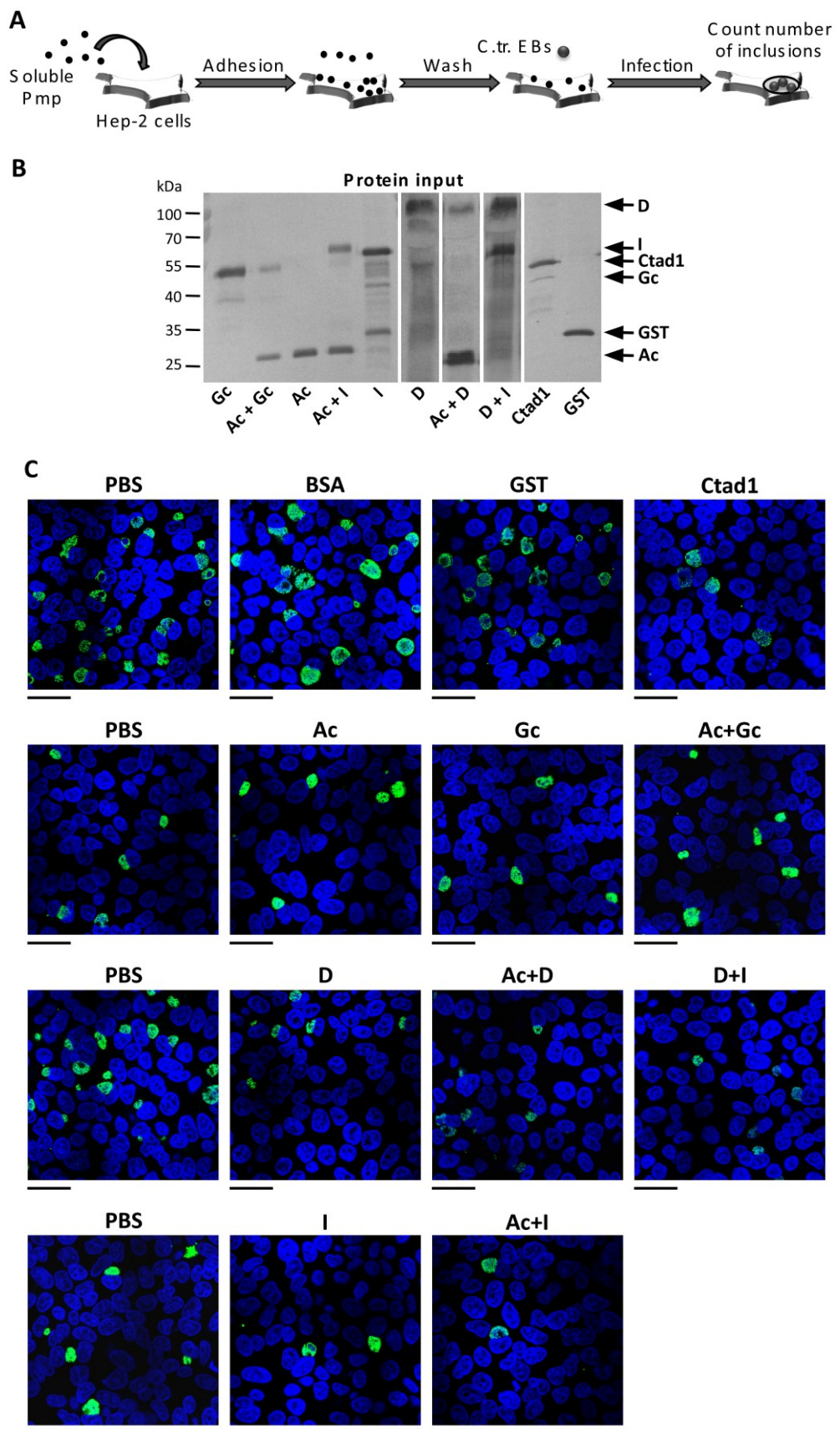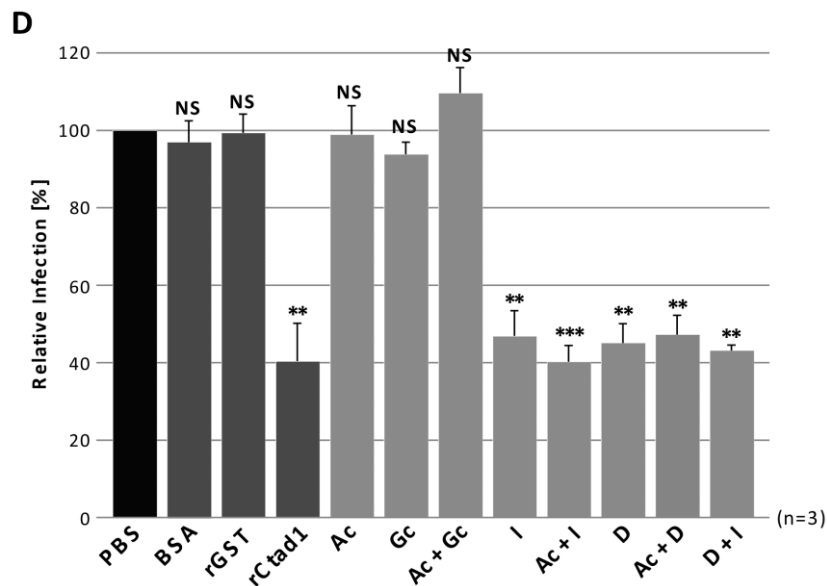
Figure 31. Homomeric and heteromeric Pmp oligomers reduce *C. trachomatis* infection to a different degree. A. Schematic representation of infection blocking assay. Soluble Pmp oligomers and control proteins (200 µg/ml final concentration) were incubated for 1 h at 37°C with confluent human epithelial HEp-2 cells. Unbound proteins were removed by washing three times with HBSS solution and infected with *C. trachomatis* EBs (MOI 10). The number of inclusions was counted at 24 hpi. **B.** Anti-His immunoblot of homomeric and co-refolded heteromeric Pmp input samples. Arrows indicate the bands of the full length Pmp proteins and of control proteins rCtad1 and rGST. **C.** Representative pictures of immunofluorescence microscopy. For detection of chlamydial inclusions, infected cells were fixed and permeabilized with 3 % PFA + 96 % methanol and stained with anti-MOMP antibody to visualize chlamydial inclusions (green), and DAPI to visualize DNA (blue). Scale bars: 25 µm. **D.** Quantifications of the infection blocking assay using recombinant homomeric and heteromeric Pmp proteins (light grey). BSA, rGST and rCtad1 were used as controls (dark grey). Infection rate was determined by counting the number of inclusions per $5.8 * 10^3$ HEp-2 cells and is expressed as a percentage of the number of inclusions determined by the PBS-treated sample (black). Results are from three separate experiments (n=3). Data shown are means + standard deviations. **: $p<0.01$, ***: $p<0.001$, NS: No significant difference compared to PBS-treated sample.

4.1.7.2 *C. trachomatis* EBs coated with homomeric and heteromeric Pmp oligomers show different capacity to infect human epithelial cells

Next, the complementary blocking experiment was performed by pre-incubating infectious EBs with recombinant Pmp proteins. *C. trachomatis* EBs were first incubated with soluble homomeric and co-refolded heteromeric Pmp oligomers and then used to infect human epithelial cells. The infection rate was quantified by counting the inclusions formed at 24 hpi (Fig. 32A) (see paragraphs 3.4.4 and 3.4.5).

All homomeric and heteromeric Pmp oligomers were able to coat *C. trachomatis* EBs, possibly binding to naturally exposed Pmp structures on the EB surface. rCtad1 and rGST control proteins also bound the EBs; Ctad1 is known for interacting with itself (Stallmann

2015) (Fig. 32B).
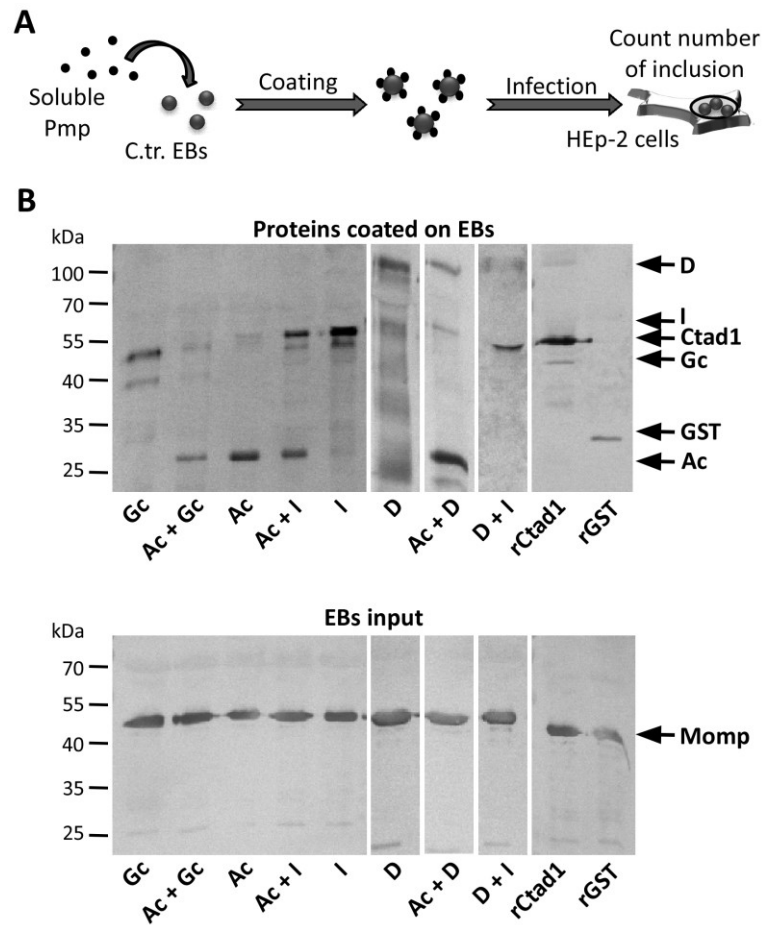
Figure 32. *C. trachomatis* EBs can be coated with soluble homomeric and heteromeric Pmp oligomers. A. Schematic representation of infection assays using EBs pre-incubated with recombinant Pmp proteins. 1 µM soluble Pmp oligomers or protein controls were incubated with *C. trachomatis* EBs for 30 minutes on ice. Unbound proteins were removed and coated EBs were used to infect human epithelial HEp-2 cells (MOI 10). The number of inclusions was counted at 24 hpi. **B.** Western Blot of EBs coated with homomeric and heteromeric Pmp oligomers or with control proteins. Recombinant Pmp oligomers and control proteins rCtad1 and rGST bound to EBs were detected with anti-His antibody (top); while *Chlamydia* EBs were detected with anti-MOMP antibody (bottom). Arrows indicate the bands of the full length Pmp proteins and of rCtad1 and rGST.

EBs coated with control proteins BSA and rGST did not influence the infection rate (108 %), compared to the PBS-treated sample; while EBs coated with control protein rCtad1 boosted the infection rate significantly (157 %), compared to the PBS-treated sample (Fig. 33). EBs coated with adhesive-incompetent homomeric Ac and Gc and heteromeric Ac+Gc Pmp oligomers showed a reduction of the infection of 51 %, 62 % and 58 % respectively, compared to the PBS-treated sample. Possibly, adhesive-incompetent Pmp oligomers are binding to and masking naturally exposed Pmp structures on EBs (Fig. 33). EBs coated with adhesive-competent homomeric I and D and with heteromeric

Ac+I, Ac+D and D+I Pmp oligomers did not influence significantly the infection rate, compared to the PBS-treated sample, with an infection rate of 78 %, 97 %, 78 %, 100 % and 101 %, respectively. Possibly, adhesive-competent Pmp oligomers are binding to naturally exposed Pmp structures on the EB surface, thus substituting their function (Fig. 33).

These data indicate that all Pmp mixtures are able to bind to the EB surface. EBs coated with adhesive-incompetent homomeric and heteromeric Pmp oligomers showed a significantly lower rate of infection; while EBs coated with adhesive-competent homomeric and heteromeric Pmp oligomers are able to mediate a *C. trachomatis* infection, proving their relevance for the infection.
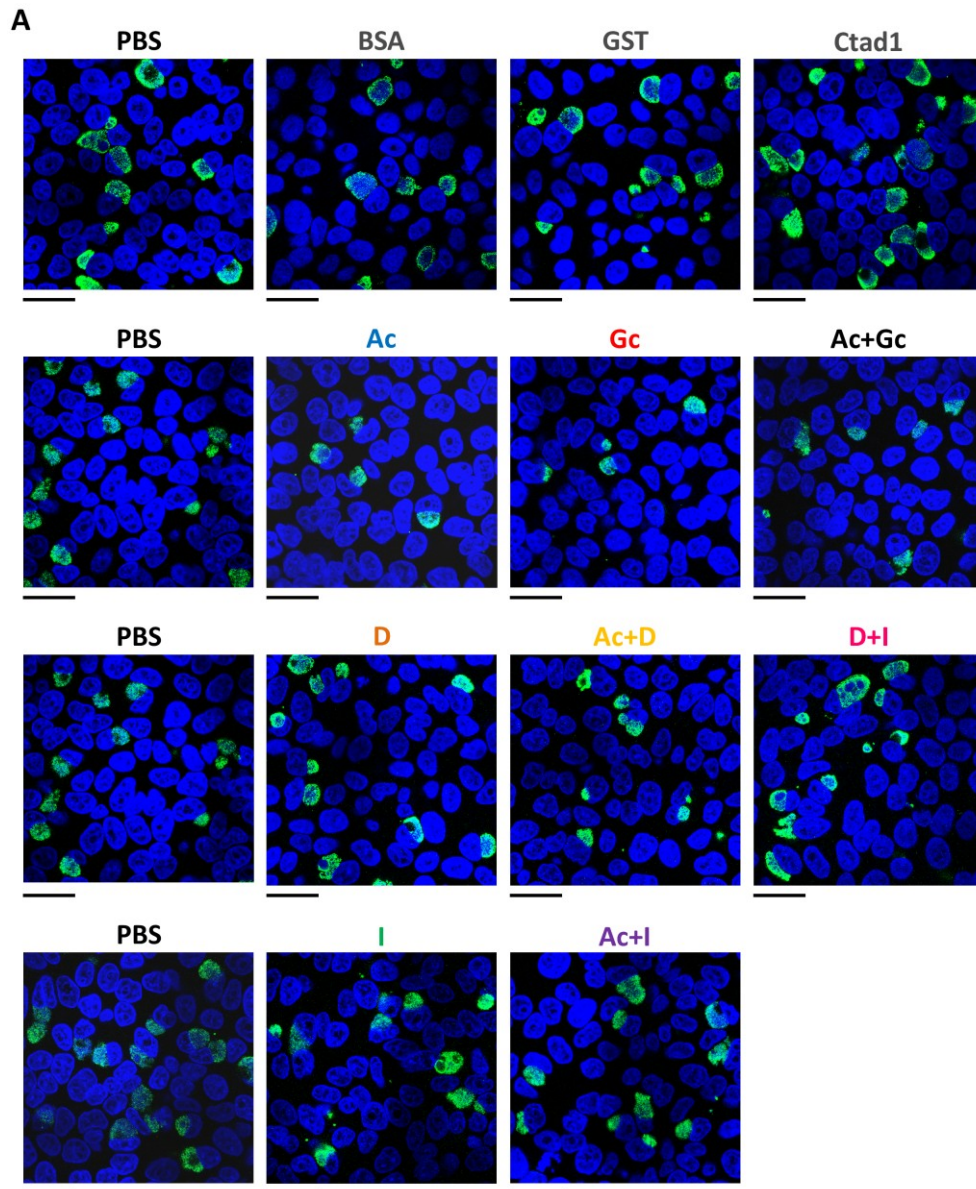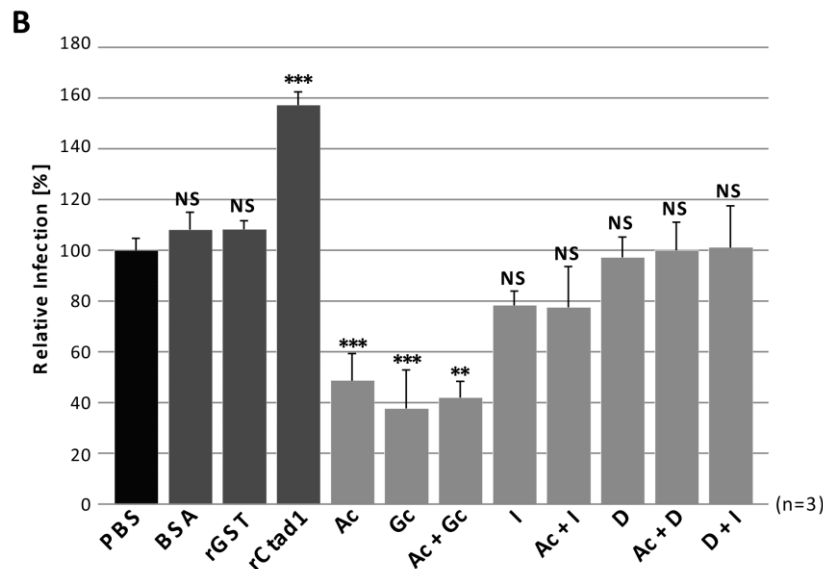
Figure 33. *C. trachomatis* **EBs coated with homomeric and heteromeric Pmp oligomers have different capacity to infect human epithelial cells. A.** Representative pictures of immunofluorescence microscopy of cells infected with protein-coated EBs. For detection of chlamydial inclusions, infected cells were fixed and permeabilized with 3 % PFA + 96 % methanol and stained with anti-MOMP antibody to visualize chlamydial inclusions (green), and DAPI to visualize DNA (blue). Scale bars: 25 μm. **B.** Infection capacity of *C. trachomatis* EBs coated with homomeric or heteromeric Pmp oligomers prior to infection of human epithelial HEp-2 cells (light grey). BSA, rGST and rCtad1 were used as controls (dark grey). Infection rate was determined by counting the number of inclusions per $5.8 * 10^3$ HEp-2 cells and is expressed as a percentage of the number of inclusions determined by the PBS-treated sample (black). Results are from three separate experiments (n=3). Data shown are means + standard deviations. ******: p<0.01, *******: p<0.001, NS: No significant difference compared to PBS-treated sample.

4.1.8 Structure prediction of *C. trachomatis* motif-poor and motif-rich Pmp fragments

The *C. trachomatis* Pmp proteins analyzed in this work presented ability to oligomerize and showed different functional properties. Therefore, we decided to look into the predicted structures of adhesion-competent (Fc, D, H and I) and adhesion-incompetent (Ac and Gc) Pmp proteins, in order to understand if they present a conserved structure, despite harboring a different number of motifs and representing different regions of the passenger domain. Previous bioinformatic analysis of *C. pneumoniae* and *C. trachomatis* Pmps predicted a 3-domain structure, composed of an α-helical N-terminal region, a β-helical central region and a C-terminal β-barrel (Henderson and Lam 2001). The β-helical core structure was detected in all Pmps in the region of the passenger domain harboring high density of motifs FxxN and GGA(I, L, V). Further bioinformatic predictions of Pmp21 and PmpD showed that the motifs are exposed at the corners of the triangular β-helix (Becker 2013). Structure predictions of *C. trachomatis* motif-poor Ac, Fc and Gc and motif-rich D,

H and I Pmp proteins were performed with Phyre2 (**P**rotein **H**omology/Analog**Y** **R**ecognition **E**ngine V **2**.0) server (http://www.sbg.bio.ic.ac.uk/phyre2).

Phyre2 is a server for protein structure prediction where the sequence of the protein of interest is scanned against a database, creating a multiple-sequence alignment, used to predict the secondary structure. The resulting secondary structure is then compared against a database of proteins with known structure and the query is modeled into the predicted final 3D model (Kelley, Mezulis et al. 2015). Motif-rich D, H and I Pmp proteins include the predicted β-helical core structure of the passenger domain, with high density of the motifs; while motif-poor Ac, Fc and Gc Pmp proteins represent the C-terminal region of the passenger domain and do not include the β-helical core structure.

When analyzed with the Phyre2 server, motif-poor Ac and Gc and motif-rich H and I Pmp proteins were modeled in the triangular β-helical structures, in agreement with the β-helical structures predicted for the full length passenger domain (Fig. 34). FxxN and GGA(I, L, V) motifs could be identified at the corners of the β-helical structure of Gc, H and I Pmp proteins, as predicted for the respective full length Pmps. The β-helical structure predicted for Pmp Ac represents only a small region of Ac sequence, which does not contain the two FxxN motifs (Fig. 34).

Motif-poor Ac, motif-poor Gc and motif-rich I Pmps show a sequence identity of 23 %, 26 % and 25 %, respectively to the C-terminal domain of a putative adhesin from *Cardicellulosiruptor kronotskyensis* (Fig. 34A-B-D). Motif-rich H shows only 13 % sequence identity to galacturonase, a pectin lyase-like protein, which folds as a single-stranded right-handed β-helix (Fig. 34C). Unfortunately, sequences of motif-poor Fc and motif-rich D Pmp fragments did not give any predicted model.
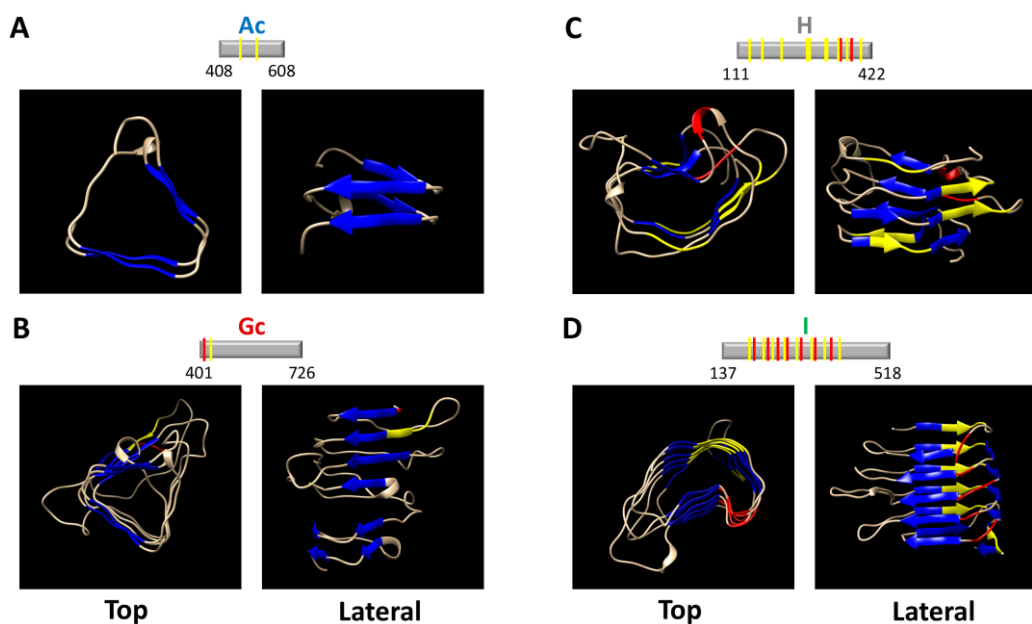
Figure 34. Predicted structures of motif-poor and motif-rich *C. trachomatis* Pmp proteins. Phyre2 structure prediction of motif-poor Ac (**A**) and Gc (**B**) and motif-rich H (**C**) and I (**D**) Pmp proteins. All Pmps exhibit a predicted triangular β-helix. Pmp proteins analyzed are shown on top of the predicted structure. Top and lateral views of the predicted structures are shown on the left and right, respectively. Blue arrows indicate predicted secondary β-strands, yellow regions represent FxxN motifs and red regions represent GGA(I, L, V) motifs. Images are processed with UCSF Chimera server (https://www.cgl.ucsf.edu/chimera/).

4.1.9 Analysis of surface exposed Pmp oligomers on EBs *in vivo*

In order to test whether homomeric and heteromeric Pmp oligomers are located on the EB surface *in vivo*, a number of initial co-immunoprecipitation assays was performed, followed by immunoblotting and mass spectrometry analysis. With the purpose of establishing a successful protocol, *C. pneumoniae* infected cells were used, due to the availability of an anti-M-Pmp21 antibody in the laboratory (Fig. 35) (see paragraphs 3.3.7 and 3.3.16.4).
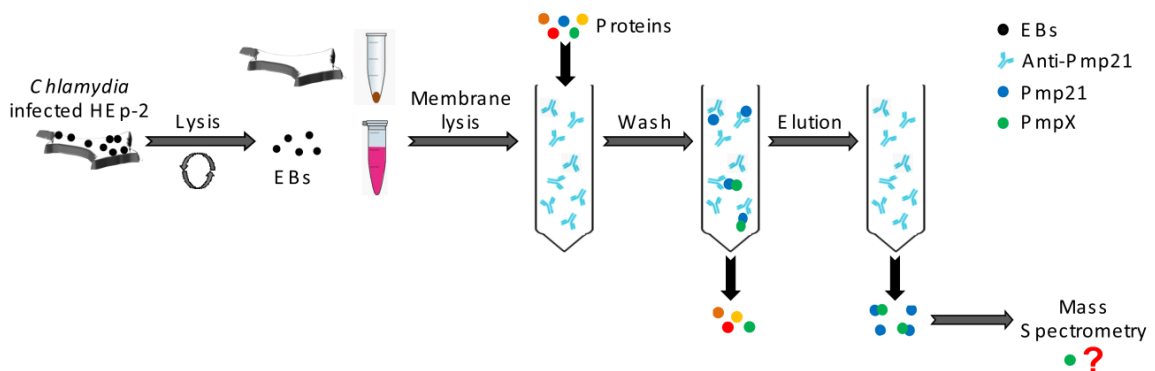
Figure 35. Schematic representation of co-immunoprecipitation from infected cells. HEp-2 cells infected with *C. pneumoniae* EBs (MOI: 10) were osmotically lysed at 80 hpi and the EB membrane components were solubilized using detergents. The obtained EB membrane components solution was incubated with an anti-Pmp21 antibody coupled on protein-G agarose and immunoprecipitation was performed. The eluted sample was then analyzed by immunoblotting and mass spectrometry.

To solubilize EB membranes, two major approaches were followed. The first approach was performed by incubating the EBs with Phospholysis buffer, followed by incubation with other detergents or reducing agents, with the purpose of disrupting and solubilizing the insoluble complexes on the EB surface. Cross-linker DTSSP was also used after Phospholysis buffer, to cross-link interacting proteins on the EB surfaces. The second approach was based on cross-linking first the interacting proteins on the EB surface with DTSSP, followed by lysis with Phospholysis buffer and other detergents or reducing agents (Fig. 36).
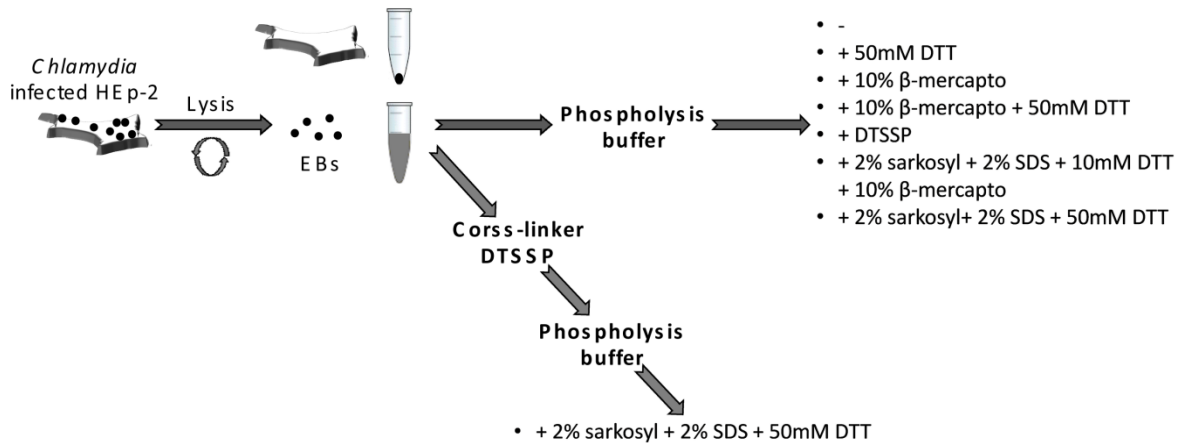
Figure 36. Schematic representation of different conditions for solubilization of EB membranes. *C. pneumoniae* infected HEp-2 cells were osmotically lysed at 80 hpi and the EB membrane components were solubilized using Phospholysis buffer or cross-link DTSSP and Phospholysis buffer, followed by the listed detergents and reducing agents.

After co-immunoprecipitation, the samples obtained were tested by immunoblotting with anti-Pmp and anti-OmcB antibodies and selected samples were sent for mass spectrometry analysis. Immunoblotting was performed with denatured proteins on the membrane and with renatured proteins on the membrane, in order to increase the sensitivity. In all experimental set-ups, enrichment of a ~60 kDa and 2 or 3 hMW bands (~ 130 kDa and higher) were detected in immunoblots of the elution fractions (Fig. 37). 60 kDa is the apparent size of the M-Pmp21 fragment. A weak band for M-Pmp21 is detected in the input sample (Fig. 37A); however, as the 60 kDa band appears in all elution fractions with all four antibodies tested, it is more likely the light chain of the antibody, which was eluted from the column (Fig. 37). Antibodies against *C. pneumoniae* Pmp6, Pmp20 and OmcB showed also enrichment in the hMW bands (Fig. 37).
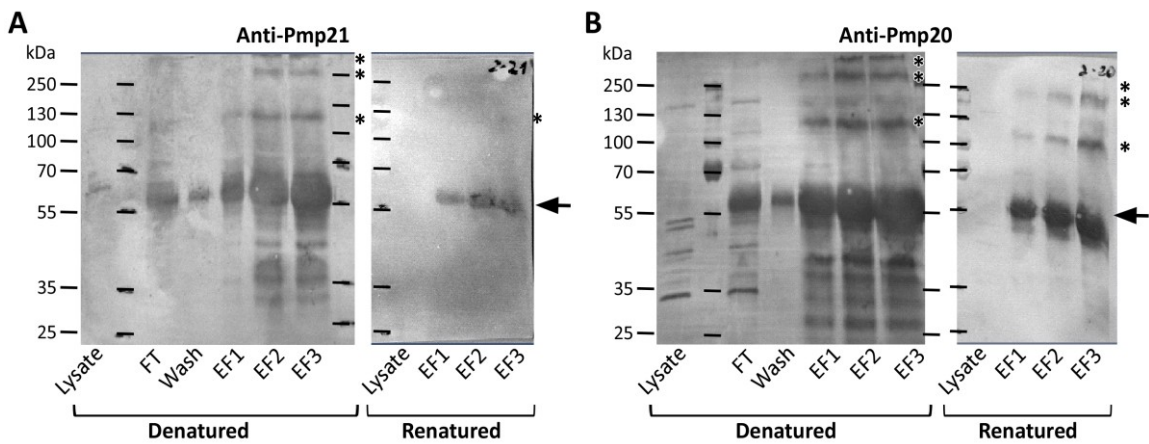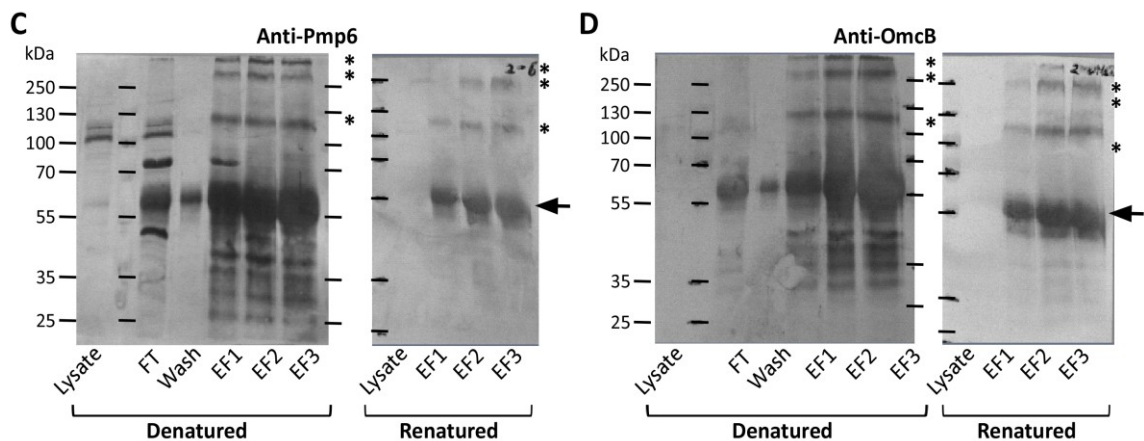
Figure 37. Analysis of a representative co-immunoprecipitation assay. Western blot analysis of samples obtained after co-immunoprecipitation performed with an anti-Pmp21 antibody. In this representative experiment, *C. pneumoniae* infected HEp-2 cells (MOI: 10) were osmotically lysed at 80 hpi; EB membranes were solubilized with Phospholysis buffer followed by incubation with 50 mM of the reducing agent DTT. 2 % of the lysate is loaded as input (Lysate), Flow-through (FT), washing sample (Wash) and three elution fractions (EF) were analyzed by immunoblotting. The denatured and renatured membranes were then incubated with anti-Pmp21 (**A**), anti-Pmp20 (**B**), anti-Pmp6 (**C**) and anti-OmcB (**D**) antibodies and visualized via secondary AP-conjugated anti-rabbit antibodies. Arrow indicates the ~60 kDa band and * indicate the hMW bands.

Samples from four conditions were analyzed by mass spectrometry (see paragraph 3.3.17).

1. Phospholysis buffer -> + 50 mM DTT
2. DTSSP -> Phospholysis buffer
3. Phospholysis buffer -> + 2 % sarkosyl+ 2 % SDS + 50 mM DTT
4. DTSSP -> Phospholysis buffer -> + 2 % sarkosyl+ 2 % SDS + 50 mM DTT

Mass spectrometry analyses were performed by Dr. Daniel Waldera-Lupa from the department of Prof. Dr. Kai Stühler at the Biological-Medical Research Center (BMFZ) at the Heinrich-Heine-University of Düsseldorf.

The results revealed that Pmp21 was detected only in the first and second set up. Outer membrane protein OmcB was also found in the first set up, together with other intra-chlamydial proteins and uncharacterized proteins (Fig. S1). However, the mass spectrometry results showed no enrichment in different Pmp proteins, therefore in the future, the experimental conditions have to be optimized.

4.1.10 Pmps: Conclusions

In this study, *C. trachomatis* Pmps were analyzed, in order to investigate their oligomerization capacities and their functional properties. Different domains of all 9 *C. trachomatis* Pmps were recombinantly produced, to have a wide representation of the whole passenger domain. The generated Pmp fragments represented the central region of the passenger domain (PD) with a high density of motifs (motif-rich), the C-terminal domains of the PD with only two motifs (motif-poor) and the N-terminal domains of the PD with a medium motif density. All different Pmp proteins tested interacted in Far-Western dot blot experiments with most, but not all other Pmp fragments of the same or of different Pmps, suggesting domain specificity for interaction. Unfortunately, a specific domain could not be identified, but the motif-rich Pmp proteins were more successful in interacting with other domains. Furthermore, most of the Pmp domains could interact with themselves.

In order to characterize in more detail the different Pmp proteins, six Pmp domains were selected: motif-poor Ac, Fc and Gc and motif-rich D, H and I.

All motif-rich and motif-poor Pmp proteins analyzed formed different species of hMW homomeric complexes, as visualized by Blue Native-PAGE and further analyzed by Size Exclusion Chromatography (SEC).

Furthermore, the motif-rich and motif-poor Pmp proteins showed interaction with each other in pull-down and MST analyses. When two different Pmp proteins were co-refolded or mixed in a 1:1 initial molar ratio, different species of hMW complexes could be detected in Blue-Native PAGE with similar or different size, compared to the two homomeric complexes alone. Second dimension SDS-PAGE revealed that the hMW complexes formed by mixed and co-refolded Pmps were composed by both protein species, but in a different ratio than the initial 1:1. SEC analysis confirmed that co-refolding of two different Pmp proteins generated hMW heteromeric complexes with different characteristics than the respective homomeric complexes alone. Moreover, motif-rich and motif-poor Pmp proteins analyzed were visualized as specific elongated protofibril-like structures of different average lengths by Transmission Electron Microscopy (TEM). Interestingly, heteromeric Pmp oligomers formed longer structures than the respective homomeric Pmp complexes. Homomeric and heteromeric Pmp complex formation is independent of the density of motifs.

Homomeric and heteromeric Pmp oligomers showed different adhesion strength to human epithelial cells, but adhesion capacity was independent of the density of motifs (e.g. motif-

poor Fc protein is strongly adhesive, while motif-poor Ac and Gc Pmps are adhesive-incompetent). Different fragments of the same Pmp with different densities of motifs showed different adhesion capacities, but a specific domain could not be identified. Thus, the adhesion capacity requires more than just the presence of motifs, and it may depend on the final 3D structure of the recombinant Pmp proteins generated.

Interestingly, adhesive-competent motif-poor Fc lost almost all its adhesive capacity when in a heteromeric complex with adhesive-incompetent Ac or Gc, possibly because the organization of adhesive-incompetent proteins in the complex masked Fc binding sites. In contrast, adhesive-incompetent Ac was found in the binding fractions when in a heteromeric complex with all the adhesive-competent motif-rich Pmps. Moreover, adhesive-competent but not adhesive-incompetent Pmp oligomers blocked a subsequent *C. trachomatis* infection, proving their relevance for the infection. Furthermore, all Pmp oligomers coated the EB surface. Adhesive-competent oligomers on EBs showed no influence on the EB infectivity, while adhesive-incompetent oligomers inhibited the infection, possibly by masking functional Pmp structures on the *Chlamydia* cell surface.

These data together indicate that *C. trachomatis* Pmps can form hMW homomeric and heteromeric complexes with elongated protofibril-like structure and functional relevance for the infection.

4.2 Characterization of Yaa3, a putative *Chlamydia pneumoniae* adhesin

C. pneumoniae adhesion to human cells is mediated by several proteins on the EB surface. In previous studies, pre-selected proteins have been tested for their adhesion properties, using a yeast display system. Three proteins (Yaa1=Cpn0473, Yaa2 and Yaa3) were identified as putative chlamydial adhesins (Fechtner 2009). Cpn0473 was characterized as a *C. pneumoniae*-specific adhesin, which directly interacts with the host cell membrane (Fechtner, Galle et al. 2016). According to a yeast display results, Yaa3 (Cpn1006) was the candidate with the strongest adhesive properties.

4.2.1 Yaa3

Yaa3 is a hypothetical protein of 161 amino acids, with a MW of 18 kDa. Yaa3 presents a predicted transmembrane hydrophobic region in the first 40 aa and almost the entire protein is composed of the DUF720 domain, which is exclusively found in several other proteins from *Chlamydia* species. However, the function of the DUF720 domain is unknown (Fig. 38A). The genomic region on the left of *yaa3* (*cpn1006*) is composed of four genes (*cpn1003, cpn1004, cpn1005* and *yaa3*) located directly adjacent to each other, forming a potential operon. Three of the four encoded proteins (Cpn1004, Cpn1005 and Yaa3) harbor a DUF720 domain (Fig. 38B). The four proteins share a relevant amino acids sequence homology and identity (Fig. 38C).

Cpn1003	Cpn1004	Cpn1005	Yaa3	Homology / Identity
100 %	21 / 14 %	20 / 13 %	23 / 18 %	Cpn1003
	100 %	31 / 20 %	31 / 26 %	Cpn1004
		100 %	33 / 21 %	Cpn1005
			100 %	Yaa3
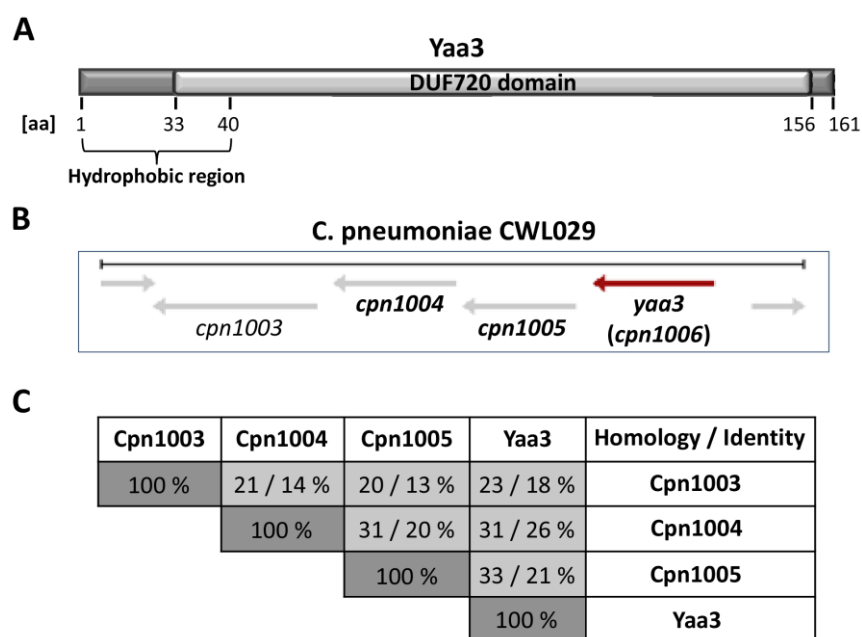
Figure 38. Yaa3. A. Schematic representation of Yaa3 protein. The amino acids indicate the

position of the DUF720 domain (light grey) and of the predicted transmembrane hydrophobic region (see paragraph 4.2.2.3). **B.** Genomic localization of *yaa3* and the three neighboring genes *cpn1003*, *cpn1004* and *cpn1005*. **C.** Amino acid homology and identity percentages among the four encoded proteins (Cpn1003, Cpn1004, Cpn1005 and Yaa3). Percentages derived from alignments of full length protein sequences in MultAlin (http://multalin.toulouse.inra.fr/multalin/) (Corpet 1988).

The same potential operon is found in all *Chlamydia* species. The orthologs proteins of Cpn1004, Cpn1005 and Yaa3 in the human pathogen *C. trachomatis* D (CT847, CT848 and CT849 respectively) also harbor the DUF720 domain and are all hypothetical proteins (Fig. S2A). Similar identity levels were found among the four *C. trachomatis* and *C. pneumoniae* proteins (between 20 and 33 %). The homologous proteins share a high full length sequence identity of 69 % for Cpn1004-CT847 and 80 % for both pairs Cpn1005-CT848 and Yaa3-CT849 (Fig. 39 and Fig. S2B).

Cpn1004	Cpn1005	Yaa3	CT847	CT848	CT849	Homology / Identity
100 %	31 / 20 %	31 / 26 %	69 / 61 %	25 / 17 %	30 / 25 %	**Cpn1004**
	100 %	33 / 21 %	26 / 19 %	80 / 73 %	29 / 18 %	**Cpn1005**
		100 %	21 / 30 %	34 / 25 %	80 / 76 %	**Yaa3**
			100 %	28 / 20 %	21 / 16 %	**CT847**
				100 %	33 / 23 %	**CT848**
					100 %	**CT849**

Figure 39. Homologous proteins identities. Amino acid homology and identity percentages among *C. pneumoniae* Cpn1004, Cpn1005, Cpn1006 and their homologous in *C. trachomatis* D CT847, CT848 and CT849. Light grey boxes indicate the homology and identity of homologous proteins. Percentages derived from alignments of full length protein sequences in MultAlin.

Database searches identified a certain amino acid similarity of the DUF720 domain from Yaa3 with only one non-chlamydial protein: P9303_01311 from *Prochlorococcus marinus*. This protein has been identified as the membrane fusion protein (MFP) component of the type 1 secretion system (T1SS). The genome area surrounding *P9303_01311* is composed of four genes (*P9303_01291-01301-01311-03121*), similar to *yaa3* genomic region. The amino acid identity between P9303_01311 and HlyD, the corresponding MFP from *E. coli* T1SS, is 24 % (34 % homology), while P9303_01311 and Yaa3 share an identity level of 22 % (31 % homology) and Yaa3 and HlyD share 15 % amino acid identity (28 % homology) (Fig. S3). A T1SS in *Chlamydia* has not yet been described.

The three *C. trachomatis* orthologous proteins CT847, CT848 and CT849 are shown to carry a functional N-terminal secretion signal in the first 20 aa, which allows the

heterologous secretion of a reporter protein via the type 3 secretion system (T3SS) in *Shigella flexeneri* or *Yersinia enterolitica* (Subtil, Delevoye et al. 2005, Chellas-Gery, Linton et al. 2007, da Cunha, Milho et al. 2014). When Yaa3 was analyzed for a T3 secretion signal sequence, conflicting results were obtained. SecretomeP 2.0 program (http://www.cbs.dtu.dk/services/SecretomeP/) indicated that the protein is not-classically secreted; on the other hand, EffectiveT3 program (http://www.effectors.org) and the Type III secretion system effector prediction program (http://gecco.org.chemie.uni-frankfurt.de/T3SS_prediction/T3SS_prediction.html) suggested presence of a T3SS signal sequence. The first 25 amino acid of Yaa3, Cpn1005 and Cpn1004 were aligned with the first 25 amino acid of CT849, CT848 and CT847, harboring the T3 secretion sequences and showed significant identity (48 %, 32 % and 28 %, respectively) (Fig. S4), opening the possibility that the three *C. pneumoniae* proteins are T3-secreted as well.

Looking into the predicted structure (Phyre2, http://www.sbg.bio.ic.ac.uk/phyre2), Yaa3, Cpn1004 and Cpn1005 mainly form α-helical structures, but the alignments showed no relevant similarities with other known proteins. Interestingly, Cpn1003, the fourth hypothetical protein encoded by this locus, presented a predicted 3D structure completely overlapping with the structure of *H. influenzae* GlpG (92 % confidence), despite the two proteins share only 16 % amino acid sequence identity (Fig. S5). The perfect superimposition of Cpn1003 and GlpG structures was suggested and identified by Prof. Dr. Lutz Schmitt, from the department of Biochemistry at the Heinrich Heine University of Düsseldorf. GlpG is a rhomboid-like protease, which cleaves proteins in their transmembrane domains (Freeman 2008).

4.2.2 Recombinant Yaa3 production

4.2.2.1 Yaa3 expression and lysis conditions

In order to characterize Yaa3 function, production of soluble recombinant protein was required. Previous attempts of expression and purification of rYaa3 performed in the laboratory were unsuccessful; therefore Yaa3 was initially fused with a C-terminal His tag (pFT31) and co-expressed with the chaperones GroES-GroEL (pGro7) in *E. coli* Xl₁Blue strain, to improve the expression levels. For the same purpose, the C-terminally His-tagged Yaa3 was fused with GST at the N-terminus (pFT28) and expressed in *E. coli* Xl₁Blue cells (see paragraphs 3.3.1, 3.3.2 and 3.3.4). Furthermore, in order to test additional conditions, *yaa3* was cloned with a C-terminal His tag in pET24a vector (pFA1) and

expressed in DE3 Rosetta and BL21 *E. coli* strains (see paragraph 3.3.1.1). The pET system has the advantage of avoiding basal expression, since its T7 promoter is activated by the T7 RNA polymerase, produced by D3 *E. coli* strains after induction with IPTG (Novagen 2003). After expression of rYaa3 for 4 hours, *E. coli* cells were lysed under different native and denaturing conditions, in order to test Yaa3 solubility (see paragraph 3.3.2) (Fig. 40A). Under native lysis conditions, Yaa3 was retained in the insoluble cell fraction, probably due to the formation of inclusion bodies. Under denaturing lysis conditions, only Guanidine-HCl was able to solubilize most of rYaa3 in the soluble fraction (Fig. 40B).

A.

Lysis	Native	Denatured
1	PBS + 1 mg/ml lysozyme + PMSF + proteases inhibitor cocktail	Buffer A1 (containing 6 M Guanidine-HCL)
2	PBS + 1 mg/ml lysozyme + PMSF + proteases inhibitor cocktail, acidic pH	Buffer A1 + 1 % triton
3	PBS + 1 mg/ml lysozyme + PMSF + proteases inhibitor cocktail, basic pH	Buffer A1 + 0,5 M NaCl
4	PBS + 1 mg/ml lysozyme + PMSF + proteases inhibitor cocktail + 1 % triton	Buffer A1 + 10 % ethanol
5	PBS + 1 mg/ml lysozyme + PMSF + proteases inhibitor cocktail + 1 % triton + 1 % sarkosyl	Buffer B (containing 8 M Urea)
6	PBS + 1 mg/ml lysozyme + PMSF + proteases inhibitor cocktail + 0,3 % SDS	Buffer B + 0,3 % SDS
7	Ripa buffer, pH 8.0	Buffer B + 0,3 % SDS + 1 % triton
8	Hepes buffer, pH 7.4	Buffer B + 300 mM NaCl
9		Buffer B + 1-2 % triton
10		Buffer B + 1 % triton + 1 % sarkosyl

Figure 40. Lysis conditions. A. Table summarizing the different native and denaturing conditions tested. **B.** Coomassie stained SDS-PAGE of representative lysed *E. coli* cells expressing C-terminal His-tagged rYaa3 (pFA1) (Lysate) and of insoluble (Pellet) and soluble (Supernatant: SN) fractions under native condition 1 (left) and denatured condition 1 (right). Arrows indicate the expected size of Yaa3.

When cells were lysed under native conditions, a band at 10 kDa was obtained both in the soluble and insoluble fractions (Fig. 40B), but was not detected in the anti-His Western blot. To test whether Yaa3 was cleaved in the N-terminal region, N-terminal His-tagged Yaa3 was produced (pFA3) (see paragraph 3.2.3), expressed in *E. coli* and cells were lysed under native and denaturing conditions (see paragraphs 3.3.1, 3.3.2). In parallel, BL21 *E. coli* strain was complemented with three sets of chaperones (GroES-GroEL, Tig and GroES-GroEL-Tig) (see 3.1.4) and, after co-expression with C-terminal and N-terminal His-tagged Yaa3 (pFA1 and pFA3), cells were lysed under native and denaturing

conditions. In all conditions tested, the 10 kDa band was still visible in the Coomassie-stained SDS-PAGE. This led to the conclusion that the 10 kDa band was indeed an *E. coli* contamination.

Furthermore, in order to obtain native rYaa3 out of *E. coli* cells, C-terminal His-tagged Yaa3 was fused with a N-terminal PelB secretion signal (pFA2) in a pET vector (pSL4) (see paragraph 3.2.3). PelB is responsible for directing polypeptides to the *E. coli* periplasm where disulfide oxidoreductases and isomerases allow proper protein folding (Sockolosky and Szoka 2013). The outer membrane of *E. coli* cells containing rYaa3 in the periplasm was lysed with TSE buffer and centrifuged. The outer membrane and periplasmic fractions were then separated from the inner membrane and cytoplasmic fractions (see paragraph 3.3.3) (Fig. 41).
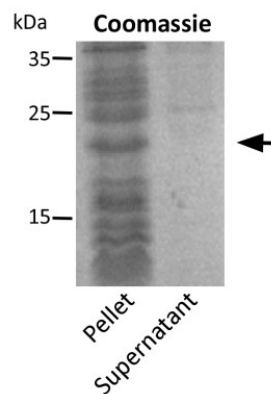
Figure 41. Yaa3 periplasmic expression. Coomassie stained SDS-PAGE of representative *E. coli* cells expressing rYaa3 fused with a PelB secretion signal (pFA2) after periplasmic fraction extraction. Pellet represents cytoplasmic and inner membrane proteins, supernatant represents periplasmic and outer membrane proteins. Arrow indicates the expected size of Yaa3.

Another attempt of obtaining rYaa3 under native conditions in the soluble fraction was performed by expressing N-terminal and C-terminal His-tagged Yaa3 in *E. coli* Arctic cells. ArcticExpress DE3 RIL cells are engineered cells, able to produce proteins at 10 °C. The low temperature only allows a slow protein expression (25 hours), improving the folding and therefore increasing the amount of soluble protein. Also in this case, Yaa3 was produced, but could not be solubilized from the cell pellet (see paragraph 3.3.1.2) (Fig. 42).
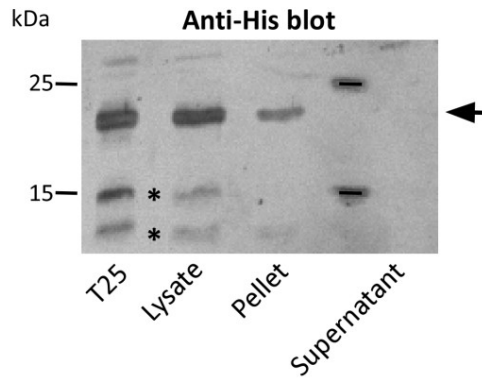
Figure 42. Yaa3 expression in *E. coli* Arctic cells. Anti-His immunoblot of Yaa3 (pFA1) expressed in *E. coli* ArcticExpress DE3 RIL cells after 25 hours of induction with IPTG at 10 °C (T25) and of lysate, insoluble (pellet) and soluble (supernatant) fractions obtained after native lysis with PBS + 1 mg/ml lysozyme + PMSF + protease inhibitor cocktail. Arrow indicates the expected size of Yaa3.

Considering all conditions and buffer tested, one method was identified as the most effective one for expression of Yaa3 and lysis of *E. coli* cells: C-terminal His-tagged rYaa3 (pFA1) was expressed in Rosetta *E. coli* strain, cells were lysed under denaturing conditions with Guanidine-HCl (Buffer A1) overnight at 4 °C and sonicated for 1 minute. Lysed cells were centrifuged at 24´000 rpm for 1 hour at 4 °C to obtain the soluble fraction, containing denatured rYaa3 (supernatant) (Figs. 40B and 43).

4.2.2.2 Yaa3 purification and refolding

Recombinant Yaa3 was purified via affinity purification with Ni-NTa agarose (see paragraph 3.3.4.3). Applying this purification method, rYaa3 was purified up to 1,3 mg/ml concentration. Under denaturing conditions, in the elution fractions Yaa3 appears as a double band (Fig. 43). The band is recognized also in Western blot analysis, confirming the identity of Yaa3 protein. Thus, it is probable that the upper band represents the full length Yaa3, which might be cleaved at the N-terminus, generating a product of 18 kDa. The presence of this band only in the elution fractions might be due to an enrichment of the protein during the affinity purification (Fig. 43).
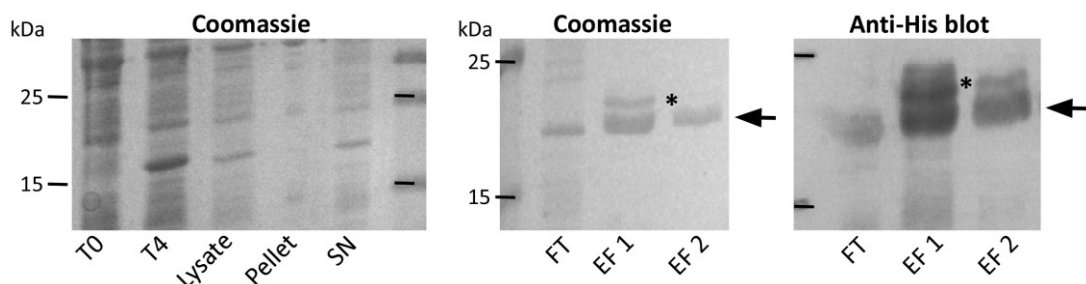
Figure 43. Purified denatured Yaa3. Coomassie staining of SDS-PAGE for Yaa3 purification.

Yaa3 expression (pFA1) was induced at time 0 (T0) and *E. coli* cells were incubated for 4 hours with shaking at 37 °C (T4). Cells were lysed with BufferA1 (Lysate) and centrifuged to separate insoluble (Pellet) and soluble (Supernatant) material. Ni-NTa affinity purification was performed (see paragraph 3.3.4.3), the supernatant containing soluble Yaa3 was run through the Ni-NTa column and washed with urea buffer to get rid of Guanidine-HCl. Unspecific proteins were removed from the Ni-NTa agarose by washing the column with urea + 40mM Imidazole (Wash). Yaa3 was obtained by elution with urea buffer containing 500mM Imidazole (EF: elution fraction). The purity of the protein was checked by SDS-PAGE analysis. FT: flow through. Arrows indicate the expected size of Yaa3. * indicates the upper Yaa3 band.

In order to perform functional assays, different dialysis conditions were tested to refold the denatured purified Yaa3 (Fig. 44A) (see paragraph 3.3.5.1). Unfortunately, in all buffers tested, Yaa3 precipitated and only a maximum of 100 µg/ml renatured soluble protein could be obtained (Fig. 44B).

Refolding	Dialysis (3 times buffer exchange in 36 hours at 4 °C)
1	PBS (4 °C or RT)
2	PBS, pH 4.0
3	PBS, pH 9.0
4	PBS + 1-2-3 % triton
5	Dialysis steps: & M, 4 M, 2 M, 1 M, 0,5 M Urea, PBS (4 °C or RT)
6	50 mM Tris-Cl + 9,6 mM NaCl + 0,4 mM KCl + 2 mM MgCl$_2$ + 2 mM CaCl$_2$ + 0,4 M sucrose + 0,5 % triton + 0,05 % polyethylene glycol + 1 mM GSH + 1 mM GSSH
7	50 mM Tris-Cl + 9,6 mM NaCl + 0,4 mM KCl + 2 mM MgCl$_2$ + 2 mM CaCl$_2$ + 50 mM Arginine + 0,4 M sucrose + 1 mM GSH + 1 mM GSSH
8	50 mM Tris-Cl + 9,6 mM NaCl + 0,4 mM KCl + 1 mM EDTA + 0,5 % triton + 1 mM DTT
9	50 mM Tris-Cl + 240 mM NaCl + 10 mM KCl + 1 mM EDTA + 50 mM Arginine + 0,5 % triton + 1 mM DTT
10	PBS + 50 mM L-Arginine + 50 mM L-Glutamine

Figure 44. Yaa3 refolding. A. Table summarizing the different refolding conditions tested. **B.** Coomassie stained SDS-PAGE of 5 % of the elution fractions (EF) of representative purified Yaa3 before (denatured) and after renaturation in dialysis buffer 1 (refolded). Arrow indicates Yaa3 expected size. * indicates a second Yaa3 band.

4.2.2.3 Yaa3 hydrophobicity region

In order to understand the high precipitation rate of Yaa3 during refolding, bioinformatic analysis of Yaa3 were performed. Both Phobius (http://phobius.sbc.su.se/) and ExPASy-ProtScale (http://web.expasy.org/protscale) programs identified a hydrophobic region in

the first 40 amino acids of the protein. Assuming that this region was the reason for the aggregation phenotype, a truncated variant of Yaa3, without the first 40 amino acids (Yaa3Δ) was cloned in a pET vector (pFA4) (Fig. 45A). After different native and denaturing lysis conditions were tested (Fig 40A), Yaa3Δ was expressed in an *E. coli* Rosetta strain, cells were lysed in Guanidine-HCl (Buffer A1) overnight at 4 °C and sonicated for 1 minute (see paragraph 3.3.2.2). Yaa3Δ was then purified under denaturing conditions at a concentration of up to 1,5 mg/ml (see paragraph 3.3.4.3). However, the absence of the predicted hydrophobic region did not solve the aggregation problem, under all refolding conditions tested (Fig. 44A). Again, Yaa3Δ precipitated and only a maximum of 100 µg/ml soluble protein was obtained (Fig. 45B). Interestingly, only one band could be detected in the elution fractions, indicating that the cleavage site is within the first 40 aa.
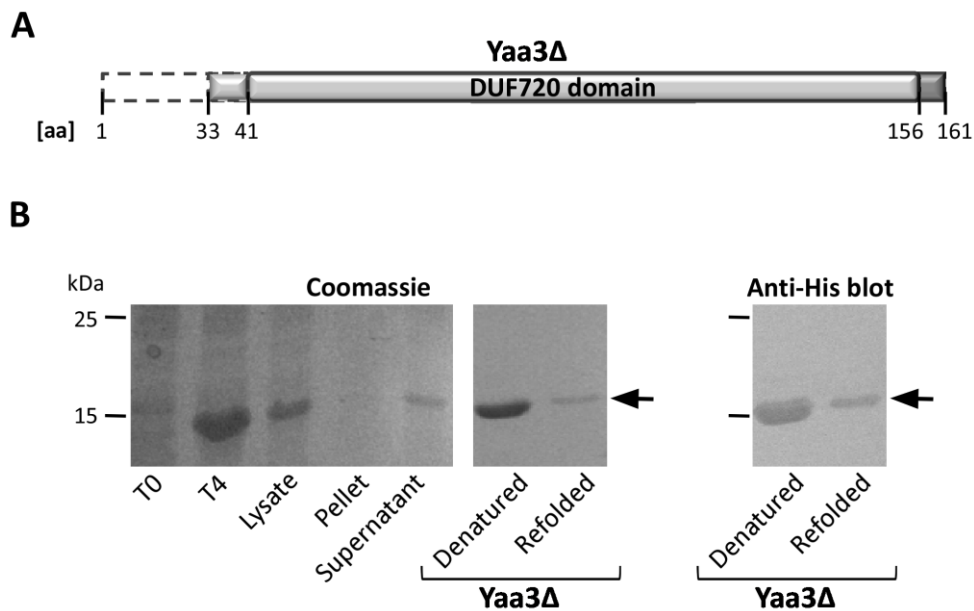
Figure 45. Yaa3Δ. A. Schematic representation of Yaa3Δ protein, without the predicted hydrophobic region, indicated by the segmented line (aa 1 to aa 40). The amino acids indicate the position of the DUF720 domain (light grey). **B.** Yaa3Δ purification and refolding. Yaa3Δ expression (pFA4) was induced at time 0 (T0) and *E. coli* cells were incubated for 4 hours with shaking at 37 °C (T4). Cells were lysed with Buffer A1 (Lysate) and centrifuged to separate insoluble (Pellet) and soluble (Supernatant) material. Ni-NTa affinity purification was performed (see paragraph 3.3.4.3) and the obtained denatured purified Yaa3Δ (Denatured) was refolded in PBS (Refolded). Coomassie-stained SDS-PAGE (left) and anti-His Western blot (right). Arrows indicate the expected size of Yaa3Δ.

4.2.2.4 Successful refolding of Yaa3

Yaa3 could be purified successfully under denaturing conditions, but it precipitated when refolded. Finally, a new refolding method based on the use of Arginine was tested by a member of the team (Philipp Hanisch) in order to refold Pmp proteins in high

concentration (Bondos and Bicknell 2003, Reddy, Lilie et al. 2005). Purified Yaa3 in urea buffer was diluted 1:20 in PBS + 200 mM Arginine and the buffer was exchanged by centrifugation of the solution in an Amicon Ultra-15 column (see paragraph 3.3.5.2). The use of Arginine and the fast refolding method prevented the aggregation phenotype and soluble native Yaa3 could be produced for further analysis (Fig. 46).
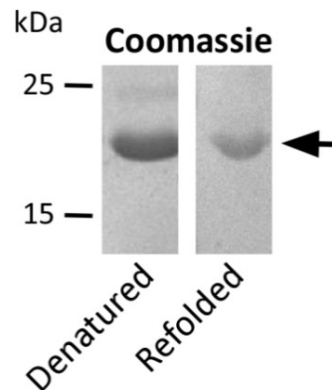
Figure 46. Successful refolding of Yaa3. Representative Coomassie-stained SDS-PAGE of purified Yaa3 (pFA1) before (denatured) and after refolding in PBS + 200 mM Arginine, using the Amicon column (refolded).

4.2.3 Functional properties of Yaa3

Soluble refolded Yaa3 was used to investigate the biological functions of the protein.

4.2.3.1 Yaa3 adhesion capacity to human epithelial cells

To confirm the adhesive characteristics observed in the yeast display system (Fechtner 2009), soluble adhesion assays were performed, (see paragraph 3.4.2) (Fig. 26). Adhesive-incompetent rGST, used as negative control, showed no binding to human cells; while rCpn0473, used as positive control, was able to bind human cells and the signal increased over time (Fig. 47A). Initially, rYaa3 was tested in absence of Arginine, therefore only 50 µg/ml of soluble protein was used to perform the assays. Soluble rYaa3 could bind to human epithelial HEp-2 cells after 15 minutes of incubation at 37°C and the binding increased over time (Fig. 47A). A possible explanation could be that Yaa3 receptors on the human cells are not saturated. Furthermore, the same adhesion assay was performed at 4°C. At this temperature, cells functions are blocked and therefore no internalization can happen. Also at 4°C, rYaa3 was able to bind to human cells, even though in a weaker manner. Also in this case the signal increased over time, suggesting that Yaa3 receptors on the human cells are not saturated (Fig. 47B). Interestingly, Yaa3Δ adhered to human cells as well (Fig. 47A), suggesting that the domain responsible for interaction is not part of the

N-terminal hydrophobic region.
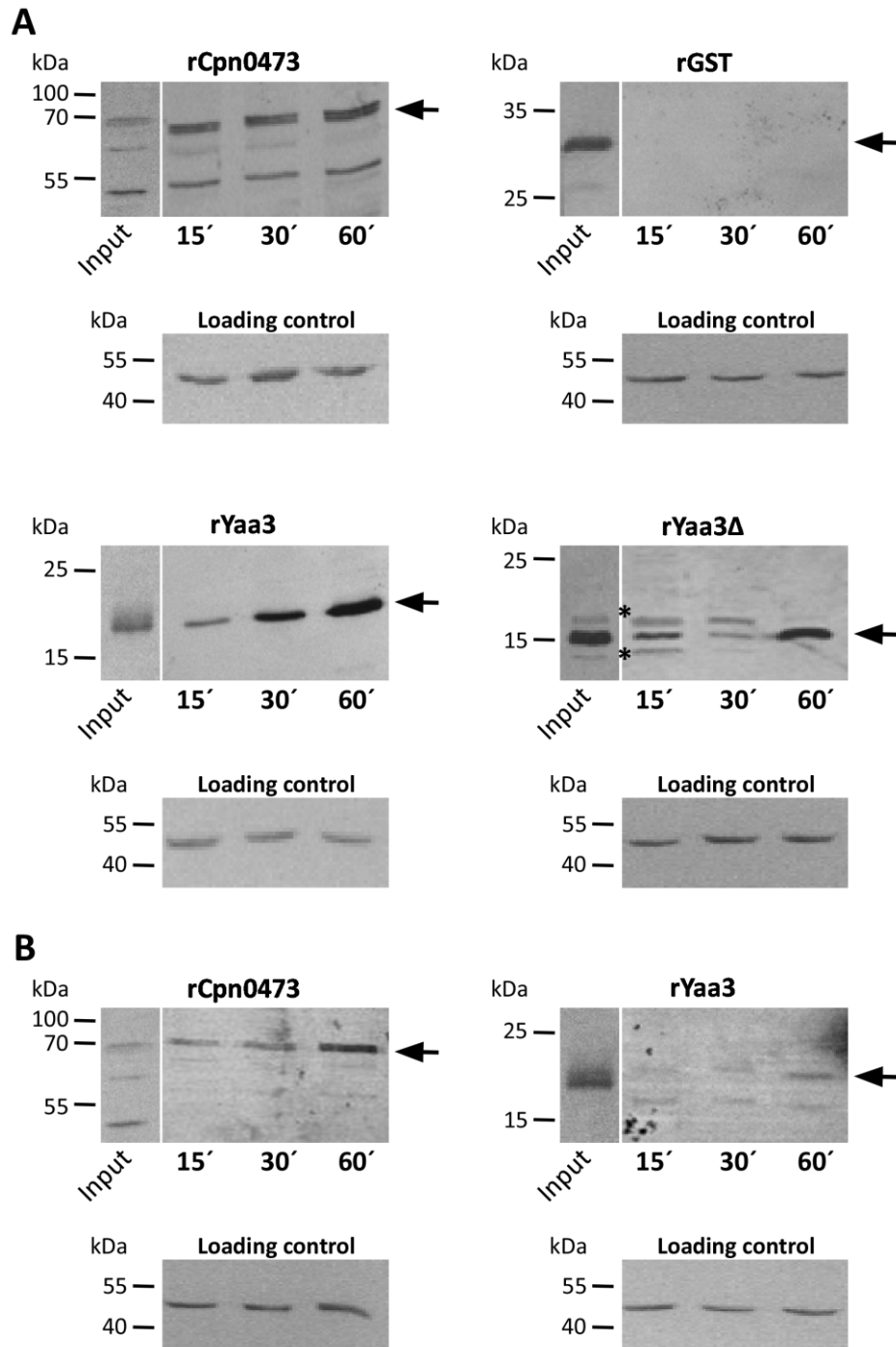
Figure 47. rYaa3 binds human epithelial cells. Adhesion capacity to human epithelial HEp-2 cells of 50 µg/ml rYaa3 or rYaa3Δ after 15, 30 and 60 minutes incubation at 37 °C (**A**) and 4 °C (**B**). rCpn0473 (*C. pneumoniae* adhesin) and rGST used as positive and negative control respectively. Anti-His antibody was used to determine the input of soluble recombinant proteins (input) and their binding capacity. Anti-actin antibodies were used to verify the amount of HEp-2 cells (loading control). Unspecific bands are indicated with *. Arrows mark the position of the proteins analyzed.

Next, Yaa3 adhesion capacity was tested in the presence of Arginine. Yaa3 refolded in the presence of 100 mM and 200 mM (shown here) Arginine could still adhere to human epithelial cells after 15 minutes of incubation, and the signal increased over time (Fig 48). Thus, the presence of Arginine did not impair functional properties of Yaa3; hence Yaa3 + 200 mM Arginine was used for all subsequent functional assays.
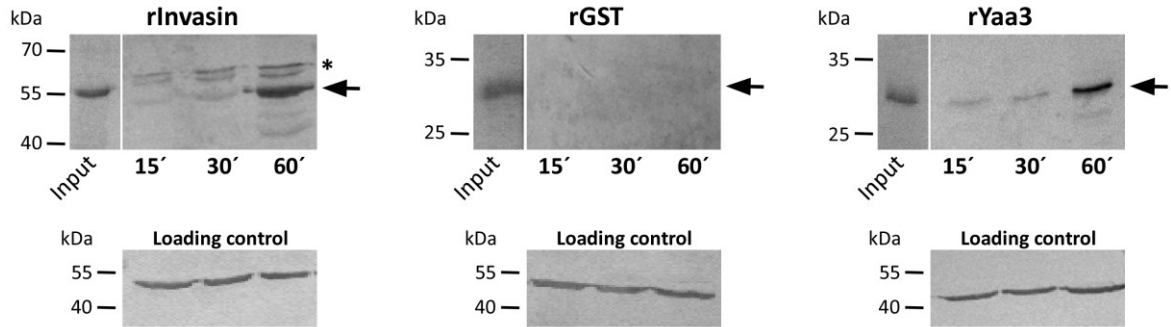
Figure 48. rYaa3 binds human epithelial cells in presence of Arginine. Adhesion capacity to human epithelial HEp-2 cells of 200 μg/ml rYaa3 refolded with 200 mM Arginine after 15, 30 and 60 minutes incubation at 37°C. rInvasin and rGST refolded in the presence of 200 mM Arginine were used as positive and negative control respectively. Anti-His antibody was used to determine the input of soluble recombinant proteins (input) and their binding capacity. Anti-actin antibodies were used to verify the amount of HEp-2 cells (loading control). Unspecific bands are indicated with *. Arrows mark the position of the proteins analyzed.

4.2.3.2 Yaa3 relevance for the *C. pneumoniae* infection

Recombinant Yaa3 could bind to human epithelial cells, but to check whether it is relevant for a *C. pneumoniae* infection, rYaa3 + 200 mM Arginine was pre-incubated with human epithelial HEp-2 cells for 1 hour, to allow binding. Then the cells were infected with *C. pneumoniae* EBs and the infection rate was quantified by counting the inclusions formed after 48 hpi (see paragraph 3.4.3) (Fig. 31A). This experiment was performed by the master student Sebastian Wintgens. Pre-incubation of HEp-2 cells with rYaa3 led to a decrease in the infection by 59 %, confirming the relevance of Yaa3 during the adhesion of *C. pneumoniae* EBs to human cells (Fig. 49).
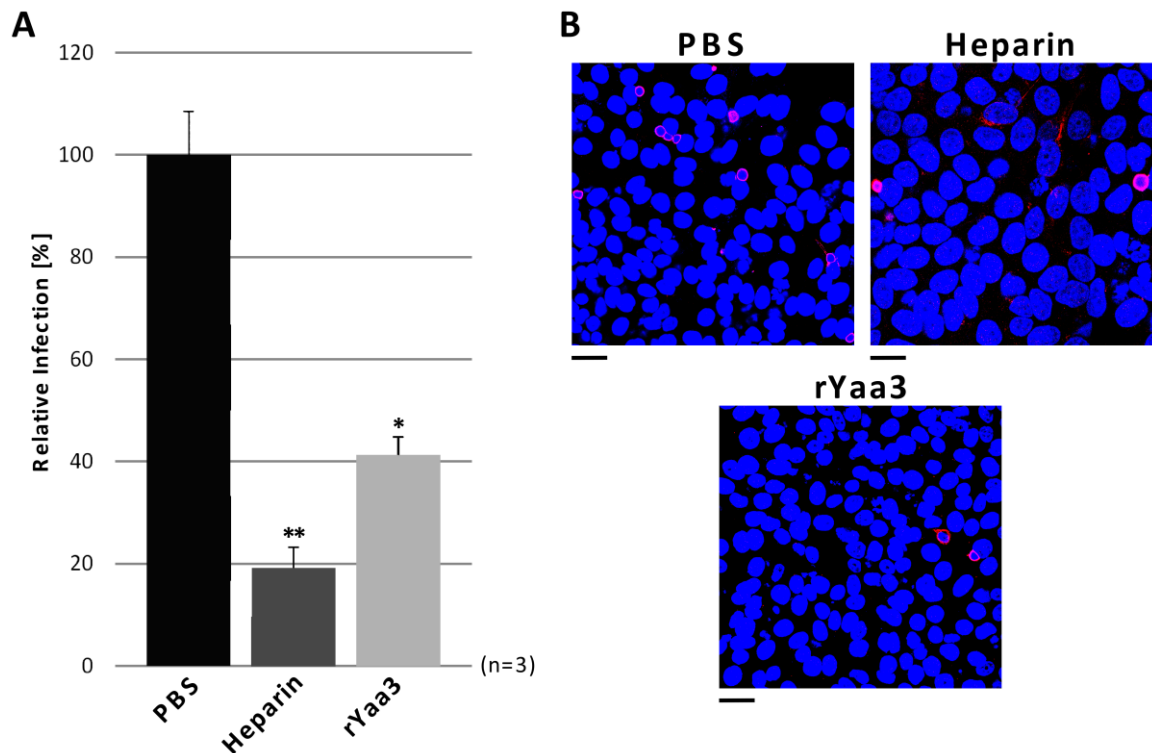
Figure 49. rYaa3 reduces *C. pneumoniae* infection. A. 50 μg/ml soluble rYaa3 was incubated for 1 hour at 37°C with confluent human epithelial HEp-2 cells. Cells were then infected with *C. pneumoniae* EBs (MOI 10). The number of inclusions was counted at 48 hpi (light grey). Infection rate was determined by counting the number of inclusions per $5.8 * 10^3$ HEp-2 cells and is expressed as a percentage of the number of inclusions determined for the PBS-treated sample (black). Results are from three separate experiments (n=3). Data shown are means + standard deviations. *: $p<0.05$, **: $p<0.01$, compared to PBS-treated sample. Heparin was used as positive control (dark grey). **B.** Representative pictures of the immunofluorescence microscopy. For detection of chlamydial inclusions, infected cells were fixed and permeabilized with 3 % PFA + 96 % methanol. DNA was stained with DAPI (1:1000) and chlamydial inclusions were stained with primary anti-Cpn147 antibody (1:50), followed by Alexa-594 conjugated secondary antibody (1:200). Scale bars: 25 μm.

4.2.4 Yaa3 expression during *C. pneumoniae* life cycle

Denatured and native rYaa3 was used to immunize rabbits (see paragraph 3.3.19) and the generated anti-Yaa3 polyclonal antibody was depleted using human HEp-2 cells lysates and antigen purified, in order to increase specificity (see paragraphs 3.3.19.1, 3.3.19.2 and 3.3.19.3) (Fig. 50A-B).

The purified anti-Yaa3 antibody was used to investigate the expression and localization of Yaa3 in human epithelial HEp-2 cells infected with *C. pneumoniae* at different time points (see paragraph 3.4.1). In order to avoid antibody cross-reactivity during immunofluorescence staining, anti-Yaa3 antibody and anti-DnaK or anti-LPS antibodies where incubated in different order.

A Yaa3 signal could not be detected at 8 hpi and 12 hpi (data not shown). At 24 hpi, Yaa3 showed co-localization with the intra-chlamydial DnaK and the extracellular LPS signal (Fig. 50C). At 48 hpi, Yaa3 showed co-localization mostly with RBs, but a lower degree of co-localization with EBs was still detected, as indicated by the merge of anti-Yaa3 antibody with the DNA signal (Fig. 50D). At the end of the cycle (72 hpi), Yaa3 co-localized with the intra-chlamydial DnaK and the extracellular LPS signal. Interestingly, single EBs, possibly leaving the inclusion, are positive for Yaa3 (Fig. 50E).
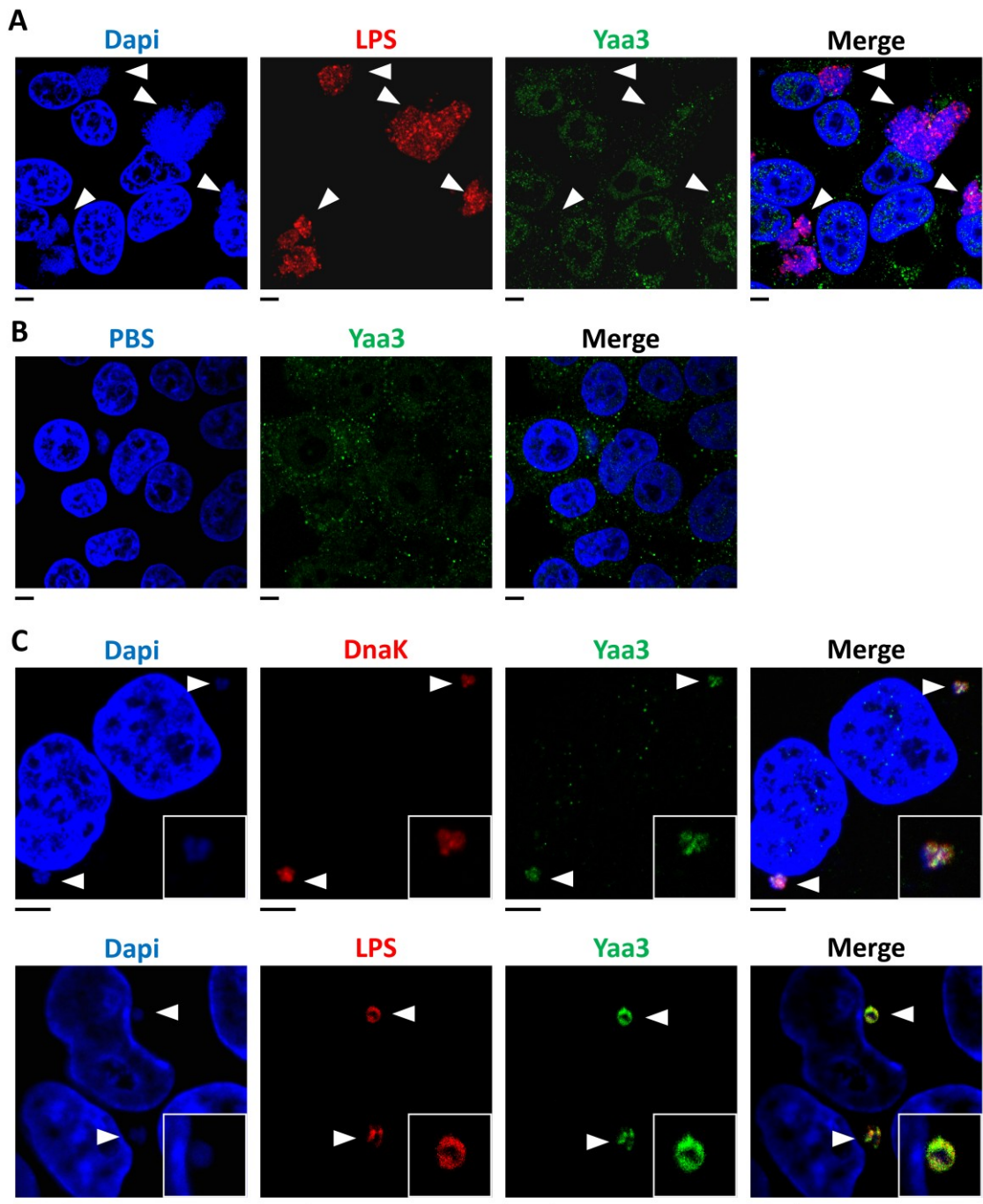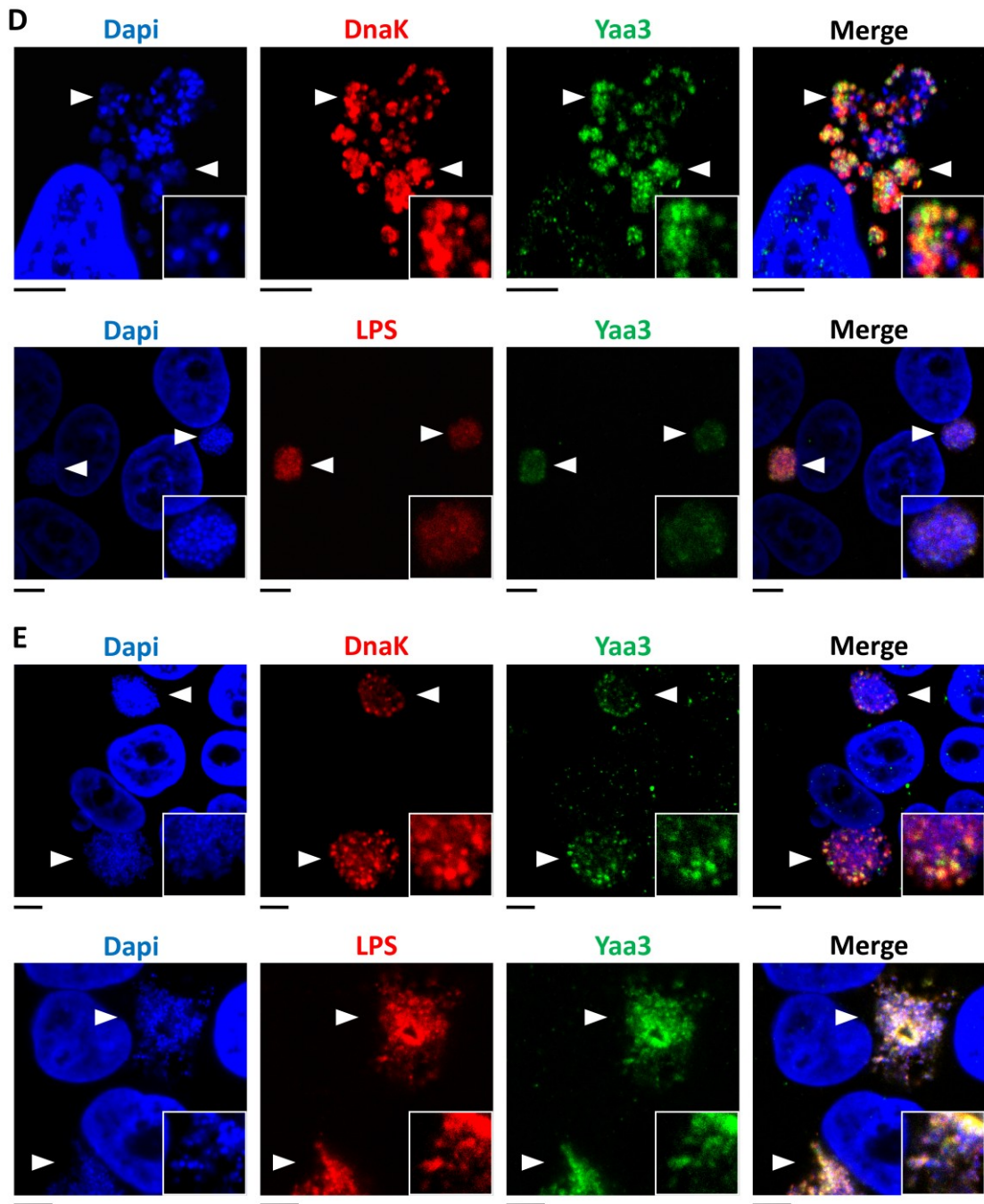
Figure 50. Immunofluorescence microscopy of Yaa3 expression during *C. pneumoniae* infection. A. Analysis of pre-immune serum (1:50) reactivity to *C. pneumoniae* infected HEp-2 cells at 48 hpi (MOI 1). **B.** Incubation of the anti-Yaa3 antibody with uninfected human HEp-2 cells. Expression and localization of Yaa3 was detected in *C. pneumoniae* infected HEp-2 cells at 24 hpi (**C**), 48 hpi (**D**) and 72 hpi (**E**). Infected and uninfected cells were fixed and permeabilized with 3 % PFA + 96 % methanol. Bacteria were detected with anti-DnaK antibodies (1:50) (top) and with anti-LPS antibodies (1:50) (bottom). DNA was stained with DAPI (1:1000) and inclusions were stained with anti-Yaa3 antibodies depleted against HEp-2 cells (1:50). To avoid cross-reactivity, the anti-Yaa3 antibodies and anti-DnaK or anti-LPS antibodies were incubated with the infected cells separately. Anti-mouse and anti-rabbit Alexa-488 and Alexa-594 conjugated antibodies were used as secondary antibodies (1:200). White arrow heads indicate relevant inclusions. Scale bars: 5 μm. 1:2 enlargements are shown at the bottom right of the pictures.

Interestingly, preliminary data showed that when *C. pneumoniae* infected cells were tested for Yaa3 expression in Western blot analysis, a band could be detected with the anti-Yaa3 antibody only at 48 hpi, but not at 24 hpi and 72 hpi, as indicated by the immunofluorescence microscopy analyses. Thus, it is possible that the band detected at 48 hpi is an unspecific band (Fig. 51).
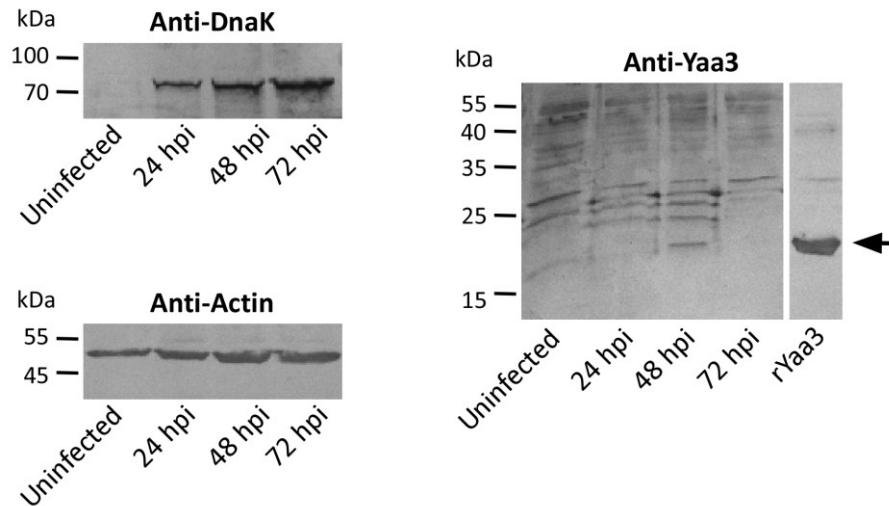
Figure 51. Western blot analysis of Yaa3 expression during *C. pneumoniae* infection. Two 25 cm^2 culture flasks with confluent HEp-2 cells were infected with *C. pneumoniae* (MOI 10) at different time points (24, 48, 72 hpi and no *Chlamydia*). The infected and uninfected cells were lysed and whole cell protein samples were generated (see paragraph 3.1.3.6). Detection of HEp-2 cells was performed with anti-actin antibody and the *Chlamydia* infection was evaluated with anti-DnaK antibody, constitutively expressed in *Chlamydia*, followed by AP-conjugated anti-mouse antibodies. Yaa3 expression was detected with depleted anti-Yaa3 antibody (1:100), followed by AP-conjugated anti-rabbit secondary antibodies. Arrow marks the position of Yaa3.

4.2.5 Yaa3: Conclusions

The hypothetical *C. pneumoniae* protein Yaa3 was analyzed, in order to characterize its functions. Bioinformatic analysis showed that Yaa3 harbor a domain on unknown function (DUF720) which is found only in three proteins in all *Chlamydia* species (Yaa3, Cpn1005 and Cpn1004 in *C. pneumoniae*). The DUF720 domain presented a certain similarity with the T1SS membrane fusion protein (MFP) of *Prochlorococcus marinus* (P9303_01311). A T1SS has not been identified in *Chlamydia*.

C. trachomatis homologs of Yaa3, Cpn1005 and Cpn1004 (CT849, CT848 and CT847), harbor a T3 secretion signal at the N-terminus in the first 20 amino acid. The first 25 amino acids of Yaa3, Cpn1005 and Cpn1004 showed a high identity with the respective *C. trachomatis* homologs, opening the possibility that the three *C. pneumoniae* proteins are T3-secreted as well. Furthermore, the first 40 amino acid of Yaa3 were identified as a high hydrophobic region, possibly representing a transmembrane domain.

In order to study Yaa3, the protein was cloned in different expression vectors and expressed in *E. coli*. Production of rYaa3 has been more challenging than initially thought. After several attempts, high amounts of rYaa3 could be purified from *E. coli* and refolded with the following protocol: Yaa3 from pFA1 expression vector was expressed in *E. coli* Rosetta strain and cells were lysed under denaturing conditions. Denatured rYaa3 was purified via affinity chromatography and refolded in PBS + 200 mM Arginine using Amicon Ultra-15 columns.

Recombinant Yaa3 showed adhesion capacity to human epithelial HEp-2 cells and the signal increased over time, suggesting binding to human receptors, which are not saturated. Interestingly, rYaa3Δ (lacking the N-terminal hydrophobic region) could also bind human cells, indicating that the adhesion domain is present within the DUF720 domain. Moreover, rYaa3 pre-incubated with human cells could block a subsequent *C. pneumoniae* infection, proving its relevance for the infection. Finally, an anti-Yaa3 polyclonal antibody was generated and used to investigate the expression and localization of Yaa3 during the *C. pneumoniae* infection. Immunofluorescence microscopy revealed that Yaa3 is expressed after 24 hpi, co-localizing with the bacteria till the end of the cycle (24, 48 and 72 hpi).

5. Discussion

Chlamydiae are obligate intracellular bacteria which cause widespread infections in humans and animals. Adhesion of the infectious EB to the host cell and its internalization are essential steps for the establishment of the infection; however this process is still not fully understood (Abdelrahman and Belland 2005).

In the first part of this work, *C. trachomatis* Polymorphic membrane proteins (Pmps) have been characterized for their oligomerization capacities and for their functional properties.

Pmps are the biggest chlamydial adhesin family, with 9 members in *C. trachomatis* and 21 in *C. pneumoniae* and represent approximately 5 % of the whole chlamydial coding capacity, suggesting a crucial role during infection (Rockey, Lenart et al. 2000, Molleken, Schmidt et al. 2010). All *C. trachomatis* Pmps are expressed on the bacterial cell surface, (Crane, Carlson et al. 2006, Tan, Hsia et al. 2009) and have a predicted autotransporter structure. The passenger domain (PD) is responsible for the protein functions and is characterized by the presence of multiple copies of the motifs FxxN and GGA(I, L, V) (Henderson and Lam 2001). Fragments with high density of motifs of all 9 *C. trachomatis* and of representative *C. pneumoniae* Pmps have been characterized as adhesins, with relevance for the infection (Molleken, Schmidt et al. 2010, Becker and Hegemann 2014); in particular, *C. trachomatis pmpD* null mutant showed a reduced infection ability *in vitro* and *in vivo* (Kari, Southern et al. 2014). Furthermore, the presence of at least 2 copies of the motifs is essential for *C. pneumoniae* Pmp21 adhesion to human cells (Molleken, Schmidt et al. 2010, Luczak, Smits et al. 2016). The exposed Pmps PD can not only mediate adhesion as a full length, but can be cleaved, generating processed forms, as it has been observed for *C. trachomatis* and *C. pneumoniae* Pmps (Vandahl, Pedersen et al. 2002, Wehrl, Brinkmann et al. 2004, Swanson, Taylor et al. 2009, Molleken, Schmidt et al. 2010, Saka, Thompson et al. 2011). Recently, it was observed that a *C. pneumoniae* Pmp21 fragment with only two copies of the motifs could form different species of hMW homomeric oligomers with amyloid properties and with protofibrillar structure. Interestingly, the presence of the two motifs is essential for Pmp21 oligomerization (Luczak, Smits et al. 2016).

In the second part of this work a new putative *C. pneumoniae* adhesin protein (Yaa3) has been analyzed for its localization, expression and function during the infection. Yaa3 was identified in a yeast display assay for its adhesive properties together with the recently characterized adhesin Cpn0473 (LIPP) (Fechtner 2009, Fechtner, Galle et al. 2016).

5.1 *C. trachomatis* Pmps form different functional homomeric and heteromeric complexes

5.1.1 Generation of motif-poor and motif-rich Pmp proteins

Pmp proteins are characterized by the presence of multiple copies of the motifs FxxN and GGA(I, L, V). *C. trachomatis* Pmps present an average of 21 motifs, with a minimum of 14 motifs in PmpH and a maximum of 37 in PmpD (Figs. 8A and 52). The role of the motifs in *C. trachomatis* Pmps has not been directly investigated so far. Central fragments of the PD of all 9 *C. trachomatis* Pmps with a high density of motifs mediate adhesion to human cells, using yeast cell display and protein-coated fluorescent beads adhesion assays, and can block a subsequent *C. trachomatis* infection (Becker and Hegemann 2014).

In this work, we decided to analyze the characteristics of *C. trachomatis* serovar E Pmp proteins in greater detail. In addition to the previously generated Pmp fragments, different portions of the PD (N-terminal domains, central domains and C-terminal domains) of all 9 *C. trachomatis* Pmps have been cloned, expressed in *E. coli* and purified. These Pmp fragments give us a wide representation of the whole Pmp PD, with fragments harboring a high density of the repeated motifs (motif-rich), fragments with a medium density of motifs (motif-low) and fragments with only two motifs (motif-poor) (Fig. 8A). These proteins have been used to investigate the presence of specific adhesion and interaction domains within the Pmps.

Three motif-poor and three motif-rich Pmp proteins have been then selected, in order to investigate their oligomerization and functional properties in more detail. Motif-rich PmpD, PmpH and PmpI fragments (D, H and I) represent the central part of the PD, harboring a high density of motifs (Fig. 8B-C). These fragments have been already characterized as adhesins and as relevant for the infection (Becker and Hegemann 2014). Motif-poor PmpA, PmpF and PmpG fragments (Ac, Fc and Gc) represent the C-terminal region of the PD and harbor only two motifs (Fig. 8B-C), similarly to the adhesive-competent motif-poor fragment of *C. pneumoniae* Pmp21 (D-Wt) (Luczak, Smits et al. 2016). Fc and Gc fragments resemble the processed peptides identified from *C. trachomatis* L2 proteasome analysis for PmpF and PmpG, respectively (Saka, Thompson et al. 2011).

5.1.2 Motif-poor and motif-rich Pmp proteins have a predicted β-helical structure

Pmps have never been crystallized so far, so the only hint regarding their structures comes from structure prediction programs. The first prediction was performed with the program BETAWRAP, which identifies β-helixes (http://groups.csail.mit.edu/cb/betawrap/). With the help of this tool, chlamydial Pmp proteins were predicted as right-handed β-helical structures (Becker 2013), like other toxins, adhesins and virulence factors from several bacteria and fungi (Bradley, Cowen et al. 2001, Cowen, Bradley et al. 2002). More recently, BETAWRAP and Phyre2 programs were adopted to predict a triangular β-helical structure for all 9 *C. trachomatis* and for *C. pneumoniae* Pmp21, with their motifs exposed at the triangular corners. The β-helical structure was identified at the N-terminal part of the PD for most Pmps, but in Pmp21, PmpB, PmpC and PmpD it was identified at the C-terminal region of the PD. Interestingly, the β-helical structure represented the motif-rich region of the Pmp PDs (Fig. 52) (Hegemann and Moelleken 2012, Becker 2013).

Motif-poor Ac and Gc and motif-rich H and I Pmp proteins, analyzed with the program Phyre2, also presented a triangular β-helical structure with the motifs FxxN and GGA(I, L, V) present at the corners, in agreement with predictions for the full length Pmps (Fig. 34). The analyzed Ac, Gc and I Pmp proteins showed relevant sequence similarity with a putative *Cardicellulosiruptor kronotskyensis* adhesin (23, 26 and 25 % respectively).

In general, β-helical structures are formed by triangular β-strands packed parallel to one another. P22 tailspike protein, for example, is a β-sheet homotrimer, where the residues of the three chains interact with each other and generate a β-sheet prism (Kreisberg, Betts et al. 2000). The β-strands forming the β-helical structure can be separated by loops, which can vary in length among different proteins and usually harbor specific domains (Jenkins, Mayans et al. 1998, Bryan, Starner-Kreinbrink et al. 2011). When the Pectin lyases from *Aspergillus niger* were analyzed, the Pectin lyase B (PLB) β-helix overlapped almost perfectly with Pectin lyase C (PLC) β-helix, but one of the T3 loops of PLB was longer than the T3 loop of PLC (Vitali, Schick et al. 1998). Furthermore, several β-helical structures present amphipathic β-helix caps at the N- and C-terminus, which may have the role of preventing aggregation. The absence of the cap in Pertactin led to uncontrolled interactions of the β-helical structures, generating oligomers and aggregates (Bryan, Starner-Kreinbrink et al. 2011). A "cap" has not been described for chlamydial Pmps;

however, structure predictions for Pmp21 suggest the presence of a globular region at the N-terminus of the predicted β-helix (Fig. 52) (Becker 2013). A structure for the N-terminal region of the β-helixes of *C. trachomatis* Pmps could not be identified using Phyre2.

In addition, oligomerization of β-helical structures is a characteristic of amyloid proteins, which leads to fibril formation, through a multi-step process, possibly initiated by conformational changes of monomeric proteins (Murphy 2007).

Moreover, *Chlamydia* Pmps are predicted autotransporters (ATs) (Figs. 4 and 52) (Henderson and Lam 2001). ATs are virulence factors with a β-helical structure, which can be processed. So far, only monomeric ATs have been described, such as the adhesin AIDA from *E. coli* (Bradley, Cowen et al. 2001, Cowen, Bradley et al. 2002).

In 2012, it was proposed that the motifs present at the corners of the predicted triangular β-helix of chlamydial Pmps might be responsible for protein-protein interaction, generating Pmp oligomers (Hegemann and Moelleken 2012, Becker 2013). In agreement with this model, it was recently shown that the motif-poor D-Wt Pmp21 harbors amyloidogenic characteristics and is able to generate protofibril-like homomeric oligomers (Luczak, Smits et al. 2016). The predicted triangular β-helical structures of Ac, Gc, H and I Pmp proteins analyzed in this work, with the motifs exposed at the corners (Fig. 34), suggest their ability of interaction.
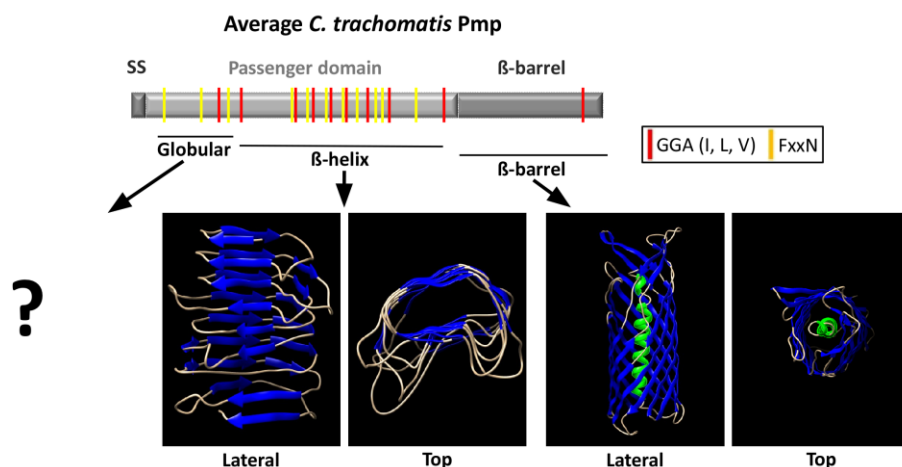
Figure 52. Schematic representation of an average *C. trachomatis* Pmp. Structure predictions performed with program Phyre2. Black lines indicate the position of the predicted structures within the Pmp. The N-terminal region of the PD is predicted as a globular structure for *C. pneumoniae* Pmp21 (aa 451-1089), modeled according to the Lipase of *Pseudomonas aeruginosa*, as shown by (Becker 2013). A globular structure for *C. trachomatis* Pmps could not be identified by Phyre2. The β-helical structure shown is the single-stranded right-handed β-helix predicted for PmpI (aa 98-330), modeled according to the Pectin lyase protein. The C-terminal β-barrel shown is the β-barrel predicted for PmpH (aa 691-1016), modeled according to the autotransporter EstA of *Pseudomonas aeruginosa*. Blue arrows indicate β-strands and α-helixes are indicated in green. The FxxN and GGA(I, L, V) motifs are shown in yellow and red, respectively. SS: signal sequences. Images are processed with UCSF Chimera server.

5.1.3 Motif-rich and motif-poor *C. trachomatis* Pmp proteins form high MW homomeric complexes

Motif-poor Ac, Fc and Gc and motif-rich D, H and I Pmp proteins (Fig. 8B-C), could interact with themselves in Far-Western-dot blot assays, but with different intensity. Biotinylated Ac, Fc and D Pmps showed a strong self-interaction; while Gc, H and I Pmps showed a weaker signal (Fig. 9). Self-interaction was confirmed by MST measurements, which revealed that motif-poor Ac, Fc and Gc self-interacted strongly, with Kd values in the range of 1,33 µM and 4,75 µM (see paragraph 4.1.2.1). To put these Kd values into context, fluorescin-labeled Protein kinase inhibitor was mixed with serial dilutions of Protein kinase A in the presence and in the absence of the cofactor and analyzed by MST. In the presence of the cofactor the two proteins could strongly interact (Kd: 2,3 ± 0,8 µM); while in the absence of the cofactor the two proteins did not interact (Kd: 489 ± 105 µM) (Jerabek-Willemsen, Wienken et al. 2011). The differences found for Gc in Far-Western-dot blot (weak interaction) and in MST (strong interaction) assays might be due to the fact that in Far-Western-dot blot the prey protein is renatured on the membrane, therefore it is possible that the protein is not folded correctly, partially masking the interaction domains. Far-Western blot analysis showed that the naturally cleaved *C. pneumoniae* fragment M-Pmp21 could self-interact, leading to the formation of hMW homomeric oligomers, as analyzed by SEC (Luczak, unpublished data; Becker 2013). Likewise, motif-poor D-Wt Pmp21 could also generate hMW oligomers of up to 839 kDa (Luczak, Smits et al. 2016).

Blue Native-PAGE (BN) and SEC analyses revealed that *C. trachomatis* motif-poor Ac, Fc and Gc and motif-rich D, H and I Pmp proteins formed hMW homomeric complexes, as it is summarized in Fig. 53. Interestingly, analysis of the same *C. trachomatis* Pmp homomeric complexes revealed differences in size when analyzed by BN and by SEC; for example Ac Pmp protein showed a main BN band at ~1300 kDa, but eluted in a main peak of ~400 kDa in SEC (Figs. 10 and 53). These discrepancies can be explained considering the different principles of the two techniques. In SEC, the proteins in soluble solution are separated by entering the pores of a solid phase, according to their size. On the other hand, BN might stabilize the hMW complexes, which enter the acrylamide gel in a more homogeneous manner. Thus, the force of separation results stronger in SEC than in BN and that might explain differences in separation of the same Pmp complexes.

Pmp	BN				SEC	
	Main bands (kDa)	Number of molecules	Complex range (kDa)	Number of molecules	Main peaks (kDa)	Number of molecules
Ac	~1300	48	~1000-5000	37-185	~400 < 67	15 1-2
Fc	~1300	34	~800-5000	21-132	n.a.	n.a.
Gc	~800 ~50	17 1	~600-1050 ~25-50	13 -23 1	~650 ~200	14 4
D	~1300 ~250	14 2	~700-5000 ~25-250	7 -52 1-2	~1000 ~669 ~140	11 7 2 degr.
H	~1000	20	~480-5000	10-100	n.a.	n.a.
I	~1250	22	~1000-5000	18-90	~2000 ~60	>36 1

Figure 53. *C. trachomatis* **Pmp proteins form different species of high molecular weight (hMW) homomeric complexes in BN and SEC.** The table summarizes the main bands for each Pmp protein identified by BN (Fig. 10A) and the main peaks of each Pmp protein identified by SEC (Fig. 10B). The number of Pmp molecules in each protein species (bands in Fig. 10A, peaks in Fig. 10B) was calculated using the apparent size of the corresponding monomers (Fig. 8C). n.a.: Not analyzed.

Furthermore, some, but not all Pmp proteins analyzed could also generate low MW complexes (Figs. 10 and 53). In particular, motif-rich D Pmp formed a ~250 kDa complex, when analyzed by BN, corresponding to 2 full length D fragments and eluted in a ~140 kDa peak in SEC, formed by a 55 kDa degradation product of PmpD, possibly forming dimers. The same PmpD degradation product is detected also in the hMW peaks, together with the full length motif-rich D Pmp fragment, suggesting that both protein species could be part of the same complex (Figs. 10B and 53).

When PmpD from *C. trachomatis* L2 was analyzed at 24 hpi, time point when PmpD transcription and expression is upregulated (Kiselev, Stamm et al. 2007, Van Lent, Creasy et al. 2016), not only the full length PmpD (p155) could be detected in EB lysates and in immunoprecipitated fraction of the EB membrane, but also two processed fragments were present, a N-terminal PD region (p73) and a C-terminal region which includes also the β-barrel (p82) (Fig. 6A). The PmpD p155, p73 and p82 fragments were detected as part of a hMW complex of ~850 kDa, when analyzed by BN and second dimension gels (Swanson, Taylor et al. 2009).

In a similar way, VacA, an autotransporter toxin of *Helicobacter pylori,* can be cleaved in two fragments (p33 and p55), which can interact, as shown by co-immunoprecipitation assays, and generate different species of hMW oligomers, up to 14 monomers (El-Bez, Adrian et al. 2005, Torres, Ivie et al. 2005, Gangwer, Mushrush et al. 2007).

Similarly, the amyloid precursor protein APP, from which the Alzheimer´s Aβ amyloid peptide is generated, can be cleaved by α- and β-secretases, generating extracellular APPα and APPβ fragments of around 110 kDa in the cerebrospinal fluid (CSF). When CSF fractions where analyzed by BN, a main band of ~240 kDa was detected, together with smear-like bands of higher MW. Immunoblotting analysis of BN gels revealed that the hMW bands are formed by full length soluble APP together with APPα and APPβ (Cuchillo-Ibanez, Lopez-Font et al. 2015). In addition, also functional surface-exposed Bap proteins from *Staphylococcus aureus* generate smear-like bands in BN analysis of bacterial lysates (Taglialegna, Navarro et al. 2016). Baps are a group of surface proteins with similar structure and function, responsible for biofilm formation and cell-cell aggregation and are characterized by a C-terminal region, which binds them to the bacterial surface, a central domain rich in serine and aspartic acid residues and with repeated motifs forming a β-sandwich, involved in cellular adhesion. The N-terminal region of the Bap protein is still of unknown function (Lasa and Penades 2006). Interestingly, Bap proteins form hMW complexes of ~700 kDa in the *S. aureus* cell wall and the degradations bands are identified by mass spectrometry analysis as peptides from the N-terminal region. These data suggest that Baps undergo proteolytical cleavage, generating several Bap fragments, responsible for building up hMW complexes (Taglialegna, Navarro et al. 2016).

As observed for APPα-β and Bap proteins, *C. trachomatis* motif-rich D, H and I and motif-poor Ac, Fc and Gc Pmp proteins do not present defined bands by BN analysis, but instead show a main band of one oligomeric species, accompanied by oligomers of higher and lower complexity (smear), indicating the presence of different species of hMW homomeric complexes generated in the same Pmp sample (Fig. 10A). The presence of different species of oligomers was confirmed by the presence of several peaks and shoulders for each Pmp sample when analyzed by SEC (Fig. 10B), similarly to what has been observed for *C. pneumoniae* M-Pmp21 and D-Wt Pmp21 (Luczak, Smits et al. 2016).

One example in the literature shows that a protein with the ability to form functional oligomers, also has the tendency to form oligomers of different sizes *in vitro*. The HIV envelope protein Gp41, a protein found in the brain of patients with HIV-associated dementia, is a trimer associated to the viral membrane and can be proteolytically cleaved, generating the Gp41 ectodomain. Sedimentation velocity assays showed that Gp41 ectodomain self-interacts, forming a big structure made of five trimers, from which hMW complexes are generated by nucleation of up to 30 Gp41 trimers. The hMW complexes accumulate in the brain causing tissue damage (Jacobs, Hartman et al. 2004). High MW

complexes were also observed for the corresponding Gp41 protein from SIV, when analyzed by SEC and electron microscopy analysis, showing that Gp41 complexes within the same sample have differences in size and shape (Caffrey, Braddock et al. 2000).

Visualization of the *C. trachomatis* Ac, Gc, D and I Pmp homomeric complexes by TEM revealed elongated structures of 32, 12, 70 and 29 nm average length, respectively (Fig. 24A). Interestingly, in the same Pmp sample different morphologies are present; for example Ac has an average length of 32 nm, with the majority of oligomers within the range of 21 and 35 nm; however some Ac structures reached 348 nm (Figs. 24A and 25A). Despite their differences in length, all homomeric Pmp structures (Ac, Gc, D and I) had a similar average width (between 13 and 20 nm), suggesting their structural specificity and excluding random aggregation (Fig. 25B). Similarly, D-Wt Pmp21 oligomers are visualized as elongated structures of 11, 27 and 61 nm average length, which can reach filaments of almost 300 nm in length, and with an average width of ~10 nm (Luczak, Smits et al. 2016).

Amyloid Alzheimer´s $A\beta_{(1-40)}$ peptide forms fibrils with parallel β-helical structures and cryo-electron microscopy and 3D reconstruction analyses showed that the $A\beta_{(1-40)}$ peptide generates fibrils with an heterogeneous morphogenesis and polymorphic fibrils can exist within the same sample (Meinhardt, Sachse et al. 2009). In addition, the $A\beta_{(12-28)}$ peptide, as analyzed by CD and FTRI spectrometry, could generate two types of oligomers; the first oligomers are generated rapidly and are characterized by small and twisted β-sheets; while the second population is formed by oligomers with multi-strand β-sheets, which are generated slowly (Mandal, Eremina et al. 2012). The generation of polymorphic oligomers from a monomer with a fixed 3D structure might be the result of different inter-residue contacts among the same peptide sequence (Meinhardt, Sachse et al. 2009).

Smear-like bands in BN, presence of several peaks in SEC and different structures by TEM analysis indicate that *C. trachomatis* motif-poor and motif-rich Pmps form a heterogeneous population of homomeric complexes, independently of the density of motifs.

The heterogeneous oligomeric population might be a result of the multi-step process of fibril formation, as described for amyloid proteins (Murphy 2007). Motif-poor D-Wt Pmp21 has been shown to have amyloid characteristics, and its similarity with *C. trachomatis* Pmps and the presence of similar structures visualized by TEM (Figs. 10 and 24A) (Luczak, Smits et al. 2016), indicate that *C. trachomatis* Pmps might behave in a similar manner. Amyloid fibril formation is initiated by conformational changes of monomers during interaction with one another, generating small and larger oligomers. The

oligomers might then generate β-helical protofibrils, with structural polymorphism. Fibril generation might occur by addition of monomers at the tip or by incorporation of small oligomers (Chiti and Dobson 2006, Murphy 2007). This multi-step process might explain why we see not only hMW Pmp oligomers, but also lower MW complexes within the same sample (Fig. 10).

5.1.4 Motif-rich and motif-poor *C. trachomatis* Pmp proteins interact with each other

The Pmps are divided in six subgroups and members belonging to the same subgroup share significant amino acid identity (e.g. PmpD-Pmp21: 33 % sequence identity), suggesting similar functionality. Nevertheless, the level of sequence identity among Pmps from different subgroups is low (e.g. PmpE-PmpD: 18 %) (Becker 2013, Vasilevsky, Stojanov et al. 2016). Despite the low sequence identity, Pmps have a predicted autotransporter structure, with the central passenger domain organized in a β-helical structure (Henderson and Lam 2001, Becker 2013). β-helical proteins and amyloid structures can associate into amyloid fibrils (Tsai, Gunasekaran et al. 2006). Pmps PDs are enriched in the FxxN and GGA(I, L, V) motifs, which, according to the structure predictions, are exposed at the corners of the triangular β-helical structure and might mediate Pmp-Pmp interaction (Hegemann and Moelleken 2012, Becker 2013). Given these premises, the structure of Pmps PD should not distinguish between different Pmps and each Pmp should be able to interact with another Pmp. Indeed, recombinant M-Pmp21, which represents a naturally occurring processed form of Pmp21, interact with itself and with representative *C. pneumoniae* Pmps when tested in Far-Western blot analysis, but does not interact with the naturally processed recombinant N-Pmp21, which has a predicted globular structure (Becker 2013).

This work now shows that different recombinant *C. trachomatis* Pmp proteins (Fig. 8A) tested in Far-Western blot analysis could interact with themselves and with most, but not all fragments of the same or of different Pmps (Figs. 9 and 11).

The ability of interaction among different Pmps was confirmed for selected Pmp fragments by MST measurements, as a proof of principle and it was shown that motif-poor Ac interacted with PmpA full length PD (Afl), Ec, Fc and Gc Pmp proteins. Interestingly, Ac interacted with Afl in a very strong manner (Kd: 0,723 ± 0,56 μM), even stronger than with itself; while the interaction with the other motif-poor Pmps was up to 25 times weaker than with Afl (see paragraph 4.1.3.2), possibly because the PmpA full length PD might

organize itself in the right natural 3D final structure, exposing the high number of motifs and allowing a more natural surface for interaction. Furthermore, the interaction ability of Pmps was confirmed with pull-down assays, where VSV-tagged motif-poor Ac interacted with His-tagged motif-poor Gc and with His-tagged motif-rich D and I Pmps (Fig. 12).

With these experiments it was demonstrated that all recombinant Pmp proteins have the capacity of interacting with different Pmps; unfortunately, a specific PD domain could not be identified as being responsible for this Pmp-Pmp interaction. However, most Pmp fragments interacted with motif-rich A, B, C, D, E, H and I Pmp proteins (Fig. 11), possibly due to the presence of the high density of the motifs. The fact that the different Pmps have a different interaction pattern and showed no interaction with all other Pmps (e.g. motif-rich C interacted with motif-rich A, but did not interact with motif-poor Ac) (Fig. 11B) may suggest that the interactions are specific and possibly depend not only on the structural conformation of the Pmp fragment, but also on the number of motifs exposed and on the protein sequence. An example in support of this hypothesis is that motif-rich H interacted with full length G PD, but did not interact with the motif-poor PD fragment Gc (Fig. 11A-B), despite the fact that both G and Gc have a predicted β-helical structure (Fig. 34B and Becker 2013).

So far in the literature only a few proteins have been described which form β-helical structures and use them to oligomerize with other β-helical proteins. An example is given by the Alzheimer Aβ peptide, which is able to interact with several other amyloid proteins, among which the Prion protein PrP is one. PrP is a protein present in the nerve cells and, when misfolded, can accumulate in the brain cells, causing Creutzfeldt-Jakob disease. PrP and Aβ peptide have been co-purified from human brain material, where the PrP N-terminal positively charged region functions as a receptor for Aβ oligomers (Luo, Warmlander et al. 2016). Functional analysis in transgenic mice suggested that PrP upregulates Aβ accumulation, acting as a seed for the Aβ peptide, making the Prion protein disease a risk factor for Alzheimer disease (Zou, Xiao et al. 2011). Interestingly, *C. pneumoniae* infection in mice leads to an accumulation of amyloid structures, correlating *C. pneumoniae* infection to Alzheimer disease (Little, Joyce et al. 2014); however the mechanisms have not been elucidated so far.

5.1.5 Motif-rich and motif-poor *C. trachomatis* Pmp proteins form high MW heteromeric complexes

This work showed that different *C. trachomatis* Pmp proteins are able to interact with each

other, thus leading to the hypothesis that Pmps might form not only homomeric hMW complexes, but also heteromeric hMW oligomers. In order to investigate the ability of Pmps to generate heteromeric oligomers on the surface of the infectious EBs, different motif-poor and motif-rich Pmp proteins (Ac, Fc, Gc, D, H and I) (Fig. 8B) were selected and their *in vitro* oligomerization ability was investigated.

5.1.5.1 Co-refolding and mixing of two different *C. trachomatis* Pmps generate hMW complexes with different characteristics

Pmps have a predicted AT structure, with the PD exposed on the EB surface (Henderson and Lam 2001). It is still not clear how the AT PD is exported and when the folding occurs. Two main models have been proposed; according to the "Hairpin model", the unfolded PD is pushed in the extracellular space, to be folded in this very moment; while the "Omp85 model" suggests that the PD folds partially in the periplasmic space, with the help of periplasmic chaperones, upon being exported in the extracellular space, where it is finally folded (Dautin and Bernstein 2007, Gawarzewski, Smits et al. 2013).

Since there is no evidence for the Pmp folding process and our experimental set up did not allow the separation of monomers from oligomers, in this work pairs of two different Pmps have been purified under denaturing conditions and co-refolded together by dialysis (Fig. 13). The co-refolding process should mimic Pmp interactions in the extracellular space, while Pmps are still not fully folded and can organize themselves in complexes, as it is discussed in the following paragraphs.

The majority of this work focuses on the characterization of co-refolded Pmps; however, complexes formed by mixing in a 1:1 molar ration of two Pmps already in their folded status were investigated (Fig. 21A). Three combinations of mixed motif-poor Pmp proteins were tested (Ac+Gc, Fc+Gc and Fc+Ac) and Blue Native-PAGE (BN) analysis showed no differences in the size of the mixed hMW complexes and of the respective co-refolded complexes (Fig. 21B). Interestingly, the mixed motif-poor Pmp complexes exhibited a slight functional difference, when tested for their adhesive capacity to human epithelial HEp-2 cells *in vitro* (Fig. 26). When adhesion-competent Fc was co-refolded with adhesion-incompetent Ac or Gc (co-refolded Ac+Fc or Fc+Gc), Fc lost almost all its adhesive capacity, indicating that Fc function is masked in the complexes (Fig. 28). On the other hand, when Fc was mixed with Ac or Gc (mixed Ac+Fc or Fc+Gc), a stronger signal for Fc was detected in the binding fraction, partially bringing also adhesion-incompetent Ac and Gc in the binding fractions (Fig. 28). These data indicate that both co-refolding of

two denatured Pmps and mixing of two Pmp proteins already in their folded status generate complexes with similar sizes, but with different functional properties, suggesting that the Pmps may interact in a different manner in the two set ups, generating complexes with a different organization of the two Pmp proteins.

When two Pmps are mixed in their already folded status at 4 °C, it is very likely that the two homomeric complexes do not dissociate to form heteromeric complexes; however the two already formed homomeric complexes with a predicted β-helical structure can form lateral associations, which do not require a high degree of energy.

Lateral association has been described for fibril formation of β-helical proteins (Murphy 2007). One example is insulin, which can generate fibrils by stacking of monomers and oligomers, associating laterally and at the filament tips, generating several intermediate aggregates, as shown by atomic force microscopy and by kinetic studies by performing light scattering measurements (Jansen, Dzwolak et al. 2005, Manno, Craparo et al. 2006).

Als5p from *Candida albicans* is another example; this protein is indeed anchored in the fungal surface and is organized in patches. When these patches are disrupted by atomic force microscope, the aggregate conformation is disturbed and unfolded domains expose their amyloid core, leading to fibril formation (Garcia, Lee et al. 2011, Chan, Joseph et al. 2015).

5.1.5.2 Two different co-refolded Pmps generate hMW complexes with different characteristics than the respective homomeric Pmp complexes

In order to investigate the ability of *C. trachomatis* Pmps to generate heteromeric oligomers and following the "Hairpin model", according to which AT PDs are exposed unfolded on the outer membrane, as described in the previous paragraph, selected motif-poor Ac, Fc and Gc and motif-rich D, H and I *C. trachomatis* Pmp proteins (Fig. 8B) have been purified under denaturing conditions and co-refolded in pairs in a 1:1 initial ratio by dialysis (Fig. 13). All co-refolded Pmps generated different hMW complexes when analyzed by Blue Native-PAGE (BN) and SEC (Figs. 14 and 22). Co-refolded motif-poor Fc+Ac migrated as a main BN band of ~1250 kDa, similarly to homomeric Fc and Ac complexes (Fig. 14A). In all other combinations (Ac+Gc, Fc+Gc, D+I, Ac+D, Ac+H and Ac+I), the co-refolded hMW complexes showed differences in size, when compared with the respective homomeric Pmp complexes (Fig. 14). In all combinations, the hMW complexes were composed by both protein species, as shown by second dimension analyses. Only in two hMW complexes the two Pmps were present in similar amounts

(Ac+D and Fc+Gc) (Figs. 16A and 17B); while the hMW complexes formed by all other Pmp pairs were composed by both protein species, but with one Pmp being more prominent than the other. Pmp Ac, for example, is the most prominent component of Ac+Gc, Fc+Ac and Ac+I hMW complexes (Figs. 16B and 17A-C), while PmpI is more prominent than PmpD in the co-refolded D+I hMW complex (Fig. 15). Furthermore, the low MW complexes of Fc+Gc and Ac+Gc were composed only by Gc Pmp protein (Fig. 17B-C). All together, these data suggest that the two Pmp species are present in the co-refolded hMW complexes with a final ratio different from the initial 1:1 ratio.

Similarly to homomeric Pmp complexes, all the co-refolded Pmp complexes did not appear as a defined band in BN analysis, but as a main band, surrounded by a smear (Fig. 14). As discussed for homomeric Pmp oligomers (see paragraph 5.1.3), the smear-like bands may be the result of a heterogeneous population of oligomers present in the same sample, which, in the case of co-refolded Pmps, might be a mixture of homomeric and different species of heteromeric complexes, due to a multi-step process of oligomers formation (Murphy 2007).

Taken together, the shift in the main BN band size and the different ratio of the two Pmp proteins in the co-refolded complexes, detected by second dimension analysis, indicate that co-refolded *C. trachomatis* Pmps generate oligomers with different characteristics than the respective homomeric Pmp oligomers.

In order to investigate in more detail the different characteristics of co-refolded Pmp and the respective homomeric complexes, motif-poor Ac+Gc was selected, because it showed the most prominent shift in BN analysis (Fig. 14A). Motif-poor Ac and Fc were used as controls, since the co-refolded Fc+Ac complex did not show a shift in size, compared to homomeric Ac and Fc complexes. The two combinations of two Pmp proteins co-refolded at different initial concentrations were tested by BN and second dimension analyses. All combinations of co-refolded Fc+Ac migrated at ~1250 kDa, as expected (Fig. 18B), while co-refolded Ac+Gc migrated in a main band of comparable size to homomeric Gc (~800 kDa), when the initial concentration of Gc was higher than the concentration of Ac (99 %, 95 % and 75 %). When Ac and Gc were co-refolded in a 50 % - 50 % initial concentration, the shift in band size became visible and the hMW complex was detected at ~1100 kDa. When the initial Ac concentration was higher than the concentration of Gc (75 % and 95 %), the co-refolded Ac+Gc complexes migrated in a main band of similar size to homomeric Ac (Fig. 18A). Second dimension analysis revealed that all the Ac+Gc

complexes from all mixtures were composed by both Ac and Gc Pmp proteins (Fig. 19). These results suggest that Ac and Gc indeed interact with each other and generate different complexes depending on the initial molar ratio. The fact that the different initial Ac and Gc concentrations influence the size of the resulting co-refolded complexes indicates that heteromeric complexes are present in the mixture.

These results were supported by co-refolding experiments of His-tagged motif-poor Gc and VSV-His-tagged motif-poor Ac Pmp proteins in an initial 1:1 ratio. Immunoblotting analysis of the BN gel with anti-His and anti-VSV antibodies showed that the co-refolded hMW complex of ~1100 kDa was composed by both Ac and Gc Pmp proteins, while band of ~30 kDa was composed by the Pmp Gc protein alone (Fig. 20), as already showed by second dimension analysis (Fig. 15C). The presence of homomeric low MW Gc band may indicate that in a 1:1 initial ratio, the resulting complex harbor more Ac protein than Gc protein. This is further supported by subsequent MST measurements showing that Ac, but not Gc, could still bind the already co-refolded Ac+Gc complex (see paragraph 4.1.4.3).

Taken together, these data indicate that *C. trachomatis* Pmp heteromeric oligomers might be formed by association of different monomeric Pmps or by association of oligomers at the tip of already formed fibrils, possibly leading to a conformational re-organization, as it is proposed for amyloid proteins (Murphy 2007).

Co-refolded Pmp complexes were further analyzed by SEC, in order to solve the different Pmp oligomers in more detail. As obtained for homomeric Pmp complexes (Fig. 10B), each co-refolded Pmp complex (Ac+Gc, Ac+I, Ac+D and D+I) presented a specific and unique elution profile. All the co-refolded complexes eluted in more than one peak, indicating the presence of a heterogeneous oligomeric population (Fig. 22). Interestingly, the main peaks of the co-refolded hMW complexes were shifted from the main peaks of the respective homomeric complexes, as shown by superimposition analysis of the SEC curves (Fig. 23). Co-refolded Ac+Gc, for example, eluted in a main peak of ~200 kDa, which overlaps with homomeric Gc, but is shifted from the homomeric Ac peak, and in a shoulder of ~500 kDa, shifted from both homomeric Ac and Gc. These data indicate the presence of at least two oligomeric species of Ac+Gc complex, with different characteristics from the two homomeric complexes alone, and composed by both Ac and Gc, as detected by immunoblotting (Figs. 22A and 23A). A shift of the main co-refolded oligomeric peaks from the respective homomeric oligomeric peaks is detected for all Pmp mixtures (Fig. 23), and, interestingly in all peaks formed by co-refolded Pmps, both Pmp

species are detected by immunoblotting analysis of SEC fractions, but in different ratios (Fig. 22). For example, co-refolded D+I eluted in one peak of ~1000 kDa, partially overlapping with homomeric D and I and containing both Pmps in similar amount; while the D+I peak of ~140 kDa, overlapping only with homomeric D, is composed mainly of I Pmp protein, and in lower concentration of D Pmp protein (Figs. 22D and 23D).

Furthermore, SEC analyses were performed also with different SEC columns (Superdex75 and Superdex200) for homomeric Ac, Gc and I and for co-refolded Ac+Gc and Ac+I. In all conditions tested, homomeric and co-refolded Pmp mixtures eluted in more than one peak with the co-refolded peaks being shifted from the respective homomeric Pmps (data not shown).

Taken together, these data show that, similarly to homomeric Pmps, co-refolded Pmps are able to generate a heterogeneous population of oligomeric species, possibly due to a multi-step process of complex formation. Different oligomeric species within the same co-refolded Pmp mixture can depend on the initial concentration of the two proteins, as shown for co-refolded Ac+Gc. Even though the presence of homomeric complexes in the hMW co-refolded Pmp complexes cannot be excluded, the shift in size of BN bands of co-refolded complexes, harboring both protein species and the changes in the SEC elution curves, again with both protein species present, showed that co-refolding of two Pmp fragments generates heteromeric complexes, with different characteristics than the respective homomeric complexes. Likely, the organization of the heteromeric complex is specific for each Pmp pair, as in all cases the final Pmp ratio in the complexes is different from the initial 1:1. Interestingly, from the experiments in this work, there is no difference in heteromeric and homomeric complex formation between motif-poor and motif-rich Pmp proteins; all of them are able to generate different species of hMW homo- and heteromeric oligomers.

While the literature knows several examples for proteins capable of forming different species of homomeric hMW oligomers (see paragraph 5.1.3), only one other family of proteins has been described so far as capable of forming multimeric protein complexes. The *Plasmodium falciparum* LCCL domain-containing proteins (PfCCp) are six secreted proteins of the malaria parasite, which contain several adhesion domains and are associated with the development of the parasite in the mosquito vector. Similarly to Pmp proteins, PfCCp proteins are heterologously expressed during the parasite cycle and are exposed on the macrogamete surface. Even though transcription of the *pfCCp* genes is independent form one another, mutant lacking *pfCCp1, 2, 3* or *4*, showed a reduced presence of all

PfCCp proteins, suggesting a co-dependent expression (Simon, Scholz et al. 2009). After expression, secreted PfCCp proteins interact with each other, assembling in multi-protein complexes, as shown by pull-down assays with recombinant proteins *in vitro* and by co-immunoprecipitation assays on gametocytes lysates *in vivo*. The PfCCp heteromeric complexes remain associated to the parasite plasma membrane by binding the membrane-anchored Psf230-Psf48/45 complex, as shown by co-immunoprecipitation assays on gametocytes lysates (Simon, Kuehn et al. 2016). Given the adhesive properties of PfCCp, the heteromeric complexes might mediate cell-cell binding of macrogametes during the sexual reproduction step of the parasite (Simon, Scholz et al. 2009).

5.1.6 Homomeric and heteromeric Pmp oligomers form protofibril-like structures

Both homomeric and heteromeric *C. trachomatis* Pmps generated elongated structures visible by TEM, independently of the density of motifs (Fig. 24). Homomeric Ac, Gc, D and I Pmp structures have an average length of 32, 12, 70 and 29 nm respectively, with an average width of 17, 13, 20 and 16 nm, respectively (Fig. 24A). Heteromeric motif-poor Ac+Gc formed heterogeneous elongated structures with an average length of 186 nm, reaching up to 2932 nm in length (Fig. 25A). Heteromeric Ac+D, Ac+I and D+I could also generate long structures with an average length of 207, 120 and 92 nm, respectively, reaching up to 749, 604 and 804 nm in length (Fig. 24B and 25). Heteromeric Ac+Gc and D+I structures presented an average length of 18 and 13 nm, respectively, comparable to the widths of the respective homomeric structures, despite Ac+Gc and D+I structures are significantly longer (Fig. 25). On the other hand, heteromeric Ac+I and Ac+D structures, which are significantly longer than the respective homomeric Pmps, are also thicker, with an average width of 52 and 48 nm, respectively (Fig. 25). These data indicate that homomeric and heteromeric Pmp structures are specific structures and not simply aggregates. The TEM pictures revealed that all homomeric and heteromeric Pmp oligomers formed a heterogeneous population of filaments, in agreement with the presence of smear-like bands in the BN analyses and of the complex elution profiles in the SEC analyses. As already mentioned, the presence of different oligomeric species within the same sample might represent a dynamic multi-step process of complex formation (Murphy 2007). Interestingly, the *C. pneumoniae* motif-poor D-Wt Pmp21 could also generate different species of oligomers, visualized as filaments of 11, 27 and 61 nm average length, and 10 nm average width, with amyloid properties and functional relevance for the infection

(Luczak, Smits et al. 2016). Whether the *C. trachomatis* Pmps also have amyloid properties needs to be analyzed, but their predicted β-helical structure, the similarity with *C. pneumoniae* Pmp21 and their TEM protofibril-like structures suggest a similar behavior. Evidently, heteromeric *C. trachomatis* Pmp structures are significantly longer than the respective homomeric Pmps, with a similar width (Fig. 25), confirming that these structures are indeed heteromeric oligomers, formed by both Pmp fragments, possibly in a different ratio than the initial 1:1, as discussed in paragraph 5.1.5, and with specific characteristics, different from the respective homomeric Pmp oligomers.

Both homomeric and heteromeric *C. trachomatis* Pmp oligomeric filaments are similar to the amyloid filaments formed by the Alzheimer's Aβ peptide, which was shown to generate different species of fibrils and oligomers within the same sample, depending on different monomeric inter-residue interactions (Meinhardt, Sachse et al. 2009, Mandal, Eremina et al. 2012). Similar structures were also visualized for the functional *E. coli* adhesin Curli, responsible for cell-cell interaction and biofilm formation. Curli fibrils are generated by highly regulated interactions of the secreted monomeric CsgA and present amyloid properties (Barnhart and Chapman 2006, Hufnagel, Depas et al. 2015).

Moreover, the trimeric autotransporter AtaA from *Acinetobacter* sp. Tol 5 has a big PD (~3000 aa), characterized by multiple domain repeats with a β-helical structure and two globular heads, forming fibers of ~200 nm on the bacterial surface (Koiwai, Hartmann et al. 2016). AtaA fibrils have amyloid properties, and are responsible for non-specific adhesion to abiotic surfaces and for cell-cell adhesion (Yoshimoto, Nakatani et al. 2016).

When analyzed by electron microscopy, immunoprecipitated complexes from the surface of *C. trachomatis* L2 EBs, using anti-PmpD antibodies, could be visualized as small protofibril-like structures, similar to *C. trachomatis* motif-poor and motif-rich Pmps, together with rare flower-like structures, and these complexes have been shown to harbor different processed PD fragments of PmpD (Swanson, Taylor et al. 2009). However, whether these structures have anything to do with the Pmp fibrils described in this work remains to be shown. So far, Pmp fibrils have not been visualized *in vivo* on the surface of the infectious EBs. Interestingly, the *H. pylori* VacA can also generate different species of flower-like oligomers, formed by the different cleaved fragments p33 and p55 (Torres, Ivie et al. 2005, Gangwer, Mushrush et al. 2007).

5.1.7 Homomeric and heteromeric Pmp oligomers have different functional properties

Recombinant *C. trachomatis* motif-poor and motif-rich Pmp proteins are able to generate different types of hMW homomeric and heteromeric complexes, with elongated protofibril-like structure and with specific characteristics. Next we decided to investigate the role that these oligomers may play during the *C. trachomatis* infection.

The first step for studying the functions of Pmp oligomers was to investigate their adhesion capacity. The protein-coated beads, often used in adhesion assays, carry a high concentration of proteins and protein loading may interfere with oligomeric structures. In order to avoid this condition and to ask whether individual protein molecules have adhesive capacity, in this work homomeric and heteromeric Pmp samples have been tested by soluble binding assays (Fig. 26). Afterwards, the Pmp oligomers were tested for their relevance during the *C. trachomatis* infection, using two different infection blocking assays (Figs. 31A and 32A).

5.1.7.1 Different homomeric Pmp proteins have different adhesion capacity

The binding capacity of homomeric Pmp fragments, representing different regions of the PD of *C. trachomatis* Pmps and harboring a different density of motifs, was investigated. For this purpose, different fragments from different Pmps were selected. Ac, Ec, Fc and Gc Pmp fragments represent the C-terminal portion of the Pmp PDs, harboring only 2 motifs (motif-poor); A, D, F, H and I Pmp fragments represent the central region of the PD with a high density of the motifs (motif-rich) and An, En and Fn Pmp fragments represent the N-terminal region of the PD, with a medium number of motifs (motif-low) (Figs. 27, 28 and 30). Surprisingly, different Pmp proteins with similar characteristics, such as position within the PD and density of motifs, behaved in a different way. For example, motif-poor Ac, Ec and Gc showed no or very weak adhesion to human epithelial HEp-2 cells, while motif-poor Fc is a strong binder (Figs. 27 and 30). In a similar manner, the Pmp fragments An and Fn with a medium density of motifs showed weak adhesion; while En, harboring similar motif numbers, bound strongly to human cells (Fig. 30). Motif-rich A, D, F, H and I fragments could both adhere to human cells (Figs. 29 and 30), confirming previous data obtained with yeast adhesion and fluorescent beads assays (Becker and Hegemann 2014). Given these results it is not possible to identify a specific common adhesive domain within the PD of different *C. trachomatis* Pmps. If we compare our *C. trachomatis* motif-poor and motif-rich Pmp fragments with the artificial and natural fragments generated from

C. pneumoniae Pmp21, motif-poor and motif-rich fragments of Pmp21 could all adhere to human cells in a similar manner, when tested by yeast adhesion assays and protein-coated beads assays, independently from the motifs density (Molleken, Schmidt et al. 2010). Furthermore, motif-rich fragments of all 9 *C. trachomatis* Pmps could also bind to human cells, but presented differences in adhesion strength when tested by protein-coated beads assays, in which PmpD showed the strongest adhesion and PmpH the least strong adhesion (Becker and Hegemann 2014). In our experiments only Pmp fragments with a limited number of motifs showed no binding (Ac, Ec, Gc and Fn) (Figs. 27 and 30), even though, according to what is known for *C. pneumoniae* Pmp21, a minimum of two motifs is enough to guarantee adhesion of protein-coated beads. A version of motif-poor Pmp21 with one of the 2 motifs mutated could no longer bind human cells in beads adhesion assay, similarly to an artificial C-terminal Pmp21 fragment harboring no motif (Molleken, Schmidt et al. 2010, Luczak, Smits et al. 2016).

In discussing the different adhesion capacities of the different *C. trachomatis* Pmp proteins, it has to be considered that these fragments generated are artificial and we have no proof that they are properly folded; therefore it is possible that the non-adhesive Pmp fragments fold themselves in an aberrant conformation, where the adhesive domains are not exposed in a proper way. It would be interesting in the future to test the non-adhesive Pmps with other adhesion assays, such as yeast display and coated-beads, in order to check whether the different conditions might influence Pmps folding and/or abilities to expose eventual functional domains. *Acinetobacter* sp. Tol 5 trimeric autotransporter AtaA, forming protofibril-like β-helical filaments on the bacterial surface, as discussed in the previous paragraph (Koiwai, Hartmann et al. 2016), is able to mediate its non-specific adhesion to abiotic surfaces only when its 3D structure is intact (Yoshimoto, Nakatani et al. 2016), suggesting that the proper folding of a protein and the exposition of the functional domains is essential even for non-specific adhesion.

Interestingly, the presence of two motifs in *C. pneumoniae* motif-poor Pmp21 is essential not only for adhesion, but also for oligomerization; when the motifs were mutated, the protein had a reduced capacity to form oligomers, and only the oligomers were able to adhere to human cells, while the monomers were not adhesive (Luczak, Smits et al. 2016).

5.1.7.2 Heteromeric Pmp oligomers have different adhesion properties

Next, heteromeric Fc+Gc, Ac+Gc, Fc+Ac, Ac+D, Ac+H, Ac+I and D+I Pmp complexes were tested for their adhesive capacity in soluble adhesion assay (Fig. 27).

Heteromeric motif-rich D+I Pmp oligomer showed adhesion, in agreement with the respective homomeric Pmp oligomers (Fig. 29); while heteromeric motif-poor Ac+Gc Pmp oligomer showed no adhesion to human cells, as the two homomeric oligomers alone (Fig. 27), despite generating very long filaments (Fig. 24A).

Interestingly, when in a heteromeric complex with adhesion-incompetent Ac or Gc (Fc+Ac and Fc+Gc), adhesion-competent motif-poor Fc signal was weaker, when compared to the homomeric Fc binding band (Fig. 27). On the other hand, adhesion-incompetent Ac was found in the binding fractions when in a heteromeric complex with adhesion-competent motif-rich D, H and I Pmps (Ac+D, Ac+H and Ac+I); while homomeric Ac alone showed no binding capacity (Fig. 29). Furthermore, different species of heteromeric and homomeric oligomers might be present in the same mixture. For example, the presence of a weak signal of Gc in the Ac+Gc sample, similar to the homomeric Gc weak signal, suggests that homomeric complexes might still be present in the mixture together with heteromeric complexes (Fig. 27). Moreover, in the Fc+Gc mixture, not only a weak band was detected for Fc, as previously mentioned, but also a band for Gc was detected as slightly stronger than the homomeric Gc alone (Fig. 27), suggesting the presence of different species of heteromeric Fc+Gc complexes.

Taken together, these data indicate that during heteromeric complex formation, the distribution and organization of the Pmps may mask or expose the functional domains of the different components. Adhesion-competent Fc might be masked by adhesive-incompetent Ac and Gc, preventing its binding; while adhesive-incompetent Ac might be used as a support for the complex formation, in order to allow adhesion-competent Pmps to reach the human receptors. Different Pmps might therefore influence each other functions when they are part of the same oligomers.

One example in this direction is given by *H. pylori* VacA. VacA fragments p55 and p33 interact with each other, generating the functional oligomeric toxin. The p55/p33 mixture could bind the host cell membrane and be internalized more efficiently than the two fragments alone (Torres, Ivie et al. 2005).

5.1.7.3 Homomeric and heteromeric Pmp oligomers show different relevance for the infection

In order to investigate the relevance of different homomeric and heteromeric Pmp oligomers for the infection, two different infection blocking assays were performed.

In the first assay, human epithelial cells were pre-incubated with soluble Pmp oligomers. Upon binding the unknown human receptor, the relevant Pmp oligomers block a subsequent *C. trachomatis* infection (Fig. 31A). In this set-up, pre-incubation of human cells with adhesion-competent homomeric D, I and heteromeric Ac+D, Ac+I and D+I Pmp oligomers blocked a subsequent *C. trachomatis* infection, up to 60 % (Fig. 31), showing their ability not only in binding human cells, but also in binding receptors relevant for the adhesion of the EBs. Relevance for the infection was also shown for motif-rich fragments of all 9 *C. trachomatis* Pmps and for *C. pneumoniae* Pmp21, Pmp20 and Pmp6, which could also block a subsequent infection, in a species-specific manner (Molleken, Schmidt et al. 2010, Becker and Hegemann 2014).

Interestingly, pre-incubation of human cells with adhesion-competent heteromeric D+I Pmp oligomer led to a reduction of the infection in a similar level as the respective homomeric D and I Pmp oligomers alone (Fig. 31). These data might indicate that the adhesive Pmps exposed in the heteromeric complex are limited (as discussed in paragraph 5.1.7.2) and, in this case, there is no difference on which is the adhesion-competent fragment exposed. These data may also indicate that *C. trachomatis* Pmps have overlapping functions, possibly acting on the same human receptors. In support of this theory, when two different Pmps from two different serotypes were mixed and pre-incubated together with human cells showed no differences in the reduction of the infection, compared to the respective Pmps alone (Becker and Hegemann 2014).

Moreover, pre-incubation with adhesive-incompetent Ac, Gc and Ac+Gc Pmp oligomers showed no effect on the infection (Fig. 31). Being homomeric Ac, Gc and heteromeric Ac+Gc Pmp oligomers not able to adhere to human cells, the human receptors are not blocked and therefore are free to interact with the EBs, allowing the establishment of the infection. In the case of *C. pneumoniae* motif-poor Pmp21, only the adhesive-competent oligomers block a *C. pneumoniae* infection, while the adhesive-incompetent monomers and the adhesive-incompetent motif-poor Pmp21 mutated in the motifs showed no effect on the infection (Luczak, Smits et al. 2016).

These data confirmed that the homomeric and heteromeric Pmp oligomers which are able to bind human cells are also crucial for the establishment of the infection.

In the second infection blocking assay, homomeric and heteromeric Pmp oligomers were first loaded onto the infectious EBs, in order to investigate their ability of interacting with natural chlamydial structures; afterwards, the Pmp-coated EBs were used to infect human cells, in order to confirm and investigate the relevance for the infection of Pmp structures in a more realistic set up (Fig. 32A).

All homomeric and heteromeric adhesion-competent and -incompetent Pmp oligomers could be coated on the surface of the EB, possibly interacting with naturally exposed Pmp structure on the cell surface (Fig. 32). The ability of Pmps of coating the EBs suggests that different Pmp oligomers could also interact *in vivo*, possibly by lateral association between different Pmp complexes or by interaction at the tip of the natural Pmp oligomer. Surprisingly, the proteins rGST and rCtad1, used as controls, could also be loaded onto the EB surface (Fig. 32). GST ability to bind chlamydial proteins has not been shown so far; therefore rGST bound the EBs by interacting with an unknown structure, which is not relevant for the infection, since the infection with GST-coated EBs shows no differences from the infection with PBS-treated EBs (Fig. 33). On the other hand, Ctad1 is a *C. trachomatis* adhesin, and rCtad1 can possibly bind to the naturally exposed Ctad1 on the EB surface, since Ctad1 self-interaction was shown *in vitro* (Stallmann 2015). Interestingly, infection with Ctad1-coated EBs results in a significant boost of the infection, when compared to the infection with PBS-treated EBs (Fig. 33). Ctad1 interacts with the β1-subunit of the integrin receptor (Stallmann and Hegemann 2016), therefore it is possible that the integrin receptors on the human cells are not saturated by the natural amount of Ctad1 on the EB surface and the presence of rCtad1 on the EBs might enhance the infection (Fig. 33).

When adhesion-incompetent Ac, Gc and Ac+Gc were coated onto the surface of the EBs, the EBs infectivity was reduced to 60 % (Fig. 33), possibly because the recombinant oligomers might bind and mask the functional domains of the naturally exposed Pmp structures, thus preventing EBs adhesion to human cells. On the other hand, EBs coated with adhesion-competent D, I, Ac+D, Ac+I and D+I did not show a reduction of the infection rate, when compared to the PBS-treated EBs (Fig. 33), possibly because the recombinant oligomers might bind the naturally exposed Pmp structures, substituting their function during the infection process. These data confirmed that adhesion-competent Pmp oligomers are functional and relevant for the infection; while, adhesion-incompetent Pmp oligomers do not play a role in the adhesion of the EBs to the human cells. It is very likely that adhesion-incompetent Pmp oligomers do not exist in nature, but are only the product

of our artificial system, as discussed in paragraph 5.1.7.1.

5.1.8 Homomeric and heteromeric Pmp oligomers during the infection

In conclusion, in this work it was shown that motif-poor and motif-rich forms of *C. trachomatis* Pmps are able to form hMW homomeric and heteromeric oligomers with protofibril-like structures, with the heteromeric complexes exhibiting properties different from those of the respective homomeric oligomers. Furthermore, not all homomeric and heteromeric Pmp oligomers are able to adhere to human cells, regardless of the number of motifs. Adhesion-competent homomeric and heteromeric Pmp complexes are able to block a subsequent infection after pre-incubation with human cells, while they mediate infection when coated on the surface of the EB, showing their relevance for a *C. trachomatis* infection. On the other hand, adhesion-incompetent Pmp oligomers do not influence the infection upon pre-incubation with human cells, but are able to prevent EBs from infecting the cells, when being coated on their cell surfaces. Interestingly, the adhesion-incompetent fragment Ac is able to generate adhesion-competent heteromeric oligomers, when co-refolded with motif-rich D, H and I Pmp proteins. The artificially produced Pmp proteins analyzed in this work show that *C. trachomatis* Pmps have the ability to generate functional homomeric and heteromeric oligomers *in vitro,* suggesting that members of this family of adhesins might generate a complex antigenic profile on the EB surfaces *in vivo*.

In this work we showed that two different Pmps are able to generate heterodimeric complexes; therefore, if one calculates the number of possible combinations generated by any two of the 9 Pmps present on the surface, using the formula 9!/[(9-2)!*2!], then 9 Pmps can form 36 different heterodimers on the EB surface. Moreover, in this work we showed that all Pmps are able to interact with other Pmps; therefore the 9 Pmps might form not only heterodimers, but hetero-oligomers and the number of possible multimers is given with the formula 9!, meaning that 9 Pmps have the ability to form up to 362.880 different complexes on the EB surface, representing a huge variability.

But there is more variability given the fact that for 7 of the 9 *C. trachomatis* Pmps on the EBs cleavage sites have been identified *in vivo* and different processed Pmp fragments have been detected during the infection by mass spectrometry and western blot analysis (Kiselev, Skinner et al. 2009, Swanson, Taylor et al. 2009, Saka, Thompson et al. 2011) (Fig. 54). The presence of several fragments for each Pmp again increases significantly the number of complexes possible on the EB surface. If one considers the fragments which could be generated, according to the cleavage sites identified by mass spectrometry by

Saka and co-workers, we have a total of 38 different Pmp fragments (full length and processed forms) (Fig. 54B). The presence of 38 Pmp proteins means that 703 heterodimers could be formed, according to the formula $38!/[(38-2)!*2!]$, and a huge variety of hetero-oligomers can be generated ($38! = 5,230226175*10^{44}$).

When *C. trachomatis* L2 PmpD processing was analyzed by mass spectrometry and western blot analysis by three different groups, different cleavage sites were identified, possibly due to the high rate of polymorphisms present in Pmps between different strains or due to differences in the technical set ups of the experiments (Fig. 54A-C-D) (Kiselev, Skinner et al. 2009, Swanson, Taylor et al. 2009, Saka, Thompson et al. 2011).
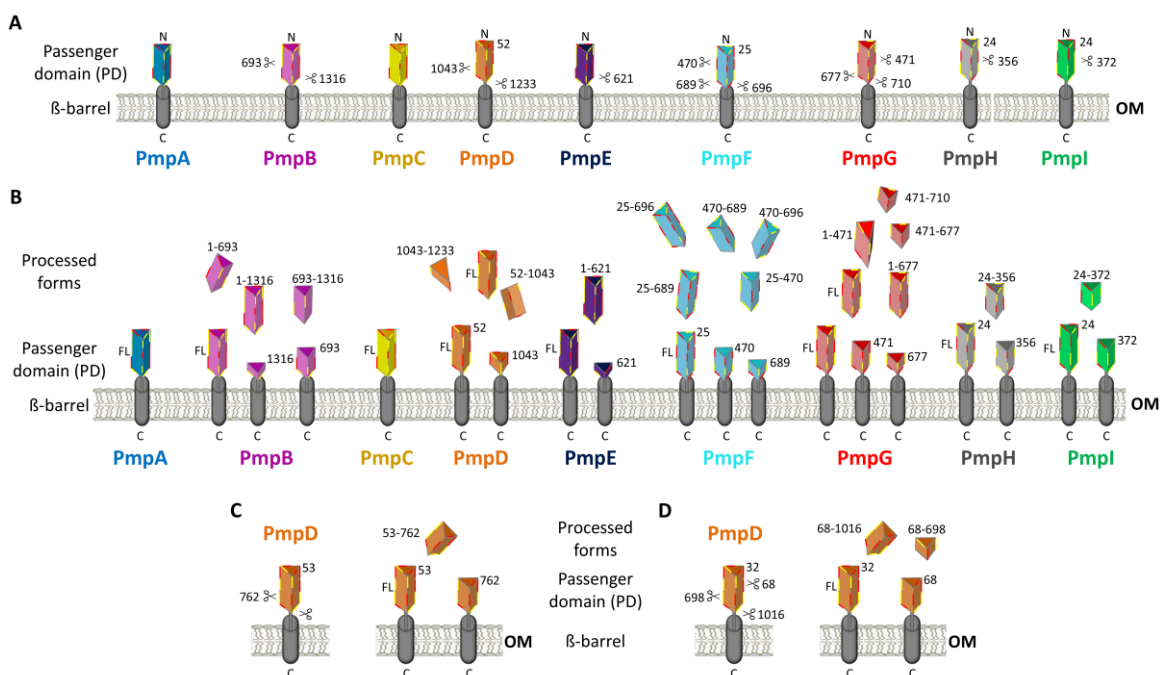
Figure 54. Processing of *C. trachomatis* Pmps. A. Most passenger domains (PD) of the 9 *C. trachomatis* L2 Pmps exposed on the EBs outer membrane (OM) can be cleaved. Position of cleavage sites along the PD, as identified by mass spectrometry by Saka and co-workers, are indicated by scissors and by the amino acid position (Saka, Thompson et al. 2011). **B.** Using the cleavage sites, several processed forms of most *C. trachomatis* L2 Pmps could hypothetically be generated. Possible processed forms are indicated for each Pmp color-coded. Numbers indicate the first and last amino acid of the fragments, according to the cleavage sites, when known. FL: full length PD (Saka, Thompson et al. 2011). **C.** Cleavage sites and processed forms of *C. trachomatis* L2 PmpD, as identified by mass spectrometry analysis, and processed forms detected as being associated with the bacterial surface (Swanson, Taylor et al. 2009). **D.** Cleavage sites and processed forms of *C. trachomatis* L2 PmpD, as identified by mass spectrometry analysis, and the relative processed forms detected (Kiselev, Skinner et al. 2009). Pmps and relative processed forms are indicated as color-codes. FxxN and GGA(I, L, V) motifs are shown in yellow and red, respectively. **A-C-D.** Different cleavage sites were identified for PmpD by mass spectrometry by the three different experimental set-ups and different PmpD processed forms were identified during the infection.

The mechanism of Pmp processing is still unknown; thus it is possible that Pmps have an autoproteolytic activity, processing their own PD; or Pmps might be cleaved by an unknown protease. Interestingly, a hypothetical protein of *C. pneumoniae* (Cpn1003) has a predicted structure which is perfectly matching the rhomboid protease GlpG from *H. influenzae* (Fig. S5). The function of Cpn1003 and of its homologue in *C. trachomatis* (CT846) (Fig. S2) should be analyzed in the future, in order to investigate their possible role in Pmp processing. If a protease is involved, it is possible that, for each Pmp, not all cleavage sites are recognized equally, increasing the possibilities of having a different ratio of different processed forms, especially if we consider for example PmpF, which has two cleavage sites very close to each other (aa 689 and 696) (Fig. 54A).

In general, it is unrealistic to expect that 10^{44} different Pmp multimers are present on the surface of the EBs; thus this process must be regulated by the bacteria somehow.

First of all, despite the fact that all 9 *C. trachomatis* Pmps have been detected on the surface of the EBs and are target for neutralizing antibodies (Crane, Carlson et al. 2006, Tan, Hsia et al. 2010), not all Pmps might be present at the same time, indicating expression heterogeneity. In a *C. trachomatis* infection *in vitro,* all Pmps could be detected within the inclusions, but, interestingly, not all at the same time in the same inclusion. Some Pmps were expressed in some inclusions, but not in others, independently from each other, suggesting an On/Off expression mechanism (Tan, Hsia et al. 2009). These data are confirmed by the antibody profiles of infected patients; all Pmps are able to induce a host humoral response and indeed all recombinant Pmps could be detected by the different sera; but, importantly, each individual serum could not recognize all Pmps (Tan, Hsia et al. 2010, Taylor, Darville et al. 2011).

Moreover, the heterogeneous expression of Pmps is further complicated by the fact that *pmp* genes are transcribed and Pmp proteins are expressed at different time points during the infection cycle and in different percentages in RBs and EBs (Kiselev, Stamm et al. 2007, Saka, Thompson et al. 2011, Van Lent, Creasy et al. 2016), suggesting that Pmps might play more than one role during the infection, in addition to their adhesion capacity (Becker and Hegemann 2014). In agreement with this hypothesis is the observation that Pmps might be cleaved differently at different time points during the infection, as has been found for PmpD, which undergoes a first proteolytical process at the early infection stage, generating three fragments likely to be present on the EB surface (Fig. 54C); and a second cleavage process late in the infection, generating two other fragments, with unknown function (Swanson, Taylor et al. 2009). Therefore, it is possible that, despite the fact that

all Pmps share a similar 3D predicted structure (Henderson and Lam 2001, Becker 2013), not all processed Pmp fragments share the same function. For example, homomeric Ac and Gc and heteromeric Ac+Gc Pmp complexes show no adhesive properties in this work, but they are able to generate hMW complexes and Ac can be part of other functional heteromeric complexes. Pmps might therefore use their heterogeneous expression pattern and their capacity for heteromeric complex formation in order to escape the immune response and to maximize their chances of infecting the human cells (Hegemann and Moelleken 2012). In this perspective, a multi-subunit vaccine would be more efficient than a vaccine based on a single Pmp, and indeed mice immunized with a mixture of PmpE, PmpF, PmpG and PmpH were more protected than the mice that were immunized with the four single Pmps individually (Yu, Karunakaran et al. 2014).

Our model proposes that *C. trachomatis* Pmps are expressed on the surface of the EBs, as full length PD and as processed forms; generating a complex mixture of motif-poor and motif-rich Pmp protein forms. The processed forms of a Pmp can interact with themselves, generating homomeric complexes, as already proposed in 2012 (Hegemann and Moelleken 2012). Additionally, as shown in this work, Pmp proteins can interact with full length and processed forms of different Pmps, generating a huge variety of hMW heteromeric complexes on the surfaces of the EBs (Fig. 55). Similarly to *C. pneumoniae* motif-poor D-Wt Pmp21 (Luczak, Smits et al. 2016), hMW homomeric and heteromeric *C. trachomatis* Pmp oligomers have a protofibril-like structure, reaching up to 3000 nm length *in vitro* (Figs. 24 and 25). Our attempts to isolate these complexes from the EB surface were unsuccessful (Fig. 35-36-37) and filaments could not be visualized on the surface of the EBs, despite their significant length *in vitro*.

It is therefore likely that homomeric and heteromeric Pmps *in vivo* do not generate long filaments, such as the filaments produced by Curli on the *E. coli* surface. Curli is an amyloid fibril generated by regulated polymerization of the secreted protein CsgA, generating long filaments. The fact that CsgA is a secreted protein makes the availability of the subunit for the polymerization almost unlimited (Barnhart and Chapman 2006). On the other hand, as already mentioned, Pmps are not secreted, but they are bound to the EB outer membrane by the β-barrel; the only membrane-free Pmps are the processed forms. Furthermore, Pmps are not expressed at the same time, resulting in a limited amount of available subunits on the EB surface, which are able to generate the homomeric and heteromeric filaments.

A similar mechanism is proposed for *Fusobacterium nucleatum* protein FadA. FadA is a secreted adhesin, which *in vitro* can generate different species of elongated oligomers, but also aggregated structures called "knots", which are relevant for adhesion to the host cell (Temoin, Wu et al. 2012). As for Pmps, FadA filaments have not been visualized yet on the *Fusobacterium nucleatum* surface, therefore it is proposed that FadA oligomers are present on the bacterial surface as short filaments or knots, which are functional and mediate adhesion to the host cell (Temoin, Wu et al. 2012).

More likely, Pmps might behave like the *Candida* Als5p protein. Als5p adhesin is an amyloid protein anchored to the fungal surface. The Als5p molecules which are in close proximity on the fungal surface are able to interact, forming small patches. Interestingly, if the patches are pulled with an atomic force microscopy (AFM), the amyloid regions of Als5p are exposed and mediate interaction with the neighboring Als5p molecules, generating visible filaments (Alsteens, Dupres et al. 2009, Garcia, Lee et al. 2011, Chan, Joseph et al. 2015).

Similarly to Als5p, Pmps are also anchored to the bacterial surface and it is probable that if we pull Pmps present on the EBs surface with an AFM, Pmp filaments could be visualized. On the other hand, Pmps can be cleaved, generating soluble processed forms, which may interact with the Pmp patches, generating complex, but likely short hetero-multimers.

We propose that Pmp full length PDs and processed PD forms can interact on the surface of the EBs, generating different species of homomeric and heteromeric complexes, which might associate in small filaments or small patches (Fig. 55). *Chlamydia* may use these Pmp structures to reach the human receptor on the host cell surface, in order to establish the infection and, given the high complex variability possible, Pmp structures may also be used as a tool for cell-type specificity. Furthermore, *Chlamydia* may use the numerous combinations of Pmp complexes as a decoy mechanism, in order to escape the host cell immune response, by increasing the Pmp antigenic variability on the EB surface (Fig. 55).

In the future, heteromeric Pmp complexes on the surface of the EBs *in vivo* should be identified by co-immunoprecipitation with specific antibodies, followed by mass spectrometry analysis. Moreover, using the available tools for *C. trachomatis* genetic manipulation, *pmp* null mutants could be created and the composition of heteromeric complexes on the bacterial cell might be identified, in order to understand how *Chlamydia* regulates Pmp expression and complex formation.
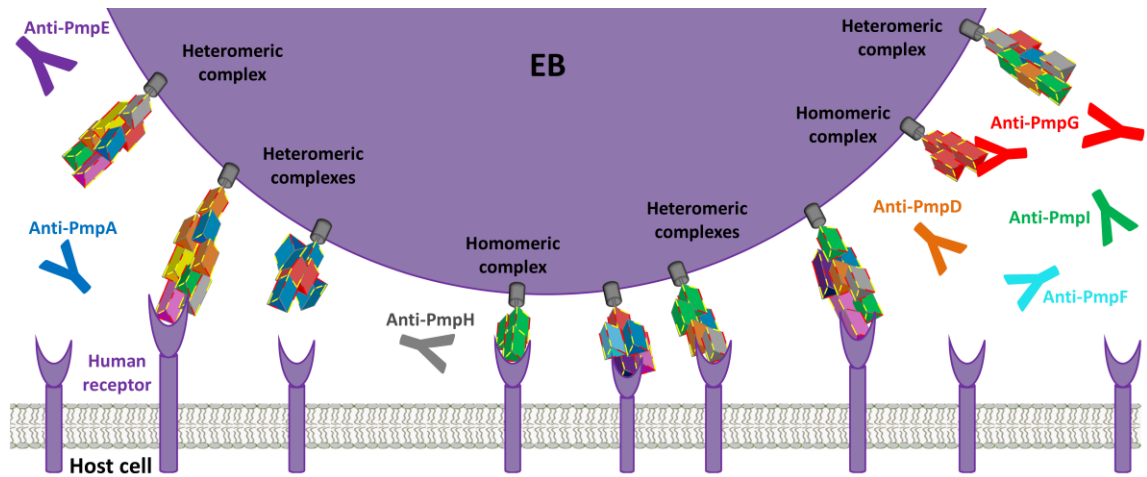
Figure 55. Model for *C. trachomatis* homomeric and heteromeric Pmps oligomers. Passenger domains (PD) of Pmps are exposed on the surface of the EBs either as full length or as processed forms. Different forms of the same or of different Pmps can interact with each other, forming homomeric and heteromeric protofibril-like oligomers. Pmp oligomers can adhere to an unknown receptor on the human cells and act as a decoy, avoiding the host immune response. Similar structures might be expected for *C. pneumoniae*.

5.2 Characterization of *C. pneumoniae* Yaa3

C. pneumoniae is one of the three species of the genus *Chlamydia,* which is able to cause infection in humans (Jama-Kmiecik, Frej-Madrzak et al. 2015). *C. pneumoniae* adhesion to human cells is a two-step process (Hegemann and Moelleken 2012), where the first reversible step is established by *Chlamydia* OmcB which binds to HS-GAGs on the human cells (Moelleken and Hegemann 2008, Fechtner, Stallmann et al. 2013) and the second and irreversible step is characterized by binding of several adhesins, such as the members of the Pmp family (Molleken, Schmidt et al. 2010) and the newly characterized Cpn0473 (LIPP) (Fechtner, Galle et al. 2016). In an attempt to identify new adhesin candidate proteins, three proteins showed adhesion ability to human cells in a yeast display adhesion assay (Fechtner 2009). One of the three proteins (Cpn0473) had been characterized as an adhesin, responsible for EB uptake in the human cell (Fechtner, Galle et al. 2016). The other two identified proteins (Yaa2 and Yaa3) are still hypothetical proteins and characterization of Yaa3 is the focus of this part of this work.

5.2.1 Yaa3 characteristics

Yaa3 (Cpn1006) is an uncharacterized *C. pneumoniae* protein of 161 amino acids, harboring a DUF720 domain of unknown function (33-156 aa) (Fig. 38A) and a N-terminal hydrophobic region, predicted as a membrane associated region (1-40 aa) (see paragraph 4.2.2.3). Nothing is known about the DUF720 domain and the bioinformatic analysis revealed that this domain is present in only three proteins in the whole *C. pneumoniae* proteasome: Yaa3, Cpn1005 and Cpn1004. Interestingly, when the *yaa3* genomic region has been investigated, *yaa3* (*cpn1006*) was found in close proximity with the genes *cpn1005* and *cpn1004* and with a third gene, whose protein does not harbor the DUF720 domain (*cpn1003*), forming a potential operon (Fig. 38B). When the four proteins encoded by the potential operon were aligned, they presented a significant amino acid sequence identity and homology (Fig. 38C), suggesting a similar function. Unfortunately nothing is known concerning the function of Cpn1004, Cpn1005 and Cpn1003.

Cpn1003 is the only protein within the operon which does not harbor a DUF720 domain and is longer than the other three proteins (235 aa). Structural predictions with Phyre2 revealed that its structure overlapped perfectly with the structure of a protein from *H. influenzae* (GlpG), despite sharing a low amino acid sequence identity (Fig. S5) (Lackner 2014). GlpG is a rhomboid-like protease, belonging to a family of transmembrane proteases which cleave proteins in their transmembrane domains (Freeman

2008). This is actually very interesting because Pmp adhesins on the surface of the EBs undergo proteolytical cleavage (Fig. 54), but it is still unknown whether it is an autoproteolytic mechanism or the result of protease activity (Vandahl, Pedersen et al. 2002, Wehrl, Brinkmann et al. 2004, Saka, Thompson et al. 2011). The presence of a protein resembling a rhomboid-like protease structure is definitely worth to further investigate.

Bioinformatic analysis revealed that not only the three *C. pneumoniae* Cpn1004, Cpn1005 and Yaa3 proteins harbor the DUF720 domain, but also the corresponding three proteins in all *Chlamydia* species. *C. trachomatis* serovar D proteins CT849, CT848 and CT847 harbor the DUF720 domain and they share significant amino acid sequence identity with *C. pneumoniae* Yaa3, Cpn1005 and Cpn1004 (between 20 and 33 %) (Fig. 39). The direct comparison of the homologous proteins from *C. pneumoniae* and *C. trachomatis* highlighted that the proteins share indeed very high sequence identity (Cpn1004-CT847: 69 %, Cpn1005-CT848: 80 % and Yaa3-CT849: 80%) (Figs. 39 and S2). The genomic localization of the three *C. trachomatis* genes *ct849, ct848* and *ct849* is comparable to the gene order found in *C. pneumoniae* (Fig. S2).

In addition to the DUF720 domain, *C. trachomatis* CT847, CT848 andCT849 harbor a type 3 secretion sequence in their first 20 amino acids, as identified by heterologous secretion assays in *Yersinia enterolitica* and *Shigella flexeneri* (Subtil, Delevoye et al. 2005, Chellas-Gery, Linton et al. 2007, da Cunha, Milho et al. 2014). Moreover, CT847, homologous to Cpn1005, was detected in RT-PCR assays to be expressed during the mid-cycle and only in RBs, but not in EBs. Furthermore, yeast two hybrid assays showed that CT847 interacts with human GCIP (Grap2 cyclin D-interacting protein) (Chellas-Gery, Linton et al. 2007). GCIP plays a role in modulating host cell transcription by binding cyclin D, preventing its interaction with the D-CDK4 kinase complex and, in this way, the phosphorylation cascade does not take place, inhibiting gene transcription (Xia, Bao et al. 2000). It is therefore hypnotized that during the mid-cycle CT847 is expressed and, binding GCIP, allows cyclin D protein to activate the phosphorylation cascade, allowing the host cells to enter the phase S of the replication cycle (Chellas-Gery, Linton et al. 2007).

Sequence alignments of the first 25 amino acid of the *C. pneumoniae* and *C. trachomatis* homologous proteins showed a very high amino acid identity (Yaa3-CT849: 48 %, Cpn1005-CT848: 32 % and Cpn1004-CT847: 24 %) (Fig. S4), suggesting that also the three *C. pneumoniae* proteins may be secreted through the T3SS.

When the DUF720 was blasted, the only non-chlamydial protein identified was the *Prochlorococcus marinus* protein P9303_01311. *Prochlorococcus marinus* is a

cyanobacterium which lives in the mid-latitude oceans (Kettler, Martiny et al. 2007). P9303_01311 is annotated as the membrane fusion protein (MFP) of the *Prochlorococcus* type 1 secretion system (T1SS) (https://www.ncbi.nlm.nih.gov/protein/123962130). P9303_01311 shares 22 % overall sequence identity with Yaa3 and 24 % with HlyD (*E. coli* MFP), and Yaa3 and HlyD share 15 % sequence identity (Fig. S3). The genomic region surrounding *P9303_01311* is composed of four genes in close proximity to each other, and the same is found for the four T1SS components of *E. coli*, similar to the *C. pneumoniae* potential operon (Fig. S3). T1SS is a Gram-negative mechanism of effector protein secretion through both the inner and outer membrane and, in the case of *E. coli*, is composed of four components: HlyB, the inner membrane bound, ATP dependent protein; HlyD, the MFP, TolC, the outer membrane protein and HlyA, the secreted toxin (Thomas, Holland et al. 2014). Even though the sequences identity among the *C. pneumoniae* Cpn1003, Cpn1004, Cpn1005 and Yaa3 proteins and the *E. coli* T1SS components is in the borderline of significance (between 11 and 28 %) (Fig. S3C), one could speculate that *Chlamydia* might harbor a T1SS.

5.2.2 Yaa3 expression, localization and functional properties during the *C. pneumoniae* infection

In order to characterize Yaa3, recombinant protein was needed. The production of rYaa3 has not been simple. Yaa3 expression was tested in different systems (see paragraph 4.2.2.1) and different native and denaturing lysis buffers were tested, in order to avoid Yaa3 precipitation after or during *E. coli* cells disruption (Fig. 40). Under native conditions, Yaa3 was insoluble, independently of how the expression was carried out in the cytoplasm or in the periplasm of *E. coli* cells (Figs. 40B and 41) or if the expression was carried out in *E. coli* Arctic cells, whose low cultivation temperature (10 °C) should improve protein folding (Fig. 42). Soluble rYaa3 could be obtained from *E. coli* cells only after denaturing lysis conditions, using 6 M Guanidine-HCl (Fig. 40B). Up to 1,3 mg/ml pure denatured rYaa3 could be purified from *E. coli* cells by Ni-NTa affinity chromatography (Fig. 43), but rYaa3 precipitated under all dialysis conditions tested (Fig. 44). Interestingly, the absence of the hydrophobic N-terminal region (1-40 aa) did not improve the solubility of Yaa3; indeed Yaa3Δ could be purified only under denaturing conditions and under all dialysis conditions tested, only a maximum of 100 μg/ml renatured soluble Yaa3Δ could be obtained (Fig. 45).

Finally, refolding of rYaa3 was only successful when buffer exchange occurred rapidly,

using centrifugation columns and a buffer harboring 200 mM Arginine (Fig. 46).

The positive influence of Arginine on Pmp protein refolding does not influence the protein functionality (Philipp Hanisch, unpublished data) (Bondos and Bicknell 2003, Reddy, Lilie et al. 2005).

Native and denatured rYaa3 was used to immunize rabbits for antibody production. The polyclonal antibody produced showed background signal in immunofluorescence microscopy and thus the specificity of the signal for Yaa3 had to be increased by depleting the serum against human HEp-2 and *E. coli* cell lysates and by antigen purification using native rYaa3 (Fig. 50A-B).

The expression of Yaa3 during the *C. pneumoniae* infection was then investigated by Immunofluorescence (IF) and western blot analysis. Yaa3 could be detected not before 24 hpi in IF (Fig. 50). The Yaa3 signal in IF co-localized with the bacteria at 24, 48 and 72 hpi, suggesting a mid-late cycle expression of Yaa3 (Fig. 50C-D-E), in agreement with the results obtained from the microarray transcription assay (Murra 2009) and similar to the adhesin Cpn0473 (Fechtner, Galle et al. 2016). At 72 hpi, single EBs could be stained for Yaa3, co-localizing with LPS (Fig. 50E).

Interestingly, Yaa3 is not detected in the cytoplasm of the host cell in all IF pictures, as it would be expected from a putative type 3 secreted protein, such as *C. trachomatis* CT622 and CT621 proteins, which clearly localize in the host cell cytoplasm at 40 hpi (Gong, Lei et al. 2011); or the Tarp protein, which, after type 3 secretion in the initial stage of the infection, co-localizes with actin filaments within the host cells (Jiwani, Alvarado et al. 2013).

When tested for its adhesive capacity in soluble adhesion assay (Fig. 26), Yaa3 could bind human HEp-2 cells at 37 °C in the presence and in the absence of Arginine and at 4 °C (Fig. 47 and 48). Both Yaa3 and Yaa3Δ binding signal increased between 15' and 60' of incubation with human cells at 37 °C (Fig. 47), similarly to the adhesion signal of adhesin and invasin Cpn0473 (Fechtner, Galle et al. 2016), but the Yaa3 binding signal is weaker and does not increase at 4 °C (Fig. 48). It can be speculated that Yaa3 can be internalized within the human cells upon adhesion in the 60' time at 37 °C, while at 4 °C the cell functions are blocked and therefore no internalization in possible. Furthermore, pre-incubation of human cells with rYaa3 (Fig. 31A) blocked a subsequent *C. pneumoniae* infection of 60 % (Fig. 49), showing the relevance of Yaa3 for the infection.

5.2.3 Yaa3 is a candidate T3 secreted adhesin

Yaa3 is a hypothetical protein, characterized by a hydrophobic region in the first 40 amino acids and by the presence of a DUF720 domain, conserved in three proteins among all *Chlamydia* species. The corresponding genes in *C. pneumoniae* (*yaa3, cpn1005* and *cpn1004*) are organized in close proximity with each other and with a fourth gene *cpn1003*, forming a potential operon, conserved in all *Chlamydia* species. Furthermore, Yaa3 presents significant sequence identity with P9303_01311, the MFP component of *Prochlorococcus marinus* T1SS and with HlyD, the MFP of *E. coli* T1SS, suggesting an inner membrane localization for Yaa3. The *C. trachomatis* proteins CT849, CT848 and CT847, homologous of Yaa3, Cpn1005 and Cpn1004 respectively, are heterologously type 3 secreted and the homologous proteins share a high sequence identity in the first 25 amino acids, suggesting that also the three *C. pneumoniae* proteins may be type 3 secreted.

Yaa3 is detected at 24, 48 and 72 hpi during the *C. pneumoniae* infection *in vitro* and co-localizes with the bacteria cells in the inclusion, but not in the host cell cytosol. Furthermore, Yaa3 is able to adhere to human cells in soluble adhesion assays and is relevant for the infection.

Considering these results, we propose two possibilities for Yaa3 function during the *C. pneumoniae* infection. The first option is that Yaa3 may be expressed during the mid-cycle of *C. pneumoniae* in the RBs. The T3SS might secret Yaa3 within the *Chlamydia* inclusion, where it can be loaded on the surface of the EBs. The Yaa3-carrying EBs may use it as an adhesin in the next round of the infection (Fig. 56). Alternatively, Yaa3 might be expressed in RBs during the mid-cycle and later in EBs. The EBs might carry Yaa3 intracellularly until the next round of the infection, during which, Yaa3 may be type 3 secreted at the stage of adhesion. After secretion, Yaa3 may facilitate the *Chlamydia* uptake within the host cell by binding to the inner leaflet of the host cell plasma membrane, given its similarity with the T1SS MFP protein (Fig. 56). It cannot be excluded that Yaa3 might function in both ways. A dual function of a protein is not uncommon; one example is the *Shigella flexeneri* virulence factor protein IcsA. IcsA is an autotransporter which is involved in the actin-based motility of the bacteria within the cell. Interestingly, when the bacteria are exposed to bile salts in the intestine site, IcsA acts as a T3SS-dependent adhesin (Brotcke Zumsteg, Goosmann et al. 2014).

In the future, it should be investigated if and at which time point Yaa3 is expressed on the surface of the EBs, for example by using differential permeabilization staining and solubilization assays from the bacterial surface. Different adhesion assays (e.g. protein-coated beads assay) might be performed, in order to confirm the adhesion ability of Yaa3. Heterologous Type 3 secretion assays might prove the presence of the secretion signal at the N-terminal of the protein. Finally, mass spectrometry from infected cells may give us a hint concerning the interaction partner of Yaa3 during the infection.
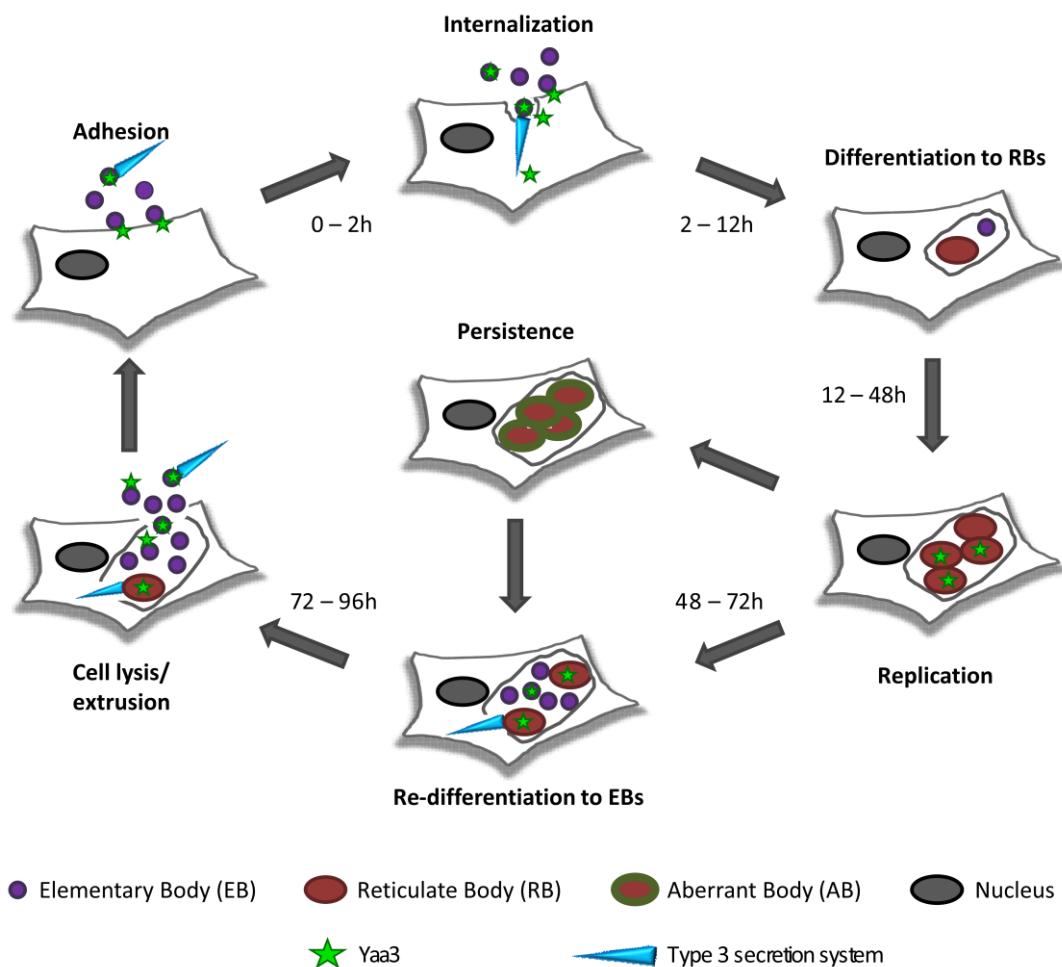
Figure 56. Model of Yaa3 expression and role during the *C. pneumoniae* infection. Yaa3 is expressed during the mid-cycle in RBs and in EBs. Yaa3 can be held within the EBs till the end of the cycle or it can be type 3 secreted during the mid-late cycle and loaded on the surface of the EBs. During the second round of the infection, Yaa3 on the surface of the EBs might act as an adhesin or Yaa3 within the EBs might be type 3 secreted and play a role in the internalization of *Chlamydia* particles.

6. Supplementary material

Accession	Description	Score	Coverage	# Proteins	# Unique Peptides	# Peptides	# aa	MW [kDa]	Calc. pI
A0A0F7XPR0	Chlamydia pneumoniae **Pmp21** [A0A0F7XPR0_CHLPN]	8889,01	27,41	3	30	30	1587	168,3	4,97
Q9S6B0	Chlamydia pneumoniae **60 kDa chaperonin GroEL** [Q9S6B0_CHLPN]	1014,08	13,48	5	5	5	497	53,1	5,25
Q9Z9A7	Chlamydia pneumoniae **Elongation factor Tu** [EFTU_CHLPN]	429,43	7,36	1	2	2	394	43,1	5,63
A0A0F7X568	Chlamydia pneumoniae **Probable DNA-binding protein HU** (Fragment) [A0A0F7X568_CHLPN]	203,07	11,83	4	1	1	93	10,7	11,05
A0A0F7WVR9	Chlamydia pneumoniae **Uncharacterized protein CPn_0443**	195,53	1,68	4	1	1	417	45,5	10,07
A0A0F7WSJ8	Chlamydia pneumoniae **Histone-like protein** [A0A0F7WSJ8_CHLPN]	168,35	6,40	2	1	1	172	18,7	12,40
A0A0F7WT76	Chlamydia pneumoniae **30S ribosomal protein** [A0A0F7WT76_CHLPN]	159,96	4,85	2	1	1	165	17,7	9,99
Q9Z7L4	Chlamydia pneumoniae **ABC Transporter Membrane Protein** [Q9Z7L4_CHLPN]	144,98	3,37	3	1	1	415	45,8	5,10
A0A0F7WTX8	Chlamydia pneumoniae **Transcription-repair-coupling factor** [A0A0F7WTX8_CHLPN]	130,74	0,92	2	1	1	1085	121,5	6,64
Q9S6B3	Chlamydia pneumoniae **Outer membrane protein 2 (OmcB)** [Q9S6B3_CHLPN]	126,86	2,53	4	1	1	395	42,2	6,62
A0A0F7WTW1	Chlamydia pneumoniae **Histone-like protein** [A0A0F7WTW1_CHLPN]	126,28	9,76	2	1	1	123	13,3	10,76
A0A0F7X3K9	Chlamydia pneumoniae **Hypothetical protein Yaa3 (Cpn1006)** [A0A0F7X3K9_CHLPN]	82,25	9,32	3	1	1	161	17,8	7,25
A0A0F7WVB8	Chlamydia pneumoniae **DNA ligase** [A0A0F7WVB8_CHLPN]	72,48	3,17	1	1	1	662	73,9	6,38
A0A0F7WYU7	Chlamydia pneumoniae **30S ribosomal protein S1** [A0A0F7WYU7_CHLPN]	28,12	3,99	3	1	1	552	61,7	5,15
Q9Z996	Chlamydia pneumoniae **Hypothetical protein (CPn0085)** [Q9Z996_CHLPN]	24,98	4,45	1	1	1	247	27,5	9,64
Q9Z7Y9	Chlamydia pneumoniae **Preprotein translocase subunit SecDF** [Q9Z7Y9_CHLPN]	23,79	3,00	1	1	1	1402	156,7	7,65

Figure S1. Mass spectrometry results of co-immunoprecipitation using M-Pmp21 antibodies. Mass spectrometry results of elution fractions obtained from co-immunoprecipitation of *C. pneumoniae* infected HEp-2 cells (MOI 10) at 80 hpi, using M-Pmp21 antibodies (see paragraph 4.1.9 and Fig. 37). Co-immunoprecipitated proteins are listed in the "Description" and the relative accession numbers (UniProt) are listed in "Accession". Mass spectrometry analyses were performed by Dr. Daniel Waldera-Lupa from the department of Prof. Dr. Kai Stühler at the Biological-Medical Research Center (BMFZ) at the Heinrich-Heine-University of Düsseldorf.

A

B
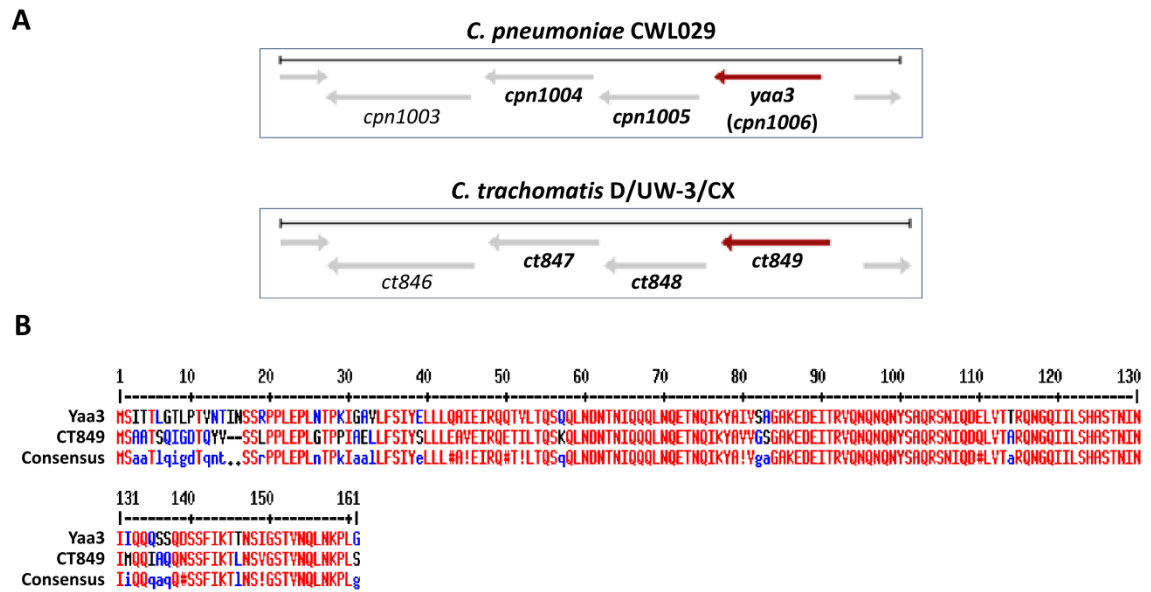
Figure S2. Yaa3 and CT849. A. Genomic localization of *yaa3* and the three neighboring genes *cpn1003*, *cpn1004* and *cpn1005* (top) and of the *C. trachomatis* homologs *ct849*, *ct846*, *ct847* and *ct848*, respectively (bottom). **B.** Alignment of full length Yaa3 and CT849 protein sequences in MultAlin (http://multalin.toulouse.inra.fr/multalin/) (Corpet 1988). Red letters in the consensus sequence indicate the identity of the amino acid in both proteins and red symbols in the consensus sequence indicate the homology of the amino acid in both proteins.
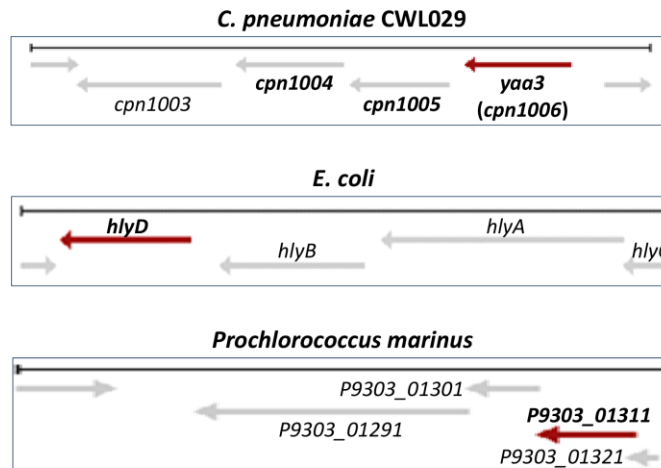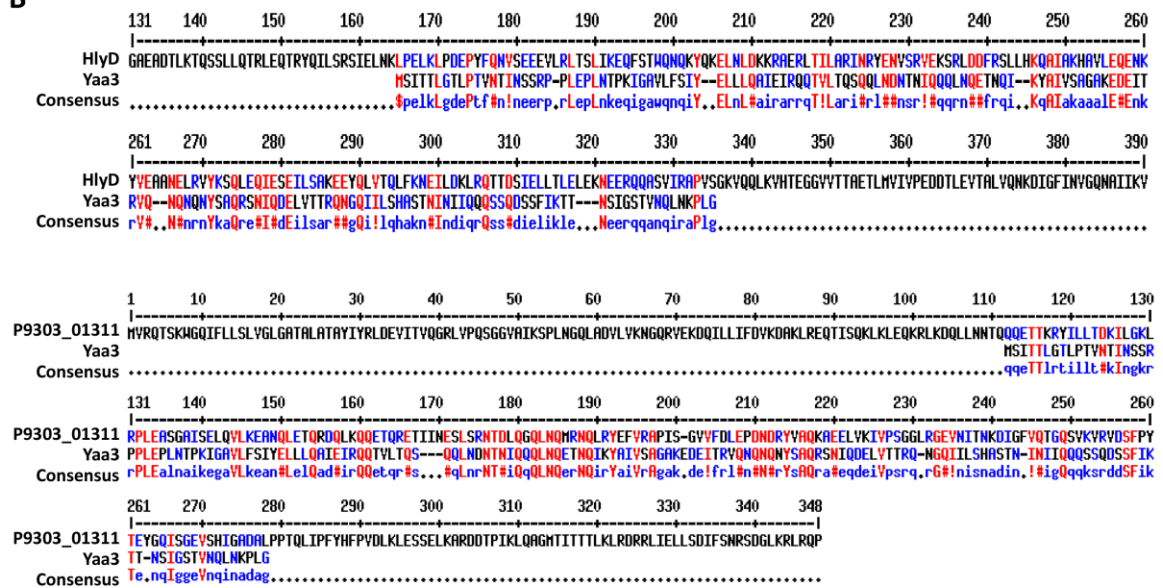
Figure S3. Yaa3 and T1SS proteins. A. Genomic localization of *yaa3* and the three neighboring genes *cpn1003*, *cpn1004* and *cpn1005* (top), compared with the *E. coli* T1SS genes *hlyD*, *hlyB*, *hlyA* and *hlyC* (center) and the *Prochlorococcus marinus* T1SS genes *P9303_01291-01301-01311-03121* (bottom). **B.** Alignment of full length Yaa3 and HlyD (top) and of Yaa3 and P9303_01311 protein sequences in MultAlin. Red letters in the consensus sequence indicate the identity of the amino acid in both proteins and red symbols in the consensus sequence indicate the homology of the amino acid in both proteins. **C.** Amino acid homology and identity percentages among *C. pneumoniae* Cpn1003, Cpn1004, Cpn1005, Yaa3 (Cpn1006) and the components of the T1SS from *E. coli* (HlyC, HlyA, HlyB and HlyD). Percentages derived from alignments of full length protein sequences in MultAlin.

T3 signal sequence

```
            1         10        20        30
            |---------+---------+---------+
     Yaa3   MSITTLGTLPTVNTINSSRPPLEPLNTPKI
    CT849   MSAATSQIGDTQYY--SSLPPLEPLGTPPI
Consensus   MSaaTlqigdTqnt..SSrPPLEPLnTPkI
```

```
            1         10        20        30
            |---------+---------+---------+
  Cpn1005   MWIIDPLSAKKPLQAAINYPGTPITGGPNT
    CT848   MWHKEPMHAVLQLPETPLYTGTTNSATADE
Consensus   MWhi#P$hAklqLqaainYpGTpnsaga#e
```

```
            1         10        20        30
            |---------+---------+---------|
  Cpn1004   MSIQPYSNTTTKADKVIPDSTKYISDSITI
    CT847    MSSAIIPTLPEKNTVIPDSTLIEPASIEI
Consensus   .miqa!inTlpea#kVIPDSTl!epaSIeI
```
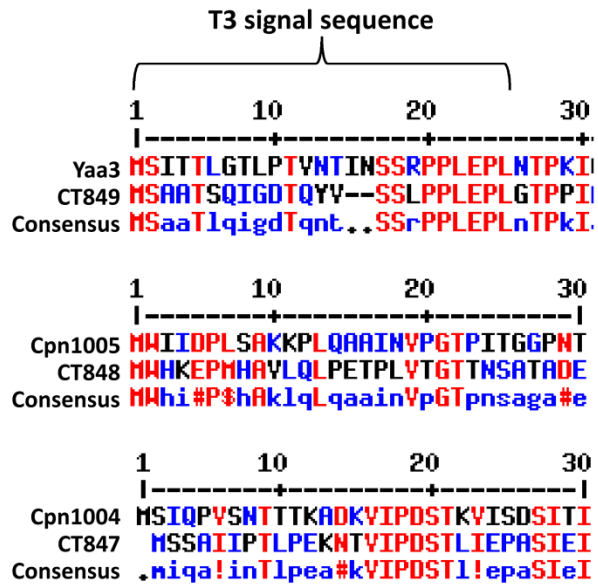
Figure S4. T3 secretion signal. Alignment of the first 25 amino acids of Yaa3 (top), Cpn1005 (center) and Cpn1004 (bottom) with the first 25 amino acids of the respective *C. trachomatis* homologs (CT849, CT848 and CT847), harboring a T3 secretion signal.

Figure S5. Cpn1003 and GlpG. A. Phyre2 structure prediction of *C. pneumoniae* Cpn1003. **B.** Phyre2 structure prediction of *H. influenzae* GlpG. **C.** Superimposition of Phyre2 predicted structures of Cpn1003 (light blue) and GlpG (light brown). Images are processed with UCSF Chimera server (https://www.cgl.ucsf.edu/chimera/). Cpn1003 and GlpG structure similarity was identified by Prof. Dr. Lutz Schmitt from the department of Biochemistry at the Heinrich Heine University of Düsseldorf. **D.** Alignment of full length Cpn1003 and GlpG protein sequences in MultAlin. Red letters in the consensus sequence indicate the identity of the amino acid in both proteins and red symbols in the consensus sequence indicate the homology of the amino acid in both proteins.

Literature

Abdelrahman, Y. M. and R. J. Belland (2005). "The chlamydial developmental cycle." <u>FEMS Microbiol Rev</u> **29**(5): 949-959.

Abromaitis, S. and R. S. Stephens (2009). "Attachment and entry of Chlamydia have distinct requirements for host protein disulfide isomerase." <u>PLoS Pathog</u> **5**(4): e1000357.

Aeberhard, L., S. Banhart, M. Fischer, N. Jehmlich, L. Rose, S. Koch, M. Laue, B. Y. Renard, F. Schmidt and D. Heuer (2015). "The Proteome of the Isolated Chlamydia trachomatis Containing Vacuole Reveals a Complex Trafficking Platform Enriched for Retromer Components." <u>PLoS Pathog</u> **11**(6): e1004883.

Ajonuma, L. C., K. L. Fok, L. S. Ho, P. K. Chan, P. H. Chow, L. L. Tsang, C. H. Wong, J. Chen, S. Li, D. K. Rowlands, Y. W. Chung and H. C. Chan (2010). "CFTR is required for cellular entry and internalization of Chlamydia trachomatis." <u>Cell Biol Int</u> **34**(6): 593-600.

Alsteens, D., V. Dupres, S. A. Klotz, N. K. Gaur, P. N. Lipke and Y. F. Dufrene (2009). "Unfolding individual als5p adhesion proteins on live cells." <u>ACS Nano</u> **3**(7): 1677-1682.

Barbour, A. G., K. Amano, T. Hackstadt, L. Perry and H. D. Caldwell (1982). "Chlamydia trachomatis has penicillin-binding proteins but not detectable muramic acid." <u>J Bacteriol</u> **151**(1): 420-428.

Barnard, T. J., N. Dautin, P. Lukacik, H. D. Bernstein and S. K. Buchanan (2007). "Autotransporter structure reveals intra-barrel cleavage followed by conformational changes." <u>Nat Struct Mol Biol</u> **14**(12): 1214-1220.

Barnhart, M. M. and M. R. Chapman (2006). "Curli biogenesis and function." <u>Annu Rev Microbiol</u> **60**: 131-147.

Bastidas, R. J., C. A. Elwell, J. N. Engel and R. H. Valdivia (2013). "Chlamydial intracellular survival strategies." <u>Cold Spring Harb Perspect Med</u> **3**(5): a010256.

Bavoil, P., B. Kaltenboeck and G. Greub (2013). "In Chlamydia veritas." <u>Pathog Dis</u> **67**(2): 89-90.

Bavoil, P. M., R. Hsia and D. M. Ojcius (2000). "Closing in on Chlamydia and its intracellular bag of tricks." <u>Microbiology</u> **146 (Pt 11)**: 2723-2731.

Beatty, W. L., R. P. Morrison and G. I. Byrne (1994). "Persistent chlamydiae: from cell culture to a paradigm for chlamydial pathogenesis." <u>Microbiol Rev</u> **58**(4): 686-699.

Becker, E. (2013). "Charakterisierung der chlamydialen Pmp Adhäsin Familie." <u>Funktionelle Genomforschung der Mikroorganismen</u> **PhD Thesis** (Düsseldorf, Heinrich-Heine-Universität).

Becker, E. and J. H. Hegemann (2014). "All subtypes of the Pmp adhesin family are implicated in chlamydial virulence and show species-specific function." <u>Microbiologyopen</u> **3**(4): 544-556.

Beeckman, D. S. and D. C. Vanrompay (2010). "Bacterial secretion systems with an emphasis on the chlamydial Type III secretion system." <u>Curr Issues Mol Biol</u> **12**(1): 17-41.

Belland, R. J., S. P. Ouellette, J. Gieffers and G. I. Byrne (2004). "Chlamydia pneumoniae and atherosclerosis." <u>Cell Microbiol</u> **6**(2): 117-127.

Bernstein, H. D. (2015). "Looks can be deceiving: recent insights into the mechanism of protein

secretion by the autotransporter pathway." Mol Microbiol **97**(2): 205-215.

Berson, J. F., A. C. Theos, D. C. Harper, D. Tenza, G. Raposo and M. S. Marks (2003). "Proprotein convertase cleavage liberates a fibrillogenic fragment of a resident glycoprotein to initiate melanosome biogenesis." J Cell Biol **161**(3): 521-533.

Betts-Hampikian, H. J. and K. A. Fields (2010). "The Chlamydial Type III Secretion Mechanism: Revealing Cracks in a Tough Nut." Front Microbiol **1**: 114.

Betts, H. J., L. E. Twiggs, M. S. Sal, P. B. Wyrick and K. A. Fields (2008). "Bioinformatic and biochemical evidence for the identification of the type III secretion system needle protein of Chlamydia trachomatis." J Bacteriol **190**(5): 1680-1690.

Birkelund, S., A. G. Lundemose and G. Christiansen (1990). "The 75-kilodalton cytoplasmic Chlamydia trachomatis L2 polypeptide is a DnaK-like protein." Infect Immun **58**(7): 2098-2104.

Birkelund, S., M. Morgan-Fisher, E. Timmerman, K. Gevaert, A. C. Shaw and G. Christiansen (2009). "Analysis of proteins in Chlamydia trachomatis L2 outer membrane complex, COMC." FEMS Immunol Med Microbiol **55**(2): 187-195.

Blasi, F., P. Tarsia and S. Aliberti (2009). "Chlamydophila pneumoniae." Clin Microbiol Infect **15**(1): 29-35.

Bodetti, T. J., E. Jacobson, C. Wan, L. Hafner, A. Pospischil, K. Rose and P. Timms (2002). "Molecular evidence to support the expansion of the hostrange of Chlamydophila pneumoniae to include reptiles as well as humans, horses, koalas and amphibians." Syst Appl Microbiol **25**(1): 146-152.

Bondos, S. E. and A. Bicknell (2003). "Detection and prevention of protein aggregation before, during, and after purification." Anal Biochem **316**(2): 223-231.

Bradley, P., L. Cowen, M. Menke, J. King and B. Berger (2001). "BETAWRAP: successful prediction of parallel beta -helices from primary sequence reveals an association with many microbial pathogens." Proc Natl Acad Sci U S A **98**(26): 14819-14824.

Brotcke Zumsteg, A., C. Goosmann, V. Brinkmann, R. Morona and A. Zychlinsky (2014). "IcsA is a Shigella flexneri adhesin regulated by the type III secretion system and required for pathogenesis." Cell Host Microbe **15**(4): 435-445.

Brunger, A. T., D. J. Cipriano and J. Diao (2015). "Towards reconstitution of membrane fusion mediated by SNAREs and other synaptic proteins." Crit Rev Biochem Mol Biol **50**(3): 231-241.

Bryan, A. W., Jr., J. L. Starner-Kreinbrink, R. Hosur, P. L. Clark and B. Berger (2011). "Structure-based prediction reveals capping motifs that inhibit beta-helix aggregation." Proc Natl Acad Sci U S A **108**(27): 11099-11104.

Caffrey, M., D. T. Braddock, J. M. Louis, M. A. Abu-Asab, D. Kingma, L. Liotta, M. Tsokos, N. Tresser, L. K. Pannell, N. Watts, A. C. Steven, M. N. Simon, S. J. Stahl, P. T. Wingfield and G. M. Clore (2000). "Biophysical characterization of gp41 aggregates suggests a model for the molecular mechanism of HIV-associated neurological damage and dementia." J Biol Chem **275**(26): 19877-19882.

Campbell, L. A. and C. C. Kuo (2006). "Interactions of Chlamydia with the host cells that mediate attachment and uptake." *Chlamydia Genomics and Pathogenesis* (Ed. Bavoil and P. B. Wyrick): 505–522.

Campbell, L. A., C. C. Kuo and J. T. Grayston (1990). "Structural and antigenic analysis of Chlamydia pneumoniae." Infect Immun **58**(1): 93-97.

Carabeo, R. A., S. S. Grieshaber, E. Fischer and T. Hackstadt (2002). "Chlamydia trachomatis induces remodeling of the actin cytoskeleton during attachment and entry into HeLa cells." Infect Immun **70**(7): 3793-3803.

Carabeo, R. A., S. S. Grieshaber, A. Hasenkrug, C. Dooley and T. Hackstadt (2004). "Requirement for the Rac GTPase in Chlamydia trachomatis invasion of non-phagocytic cells." Traffic **5**(6): 418-425.

Carrasco, J. A., C. Tan, R. G. Rank, R. C. Hsia and P. M. Bavoil (2011). "Altered developmental expression of polymorphic membrane proteins in penicillin-stressed Chlamydia trachomatis." Cell Microbiol **13**(7): 1014-1025.

Casali, N., M. Konieczny, M. A. Schmidt and L. W. Riley (2002). "Invasion activity of a Mycobacterium tuberculosis peptide presented by the Escherichia coli AIDA autotransporter." Infect Immun **70**(12): 6846-6852.

Chan, C. X., I. G. Joseph, A. Huang, D. N. Jackson and P. N. Lipke (2015). "Quantitative Analyses of Force-Induced Amyloid Formation in Candida albicans Als5p: Activation by Standard Laboratory Procedures." PLoS One **10**(6): e0129152.

Charbonneau, M. E., F. Berthiaume and M. Mourez (2006). "Proteolytic processing is not essential for multiple functions of the Escherichia coli autotransporter adhesin involved in diffuse adherence (AIDA-I)." J Bacteriol **188**(24): 8504-8512.

Chatterjee, S., S. Chaudhury, A. C. McShan, K. Kaur and R. N. De Guzman (2013). "Structure and biophysics of type III secretion in bacteria." Biochemistry **52**(15): 2508-2517.

Chavez, J. M., R. D. Vicetti Miguel and T. L. Cherpes (2011). "Chlamydia trachomatis infection control programs: lessons learned and implications for vaccine development." Infect Dis Obstet Gynecol **2011**: 754060.

Chellas-Gery, B., C. N. Linton and K. A. Fields (2007). "Human GCIP interacts with CT847, a novel Chlamydia trachomatis type III secretion substrate, and is degraded in a tissue-culture infection model." Cell Microbiol **9**(10): 2417-2430.

Chen, J. C., J. P. Zhang and R. S. Stephens (1996). "Structural requirements of heparin binding to Chlamydia trachomatis." J Biol Chem **271**(19): 11134-11140.

Chen, X. (2016). "Yeast cell surface display: An efficient strategy for improvement of bioethanol fermentation performance." Bioengineered: 1-5.

Chen, Y. S., R. J. Bastidas, H. A. Saka, V. K. Carpenter, K. L. Richards, G. V. Plano and R. H. Valdivia (2014). "The Chlamydia trachomatis type III secretion chaperone Slc1 engages multiple early effectors, including TepP, a tyrosine-phosphorylated protein required for the recruitment of CrkI-II to nascent inclusions and innate immune signaling." PLoS Pathog **10**(2): e1003954.

Chiti, F. and C. M. Dobson (2006). "Protein misfolding, functional amyloid, and human disease." Annu Rev Biochem **75**: 333-366.

Clarke, I. N. (2011). "Evolution of Chlamydia trachomatis." Ann N Y Acad Sci **1230**: E11-18.

Clifton, D. R., C. A. Dooley, S. S. Grieshaber, R. A. Carabeo, K. A. Fields and T. Hackstadt (2005). "Tyrosine phosphorylation of the chlamydial effector protein Tarp is species specific and

not required for recruitment of actin." Infect Immun **73**(7): 3860-3868.

Clifton, D. R., K. A. Fields, S. S. Grieshaber, C. A. Dooley, E. R. Fischer, D. J. Mead, R. A. Carabeo and T. Hackstadt (2004). "A chlamydial type III translocated protein is tyrosine-phosphorylated at the site of entry and associated with recruitment of actin." Proc Natl Acad Sci U S A **101**(27): 10166-10171.

Coler, R. N., A. Bhatia, J. F. Maisonneuve, P. Probst, B. Barth, P. Ovendale, H. Fang, M. Alderson, Y. Lobet, J. Cohen, P. Mettens and S. G. Reed (2009). "Identification and characterization of novel recombinant vaccine antigens for immunization against genital Chlamydia trachomatis." FEMS Immunol Med Microbiol **55**(2): 258-270.

Confer, A. W. and S. Ayalew (2013). "The OmpA family of proteins: roles in bacterial pathogenesis and immunity." Vet Microbiol **163**(3-4): 207-222.

Coombes, B. K. and J. B. Mahony (2002). "Identification of MEK- and phosphoinositide 3-kinase-dependent signalling as essential events during Chlamydia pneumoniae invasion of HEp2 cells." Cell Microbiol **4**(7): 447-460.

Cornelis, G. R. (2006). "The type III secretion injectisome." Nat Rev Microbiol **4**(11): 811-825.

Corpet, F. (1988). "Multiple sequence alignment with hierarchical clustering." Nucleic Acids Res **16**(22): 10881-10890.

Costa, T. R., C. Felisberto-Rodrigues, A. Meir, M. S. Prevost, A. Redzej, M. Trokter and G. Waksman (2015). "Secretion systems in Gram-negative bacteria: structural and mechanistic insights." Nat Rev Microbiol **13**(6): 343-359.

Cowen, L., P. Bradley, M. Menke, J. King and B. Berger (2002). "Predicting the beta-helix fold from protein sequence data." J Comput Biol **9**(2): 261-276.

Crane, D. D., J. H. Carlson, E. R. Fischer, P. Bavoil, R. C. Hsia, C. Tan, C. C. Kuo and H. D. Caldwell (2006). "Chlamydia trachomatis polymorphic membrane protein D is a species-common pan-neutralizing antigen." Proc Natl Acad Sci U S A **103**(6): 1894-1899.

Cuchillo-Ibanez, I., I. Lopez-Font, A. Boix-Amoros, G. Brinkmalm, K. Blennow, J. L. Molinuevo and J. Saez-Valero (2015). "Heteromers of amyloid precursor protein in cerebrospinal fluid." Mol Neurodegener **10**: 2.

da Cunha, M., C. Milho, F. Almeida, S. V. Pais, V. Borges, R. Mauricio, M. J. Borrego, J. P. Gomes and L. J. Mota (2014). "Identification of type III secretion substrates of Chlamydia trachomatis using Yersinia enterocolitica as a heterologous system." BMC Microbiol **14**: 40.

Damiani, M. T., J. Gambarte Tudela and A. Capmany (2014). "Targeting eukaryotic Rab proteins: a smart strategy for chlamydial survival and replication." Cell Microbiol **16**(9): 1329-1338.

Darville, T. and T. J. Hiltke (2010). "Pathogenesis of genital tract disease due to Chlamydia trachomatis." J Infect Dis **201 Suppl 2**: S114-125.

Dautin, N. and H. D. Bernstein (2007). "Protein secretion in gram-negative bacteria via the autotransporter pathway." Annu Rev Microbiol **61**: 89-112.

Dautry-Varsat, A., A. Subtil and T. Hackstadt (2005). "Recent insights into the mechanisms of Chlamydia entry." Cell Microbiol **7**(12): 1714-1722.

Davis, C. H. and P. B. Wyrick (1997). "Differences in the association of Chlamydia trachomatis

serovar E and serovar L2 with epithelial cells in vitro may reflect biological differences in vivo." Infect Immun **65**(7): 2914-2924.

de la Maza, M. A. and L. M. de la Maza (1995). "A new computer model for estimating the impact of vaccination protocols and its application to the study of Chlamydia trachomatis genital infections." Vaccine **13**(1): 119-127.

Di Francesco, A., A. Favaroni and M. Donati (2013). "Host defense peptides: general overview and an update on their activity against Chlamydia spp." Expert Rev Anti Infect Ther **11**(11): 1215-1224.

Donati, M., H. Huot-Creasy, M. Humphrys, M. Di Paolo, A. Di Francesco and G. S. Myers (2014). "Genome Sequence of Chlamydia suis MD56, Isolated from the Conjunctiva of a Weaned Piglet." Genome Announc **2**(3).

El-Bez, C., M. Adrian, J. Dubochet and T. L. Cover (2005). "High resolution structural analysis of Helicobacter pylori VacA toxin oligomers by cryo-negative staining electron microscopy." J Struct Biol **151**(3): 215-228.

Elwell, C., K. Mirrashidi and J. Engel (2016). "Chlamydia cell biology and pathogenesis." Nat Rev Microbiol **14**(6): 385-400.

Emsley, P., I. G. Charles, N. F. Fairweather and N. W. Isaacs (1996). "Structure of Bordetella pertussis virulence factor P.69 pertactin." Nature **381**(6577): 90-92.

Entian, K. D., T. Schuster, J. H. Hegemann, D. Becher, H. Feldmann, U. Guldener, R. Gotz, M. Hansen, C. P. Hollenberg, G. Jansen, W. Kramer, S. Klein, P. Kotter, J. Kricke, H. Launhardt, G. Mannhaupt, A. Maierl, P. Meyer, W. Mewes, T. Munder, R. K. Niedenthal, M. Ramezani Rad, A. Rohmer, A. Romer, A. Hinnen and et al. (1999). "Functional analysis of 150 deletion mutants in Saccharomyces cerevisiae by a systematic approach." Mol Gen Genet **262**(4-5): 683-702.

Everett, K. D. and A. A. Andersen (1997). "The ribosomal intergenic spacer and domain I of the 23S rRNA gene are phylogenetic markers for Chlamydia spp." Int J Syst Bacteriol **47**(2): 461-473.

Everett, K. D., R. M. Bush and A. A. Andersen (1999). "Emended description of the order Chlamydiales, proposal of Parachlamydiaceae fam. nov. and Simkaniaceae fam. nov., each containing one monotypic genus, revised taxonomy of the family Chlamydiaceae, including a new genus and five new species, and standards for the identification of organisms." Int J Syst Bacteriol **49 Pt 2**: 415-440.

Everett, K. D. and T. P. Hatch (1995). "Architecture of the cell envelope of Chlamydia psittaci 6BC." J Bacteriol **177**(4): 877-882.

Fadel, S. and A. Eley (2008). "Is lipopolysaccharide a factor in infectivity of Chlamydia trachomatis?" J Med Microbiol **57**(Pt 3): 261-266.

Fechtner, T. (2009). "Funktionelle Analyse des chlamydialen Adhäsins OmcB und Identifizierung neuer, potentieller Adhäsine." Funktionelle Genomforschung der Mikroorganismen **Diploma thesis**(Düsseldorf, Heinrich-Heine-Universität).

Fechtner, T., J. N. Galle and J. H. Hegemann (2016). "The novel chlamydial adhesin CPn0473 mediates the lipid raft-dependent uptake of Chlamydia pneumoniae." Cell Microbiol **18**(8): 1094-1105.

Fechtner, T., S. Stallmann, K. Moelleken, K. L. Meyer and J. H. Hegemann (2013). "Characterization of the interaction between the chlamydial adhesin OmcB and the human host

cell." J Bacteriol **195**(23): 5323-5333.

Feher, V. A., A. Randall, P. Baldi, R. M. Bush, L. M. de la Maza and R. E. Amaro (2013). "A 3-dimensional trimeric beta-barrel model for Chlamydia MOMP contains conserved and novel elements of Gram-negative bacterial porins." PLoS One **8**(7): e68934.

Fields, K. A. and T. Hackstadt (2002). "The chlamydial inclusion: escape from the endocytic pathway." Annu Rev Cell Dev Biol **18**: 221-245.

Fields, K. A., D. J. Mead, C. A. Dooley and T. Hackstadt (2003). "Chlamydia trachomatis type III secretion: evidence for a functional apparatus during early-cycle development." Mol Microbiol **48**(3): 671-683.

Finco, O., A. Bonci, M. Agnusdei, M. Scarselli, R. Petracca, N. Norais, G. Ferrari, I. Garaguso, M. Donati, V. Sambri, R. Cevenini, G. Ratti and G. Grandi (2005). "Identification of new potential vaccine candidates against Chlamydia pneumoniae by multiple screenings." Vaccine **23**(9): 1178-1188.

Fink, G. R., H. J.B. and S. F. (1983). "Methods in yeast genetics, laboratory manual Cold Sprng Harbor Laboratory, New York.".

Fowler, D. M., A. V. Koulov, W. E. Balch and J. W. Kelly (2007). "Functional amyloid--from bacteria to humans." Trends Biochem Sci **32**(5): 217-224.

Freeman, M. (2008). "Rhomboid proteases and their biological functions." Annu Rev Genet **42**: 191-210.

Fukushi, H. and K. Hirai (1992). "Proposal of Chlamydia pecorum sp. nov. for Chlamydia strains derived from ruminants." Int J Syst Bacteriol **42**(2): 306-308.

Gabel, B. R., C. Elwell, S. C. van Ijzendoorn and J. N. Engel (2004). "Lipid raft-mediated entry is not required for Chlamydia trachomatis infection of cultured epithelial cells." Infect Immun **72**(12): 7367-7373.

Gangwer, K. A., D. J. Mushrush, D. L. Stauff, B. Spiller, M. S. McClain, T. L. Cover and D. B. Lacy (2007). "Crystal structure of the Helicobacter pylori vacuolating toxin p55 domain." Proc Natl Acad Sci U S A **104**(41): 16293-16298.

Garcia, M. C., J. T. Lee, C. B. Ramsook, D. Alsteens, Y. F. Dufrene and P. N. Lipke (2011). "A role for amyloid in cell aggregation and biofilm formation." PLoS One **6**(3): e17632.

Gauliard, E., S. P. Ouellette, K. J. Rueden and D. Ladant (2015). "Characterization of interactions between inclusion membrane proteins from Chlamydia trachomatis." Front Cell Infect Microbiol **5**: 13.

Gawarzewski, I., S. H. Smits, L. Schmitt and J. Jose (2013). "Structural comparison of the transport units of type V secretion systems." Biol Chem **394**(11): 1385-1398.

Gerard, H. C., E. Fomicheva, J. A. Whittum-Hudson and A. P. Hudson (2008). "Apolipoprotein E4 enhances attachment of Chlamydophila (Chlamydia) pneumoniae elementary bodies to host cells." Microb Pathog **44**(4): 279-285.

Gerlach, R. G. and M. Hensel (2007). "Protein secretion systems and adhesins: the molecular armory of Gram-negative pathogens." Int J Med Microbiol **297**(6): 401-415.

Gietz, R. D., R. H. Schiestl, A. R. Willems and R. A. Woods (1995). "Studies on the transformation

of intact yeast cells by the LiAc/SS-DNA/PEG procedure." <u>Yeast</u> **11**(4): 355-360.

Gomes, J. P., A. Nunes, W. J. Bruno, M. J. Borrego, C. Florindo and D. Dean (2006). "Polymorphisms in the nine polymorphic membrane proteins of Chlamydia trachomatis across all serovars: evidence for serovar Da recombination and correlation with tissue tropism." <u>J Bacteriol</u> **188**(1): 275-286.

Gong, S., L. Lei, X. Chang, R. Belland and G. Zhong (2011). "Chlamydia trachomatis secretion of hypothetical protein CT622 into host cell cytoplasm via a secretion pathway that can be inhibited by the type III secretion system inhibitor compound 1." <u>Microbiology</u> **157**(Pt 4): 1134-1144.

Gophna, U., T. A. Oelschlaeger, J. Hacker and E. Z. Ron (2002). "Role of fibronectin in curli-mediated internalization." <u>FEMS Microbiol Lett</u> **212**(1): 55-58.

Grayston, J. T. (1989). "Chlamydia pneumoniae, strain TWAR." <u>Chest</u> **95**(3): 664-669.

Grayston, J. T., C. C. Kuo, S. P. Wang and J. Altman (1986). "A new Chlamydia psittaci strain, TWAR, isolated in acute respiratory tract infections." <u>N Engl J Med</u> **315**(3): 161-168.

Greub, G. (2010). "International Committee on Systematics of Prokaryotes. Subcommittee on the taxonomy of the Chlamydiae: minutes of the closed meeting, 21 June 2010, Hof bei Salzburg, Austria." <u>Int J Syst Evol Microbiol</u> **60**(Pt 11): 2694.

Grieshaber, N. A., E. R. Fischer, D. J. Mead, C. A. Dooley and T. Hackstadt (2004). "Chlamydial histone-DNA interactions are disrupted by a metabolite in the methylerythritol phosphate pathway of isoprenoid biosynthesis." <u>Proc Natl Acad Sci U S A</u> **101**(19): 7451-7456.

Grieshaber, S. S., N. A. Grieshaber, N. Miller and T. Hackstadt (2006). "Chlamydia trachomatis causes centrosomal defects resulting in chromosomal segregation abnormalities." <u>Traffic</u> **7**(8): 940-949.

Grimwood, J., L. Olinger and R. S. Stephens (2001). "Expression of Chlamydia pneumoniae polymorphic membrane protein family genes." <u>Infect Immun</u> **69**(4): 2383-2389.

Grimwood, J. and R. S. Stephens (1999). "Computational analysis of the polymorphic membrane protein superfamily of Chlamydia trachomatis and Chlamydia pneumoniae." <u>Microb Comp Genomics</u> **4**(3): 187-201.

Guo, W., J. Li, B. Kaltenboeck, J. Gong, W. Fan and C. Wang (2016). "Chlamydia gallinacea, not C. psittaci, is the endemic chlamydial species in chicken (Gallus gallus)." <u>Sci Rep</u> **6**: 19638.

Hackstadt, T. (2000). "Redirection of host vesicle trafficking pathways by intracellular parasites." <u>Traffic</u> **1**(2): 93-99.

Hackstadt, T., W. J. Todd and H. D. Caldwell (1985). "Disulfide-mediated interactions of the chlamydial major outer membrane protein: role in the differentiation of chlamydiae?" <u>J Bacteriol</u> **161**(1): 25-31.

Hammerschlag, M. R. (2002). "The intracellular life of chlamydiae." <u>Semin Pediatr Infect Dis</u> **13**(4): 239-248.

Hatch, T. P. (1996). "Disulfide cross-linked envelope proteins: the functional equivalent of peptidoglycan in chlamydiae?" <u>J Bacteriol</u> **178**(1): 1-5.

Hegemann, J. H. and K. Moelleken (2012). "Chlamydial adhesions and adhesins." <u>*Intracellular Pathogens 1: Chlamydiales Vol. 1*</u> (Ed. Tan, M. & Bavoil, P. M.) **97–125**.

Henderson, I. R. and A. C. Lam (2001). "Polymorphic proteins of Chlamydia spp.--autotransporters beyond the Proteobacteria." Trends Microbiol **9**(12): 573-578.

Henderson, I. R., F. Navarro-Garcia, M. Desvaux, R. C. Fernandez and D. Ala'Aldeen (2004). "Type V protein secretion pathway: the autotransporter story." Microbiol Mol Biol Rev **68**(4): 692-744.

Henrichfreise, B., A. Schiefer, T. Schneider, E. Nzukou, C. Poellinger, T. J. Hoffmann, K. L. Johnston, K. Moelleken, I. Wiedemann, K. Pfarr, A. Hoerauf and H. G. Sahl (2009). "Functional conservation of the lipid II biosynthesis pathway in the cell wall-less bacteria Chlamydia and Wolbachia: why is lipid II needed?" Mol Microbiol **73**(5): 913-923.

Herlyn, H. and H. Zischler (2008). "The molecular evolution of sperm zonadhesin." Int J Dev Biol **52**(5-6): 781-790.

Hillman, R. D., Jr., Y. M. Baktash and J. J. Martinez (2013). "OmpA-mediated rickettsial adherence to and invasion of human endothelial cells is dependent upon interaction with alpha2beta1 integrin." Cell Microbiol **15**(5): 727-741.

Hogan, R. J., S. A. Mathews, S. Mukhopadhyay, J. T. Summersgill and P. Timms (2004). "Chlamydial persistence: beyond the biphasic paradigm." Infect Immun **72**(4): 1843-1855.

Holzer, M., K. Laroucau, H. H. Creasy, S. Ott, F. Vorimore, P. M. Bavoil, M. Marz and K. Sachse (2016). "Whole-Genome Sequence of Chlamydia gallinacea Type Strain 08-1274/3." Genome Announc **4**(4).

Hu, V. H., E. M. Harding-Esch, M. J. Burton, R. L. Bailey, J. Kadimpeul and D. C. Mabey (2010). "Epidemiology and control of trachoma: systematic review." Trop Med Int Health **15**(6): 673-691.

Hua-Feng, X., W. Yue-Ming, L. Hong and D. Junyi (2015). "A meta-analysis of the association between Chlamydia pneumoniae infection and lung cancer risk." Indian J Cancer **52 Suppl 2**: e112-115.

Hufnagel, D. A., W. H. Depas and M. R. Chapman (2015). "The Biology of the Escherichia coli Extracellular Matrix." Microbiol Spectr **3**(3).

Hulin, V., S. Oger, F. Vorimore, R. Aaziz, B. de Barbeyrac, J. Berruchon, K. Sachse and K. Laroucau (2015). "Host preference and zoonotic potential of Chlamydia psittaci and C. gallinacea in poultry." Pathog Dis **73**(1): 1-11.

Hybiske, K. and R. S. Stephens (2007). "Mechanisms of host cell exit by the intracellular bacterium Chlamydia." Proc Natl Acad Sci U S A **104**(27): 11430-11435.

Jacobs, A., K. Hartman, T. Laue and M. Caffrey (2004). "Sedimentation velocity studies of the high-molecular weight aggregates of the HIV gp41 ectodomain." Protein Sci **13**(10): 2811-2813.

Jacquier, N., P. H. Viollier and G. Greub (2015). "The role of peptidoglycan in chlamydial cell division: towards resolving the chlamydial anomaly." FEMS Microbiol Rev **39**(2): 262-275.

Jama-Kmiecik, A., M. Frej-Madrzak, J. Sarowska and I. Choroszy-Krol (2015). "[Selected aspects of Chlamydophila pneumoniae infections]." Postepy Hig Med Dosw (Online) **69**: 612-623.

Jansen, R., W. Dzwolak and R. Winter (2005). "Amyloidogenic self-assembly of insulin aggregates probed by high resolution atomic force microscopy." Biophys J **88**(2): 1344-1353.

Jantos, C. A., S. Heck, R. Roggendorf, M. Sen-Gupta and J. H. Hegemann (1997). "Antigenic and

molecular analyses of different Chlamydia pneumoniae strains." J Clin Microbiol **35**(3): 620-623.

Jeffrey, B. M., R. J. Suchland, K. L. Quinn, J. R. Davidson, W. E. Stamm and D. D. Rockey (2010). "Genome sequencing of recent clinical Chlamydia trachomatis strains identifies loci associated with tissue tropism and regions of apparent recombination." Infect Immun **78**(6): 2544-2553.

Jenkins, J., O. Mayans and R. Pickersgill (1998). "Structure and evolution of parallel beta-helix proteins." J Struct Biol **122**(1-2): 236-246.

Jerabek-Willemsen, M., C. J. Wienken, D. Braun, P. Baaske and S. Duhr (2011). "Molecular interaction studies using microscale thermophoresis." Assay Drug Dev Technol **9**(4): 342-353.

Jiwani, S., S. Alvarado, R. J. Ohr, A. Romero, B. Nguyen and T. J. Jewett (2013). "Chlamydia trachomatis Tarp harbors distinct G and F actin binding domains that bundle actin filaments." J Bacteriol **195**(4): 708-716.

Kalman, S., W. Mitchell, R. Marathe, C. Lammel, J. Fan, R. W. Hyman, L. Olinger, J. Grimwood, R. W. Davis and R. S. Stephens (1999). "Comparative genomes of Chlamydia pneumoniae and C. trachomatis." Nat Genet **21**(4): 385-389.

Kari, L., T. R. Southern, C. J. Downey, H. S. Watkins, L. B. Randall, L. D. Taylor, G. L. Sturdevant, W. M. Whitmire and H. D. Caldwell (2014). "Chlamydia trachomatis polymorphic membrane protein D is a virulence factor involved in early host-cell interactions." Infect Immun **82**(7): 2756-2762.

Kari, L., W. M. Whitmire, D. D. Crane, N. Reveneau, J. H. Carlson, M. M. Goheen, E. M. Peterson, S. Pal, L. M. de la Maza and H. D. Caldwell (2009). "Chlamydia trachomatis native major outer membrane protein induces partial protection in nonhuman primates: implication for a trachoma transmission-blocking vaccine." J Immunol **182**(12): 8063-8070.

Karunakaran, K. P., J. Rey-Ladino, N. Stoynov, K. Berg, C. Shen, X. Jiang, B. R. Gabel, H. Yu, L. J. Foster and R. C. Brunham (2008). "Immunoproteomic discovery of novel T cell antigens from the obligate intracellular pathogen Chlamydia." J Immunol **180**(4): 2459-2465.

Karunakaran, K. P., H. Yu, X. Jiang, Q. Chan, K. M. Moon, L. J. Foster and R. C. Brunham (2015). "Outer membrane proteins preferentially load MHC class II peptides: implications for a Chlamydia trachomatis T cell vaccine." Vaccine **33**(18): 2159-2166.

Kelley, L. A., S. Mezulis, C. M. Yates, M. N. Wass and M. J. Sternberg (2015). "The Phyre2 web portal for protein modeling, prediction and analysis." Nat Protoc **10**(6): 845-858.

Kettler, G. C., A. C. Martiny, K. Huang, J. Zucker, M. L. Coleman, S. Rodrigue, F. Chen, A. Lapidus, S. Ferriera, J. Johnson, C. Steglich, G. M. Church, P. Richardson and S. W. Chisholm (2007). "Patterns and implications of gene gain and loss in the evolution of Prochlorococcus." PLoS Genet **3**(12): e231.

Kikuchi, T., Y. Mizunoe, A. Takade, S. Naito and S. Yoshida (2005). "Curli fibers are required for development of biofilm architecture in Escherichia coli K-12 and enhance bacterial adherence to human uroepithelial cells." Microbiol Immunol **49**(9): 875-884.

Kim, J. H., S. Jiang, C. A. Elwell and J. N. Engel (2011). "Chlamydia trachomatis co-opts the FGF2 signaling pathway to enhance infection." PLoS Pathog **7**(10): e1002285.

Kim, S. K. and R. DeMars (2001). "Epitope clusters in the major outer membrane protein of Chlamydia trachomatis." Curr Opin Immunol **13**(4): 429-436.

Kiselev, A. O., M. C. Skinner and M. F. Lampe (2009). "Analysis of pmpD expression and PmpD post-translational processing during the life cycle of Chlamydia trachomatis serovars A, D, and L2." PLoS One **4**(4): e5191.

Kiselev, A. O., W. E. Stamm, J. R. Yates and M. F. Lampe (2007). "Expression, processing, and localization of PmpD of Chlamydia trachomatis Serovar L2 during the chlamydial developmental cycle." PLoS One **2**(6): e568.

Klockner, A., C. Otten, A. Derouaux, W. Vollmer, H. Buhl, S. De Benedetti, D. Munch, M. Josten, K. Molleken, H. G. Sahl and B. Henrichfreise (2014). "AmiA is a penicillin target enzyme with dual activity in the intracellular pathogen Chlamydia pneumoniae." Nat Commun **5**: 4201.

Koiwai, K., M. D. Hartmann, D. Linke, A. N. Lupas and K. Hori (2016). "Structural Basis for Toughness and Flexibility in the C-terminal Passenger Domain of an Acinetobacter Trimeric Autotransporter Adhesin." J Biol Chem **291**(8): 3705-3724.

Korhonen, J. T., M. Puolakkainen, A. Haveri, A. Tammiruusu, M. Sarvas and R. Lahesmaa (2012). "Chlamydia pneumoniae entry into epithelial cells by clathrin-independent endocytosis." Microb Pathog **52**(3): 157-164.

Kreisberg, J. F., S. D. Betts and J. King (2000). "Beta-helix core packing within the triple-stranded oligomerization domain of the P22 tailspike." Protein Sci **9**(12): 2338-2343.

Kuo, C. C. and T. Grayston (1976). "Interaction of Chlamydia trachomatis organisms and HeLa 229 cells." Infect Immun **13**(4): 1103-1109.

Kuo, C. C., S. P. Wang and J. T. Grayston (1973). "Effect of polycations, polyanions and neuraminidase on the infectivity of trachoma-inclusin conjunctivitis and lymphogranuloma venereum organisms HeLa cells: sialic acid residues as possible receptors for trachoma-inclusion conjunction." Infect Immun **8**(1): 74-79.

Lackner, J. (2014). "Klonierung und Expression des hypothetischen Proteins Cpn1003 aus Chlamydia pneumoniae." Funktionelle Genomforschung der Mikroorganismen **Bachelor thesis**(Düsseldorf, Heinrich-Heine-Universität).

Lara-Tejero, M., J. Kato, S. Wagner, X. Liu and J. E. Galan (2011). "A sorting platform determines the order of protein secretion in bacterial type III systems." Science **331**(6021): 1188-1191.

Laroucau, K., R. Aaziz, L. Meurice, V. Servas, I. Chossat, H. Royer, B. de Barbeyrac, V. Vaillant, J. L. Moyen, F. Meziani, K. Sachse and P. Rolland (2015). "Outbreak of psittacosis in a group of women exposed to Chlamydia psittaci-infected chickens." Euro Surveill **20**(24).

Lasa, I. and J. R. Penades (2006). "Bap: a family of surface proteins involved in biofilm formation." Res Microbiol **157**(2): 99-107.

Leo, J. C., I. Grin and D. Linke (2012). "Type V secretion: mechanism(s) of autotransport through the bacterial outer membrane." Philos Trans R Soc Lond B Biol Sci **367**(1592): 1088-1101.

Liechti, G., E. Kuru, M. Packiam, Y. P. Hsu, S. Tekkam, E. Hall, J. T. Rittichier, M. VanNieuwenhze, Y. V. Brun and A. T. Maurelli (2016). "Pathogenic Chlamydia Lack a Classical Sacculus but Synthesize a Narrow, Mid-cell Peptidoglycan Ring, Regulated by MreB, for Cell Division." PLoS Pathog **12**(5): e1005590.

Liechti, G. W., E. Kuru, E. Hall, A. Kalinda, Y. V. Brun, M. VanNieuwenhze and A. T. Maurelli (2014). "A new metabolic cell-wall labelling method reveals peptidoglycan in Chlamydia trachomatis." Nature **506**(7489): 507-510.

Little, C. S., T. A. Joyce, C. J. Hammond, H. Matta, D. Cahn, D. M. Appelt and B. J. Balin (2014). "Detection of bacterial antigens and Alzheimer's disease-like pathology in the central nervous system of BALB/c mice following intranasal infection with a laboratory isolate of Chlamydia pneumoniae." Front Aging Neurosci **6**: 304.

Liu, X., M. Afrane, D. E. Clemmer, G. Zhong and D. E. Nelson (2010). "Identification of Chlamydia trachomatis outer membrane complex proteins by differential proteomics." J Bacteriol **192**(11): 2852-2860.

Longbottom, D., M. Russell, G. E. Jones, F. A. Lainson and A. J. Herring (1996). "Identification of a multigene family coding for the 90 kDa proteins of the ovine abortion subtype of Chlamydia psittaci." FEMS Microbiol Lett **142**(2-3): 277-281.

Luczak, S. E., S. H. Smits, C. Decker, L. Nagel-Steger, L. Schmitt and J. H. Hegemann (2016). "The Chlamydia pneumoniae Adhesin Pmp21 forms Oligomers with Adhesive Properties." J Biol Chem.

Luo, J., S. K. Warmlander, A. Graslund and J. P. Abrahams (2016). "Cross-interactions between the Alzheimer Disease Amyloid-beta Peptide and Other Amyloid Proteins: A Further Aspect of the Amyloid Cascade Hypothesis." J Biol Chem **291**(32): 16485-16493.

Lutter, E. I., C. Martens and T. Hackstadt (2012). "Evolution and conservation of predicted inclusion membrane proteins in chlamydiae." Comp Funct Genomics **2012**: 362104.

Maji, S. K., M. H. Perrin, M. R. Sawaya, S. Jessberger, K. Vadodaria, R. A. Rissman, P. S. Singru, K. P. Nilsson, R. Simon, D. Schubert, D. Eisenberg, J. Rivier, P. Sawchenko, W. Vale and R. Riek (2009). "Functional amyloids as natural storage of peptide hormones in pituitary secretory granules." Science **325**(5938): 328-332.

Makin, O. S. and L. C. Serpell (2005). "Structures for amyloid fibrils." FEBS J **272**(23): 5950-5961.

Malhotra, M., S. Sood, A. Mukherjee, S. Muralidhar and M. Bala (2013). "Genital Chlamydia trachomatis: an update." Indian J Med Res **138**(3): 303-316.

Mandal, P., N. Eremina and A. Barth (2012). "Formation of oligomers in the early phase of pH-induced aggregation of the Alzheimer Abeta(12-28) peptide [corrected]." J Phys Chem B **116**(41): 12389-12397.

Manno, M., E. F. Craparo, V. Martorana, D. Bulone and P. L. San Biagio (2006). "Kinetics of insulin aggregation: disentanglement of amyloid fibrillation from large-size cluster formation." Biophys J **90**(12): 4585-4591.

McCoy, A. J. and A. T. Maurelli (2006). "Building the invisible wall: updating the chlamydial peptidoglycan anomaly." Trends Microbiol **14**(2): 70-77.

McCoy, A. J., R. C. Sandlin and A. T. Maurelli (2003). "In vitro and in vivo functional activity of Chlamydia MurA, a UDP-N-acetylglucosamine enolpyruvyl transferase involved in peptidoglycan synthesis and fosfomycin resistance." J Bacteriol **185**(4): 1218-1228.

Mehlitz, A. and T. Rudel (2013). "Modulation of host signaling and cellular responses by Chlamydia." Cell Commun Signal **11**: 90.

Meinhardt, J., C. Sachse, P. Hortschansky, N. Grigorieff and M. Fandrich (2009). "Abeta(1-40) fibril polymorphism implies diverse interaction patterns in amyloid fibrils." J Mol Biol **386**(3): 869-877.

Mikami, T. and H. Kitagawa (2016). "Sulfated glycosaminoglycans: their distinct roles in stem cell biology." Glycoconj J.

Miyairi, I., J. D. Laxton, X. Wang, C. A. Obert, V. R. Arva Tatireddigari, N. van Rooijen, T. P. Hatch and G. I. Byrne (2011). "Chlamydia psittaci genetic variants differ in virulence by modulation of host immunity." J Infect Dis 204(4): 654-663.

Moelleken, K. and J. H. Hegemann (2008). "The Chlamydia outer membrane protein OmcB is required for adhesion and exhibits biovar-specific differences in glycosaminoglycan binding." Mol Microbiol 67(2): 403-419.

Mojica, S., H. Huot Creasy, S. Daugherty, T. D. Read, T. Kim, B. Kaltenboeck, P. Bavoil and G. S. Myers (2011). "Genome sequence of the obligate intracellular animal pathogen Chlamydia pecorum E58." J Bacteriol 193(14): 3690.

Molleken, K., E. Becker and J. H. Hegemann (2013). "The Chlamydia pneumoniae invasin protein Pmp21 recruits the EGF receptor for host cell entry." PLoS Pathog 9(4): e1003325.

Molleken, K., E. Schmidt and J. H. Hegemann (2010). "Members of the Pmp protein family of Chlamydia pneumoniae mediate adhesion to human cells via short repetitive peptide motifs." Mol Microbiol 78(4): 1004-1017.

Montigiani, S., F. Falugi, M. Scarselli, O. Finco, R. Petracca, G. Galli, M. Mariani, R. Manetti, M. Agnusdei, R. Cevenini, M. Donati, R. Nogarotto, N. Norais, I. Garaguso, S. Nuti, G. Saletti, D. Rosa, G. Ratti and G. Grandi (2002). "Genomic approach for analysis of surface proteins in Chlamydia pneumoniae." Infect Immun 70(1): 368-379.

Moore, E. R. and S. P. Ouellette (2014). "Reconceptualizing the chlamydial inclusion as a pathogen-specified parasitic organelle: an expanded role for Inc proteins." Front Cell Infect Microbiol 4: 157.

Moorhead, A. M., J. Y. Jung, A. Smirnov, S. Kaufer and M. A. Scidmore (2010). "Multiple host proteins that function in phosphatidylinositol-4-phosphate metabolism are recruited to the chlamydial inclusion." Infect Immun 78(5): 1990-2007.

Morrison, R. P., K. Feilzer and D. B. Tumas (1995). "Gene knockout mice establish a primary protective role for major histocompatibility complex class II-restricted responses in Chlamydia trachomatis genital tract infection." Infect Immun 63(12): 4661-4668.

Moulder, J. W. (1966). "The relation of the psittacosis group (Chlamydiae) to bacteria and viruses." Annu Rev Microbiol 20: 107-130.

Moulder, J. W. (1993). "Why is Chlamydia sensitive to penicillin in the absence of peptidoglycan?" Infect Agents Dis 2(2): 87-99.

Moulder, J. W., N. J. Levy and L. P. Schulman (1980). "Persistent infection of mouse fibroblasts (L cells) with Chlamydia psittaci: evidence for a cryptic chlamydial form." Infect Immun 30(3): 874-883.

Mueller, K. E., G. V. Plano and K. A. Fields (2014). "New frontiers in type III secretion biology: the Chlamydia perspective." Infect Immun 82(1): 2-9.

Muramatsu, M. K., J. A. Brothwell, B. D. Stein, T. E. Putman, D. D. Rockey and D. E. Nelson (2016). "Beyond Tryptophan Synthase: Identification of Genes That Contribute to Chlamydia trachomatis Survival during Gamma Interferon-Induced Persistence and Reactivation." Infect Immun 84(10): 2791-2801.

Murphy, R. M. (2007). "Kinetics of amyloid formation and membrane interaction with amyloidogenic proteins." Biochim Biophys Acta **1768**(8): 1923-1934.

Murra, G. (2009). "Identifizierung und Charakterisierung von Adhaesionsproteinen des Humanpathogenen Erregers *Chlamydia pneumoniae*." Funktionelle Genomforschung der Mikroorganismen **PhD Thesis**(Düsseldorf, Heinrich-Heine-Universität).

Myers, G. S., S. A. Mathews, M. Eppinger, C. Mitchell, K. K. O'Brien, O. R. White, F. Benahmed, R. C. Brunham, T. D. Read, J. Ravel, P. M. Bavoil and P. Timms (2009). "Evidence that human Chlamydia pneumoniae was zoonotically acquired." J Bacteriol **191**(23): 7225-7233.

Mygind, P. H., G. Christiansen, P. Roepstorff and S. Birkelund (2000). "Membrane proteins PmpG and PmpH are major constituents of Chlamydia trachomatis L2 outer membrane complex." FEMS Microbiol Lett **186**(2): 163-169.

Nans, A., H. R. Saibil and R. D. Hayward (2014). "Pathogen-host reorganization during Chlamydia invasion revealed by cryo-electron tomography." Cell Microbiol **16**(10): 1457-1472.

Nguyen, B. D., D. Cunningham, X. Liang, X. Chen, E. J. Toone, C. R. Raetz, P. Zhou and R. H. Valdivia (2011). "Lipooligosaccharide is required for the generation of infectious elementary bodies in Chlamydia trachomatis." Proc Natl Acad Sci U S A **108**(25): 10284-10289.

Nicholson, T. L., L. Olinger, K. Chong, G. Schoolnik and R. S. Stephens (2003). "Global stage-specific gene regulation during the developmental cycle of Chlamydia trachomatis." J Bacteriol **185**(10): 3179-3189.

Niessner, A., C. Kaun, G. Zorn, W. Speidl, Z. Turel, G. Christiansen, A. S. Pedersen, S. Birkelund, S. Simon, A. Georgopoulos, W. Graninger, R. de Martin, J. Lipp, B. R. Binder, G. Maurer, K. Huber and J. Wojta (2003). "Polymorphic membrane protein (PMP) 20 and PMP 21 of Chlamydia pneumoniae induce proinflammatory mediators in human endothelial cells in vitro by activation of the nuclear factor-kappaB pathway." J Infect Dis **188**(1): 108-113.

Nobbs, A. H., M. M. Vickerman and H. F. Jenkinson (2010). "Heterologous expression of Candida albicans cell wall-associated adhesins in Saccharomyces cerevisiae Reveals differential specificities in adherence and biofilm formation and in binding oral Streptococcus gordonii." Eukaryot Cell **9**(10): 1622-1634.

Novagen (2003). "pET System Manual." EMD Biosciences **10th Edition**.

Nunes, A., J. P. Gomes, S. Mead, C. Florindo, H. Correia, M. J. Borrego and D. Dean (2007). "Comparative expression profiling of the Chlamydia trachomatis pmp gene family for clinical and reference strains." PLoS One **2**(9): e878.

Oh, Y. J., M. Hubauer-Brenner, H. J. Gruber, Y. Cui, L. Traxler, C. Siligan, S. Park and P. Hinterdorfer (2016). "Curli mediate bacterial adhesion to fibronectin via tensile multiple bonds." Sci Rep **6**: 33909.

Olivares-Zavaleta, N., W. Whitmire, D. Gardner and H. D. Caldwell (2010). "Immunization with the attenuated plasmidless Chlamydia trachomatis L2(25667R) strain provides partial protection in a murine model of female genitourinary tract infection." Vaccine **28**(6): 1454-1462.

Olzscha, H., S. M. Schermann, A. C. Woerner, S. Pinkert, M. H. Hecht, G. G. Tartaglia, M. Vendruscolo, M. Hayer-Hartl, F. U. Hartl and R. M. Vabulas (2011). "Amyloid-like aggregates sequester numerous metastable proteins with essential cellular functions." Cell **144**(1): 67-78.

Omsland, A., B. S. Sixt, M. Horn and T. Hackstadt (2014). "Chlamydial metabolism revisited:

interspecies metabolic variability and developmental stage-specific physiologic activities." FEMS Microbiol Rev **38**(4): 779-801.

Ortega, N., M. R. Caro, M. C. Gallego, A. Murcia-Belmonte, D. Alvarez, L. Del Rio, F. Cuello, A. J. Buendia and J. Salinas (2015). "Isolation of Chlamydia abortus from a laboratory worker diagnosed with atypical pneumonia." Ir Vet J **69**: 8.

Otto, B. R., R. Sijbrandi, J. Luirink, B. Oudega, J. G. Heddle, K. Mizutani, S. Y. Park and J. R. Tame (2005). "Crystal structure of hemoglobin protease, a heme binding autotransporter protein from pathogenic Escherichia coli." J Biol Chem **280**(17): 17339-17345.

Pannekoek, Y., Q. Qi-Long, Y. Z. Zhang and A. van der Ende (2016). "Genus delineation of Chlamydiales by analysis of the percentage of conserved proteins justifies the reunifying of the genera Chlamydia and Chlamydophila into one single genus Chlamydia." Pathog Dis **74**(6).

Pedersen, A. S., G. Christiansen and S. Birkelund (2001). "Differential expression of Pmp10 in cell culture infected with Chlamydia pneumoniae CWL029." FEMS Microbiol Lett **203**(2): 153-159.

Pedersen, J. S., G. Christensen and D. E. Otzen (2004). "Modulation of S6 fibrillation by unfolding rates and gatekeeper residues." J Mol Biol **341**(2): 575-588.

Perry, L. L., K. Feilzer and H. D. Caldwell (1997). "Immunity to Chlamydia trachomatis is mediated by T helper 1 cells through IFN-gamma-dependent and -independent pathways." J Immunol **158**(7): 3344-3352.

Peters, J., D. P. Wilson, G. Myers, P. Timms and P. M. Bavoil (2007). "Type III secretion a la Chlamydia." Trends Microbiol **15**(6): 241-251.

Peterson, E. M., L. M. de la Maza, L. Brade and H. Brade (1998). "Characterization of a neutralizing monoclonal antibody directed at the lipopolysaccharide of Chlamydia pneumoniae." Infect Immun **66**(8): 3848-3855.

Peterson, E. M., J. Z. You, V. Motin and L. M. de la Maza (1999). "Intranasal immunization with Chlamydia trachomatis, serovar E, protects from a subsequent vaginal challenge with the homologous serovar." Vaccine **17**(22): 2901-2907.

Pillonel, T., C. Bertelli, N. Salamin and G. Greub (2015). "Taxogenomics of the order Chlamydiales." Int J Syst Evol Microbiol **65**(Pt 4): 1381-1393.

Qin, Q. L., B. B. Xie, X. Y. Zhang, X. L. Chen, B. C. Zhou, J. Zhou, A. Oren and Y. Z. Zhang (2014). "A proposed genus boundary for the prokaryotes based on genomic insights." J Bacteriol **196**(12): 2210-2215.

Quan, S., A. Hiniker, J. F. Collet and J. C. Bardwell (2013). "Isolation of bacteria envelope proteins." Methods Mol Biol **966**: 359-366.

Rapsinski, G. J., M. A. Wynosky-Dolfi, G. O. Oppong, S. A. Tursi, R. P. Wilson, I. E. Brodsky and C. Tukel (2015). "Toll-like receptor 2 and NLRP3 cooperate to recognize a functional bacterial amyloid, curli." Infect Immun **83**(2): 693-701.

Raulston, J. E. (1995). "Chlamydial envelope components and pathogen-host cell interactions." Mol Microbiol **15**(4): 607-616.

Reddy, K. R., H. Lilie, R. Rudolph and C. Lange (2005). "L-Arginine increases the solubility of unfolded species of hen egg white lysozyme." Protein Sci **14**(4): 929-935.

Rejman Lipinski, A., J. Heymann, C. Meissner, A. Karlas, V. Brinkmann, T. F. Meyer and D. Heuer (2009). "Rab6 and Rab11 regulate Chlamydia trachomatis development and golgin-84-dependent Golgi fragmentation." PLoS Pathog **5**(10): e1000615.

Resnikoff, S., D. Pascolini, D. Etya'ale, I. Kocur, R. Pararajasegaram, G. P. Pokharel and S. P. Mariotti (2004). "Global data on visual impairment in the year 2002." Bull World Health Organ **82**(11): 844-851.

Rockey, D. D., J. Lenart and R. S. Stephens (2000). "Genome sequencing and our understanding of chlamydiae." Infect Immun **68**(10): 5473-5479.

Rodolakis, A. and K. Laroucau (2015). "Chlamydiaceae and chlamydial infections in sheep or goats." Vet Microbiol **181**(1-2): 107-118.

Rohde, G., E. Straube, A. Essig, P. Reinhold and K. Sachse (2010). "Chlamydial zoonoses." Dtsch Arztebl Int **107**(10): 174-180.

Romero, D. and R. Kolter (2014). "Functional amyloids in bacteria." Int Microbiol **17**(2): 65-73.

Ruiz-Perez, F., I. R. Henderson and J. P. Nataro (2010). "Interaction of FkpA, a peptidyl-prolyl cis/trans isomerase with EspP autotransporter protein." Gut Microbes **1**(5): 339-344.

Rund, S., B. Lindner, H. Brade and O. Holst (1999). "Structural analysis of the lipopolysaccharide from Chlamydia trachomatis serotype L2." J Biol Chem **274**(24): 16819-16824.

Sachse, K., K. Laroucau, K. Riege, S. Wehner, M. Dilcher, H. H. Creasy, M. Weidmann, G. Myers, F. Vorimore, N. Vicari, S. Magnino, E. Liebler-Tenorio, A. Ruettger, P. M. Bavoil, F. T. Hufert, R. Rossello-Mora and M. Marz (2014). "Evidence for the existence of two new members of the family Chlamydiaceae and proposal of Chlamydia avium sp. nov. and Chlamydia gallinacea sp. nov." Syst Appl Microbiol **37**(2): 79-88.

Saikku, P. (2000). "Epidemiologic association of Chlamydia pneumoniae and atherosclerosis: the initial serologic observation and more." J Infect Dis **181 Suppl 3**: S411-413.

Saka, H. A., J. W. Thompson, Y. S. Chen, Y. Kumar, L. G. Dubois, M. A. Moseley and R. H. Valdivia (2011). "Quantitative proteomics reveals metabolic and pathogenic properties of Chlamydia trachomatis developmental forms." Mol Microbiol **82**(5): 1185-1203.

Sambrook, J. and T. Maniatis (1989). "Cold Spring Harbor, N. Y., Cold Spring Harbor laboratory." Molecular cloning: A laboratory manual.

Schautteet, K., E. De Clercq and D. Vanrompay (2011). "Chlamydia trachomatis vaccine research through the years." Infect Dis Obstet Gynecol **2011**: 963513.

Scheller, E. V. and P. A. Cotter (2015). "Bordetella filamentous hemagglutinin and fimbriae: critical adhesins with unrealized vaccine potential." Pathog Dis **73**(8): ftv079.

Shaw, E. I., C. A. Dooley, E. R. Fischer, M. A. Scidmore, K. A. Fields and T. Hackstadt (2000). "Three temporal classes of gene expression during the Chlamydia trachomatis developmental cycle." Mol Microbiol **37**(4): 913-925.

Shima, K., J. Coopmeiners, S. Graspeuntner, K. Dalhoff and J. Rupp (2016). "Impact of micro-environmental changes on respiratory tract infections with intracellular bacteria." FEBS Lett.

Simon, N., A. Kuehn, K. C. Williamson and G. Pradel (2016). "Adhesion protein complexes of malaria gametocytes assemble following parasite transmission to the mosquito." Parasitol Int **65**(1):

27-30.

Simon, N., S. M. Scholz, C. K. Moreira, T. J. Templeton, A. Kuehn, M. A. Dude and G. Pradel (2009). "Sexual stage adhesion proteins form multi-protein complexes in the malaria parasite Plasmodium falciparum." J Biol Chem **284**(21): 14537-14546.

Sipe, J. D. and A. S. Cohen (2000). "Review: history of the amyloid fibril." J Struct Biol **130**(2-3): 88-98.

Sixt, B. S. and R. H. Valdivia (2016). "Molecular Genetic Analysis of Chlamydia Species." Annu Rev Microbiol **70**: 179-198.

Sockolosky, J. T. and F. C. Szoka (2013). "Periplasmic production via the pET expression system of soluble, bioactive human growth hormone." Protein Expr Purif **87**(2): 129-135.

Spaeth, K. E., Y. S. Chen and R. H. Valdivia (2009). "The Chlamydia type III secretion system C-ring engages a chaperone-effector protein complex." PLoS Pathog **5**(9): e1000579.

Stallmann, S. (2015). "Identifizierung und Charakterisierung neuer Adhäsine bei Chlamydia trachomatis." Funktionelle Genomforschung der Mikroorganismen **PhD Thesis** (Düsseldorf, Heinrich-Heine-Universität).

Stallmann, S. and J. H. Hegemann (2016). "The Chlamydia trachomatis Ctad1 invasin exploits the human integrin beta1 receptor for host cell entry." Cell Microbiol **18**(5): 761-775.

Stephens, R. S., S. Kalman, C. Lammel, J. Fan, R. Marathe, L. Aravind, W. Mitchell, L. Olinger, R. L. Tatusov, Q. Zhao, E. V. Koonin and R. W. Davis (1998). "Genome sequence of an obligate intracellular pathogen of humans: Chlamydia trachomatis." Science **282**(5389): 754-759.

Stephens, R. S., K. Koshiyama, E. Lewis and A. Kubo (2001). "Heparin-binding outer membrane protein of chlamydiae." Mol Microbiol **40**(3): 691-699.

Stephens, R. S., G. Myers, M. Eppinger and P. M. Bavoil (2009). "Divergence without difference: phylogenetics and taxonomy of Chlamydia resolved." FEMS Immunol Med Microbiol **55**(2): 115-119.

Stoner, B. P. and S. E. Cohen (2015). "Lymphogranuloma Venereum 2015: Clinical Presentation, Diagnosis, and Treatment." Clin Infect Dis **61 Suppl 8**: S865-873.

Su, H., L. Raymond, D. D. Rockey, E. Fischer, T. Hackstadt and H. D. Caldwell (1996). "A recombinant Chlamydia trachomatis major outer membrane protein binds to heparan sulfate receptors on epithelial cells." Proc Natl Acad Sci U S A **93**(20): 11143-11148.

Subbarayal, P., K. Karunakaran, A. C. Winkler, M. Rother, E. Gonzalez, T. F. Meyer and T. Rudel (2015). "EphrinA2 receptor (EphA2) is an invasion and intracellular signaling receptor for Chlamydia trachomatis." PLoS Pathog **11**(4): e1004846.

Subtil, A., C. Delevoye, M. E. Balana, L. Tastevin, S. Perrinet and A. Dautry-Varsat (2005). "A directed screen for chlamydial proteins secreted by a type III mechanism identifies a translocated protein and numerous other new candidates." Mol Microbiol **56**(6): 1636-1647.

Subtil, A., B. Wyplosz, M. E. Balana and A. Dautry-Varsat (2004). "Analysis of Chlamydia caviae entry sites and involvement of Cdc42 and Rac activity." J Cell Sci **117**(Pt 17): 3923-3933.

Sun, G., S. Pal, A. K. Sarcon, S. Kim, E. Sugawara, H. Nikaido, M. J. Cocco, E. M. Peterson and L. M. de la Maza (2007). "Structural and functional analyses of the major outer membrane protein

of Chlamydia trachomatis." J Bacteriol **189**(17): 6222-6235.

Swanson, K. A., L. D. Taylor, S. D. Frank, G. L. Sturdevant, E. R. Fischer, J. H. Carlson, W. M. Whitmire and H. D. Caldwell (2009). "Chlamydia trachomatis polymorphic membrane protein D is an oligomeric autotransporter with a higher-order structure." Infect Immun **77**(1): 508-516.

Taglialegna, A., S. Navarro, S. Ventura, J. A. Garnett, S. Matthews, J. R. Penades, I. Lasa and J. Valle (2016). "Staphylococcal Bap Proteins Build Amyloid Scaffold Biofilm Matrices in Response to Environmental Signals." PLoS Pathog **12**(6): e1005711.

Tan, C., R. C. Hsia, H. Shou, J. A. Carrasco, R. G. Rank and P. M. Bavoil (2010). "Variable expression of surface-exposed polymorphic membrane proteins in in vitro-grown Chlamydia trachomatis." Cell Microbiol **12**(2): 174-187.

Tan, C., R. C. Hsia, H. Shou, C. L. Haggerty, R. B. Ness, C. A. Gaydos, D. Dean, A. M. Scurlock, D. P. Wilson and P. M. Bavoil (2009). "Chlamydia trachomatis-infected patients display variable antibody profiles against the nine-member polymorphic membrane protein family." Infect Immun **77**(8): 3218-3226.

Tanzer, R. J. and T. P. Hatch (2001). "Characterization of outer membrane proteins in Chlamydia trachomatis LGV serovar L2." J Bacteriol **183**(8): 2686-2690.

Taylor, B. D., T. Darville, C. Tan, P. M. Bavoil, R. B. Ness and C. L. Haggerty (2011). "The role of Chlamydia trachomatis polymorphic membrane proteins in inflammation and sequelae among women with pelvic inflammatory disease." Infect Dis Obstet Gynecol **2011**: 989762.

Taylor, J. D., W. J. Hawthorne, J. Lo, A. Dear, N. Jain, G. Meisl, M. Andreasen, C. Fletcher, M. Koch, N. Darvill, N. Scull, A. Escalera-Maurer, L. Sefer, R. Wenman, S. Lambert, J. Jean, Y. Xu, B. Turner, S. G. Kazarian, M. R. Chapman, D. Bubeck, A. de Simone, T. P. Knowles and S. J. Matthews (2016). "Electrostatically-guided inhibition of Curli amyloid nucleation by the CsgC-like family of chaperones." Sci Rep **6**: 24656.

Taylor, L. D., D. E. Nelson, D. W. Dorward, W. M. Whitmire and H. D. Caldwell (2010). "Biological characterization of Chlamydia trachomatis plasticity zone MACPF domain family protein CT153." Infect Immun **78**(6): 2691-2699.

Temoin, S., K. L. Wu, V. Wu, M. Shoham and Y. W. Han (2012). "Signal peptide of FadA adhesin from Fusobacterium nucleatum plays a novel structural role by modulating the filament's length and width." FEBS Lett **586**(1): 1-6.

Thomas, S., I. B. Holland and L. Schmitt (2014). "The Type 1 secretion pathway - the hemolysin system and beyond." Biochim Biophys Acta **1843**(8): 1629-1641.

Thornton, D. J., K. Rousseau and M. A. McGuckin (2008). "Structure and function of the polymeric mucins in airways mucus." Annu Rev Physiol **70**: 459-486.

Tifrea, D. F., S. Pal, J. L. Popot, M. J. Cocco and L. M. de la Maza (2014). "Increased immunoaccessibility of MOMP epitopes in a vaccine formulated with amphipols may account for the very robust protection elicited against a vaginal challenge with Chlamydia muridarum." J Immunol **192**(11): 5201-5213.

Ting, L. M., R. C. Hsia, C. G. Haidaris and P. M. Bavoil (1995). "Interaction of outer envelope proteins of Chlamydia psittaci GPIC with the HeLa cell surface." Infect Immun **63**(9): 3600-3608.

Torres, V. J., S. E. Ivie, M. S. McClain and T. L. Cover (2005). "Functional properties of the p33 and p55 domains of the Helicobacter pylori vacuolating cytotoxin." J Biol Chem **280**(22): 21107-

21114.

Tsai, H. H., K. Gunasekaran and R. Nussinov (2006). "Sequence and structure analysis of parallel beta helices: implication for constructing amyloid structural models." Structure **14**(6): 1059-1072.

Van Lent, S., H. H. Creasy, G. S. Myers and D. Vanrompay (2016). "The Number, Organization, and Size of Polymorphic Membrane Protein Coding Sequences as well as the Most Conserved Pmp Protein Differ within and across Chlamydia Species." J Mol Microbiol Biotechnol **26**(5): 333-344.

Vandahl, B. B., A. S. Pedersen, K. Gevaert, A. Holm, J. Vandekerckhove, G. Christiansen and S. Birkelund (2002). "The expression, processing and localization of polymorphic membrane proteins in Chlamydia pneumoniae strain CWL029." BMC Microbiol **2**: 36.

Vasilevsky, S., M. Stojanov, G. Greub and D. Baud (2016). "Chlamydial polymorphic membrane proteins: regulation, function and potential vaccine candidates." Virulence **7**(1): 11-22.

Vicinanza, M., G. D'Angelo, A. Di Campli and M. A. De Matteis (2008). "Function and dysfunction of the PI system in membrane trafficking." EMBO J **27**(19): 2457-2470.

Vitali, J., B. Schick, H. C. Kester, J. Visser and F. Jurnak (1998). "The tree-dimensional structure of aspergillus niger pectin lyase B at 1.7-A resolution." Plant Physiol **116**(1): 69-80.

Voigt, A., G. Schofl and H. P. Saluz (2012). "The Chlamydia psittaci genome: a comparative analysis of intracellular pathogens." PLoS One **7**(4): e35097.

Vorimore, F., R. C. Hsia, H. Huot-Creasy, S. Bastian, L. Deruyter, A. Passet, K. Sachse, P. Bavoil, G. Myers and K. Laroucau (2013). "Isolation of a New Chlamydia species from the Feral Sacred Ibis (Threskiornis aethiopicus): Chlamydia ibidis." PLoS One **8**(9): e74823.

Walsh, D. M., D. M. Hartley, Y. Kusumoto, Y. Fezoui, M. M. Condron, A. Lomakin, G. B. Benedek, D. J. Selkoe and D. B. Teplow (1999). "Amyloid beta-protein fibrillogenesis. Structure and biological activity of protofibrillar intermediates." J Biol Chem **274**(36): 25945-25952.

Wang, A., S. C. Johnston, J. Chou and D. Dean (2010). "A systemic network for Chlamydia pneumoniae entry into human cells." J Bacteriol **192**(11): 2809-2815.

Wang, Y., S. Kahane, L. T. Cutcliffe, R. J. Skilton, P. R. Lambden and I. N. Clarke (2011). "Development of a transformation system for Chlamydia trachomatis: restoration of glycogen biosynthesis by acquisition of a plasmid shuttle vector." PLoS Pathog **7**(9): e1002258.

Wehrl, W., V. Brinkmann, P. R. Jungblut, T. F. Meyer and A. J. Szczepek (2004). "From the inside out--processing of the Chlamydial autotransporter PmpD and its role in bacterial adhesion and activation of human host cells." Mol Microbiol **51**(2): 319-334.

Wells, T. J., M. Totsika and M. A. Schembri (2010). "Autotransporters of Escherichia coli: a sequence-based characterization." Microbiology **156**(Pt 8): 2459-2469.

Wheelhouse, N. M., M. Sait, K. Aitchison, M. Livingstone, F. Wright, K. McLean, N. F. Inglis, D. G. Smith and D. Longbottom (2012). "Processing of Chlamydia abortus polymorphic membrane protein 18D during the chlamydial developmental cycle." PLoS One **7**(11): e49190.

WHO (2016). WHO Guidelines for the Treatment of Chlamydia trachomatis Geneva.

Wilson, D. P., P. Timms, D. L. McElwain and P. M. Bavoil (2006). "Type III secretion, contact-dependent model for the intracellular development of chlamydia." Bull Math Biol **68**(1): 161-178.

Witkin, S. S. and I. M. Linhares (2002). "Chlamydia trachomatis in subfertile women undergoing uterine instrumentation: an alternative to direct microbial testing or prophylactic antibiotic treatment." Hum Reprod **17**(8): 1938-1941.

Wolf, K., E. Fischer and T. Hackstadt (2000). "Ultrastructural analysis of developmental events in Chlamydia pneumoniae-infected cells." Infect Immun **68**(4): 2379-2385.

Wuppermann, F. N., J. H. Hegemann and C. A. Jantos (2001). "Heparan sulfate-like glycosaminoglycan is a cellular receptor for Chlamydia pneumoniae." J Infect Dis **184**(2): 181-187.

Wuppermann, F. N., K. Molleken, M. Julien, C. A. Jantos and J. H. Hegemann (2008). "Chlamydia pneumoniae GroEL1 protein is cell surface associated and required for infection of HEp-2 cells." J Bacteriol **190**(10): 3757-3767.

Wyrick, P. B. (2010). "Chlamydia trachomatis persistence in vitro: an overview." J Infect Dis **201 Suppl 2**: S88-95.

Xia, C., Z. Bao, F. Tabassam, W. Ma, M. Qiu, S. Hua and M. Liu (2000). "GCIP, a novel human grap2 and cyclin D interacting protein, regulates E2F-mediated transcriptional activity." J Biol Chem **275**(27): 20942-20948.

Yan, Y., S. Silvennoinen-Kassinen, M. Leinonen and P. Saikku (2006). "Inhibitory effect of heparan sulfate-like glycosaminoglycans on the infectivity of Chlamydia pneumoniae in HL cells varies between strains." Microbes Infect **8**(3): 866-872.

Yoshimoto, S., H. Nakatani, K. Iwasaki and K. Hori (2016). "An Acinetobacter trimeric autotransporter adhesin reaped from cells exhibits its nonspecific stickiness via a highly stable 3D structure." Sci Rep **6**: 28020.

Yu, H., X. Jiang, C. Shen, K. P. Karunakaran and R. C. Brunham (2009). "Novel Chlamydia muridarum T Cell Antigens Induce Protective Immunity against Lung and Genital Tract Infection in Murine Models." The Journal of Immunology **182**(3): 1602-1608.

Yu, H., K. P. Karunakaran, X. Jiang and R. C. Brunham (2014). "Evaluation of a multisubunit recombinant polymorphic membrane protein and major outer membrane protein T cell vaccine against Chlamydia muridarum genital infection in three strains of mice." Vaccine **32**(36): 4672-4680.

Yu, H., K. P. Karunakaran, X. Jiang, C. Shen, P. Andersen and R. C. Brunham (2012). "Chlamydia muridarum T cell antigens and adjuvants that induce protective immunity in mice." Infect Immun **80**(4): 1510-1518.

Yu, H., K. P. Karunakaran, I. Kelly, C. Shen, X. Jiang, L. J. Foster and R. C. Brunham (2011). "Immunization with live and dead Chlamydia muridarum induces different levels of protective immunity in a murine genital tract model: correlation with MHC class II peptide presentation and multifunctional Th1 cells." J Immunol **186**(6): 3615-3621.

Zhang, J. P. and R. S. Stephens (1992). "Mechanism of C. trachomatis attachment to eukaryotic host cells." Cell **69**(5): 861-869.

Ziklo, N., W. M. Huston, J. S. Hocking and P. Timms (2016). "Chlamydia trachomatis Genital Tract Infections: When Host Immune Response and the Microbiome Collide." Trends Microbiol **24**(9): 750-765.

Zogaj, X., W. Bokranz, M. Nimtz and U. Romling (2003). "Production of Cellulose and Curli Fimbriae by Members of the Family Enterobacteriaceae Isolated from the Human Gastrointestinal

Tract." <u>Infection and Immunity</u> **71**(7): 4151-4158.

Zou, W. Q., X. Xiao, J. Yuan, G. Puoti, H. Fujioka, X. Wang, S. Richardson, X. Zhou, R. Zou, S. Li, X. Zhu, P. L. McGeer, J. McGeehan, G. Kneale, D. E. Rincon-Limas, P. Fernandez-Funez, H. G. Lee, M. A. Smith, R. B. Petersen and J. P. Guo (2011). "Amyloid-beta42 interacts mainly with insoluble prion protein in the Alzheimer brain." <u>J Biol Chem</u> **286**(17): 15095-15105.

List of figures

Acknowledgments

First of all, I would like to thank Prof. Dr. Johannes H. Hegemann for giving me the possibility to work in his lab, for his guidance in the development of the projects, which allowed me to evolve a scientific thinking.

I am grateful to Prof. Dr. Klaus Pfeffer for having accepted to co-supervise my work and for his always useful advices.

Thanks to Prof. Dr. Ursula Fleig for her helpful comments and inputs during my time in the lab.

Thanks to Prof. Dr. Lutz Schmitt and to Prof. Dr. Joachim Ernst for allowing me to use their facilities for my SEC and MST analyses.

Many thanks to Dr. Inge Krümpelbeck for always being present and patient to solve every problem.

Special thanks to Dr. Katja Mölleken for her support in discussing any kind of doubt, question and solution; and, in particular, for her encouragement.

I would like to thank all the previous and present members of the "Chlamydia" and "Pombe" teams for the nice environment, which made me gain self-confidence and learn very much, professionally and personally. Special thanks to Sören, for living the "Pmp experience" with me, my PhD would not have reached this far without your help. Thanks to all the colleagues of the MOI II graduate school. It was a pleasure being part of this group. I wish you great success!

To Marina, Coco and Natascha. I can´t express in words how lucky and grateful I feel that we got to share this experience together. I could not have done it without you! We always got our backs in difficult times and celebrated together the good times; we cried and laughed through these years and became a family! Thank you for being able to deal with my obsessions, my weaknesses and to read my very long quotes! I will miss you very much!

To my "lifetime" friends in Italy and in the rest of the world (Maria, Alice, Corinne, Benedetta, Ilaria, Federico, Giulia, Francesca, Irene, Andrea, Milena, Angelica, Diego, Valentina, Daniele, Jacopo, Andrea, Alessandro, Fabrizio, Erica), for making me feel like "distance" is just a word.

To my mom and my dad, thank you for always believing in me, for all the sacrifices you made to make it possible for me to be who I am today. Thank you for loving me so much to face all challenges that my life has brought along the way.

To the rest of my big italian family (my aunts, uncles, cousins, nieces, nephews and to my family in-law) for your love and support.

At last, to Selene. Thank you for being by my side for six years, for supporting me in all my decisions, for always putting me first, for pushing me when I am afraid to move forward, for comforting me when I fail and for celebrating my successes. Thanks for reminding me that everything is possible, that we can have it all and guess what!? We have it already!

Ringraziamenti

Vorrei ringraziare Prof. Dr. Johannes Hegemann per avermi dato l'opportunità di lavorare nel lab, per la sua guida nello sviluppo dei progetti, che mi ha permesso di evolvere un pensiero scientifico.

Sono grata a Prof. Dr. Klaus Pfeffer, per aver accettato di essere il mio co-supervisor e per i suoi sempre utili consigli.

Grazie a Prof. Dr. Ursula Fleig, per i suoi utili commenti e input durante il mio percorso nel lab.

Grazie a Prof. Dr. Lutz Schmitt e Prof. Dr. Joachim Ernst per avermi permesso di usare i loro strumenti per le mie analisi di SEC e MST.

Molte grazie a Dr. Inge Krümpelbeck, per essere sempre presente per risolvere ogni problema.

Un grazie speciale a Dr. Katja Mölleken, per il suo sostegno in discutere ogni tipo di dubbio, domanda e soluzione; e, soprattutto, per il suo incoraggiamento.

Vorrei inoltre ringraziare tutti i passati e gli attuali componenti dei "Chlamydia" e "Pombe" teams, per la bella atmosfera, che ha fatto sviluppare la mia autostima e mi ha fatto imparare molto, professionalmente e personalmente. Un grazie particolare a Sören, per aver vissuto con me la "Pmp experience", il mio PhD non avrebbe avuto questi risultati senza il tuo aiuto!

Grazie a tutti i colleghi della scuola di dottorato MOI II. È stato un piacere far parte di questo gruppo. Vi auguro di avere successo nelle vostre carriere e nelle vostre vite!

A Marina, Coco e Natascha, non so esprimere a parole quanto mi senta fortunata e grata di aver condiviso questa esperienza con voi. Non ce l'avrei fatta senza di voi! Ci siamo sempre sostenute nei momenti difficili e abbiamo celebrato insieme i momenti belli, abbiamo pianto e riso attraverso questi anni e siamo diventate una famiglia! Grazie per essere state in grado di tollerare le mie ossessioni, debolezze e per leggere le mie lunghe citazioni! Mi mancherete moltissimo!

Ai miei amici di sempre in Italia e nel resto del mondo (Maria, Alice, Corinne, Benedetta, Ilaria, Federico, Giulia, Francesca, Irene, Andrea, Milena, Angelica, Diego, Valentina, Daniele, Jacopo, Andrea, Alessandro, Fabrizio, Erica), per avermi dimostrato che "lontananza" è solo una parola.

A mia mamma e mio papà, grazie per credere sempre in me, per tutti i sacrifici che avete fatto per permettermi di essere chi sono oggi. Grazie per amarmi così tanto da affrontare tutte le sfide che la mia vita ha portato lungo il cammino.

Al resto della mia famiglia (zie, zii, cugini, nipoti e alla mia famiglia acquisita), per il vostro amore e sostegno.

In fine, a Selene. Grazie per essere al mio fianco da ben sei anni, per sostenermi in tutte le mie scelte, per mettermi sempre al primo posto, per spronarmi quando ho paura di andare avanti, per confortarmi quando fallisco e per celebrare i miei successi.

Grazie per ricordarmi che tutto è possibile, che possiamo avere tutto e indovina? Lo abbiamo già!

Statutory declaration

Düsseldorf, 10.02.2017

I declare under oath that I have compiled my dissertation independently and without any undue assistance by third parties, under consideration of the 'Principles for the Safeguarding of Good Scientific Practice at Heinrich Heine University Düsseldorf'.

I declare that I have not used sources or means without declaration in the text. All the passages taken from other works in the wording or in the meaning have been clearly indicated with sources. This thesis has not been used in the same or similar version to achieve an academic grading or is being published elsewhere.

Alison Favaroni

.